



DOTTORATO DI RICERCA IN INGEGNERIA MECCANICA INDUSTRIALE

CICLO DI DOTTORATO

XXVI

# COOL MATERIALS PERFORMANCES ANALYSIS IN BUILDING AND URBAN SCALE

DOTTORANDO:

Emiliano Carnielo

TUTOR:

Prof. Ing. Aldo Fanchiotti

COORDINATORE:

Prof. Ing. Edoardo Bemporad

# Abstract

---

Climate changes have in global warming one of the most obvious manifestations. The increase in temperature is a generalised phenomenon, associated with a number of environmental energy risks. The urban heat island is a typical effect, in which global phenomena are in addition to specific local conditions that lead to significant temperature rises in densely urbanised areas with respect to rural ones. Another trend is the increase in consumption for air conditioning in summer and, consequently, of electricity in the civil sector, as demonstrated by data collected in recent years, at national and European level, regarding consumption by sector.

Cool materials represent a possibility to mitigate both phenomena, since they allow to reduce the overheating of construction materials due to the high absorption of solar radiation. Cool materials, characterised by high solar reflectance and thermal emissivity, have many possible applications and are the subject of numerous studies to optimise their thermal-physical properties and check their effects on urban area and on buildings. This study aims at evaluating the efficiency of the cool material both on building scale and on urban scale.

Among cool materials there are products used as building roof coatings, the so-called cool roofs. These products are available in the European market for nearly a decade and nearly two decades in American ones. Although they are a consolidated technology, their use remains limited to a few buildings mostly experimental. This also makes impossible to massively exploit their properties.

Within this report, the application of a cool roof has been tested on a single floor building with a low-sloped roof. The experimental and numerical analyses have shown the potential of this passive technique on increasing in thermo-hygrometric comfort influencing the decrease in internal temperatures of about 2.5 °C as well as the energy savings associated with the energy demand for cooling.

A little investigated aspect of this technology is the study of the decay of the reflection power related to natural phenomena of ageing and soiling. A measurement campaign still in progress aims at assessing the reflectance of materials used as roof coatings with regular experimental analyses. After 18 months there was a decrease of about 24% of the reflection power for samples that had an initial solar reflectance greater than 0.8. In general, this decay is a function of roughness and reflectance spectral response shape. Nonetheless in many cases spectral data measured after 12 and 18 months demonstrate a convergence trend with broadband values however higher than that of conventional materials.

Despite the benefits reported in this and other studies on real applications, there are no procedures for the energy classification of these materials. National energy policies are aimed at reducing consumption related to space heating, with restrictions on thermal transmittance values of the building envelope, neglecting those related to space cooling. For this reason it has been proposed a cool roof classification system as a function of their thermal properties and their influence on the energy performance of buildings normalised as a function of the geometry of some reference buildings and climatic zones.

The cool materials used for urban applications as asphalt and concrete tints, the cool paving, are a technology still in its infancy, with a negligible market penetration. The optical and solar characterisation of these products confirmed their high reflectance especially compared to conventional materials with surface temperatures even lower than 20 °C. A lower surface temperature reduces the heat transferred to the air for convection. The potentialities of these materials applied on the asphalt of a neighbourhood of Rome were analysed by numerical analysis with a type SVAT tool (Soil, Vegetation, Atmosphere, and Transfer). Results showed a decrease in average air temperature of 5.5 °C compared to those obtained in presence of conventional asphalts. The temperature decrease is also reflected at an altitude over the average height of buildings. This shows how cool materials, when used on an urban scale, can be exploited as a contributory factor to the reduction of the heat island.

The use of different energy analysis tools employed for numerical purposes has highlighted a limit concerning the modelling of the building surfaces of the buildings. These models consider the reflectance as a constant and independent on the incidence angle of radiation that hits the surfaces (Lambertian reflection). Instead, the building materials, especially those used as roof coatings, present mixed reflection modalities with not negligible regular components, which are a function of angle of incidence as demonstrated in the experimental campaign shown in this report. Thus, it was obtained a function that linked the solar reflectance to incidence angle starting from the measured data. It has been used in order to modify the calculation model of a dynamic tool in order to optimise the solar gains calculation. The results demonstrate the limits of current thermo-physical models generally used to conduct energy analyses.

*Keywords:* Cool, Reflectance, Emissivity, Solar, Energy.

## Sintesi

---

I cambiamenti climatici hanno nel riscaldamento globale una delle manifestazioni più evidenti. L'aumento delle temperature è un fenomeno generalizzato, cui si associano una serie di rischi ambientali ed energetici. L'isola di calore urbana è un tipico effetto, in cui fenomeni globali si sommano a specificità locali che portano ad innalzamenti di temperatura significativi in aree densamente urbanizzate. Altra tendenza è l'aumento dei consumi per la climatizzazione estiva e, conseguentemente, di energia elettrica nel settore civile, come dimostrato dai dati raccolti in questi anni su scala nazionale ed europea riguardanti i consumi per settore.

I cool material rappresentano una possibilità per mitigare entrambi i fenomeni, dal momento che consentono di ridurre il surriscaldamento dei materiali da costruzione per effetto dell'elevato assorbimento della radiazione solare. I cool material, caratterizzati da riflettanza solare ed emissività termica elevate, hanno numerose possibilità applicative e sono oggetto di numerosi studi per ottimizzarne le proprietà termo-fisiche e verificarne gli effetti su aree urbane e sugli edifici. Questo studio ha lo scopo di valutare l'efficienza dei cool material sia su scala di edificio sia su scala urbana.

Tra i cool material esistono dei prodotti utilizzati come rivestimento per i tetti degli edifici, definiti cool roof. Tali prodotti sono presenti nei mercati europei da circa un decennio e da circa due decenni in quelli americani. Sebbene siano una tecnologia ormai consolidata, il loro utilizzo resta limitato a pochi edifici perlopiù sperimentali. Ciò non rende possibile uno sfruttamento massivo delle loro proprietà.

All'interno di questa relazione, è stata testata l'applicazione di un cool roof su un edificio sviluppato su un piano singolo con tetto orizzontale. Le analisi sperimentali e numeriche hanno dimostrato le potenzialità di questa tecnica passiva sia sul benessere termo-igrometrico, influenzando sulla diminuzione delle temperature interne di circa 2.5 °C, sia sul risparmio energetico associato alla richiesta di energia per il raffrescamento.

Un aspetto poco investigato di questa tecnologia riguarda lo studio del decadimento del potere di riflessione legato a fenomeni di invecchiamento e sporcamento naturali. Una campagna di misura tuttora in atto ha come obiettivo la valutazione della riflettanza di materiali utilizzati come rivestimento dei tetti con analisi sperimentali periodiche. Dopo 18 mesi è stata riscontrata una diminuzione di circa il 24% del potere di riflessione per i campioni che presentavano una riflettanza solare iniziale superiore a 0.8. In generale questo decadimento è funzione della rugosità e dello spettro di riflessione. Nonostante ciò, in molti casi, i valori di riflettanza spettrale misurati dopo 12 e 18 mesi sembrano iniziare a convergere con valori integrati comunque più alti rispetto a quelli dei materiali convenzionali.

Nonostante i benefici rilevati in questo e in altri studi su applicazioni reali, non esistono procedure di classificazione energetica di questi materiali. Le politiche energetiche nazionali sono mirate a ridurre i consumi legati al riscaldamento degli edifici, con restrizioni sempre maggiori sui valori di trasmittanza termica dell'involucro edilizio, trascurando invece quelli legati al raffrescamento estivo. Per questo motivo è stato proposto un sistema di classificazione per i cool roof in funzione delle loro proprietà termiche e della loro influenza sulle prestazioni energetiche degli edifici normalizzate in funzione della geometria di alcune strutture di riferimento e delle fasce climatiche.

I cool material utilizzati per applicazioni urbane come tinte per asfalti e calcestruzzi sono una tecnologia ancora in fase embrionale, con una trascurabile penetrazione nei mercati. La caratterizzazione ottica e solare di questi prodotti ha confermato la loro elevata riflettanza soprattutto rispetto ai materiali convenzionali con temperature superficiali, rispetto a questi ultimi, anche inferiori di 20 °C. Una temperatura superficiale inferiore riduce il calore ceduto all'aria per convezione. Le potenzialità di questi materiali applicati sull'asfalto di un quartiere di Roma sono state analizzate tramite analisi numeriche con un software di tipo S.V.A.T. (Soil, Vegetation, Atmosphere, Transfer). Si sono ottenute diminuzioni della temperatura media dell'aria anche di 5.5 °C rispetto a quelle ottenute in presenza di asfalti convenzionali. La diminuzione di temperatura si



ripercuote anche a quote superiori all'altezza media degli edifici. Ciò dimostra come i cool material, se utilizzati su scala urbana, possano essere sfruttati come fattore che contribuirebbe alla diminuzione dell'effetto isola di calore.

L'utilizzo di diversi software per l'analisi energetica impiegati come strumento numerico ha permesso di evidenziare un limite riguardante la modellizzazione delle superfici degli edifici. Questi modelli considerano la riflettanza come costante e indipendente dall'angolo di incidenza della radiazione che li colpisce (riflessione Lambertiana). In realtà i materiali da costruzione, soprattutto quelli utilizzati per il rivestimento superficiale dei tetti, presentano modalità di riflessione miste con componenti regolari, che sono funzione dell'angolo di incidenza, a volte non trascurabili come dimostrato nella campagna sperimentale riportata in questa relazione. È stata ricavata quindi una funzione che legasse la riflettanza solare all'angolo di incidenza a partire dai valori misurati. Essa è stata utilizzata in modo da modificare il modello di calcolo di un software dinamico al fine di ottimizzare il calcolo dei carichi solari. I risultati hanno dimostrato i limiti dei modelli termo-fisici generalmente utilizzati per condurre analisi energetiche.

*Parole chiave:* Cool, Riflettanza, Emissività, Solare, Energia.

# Acknowledgements

---

It was possible to carry out this work thanks to the funds allocated by the Italian Ministry for Economic Development under the framework of RSE - Ricerca Sistema Elettrico, for the following projects:

- Impatto di tecnologie Cool Roof sulle prestazioni energetiche degli edifici. Caso studio;
- Impatto di tecnologie Cool Roof sulle prestazioni energetiche di edifici residenziali in area mediterranea;
- Impatto delle protezioni solari trattate con vernici innovative ad elevata riflettanza all'infrarosso vicino sulle prestazioni energetiche di edifici residenziali in regime estivo;
- Impatto di cool material sulla mitigazione dell'isola di calore urbana e sui livelli di comfort termico negli edifici;
- Determinazione delle proprietà termofisiche di materiali ad elevata riflettanza solare per applicazioni a scala urbana: limiti e potenzialità;
- Caratterizzazione e valutazione di pavimentazioni riflettenti per applicazioni urbane. Ricerca di sistema elettrico;
- Sviluppo di materiali e tecnologie per la riduzione degli effetti della radiazione solare.

Moreover a special thanks goes to Prof. Aldo Fanchiotti of Engineering Department of Roma Tre University for giving me the opportunity to carry on this research, to Dr. Michele Zinzi of UTEE of ENEA Casaccia Research Centre for the forwarded experience, to Dr. Tiziana Poli and to Dr. Riccardo Paolini of ABC Department of Politecnico di Milano and to Dr. Giuseppe Rossi of INRIM for their technical and theoretical support.

# Table of Contents

<b>ABSTRACT.....</b>	<b>2</b>
<b>SINTESI.....</b>	<b>4</b>
<b>ACKNOWLEDGEMENTS.....</b>	<b>6</b>
<b>SECTION 1: OVERVIEW.....</b>	<b>11</b>
<b>1. Introduction.....</b>	<b>12</b>
1.1 Research Topic.....	12
1.2 General Framework.....	12
1.3 Cool Materials: Properties.....	16
1.4 References.....	18
<b>2. Theoretical references.....</b>	<b>19</b>
2.1 Introduction.....	19
2.2 Nomenclature.....	20
2.3 Solar Radiation and Optical Quantities.....	20
2.3.1 Solar Radiation Characteristics.....	20
2.3.2 Materials and Solar Radiation.....	22
2.3.3 Optical and Solar Properties of Materials.....	24
2.4 Wall Exposed to Solar Radiation.....	24
2.5 Outline of Black Body Theory.....	26
<b>SECTION 2: EXPERIMENTAL AND NUMERICAL ANALYSES.....</b>	<b>29</b>
<b>3. Instruments for solar and thermal characterisation of materials.....</b>	<b>30</b>
3.1 Introduction.....	30
3.2 Nomenclature.....	31
3.3 Spectrophotometer.....	31
3.3.1 Commercial Spectrophotometer.....	32
3.3.2 Experimental Facility.....	34
3.4 Gonio-Photometer.....	35
3.5 Emissometer.....	39
3.6 References.....	40
<b>4. Cool Roofs.....</b>	<b>41</b>
4.1 Topic.....	41

4.2	Introduction .....	41
4.2.1	Cool Roofing in General .....	41
4.2.2	Cool Roof Types .....	42
4.2.3	Main Cool Roof Products .....	43
	White Cool Roofs.....	43
	Metal Materials .....	43
	Cool Coloured Materials .....	44
	Other Cool Materials.....	44
	Thermo-Chromic Materials .....	44
4.3	Case study: Cool Roof Application in a Non-Residential Building.....	45
4.3.1	Building Description .....	45
4.3.2	Cool roof application .....	47
4.3.3	Methodology .....	47
4.3.4	Experimental .....	47
	Optical and Thermal Characterisation of Roof Coating Surfaces .....	47
	Positioning of the Outdoor Equipment.....	48
	A Drawback for the Membrane.....	49
	Comparative Analysis of Measured Data .....	50
4.3.5	Numerical Analyses .....	52
	The Software .....	52
	The Model.....	52
	Simulations Results: Operative Temperatures.....	54
	Simulations Results: Cooling Energy Demands.....	56
4.4	Effects of Ageing and Soiling on Solar Reflectance of Roofing Membranes .....	58
4.4.1	Nomenclature .....	58
4.4.2	Selected Materials.....	59
4.4.3	Exposure Sites and Sample Positioning .....	59
4.4.4	Methodology .....	59
4.4.5	Experimental Results .....	60
4.5	Cool Roofs Energy Rating System Proposal.....	66
4.5.1	Methodology .....	66
4.5.2	Climatic Conditions .....	67
4.5.3	The Reference Buildings.....	67
4.5.4	Numerical Analysis.....	68
	Software .....	68
	Numerical Analysis Results .....	69

4.5.5	The Rating Procedure .....	72
	Climate Dependent Energy Rating.....	72
	Climate Independent Cooling Energy Rating .....	74
4.6	Chapter Conclusions .....	76
4.7	References.....	76
<b>5.</b>	<b>Cool Paving .....</b>	<b>78</b>
5.1	Topic .....	78
5.2	Introduction .....	78
5.3	The Urban Heat Island effect.....	80
5.3.1	Measurement of the Intensity of the Urban Heat Island in the City of Rome.....	81
5.4	Photo-Catalytic Tints for Asphalts.....	86
5.4.1	Samples Description .....	86
5.4.2	Methodology .....	86
5.4.3	Experimental .....	86
	Thermo-Graphic Analysis .....	86
	Solar and Optical Characterisation.....	87
	Surface Temperatures Analysis .....	88
5.5	Porous Concrete Draining Paving .....	91
5.5.1	Selected Materials.....	91
5.5.2	Experimental .....	91
5.6	Calculation of Urban Environment Temperatures: Numerical Analysis.....	93
5.6.1	Description of the Calculation Software: ENVI-met .....	93
5.6.2	ENVI-met Model of a Neighbourhood of Rome: Prati .....	93
5.6.3	Simulations Result .....	97
	Buildings and Asphalt Surfaces.....	97
	Asphalt Surfaces: Photo-Catalytic Tints .....	101
	Asphalt Surfaces: Concrete Draining Paving .....	106
5.7	Chapter Conclusions .....	111
5.8	References.....	111
	<b>SECTION 3: DEVELOPMENT OF NUMERICAL METHODS.....</b>	<b>114</b>
<b>6.</b>	<b>Solar reflectance angular dependence of opaque construction materials .....</b>	<b>115</b>
6.1	Introduction .....	115
6.2	Nomenclature.....	116
6.3	Methodology .....	116
6.4	Description of Selected Materials .....	118

6.5	Experimental .....	119
6.5.1	Gonio-Photometric Measurements .....	119
6.6	Spectrophotometric Measurements .....	123
6.7	Comparison Between the Two Instruments Results.....	126
6.8	Numerical Analysis Calculation .....	127
6.8.1	Preliminary Comparisons Between Experimental and Theoretical Solar Reflectance ....	127
6.8.2	Model Description .....	129
6.8.3	Results .....	129
6.9	Chapter Discussions and Conclusions .....	133
6.10	References.....	133
<b>7.</b>	<b>Conclusions .....</b>	<b>134</b>
7.1	Achievements .....	134
7.2	Future developments .....	136

# Section 1: *Overview*

# 1. Introduction

---

## 1.1 Research Topic

---

This research is focused on the study of the efficiency of innovative materials used as passive technique for energy savings in buildings and as a contributory factor to limit the overheating phenomenon of urban areas: the urban heat island. These materials, characterised by high solar reflectance and thermal emissivity, were the subjects of tests carried out in laboratory and outdoors. The results supported by numerical analysis allowed to establish their limits and potentialities.

## 1.2 General Framework

---

Phenomena such as climate change and global warming are known to the public opinion, as well as the associated risks. They are present on a global scale, regardless of latitude and economic development, although with different intensity and consequences. One of the areas at risk is the Mediterranean basin with a predicted rise in average air temperatures of 2 °C by 2030 and even further by 2100 [1.1]. Some estimates foreshadow very drastic scenarios: increase of tropical nights, where the temperature never drops below 20 °C and 30% reduction in annual rainfall in comparison to the current standards.

The data on the increase of the concentration of carbon dioxide show a strong link to the anthropogenic activities. The trend shown in Figure 1.1 highlights how radically changed the amount of CO<sub>2</sub> emissions resulting from fossil fuels in atmosphere since the mid-1700s. Emissions are literally exploded in the second half of the twentieth century in large part due to energy uses. The data comes from CDIAC (Carbon Dioxide Information Analysis Center) of the Department of Energy (DOE) of United States.



## Section 1: Overview

The increase of CO<sub>2</sub> concentration in atmosphere, the main greenhouse gas, has a significant impact on temperature rising. From this point of view, it is interesting to observe the evolution in Figure 1.2. The figure refers to the annual average temperature of the Earth surface. It is important to note the growing trend, especially in recent decades. Once again, data confirm a planet thermal equilibrium alteration due to anthropogenic factors.

A much debated topic wonders if these changes are natural or caused by human activity, being the second option considered the most plausible by the majority of the scientific community. The latter argues that global warming will lead to many irreversible risks and changes if the increase in temperature will exceed 2 °C.

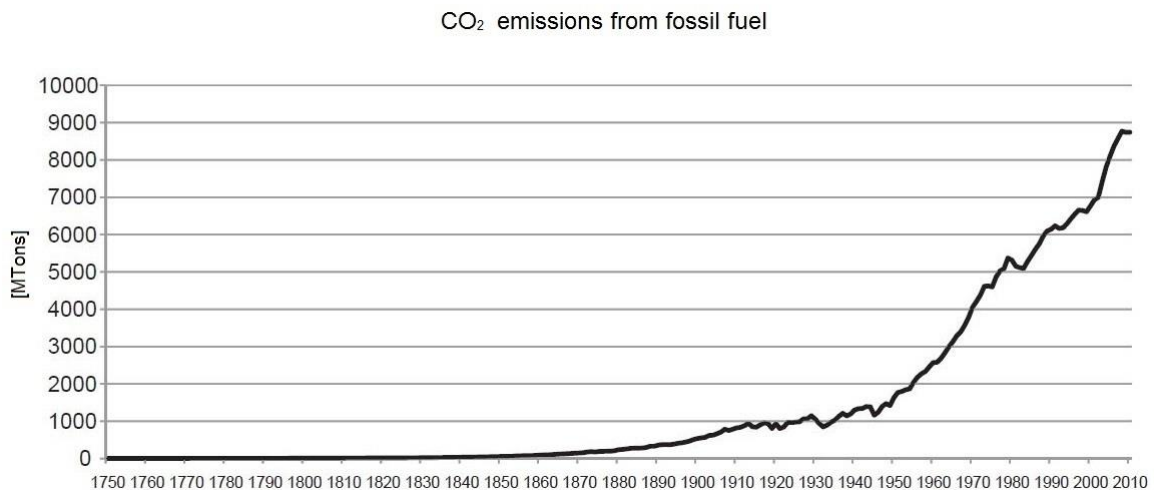


Figure 1.1: CO<sub>2</sub> emissions in atmosphere since 1700.

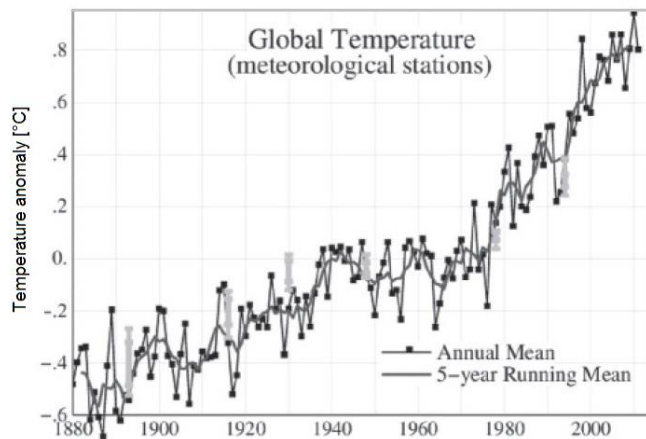


Figure 1.2: Annual average temperature of Earth surface (source: NASA).

Most of development and production activities of industrialised countries required an enormous amount of energy produced and used. All this happened for decades and only in the last 20 - 30 years the energetic and environmental problems have been globally recognised, without arriving at shared solutions to limit it. Furthermore, the appearance of new and formidable economies makes this problem resolution definitely more complex.

Some interesting data are retrievable from RAEE (Rapporto Energia e Ambiente), annually published by ENEA [1.2]. The global energy end uses in 2009 amounted to about 7.5 billion of toe (tons of oil equivalent, a unit of measurement that expresses the energy released by the combustion of a ton of oil) corresponding to an increase by 34% if compared to 1990.

The previous figure is alarming but in the euro zone the trend is downward. Looking at the national data, considering the available data, the energy end uses decreased of about 5.2% from

## Section 1: Overview

2011 to 2012, following the positive trend of the previous year in which they decreased of about 2.65%. In fact the end uses consumptions reached in these years the values they had in 1997 denoting a collective effort that has reversed the trend of growth.

On the other hand, ENEA data also reported that the civil sector does not follow this positive trend. The impact of this sector on total energy end uses increased from 30.8% in 2004 to 36.7% in 2012, proving to be the sector with the highest energy consumption in Italy. Figure 1.3 shows the distribution of end uses of energy sector for the year 2012.

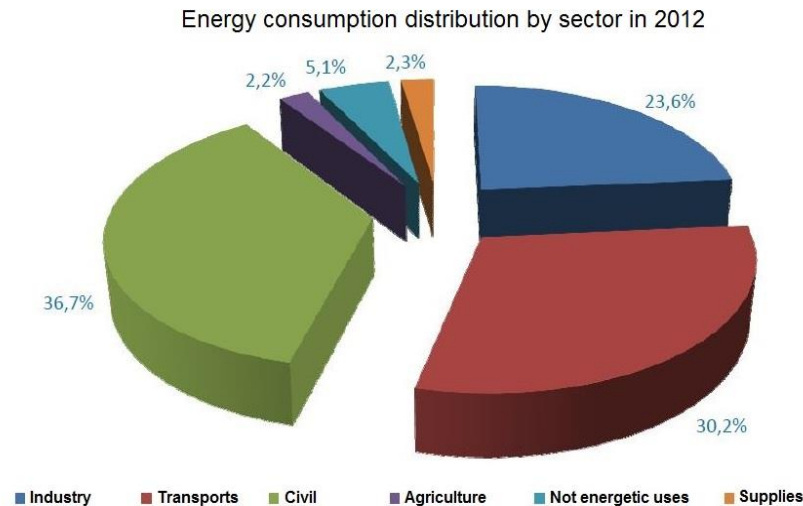


Figure 1.3: Percentage distribution of energy end uses in Italy, 2012 (source: Data processing by ENEA - Data provided by the Italian Ministry of Economic Development).

Figure 1.4 shows the energy consumption trend for the main sectors over the years. In the last years the civil sector (residential and services) has overtaken the industry, which has experienced a period of undeniable energy efficiency, and the transport sector, traditionally the more consistent consumption item.

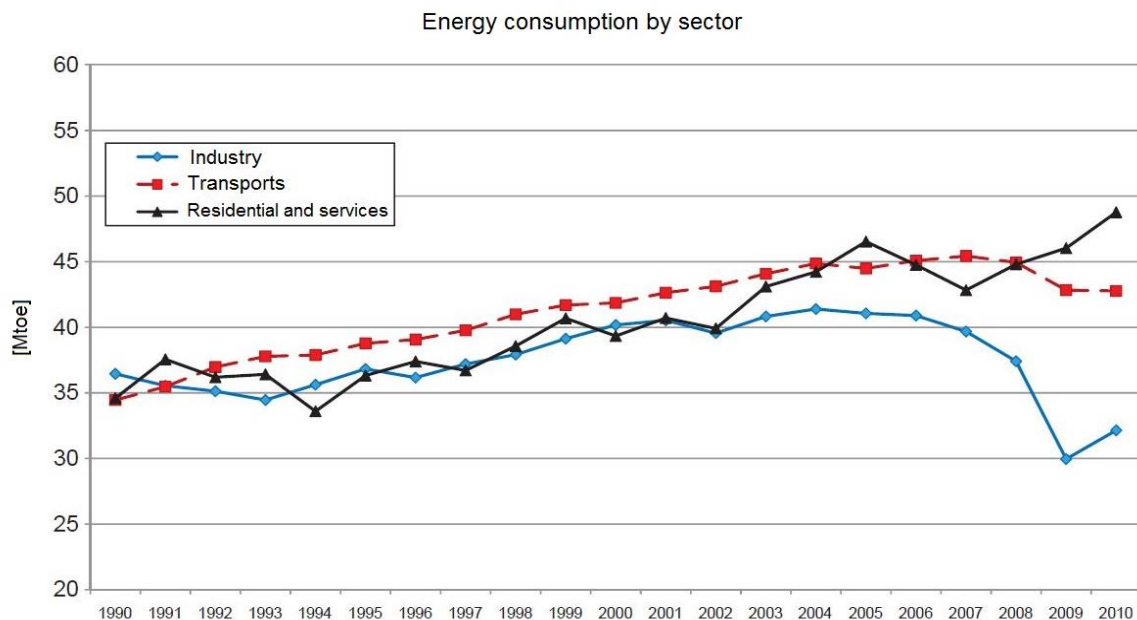


Figure 1.4: Energy end uses trend by sector (source: Data processing by ENEA - Data provided by the Italian Ministry of Economic Development).

Consumption increase in the civil sector is due to the increase in electricity consumption. Although in the residential sector is registered a slight energy consumption growing in recent years

## Section 1: Overview

(+0.8% from 2010 to 2011), the services sector shows a strong increasing trend. In particular, the electricity consumption per worker in trade sector has more than doubled in the last twenty years.

The constant increase in sales of compact units for air conditioning and in size of large cooling systems, demonstrates the critical point, as well as the increasing in comfort demand from the growing population.

The phenomenon seems to be linked to the continuous urbanisation which sets in motion millions of people from rural to urban and suburban areas, with significant problems of environmental degradation. One of these problems is the urban heat island effect, a phenomenon for which the average or peak temperatures of urban areas becomes a few degrees higher than the ones of rural areas.

The aspects related to energy and environmental issues listed in this paragraph assume an even more serious connotation considering that they are related in a cyclic manner, as shown in Figure 1.5.

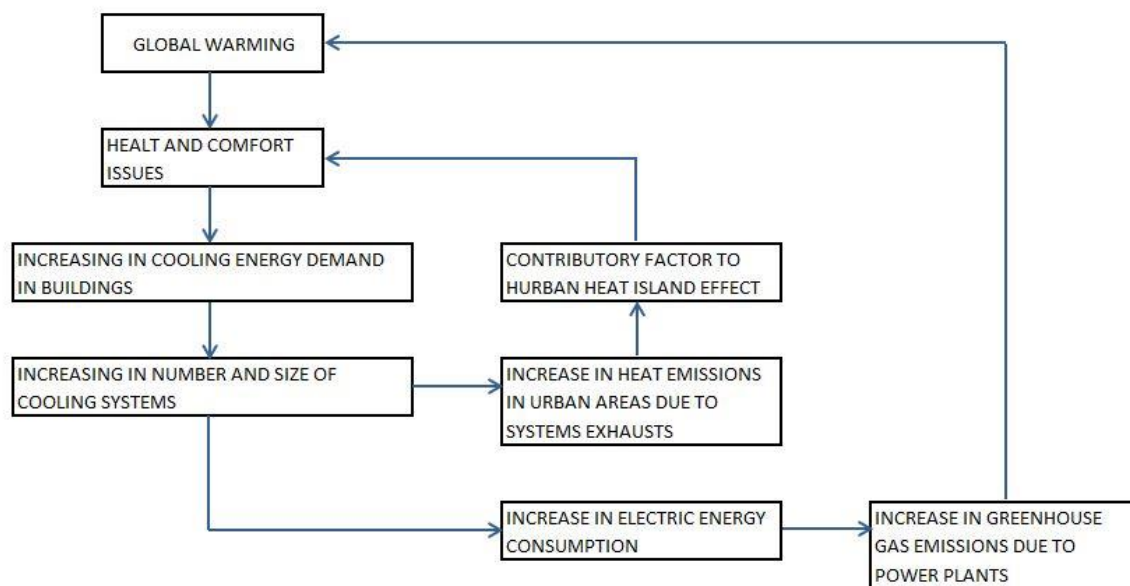


Figure 1.5: Cause and effect diagram of energy and environment problems.

The need to cool buildings and cities become crucial in a context of great environmental commitment recruited on an international scale. The problem is not only Italian; in fact buildings are responsible for the 40% of global energy consumption in the European Union. Therefore, in the European Directive 91/2002 issued by the European Parliament the dictates to follow to reduce energy consumption in buildings are reported [1.3]. The Directive covers different fields and introduces key aspects such as energy certification of buildings, the requirement to take into account for the different energy uses and not only for heating, i.e.: cooling demand; ventilation; lighting; production of domestic hot water. In 2010 was enacted the Directive 31, which updates the Directive 91/2002, introducing other aspects, such as the obligation to almost zero energy consumption for new buildings here in a few years [1.4]. The ultimate goal is to contribute to the achievement of the reduction of greenhouse gas emissions by 20% compared to 1990 levels by 2020 as required by the Kyoto Protocol.

Many techniques for energy saving in buildings were proposed in recent years. Some proposals are related to increase cooling and heating systems performances, such as systems that use absorption heat pumps powered by hot fluids obtained as result of regeneration or through solar collectors (solar cooling). Unfortunately, these systems have very high initial costs that justify their use only for high peak powers and therefore are not suitable for residential use. In Europe, thanks to incentive policies, household photovoltaic systems are taking hold to allow to feed with the electrical energy stored in batteries the heat pumps for heating and cooling.

There are also passive techniques designed to make the building envelope more efficient. Among these, there are some that are aimed at a reduction of solar load on the external surfaces. The study concerning solar gains through the opaque components of the building envelope is assuming significant importance in both residential and non-residential buildings. The need to improve the energy performance of buildings, reducing energy consumption for cooling is leading to the development of new materials that are designed to modulate solar gains. These materials represent a viable and economical technique for passive cooling of buildings. They are characterised by a higher reflection power of solar radiation than conventional materials and, used as coatings for external surfaces, play an important role in the heat exchange. These products are defined “cool materials”.

The high reflection limits the increase of surface temperature in presence of solar radiation, reducing both the heat exchanged with the environment by convection and the incoming heat in buildings by conduction. The final consequence is, in the first case, the urban heat island reduction, in the second case the cooling demand reduction in buildings. Projects and studies conducted in recent years show the impact of technology by means of numerical analysis [1.5 - 1.9], and by means of experimental campaigns in real buildings [1.10 - 1.17].

### 1.3 Cool Materials: Properties

Cool materials are a passive technique used for energy savings. They are used as coatings for the building envelope. This technology is based on a high solar reflectance and a high thermal emissivity.

The reflectance is a characteristic of materials surface. It is defined as the ratio between the intensity of the radiant flux reflected from a surface and the radiant flux incident on it (see paragraph 2.3.2). Cool materials have a high reflectance in the solar spectrum.

Figure 1.6 shows the solar spectrum emission outside atmosphere and at sea level. Having an ideal white colour surface means reflecting the full emission spectrum in the visible band (380 - 780 nm), at each wavelength, equivalent to approximately 55% of the whole power contained in the solar spectrum. Having an ideal black colour material means absorbing the whole energy emission of the visible band. This is the reason why the light colours materials tend to heat up less compared to dark colour materials. The phenomenon is well known and used in the building since ancient times as shown in Figure 1.7 which shows an ancient structure in use in southern Italy: The “trullo”.

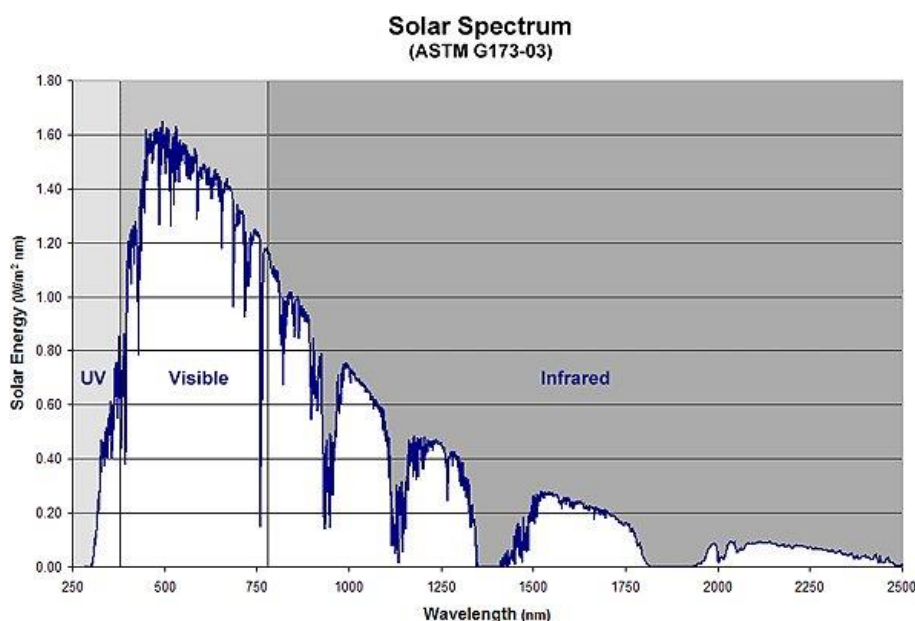


Figure 1.6: Solar spectrum. Ultra – violet (UV), visible (VIS) and near infra-red (NIR) bands.



Figure 1.7: Trullo in southern Italy.

Figure 1.6 also highlights how the sun emits a significant amount of energy over the visible band and distributed in a larger band: The NIR band (Near Infra-Red) that ranges from 780 to 2500 nm. A high reflection power in this band is the peculiar characteristic of cool materials.

High reflection in visible band depends mainly on the surface colour, while the cool materials have a high reflectivity in the entire solar spectrum being equal the surface colour reflecting a greater amount of solar radiation compared to a conventional material. This depends on the reflectance in the NIR band.

For example Figure 1.8 shows the reflectance as a function of wavelength, in the solar spectrum of two materials with the same colour, one of which is a cool coloured material [1.17]. The colour of these materials is dark grey, for this reason the reflectance in the visible band remains below 0.1. Beyond 780 nm the reflectance of the conventional material stay at a nearly constant value between 0.05 and 0.07, while the reflectance of the cool coloured material increases in a clear manner, reaching a peak value of 0.7 at 1600 nm, greater than an order of magnitude compared to the conventional material one.

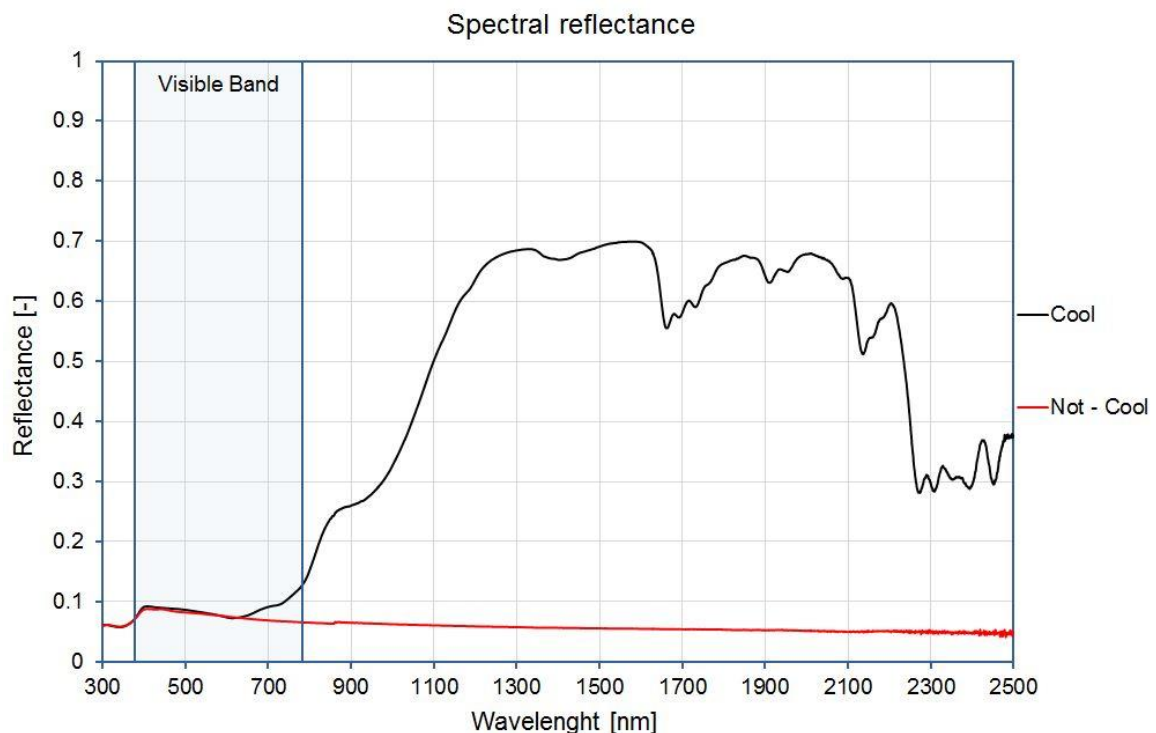


Figure 1.8: Spectral reflectance comparison between cool and not cool materials.



## Section 1: Overview

To express the physical concept of thermal emissivity, it is useful to take into account the theory of the black body (see paragraph 2.5). It is a physical entity capable of absorbing the full electromagnetic radiation and, for the energy conservation, is able to re-irradiate (or emit) it entirely.

The emittance of a body is the ability that the body has to emit a quantity of energy at a certain temperature and it represents a power per unit area ( $W / m^2$ ).

The emissivity is defined as the ratio between the global emittance of a real body and the global emittance of a black body at the same temperature considered.

The construction materials typically have a very high value of emissivity of around 0.9 with the exception of the metals which have lower values (0.2 - 0.7). Generally cool materials have a high thermal emissivity in order to facilitate the dissipation during the night of the heat accumulated during daylight hours due to radiative and convective heat transfer.

### 1.4 References

---

- [1.1] Climate change: Intergovernmental Panel on Climate Change (IPCC); 2007.
- [1.2] RAEE Rapporto Annuale Efficienza Energetica: ENEA; 2014. [www.enea.it](http://www.enea.it); available online at.
- [1.3] Eu Directive 2002/91/Ec. On The Energy Performance Of Buildings; 2002.
- [1.4] Eu Directive 2010/31. On The Energy Performance Of Buildings (recast); 2010.
- [1.5] Akbari H, Bretz S, Kurn D, Hartford H. 'Peak power and cooling energy savings of high albedo roofs'. Energy and Buildings; 1997; 25: 117 - 126.
- [1.6] Christen A, Vogt R. 'Energy and radiation balance of a central European city'. International Journal of Climatology; 2004; 24: 1395 - 1421.
- [1.7] Suehrcke H, Peterson EL, Selby N. 'Effect of roof solar reflectance on the building heat gain in a hot climate'. Energy and Buildings; 2008; 40: 2224 - 2235.
- [1.8] Synnefa A, Santamouris M, Akbari H. 'Estimating the effect of using cool coatings on energy loads and thermal comfort in residential buildings in various climatic conditions'. Energy and Buildings; 2007; 39(11): 1167 - 1174.
- [1.9] Zinzi M. 'Cool materials and cool roofs: Potentialities in Mediterranean buildings'. Advances in Building Energy Research; 2010; 4: 201 - 266.
- [1.10] Bozonnet E, Doya M, Allard F. 'Cool roofs impact on building thermal response: A French case study'. Energy and Buildings; 2011; 43(11): 3006 - 3012.
- [1.11] Carnielo E, Fanchiotti A., Zinzi M. 'Energy and comfort benefits of a cool roof application in a non - residential building belonging to Roma Tre University'. World Renewable Energy Congress, 8 -13 May, Linköping, Sweden; 2011.
- [1.12] Kolokotsa D, Diakaki C, Papantoniou S, Vlissidis A. 'Numerical and experimental analysis of cool roofs application on a laboratory building in Iraklion'. Energy and Buildings; 2011; 55: 85 - 93.
- [1.13] Paolini R, Zinzi M, Poli T, Carnielo E, Fiori M, Mainini AG. 'Evolution over time of UV – VIS - NIR reflectance of cool roofing materials in urban environments'. 34th AIVC conference, 25 – 26 September, Athens, Greece; 2013.
- [1.14] Parker D, Huang J, Konopacki S, Gartland L, Sherwin J, Gu L. 'Measured and simulated performance of reflective roofing systems in residential buildings'. ASHRAE Trans; 1998; 104(1): 963 - 975.
- [1.15] Romeo C, Zinzi M. 'Impact of a cool roof application on the energy and comfort performance in an existing non - residential building. A Sicilian case study'. Energy and Buildings; 2011; 67: 647 - 657.
- [1.16] Synnefa A, Saliari M, Santamouris M. 'Experimental and numerical assessment of the impact of increased roof reflectance on a school building in Athens'. Energy and Buildings; 2012; 55: 7 - 15.
- [1.17] Zinzi, M, Carnielo E, Agnoli S. 'Characterization and assessment of cool coloured solar protection devices for Mediterranean residential buildings application'. Energy and Buildings; 2012; 50: 111 -119.

## 2. Theoretical references

---

### 2.1 Introduction

---

The building envelope is the boundary which delimits the built environment from the external one and, for that reason, it is subject to a series of thermal fluxes, having a direction dependent on external and indoor conditions.

Referring to Figure 2.1, the following thermal fluxes can be highlighted:

- Transmission: A function of temperature difference between indoor and outdoor;
- Solar gains: A function of solar radiation, both direct and diffuse, which affects opaque and transparent surfaces;
- Ventilation: Outdoor air intentionally introduced into the environment to ensure the indoor air healthiness;
- Infiltration: Amount of the non-controlled air that penetrates through the building envelope, which is not perfectly sealed.

According to the European Directive EPBD and later recast in 2010, energy uses to be considered in the energy balance of building are: heating, cooling, ventilation, lighting, hot water. The opaque components of the building involved in energy balance by influencing the cooling and heating demand.

This chapter describes the main thermo-physical properties of the opaque components and illustrates the way in which they enter into the heat balance of the building. These basics are necessary for fully understanding the following chapters, in which the characteristics of different materials used as building coatings will be widely discussed.

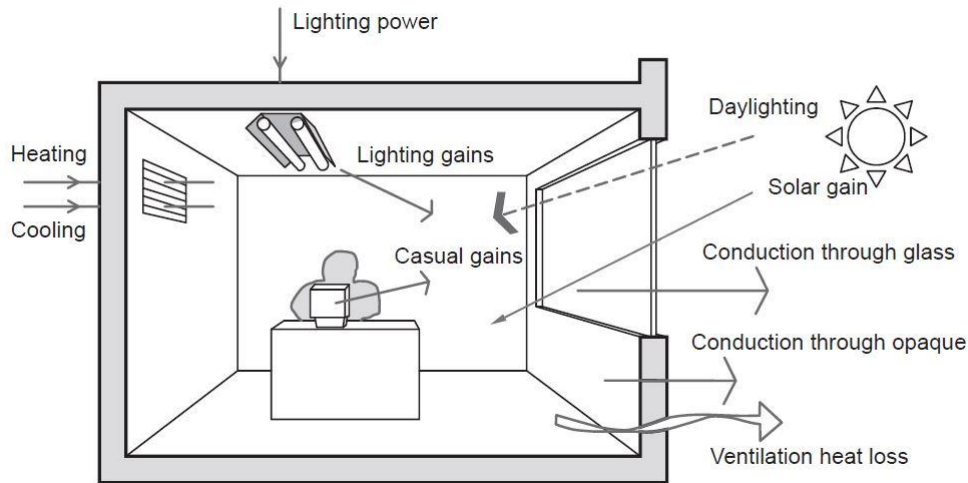


Figure 2.1: Heat fluxes affecting the building envelope.

## 2.2 Nomenclature

Table 2.1 shows the symbols reported in chapter 2.

Table 2.1: Chapter 2 nomenclature.

$I$	Irradiance	$[W/m^2]$	$h$	Adduction coefficient	$[W/m^2 K]$	$J$	Emittance	$[W/m^2]$
$\alpha$	Absorptance	$[-]$	$K$	Thermal transmittance	$[W/m^2 K]$	$T$	Temperature	$[K]$
$\lambda$	Wavelength	$[nm]$	$q$	Heat flux	$[W/m^2]$	$\varepsilon$	Emissivity	$[-]$
$\theta$	Incidence angle	$[^\circ]$	$s$	thickness	$[m]$			
$\rho$	Reflectance	$[-]$	$T$	Temperature	$[^\circ C]$			
$\tau$	Transmittance	$[-]$	$\gamma$	Thermal conductivity	$[W/m K]$			

### Subscript

$0$	Normal	$s$	Surface	$G$	Global
$e$	Solar	$ext$	externale	$M$	Maximum
$v$	Visible	$int$	internal		
$\alpha$	Absorbed	$as$	air - sun		
$\rho$	Reflected				
$\tau$	Transmitted				

## 2.3 Solar Radiation and Optical Quantities

### 2.3.1 Solar Radiation Characteristics

The sun is a gaseous spherical mass with a diameter equal to  $1.4 \cdot 10^6$  km and a temperature on the order of millions of degrees in the central regions, which emits energy in the form of oscillating electromagnetic field. Among the many chemical reactions that take place inside the star, there is the fundamental transformation of hydrogen into helium, a reaction that gives rise to spontaneous emission of energy. The energy is then transferred through convection to the sun surface and radiated into the space according to a very complex process. Solar radiation is the result of many layers that emit and absorb radiant energy at variable wavelengths. In the physical-technical analysis is permissible to approximate the sun as a black body having an effective temperature that range about between 5800 and 6300 K.



## Section 1: Overview

The sun is located at a distance from the Earth equal in average to  $1.495 \cdot 10^{11}$  m (about 150 million km), with a variation of  $\pm 1.7\%$ , due to the elliptical shape of the trajectory of motion of the Earth around the star. The characteristics of the sun and the geometric relationships between it and the Earth induce almost constant intensity of solar radiation outside the atmosphere. This consideration allows to introduce the solar constant  $I_s$ , a quantity defined as the energy coming from the sun which affects, in the unit time, the unit area of a surface perpendicular to the direction of radiation propagation and placed in the space at a distance equal to the average distance Earth-Sun. The most recent measurements assign to the solar constant a value between 1353 - 1367  $\text{W/m}^2$ .

In addition to the total energy emitted by the sun, it is also important to know its spectral distribution. The emitted radiation is actually the overlap of a series of waves having wavelengths in a range theoretically infinite, but practically between 150 nm and 10  $\mu\text{m}$ . The following spectral portions can be therefore identified:

- Ultraviolet spectrum (150 - 380 nm), harmful to health and to the deterioration of many materials, particularly plastic ones (polymerisation);
- Visible spectrum (380 - 780 nm), part of the solar spectrum that is sensitive to the human eye and, therefore, the most important for the study of natural lighting;
- Infrared spectrum (780 nm - 10 microns), spectral area with significant impact on heat transfer. Reference standards define as NIR (Near Infra-Red) a region between 780 and 2500 nm. Medium and far infrared are related to portions of spectrum to higher wavelength.

The spectral distribution of solar radiation indicates that about 7% of the radiation falls within the ultraviolet spectrum, about 55% in the visible spectrum and the rest in the NIR spectrum being the contribution in the far infra-red only a few percentage points. It is important to note that the spectral distribution, beyond its own nature, is often defined differently in various international standards.

Figure 2.2 shows the spectral trend normalised to the peak of the solar radiation and the cumulative distribution of the radiation itself, which shows that more than 90% of solar energy falls within 1700 nm.

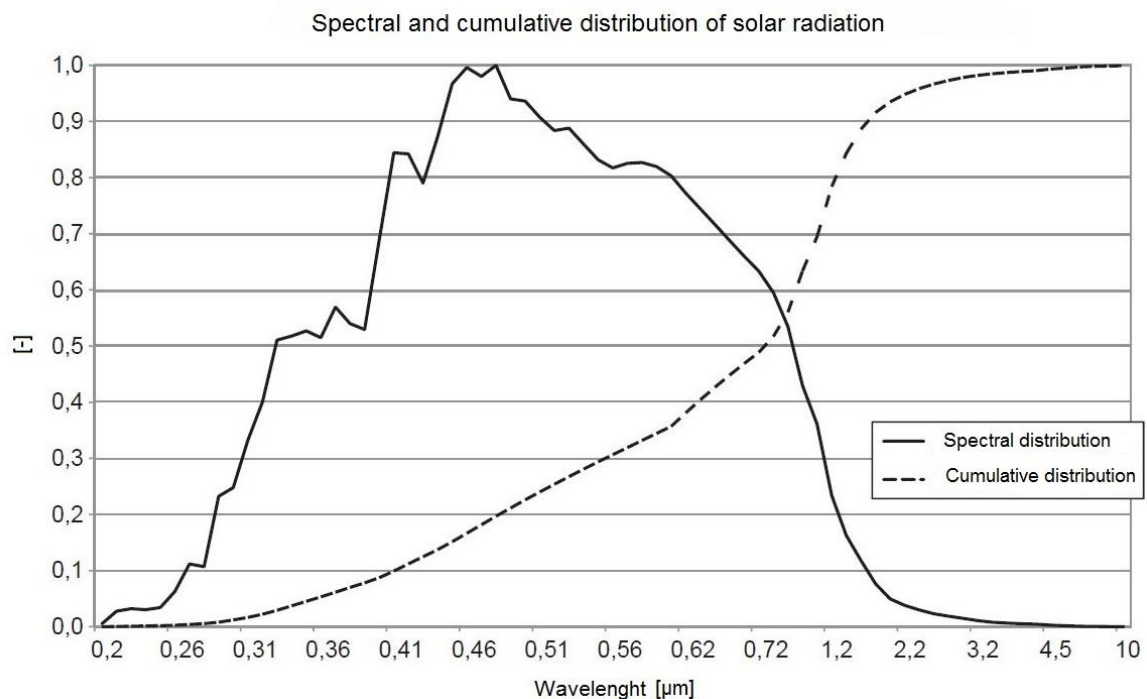


Figure 2.2: Solar radiation trend.

## Section 1: Overview

The radiation coming from the sun propagates as a beam of parallel rays but, in crossing the atmosphere, undergoes three changes, due to the effect of the gases, water vapour, water droplets and suspended solid particles which constitute the atmosphere itself:

- A substantial reduction, due to the fact that the radiation is partly absorbed by the atmosphere and in part reflected to the outer space;
- A variation of the spectral distribution, due to the selective behaviour of some of the atmosphere components ( $O_2$ ,  $O_3$ ,  $CO_2$ ,  $H_2O$ );
- A dispersion in the atmosphere (scattering), due to multiple reflection phenomena that diffuse the radiation reaching the ground in addition to the collimated one coming directly from the direction of the sun (direct radiation).

The consistency of these phenomena depends on thickness and composition of the atmosphere layer passed through by the radiation. It is useful to remember that the solar constant is a value much higher than the normal values found on Earth surface both for filtering effect due to the atmosphere and for the geometrical conditions between the sun and an oriented surface. Hence, the amount of stored solar energy in a surface depends on the inclination and orientation of the surface itself. Figure 2.3 shows the monthly average values of solar radiation ( $W / m^2$ ) on surfaces oriented in a different way, and this demonstrates what is stated above.

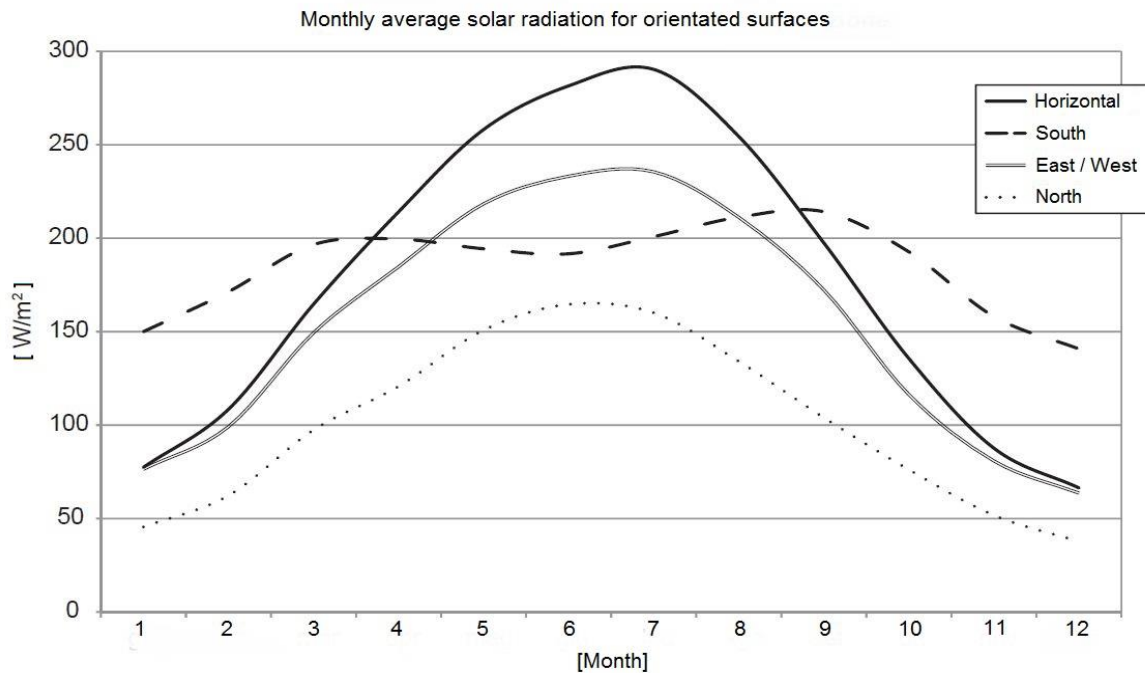


Figure 2.3: Monthly average solar radiation for several orientations – Rome.

### 2.3.2 Materials and Solar Radiation

When solar radiation hits a surface material is decomposed into several components as a function of parameters that affect the characteristics of the radiation, such as the spectral distribution, the angle of incidence, and the material type.

Solar reflection can be transmitted, reflected and absorbed:

- The ratio between the transmitted radiation and the incident radiation is called transmittance, generally indicated with “ $\tau$ ”.

$$\tau = \frac{I_{\tau}}{I} \quad (2.1)$$

## Section 1: Overview

- The ratio between the reflected radiation and the incident radiation is called reflectance, generally indicated with “ $\rho$ ”.

$$\rho = \frac{I_{\rho}}{I} \quad (2.2)$$

- The ratio between the absorbed radiation and the incident radiation is called absorptance, generally indicated with “ $\alpha$ ”.

$$\alpha = \frac{I_{\alpha}}{I} \quad (2.3)$$

These quantities can be expressed similarly in dimensionless value (from 0 to 1) or with a percentage (from 0% to 100%). The three coefficients are related by the following equation.

$$\tau + \rho + \alpha = 1 \quad (2.4)$$

Opaque materials, for their own definition do not allow to be passed through by solar radiation, for this reason  $\tau = 0$ . The previous equation 2.4 becomes:

$$\rho + \alpha = 1 \quad (2.5)$$

These quantities are not constant if considered in the whole solar spectrum but they depend on wavelength. The equation 2.2 can be rewritten as:

$$\rho(\lambda) = \frac{I_{\rho}(\lambda)}{I(\lambda)} \quad (2.6)$$

And similarly it is possible to rewrite the quantities reported in equations 2.1 and 2.3. Figure 2.4 shows the spectral reflectance trend of an opaque material.

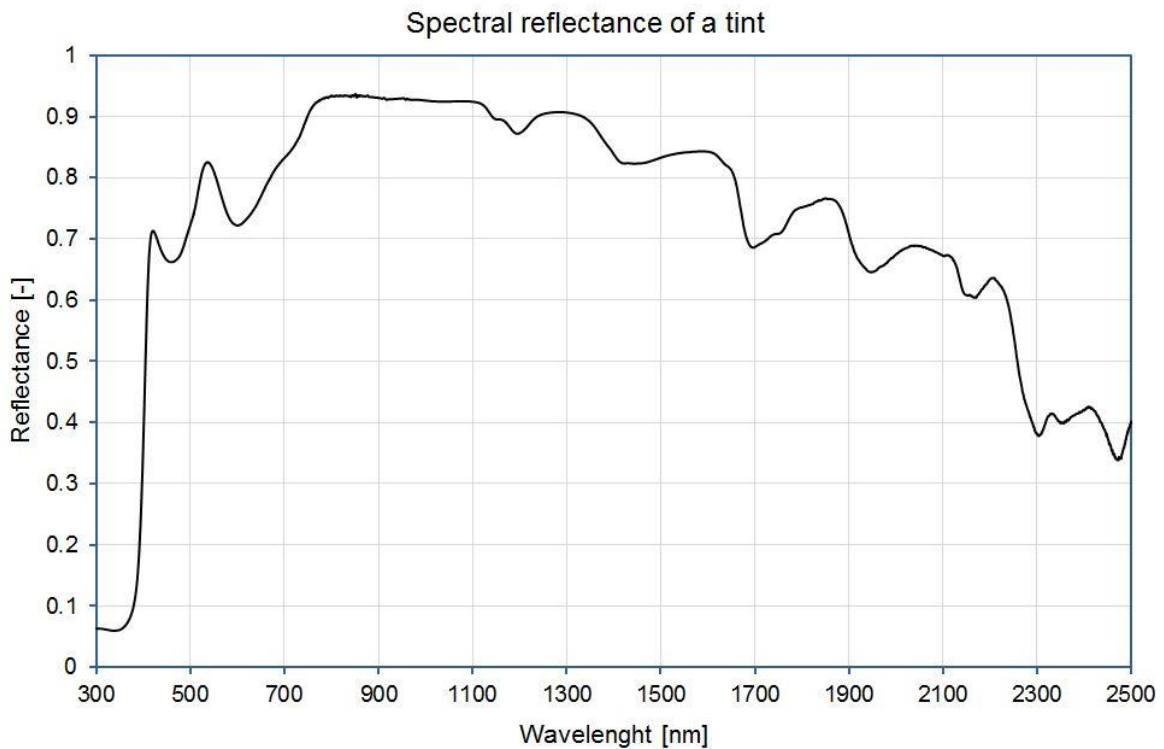


Figure 2.4: Spectral reflectance of an opaque material.

## Section 1: Overview

It has to be noted that the reflectance indicates only the amount of radiation reflected and nothing about the way in which the phenomenon occurs. This clarification is essential when treated opaque materials in densely urbanised areas to avoid concentrated inter-reflections both for health and safety issues. The incident radiation can be reflected in such a way:

- Regular, the beam is reflected with an angle equal to the angle of the incident radiation;
- Diffuse (Lambertian), according to the cosine law, the incident beam is reflected as the sum of infinite rays emitted in all directions following the equation:

$$\rho \cdot I_{\theta} = \rho \cdot I_0 \cdot \cos \theta \quad (2.7)$$

The reflected radiation, in the direction defined by the angle  $\theta$ , that the direction itself do with the surface normal, is equal to the normal reflected radiation  $\rho \cdot I_0$  multiplied by the cosine of the angle. The materials of this type are purely theoretical and do not exist in nature. The term “diffuse” generally refers to those materials that have an opening angle with respect to the normal between  $60^\circ$  and  $90^\circ$  (being the latter the angle of a Lambertian material);

- Partially diffuse (scattering), the incident beam is reflected more or less diffusely, keeping a preferential direction as a function of the incidence angle.

Those considerations can be applied similarly to transmittance and absorptance.

### 2.3.3 Optical and Solar Properties of Materials

---

The spectral quantities for practical applications can be traced to singular broadband values, by means of integration operations on reference spectra.

Referring for simplicity only to reflectance, it is defined solar reflectance (indicated with subscript “e”) the value expressed by the following equation.

$$\rho_e = \frac{\int \rho(\lambda) \cdot E(\lambda) \cdot d\lambda}{\int E(\lambda) \cdot d\lambda} \quad (2.8)$$

having indicated with  $E(\lambda)$  the reference solar spectrum, the integration limits are the reference solar spectrum limits. Likewise it is defined the luminous or visible reflectance (indicated with the subscript “v”) the value expressed in the following equation.

$$\rho_v = \frac{\int \rho(\lambda) \cdot D(\lambda) \cdot V(\lambda) \cdot d\lambda}{\int D(\lambda) \cdot V(\lambda) \cdot d\lambda} \quad (2.9)$$

The spectral reflectance is multiplied by two reference curves: One corresponding to a white illuminant  $D(\lambda)$  and one corresponding to the sensitivity curve of the human eye  $V(\lambda)$ . The integration limits correspond to minimum and maximum wavelength detected by the human eye.

## 2.4 Wall Exposed to Solar Radiation

---

In paragraph 2.1 solar gains have been defined as one of the main thermal fluxes involved in the energy balance of a building. This section is intended to define how they can be included in the calculation of the heat exchange through a flat wall, giving for granted the other basic concepts.

In the hypothesis of steady thermal flux a flat wall composed by “n” layers separates two environments characterised by two different temperatures  $T_{\text{ext}}$  and  $T_{\text{int}}$ . The thermal transmittance “K” of the wall is (see table 1 for the used symbols):

$$K = \frac{1}{\frac{1}{h_{\text{ext}}} + \frac{s_1}{\gamma_1} + \frac{s_2}{\gamma_2} + \dots + \frac{s_n}{\gamma_n} + \frac{1}{h_{\text{int}}}} \quad (2.10)$$

## Section 1: Overview

The wall is hit by solar radiation  $I$  [W/m<sup>2</sup>] on the external surface. The wall absorbs " $\alpha \cdot I$ " being " $\alpha$ " its solar absorptance.

The layer of the wall which absorbs the radiation reaches a temperature  $T_s$  in order to ensure the balance, namely that the radiation absorbed by the unit area in the unit time is transferred from the layer both outwards ( $q'$ ) and through the wall ( $q''$ ) to environment with temperature  $T_{int}$ :

$$\alpha \cdot I = q' + q'' \quad (2.11)$$

The two heat fluxes can be expressed as the ratio between the corresponding difference in temperatures and the thermal resistances:

$$q' = \frac{T_s - T_{ext}}{\frac{1}{h_{ext}}} = h_{ext} \cdot (T_s - T_{ext}) \quad (2.12)$$

$$q'' = \frac{T_s - T_{int}}{\frac{s_1}{\lambda_1} + \frac{s_2}{\lambda_2} + \dots + \frac{s_n}{\lambda_n} + \frac{1}{h_{int}}} = B(T_s - T_{int}) \quad (2.13)$$

having indicated with  $B$  and the inverse of the sum of all the resistances offered by the layers of the wall plus the resistance associated to the internal advection coefficient. Namely:

$$\frac{1}{B} = \frac{1}{K} = \frac{1}{h_{ext}} \quad (2.14)$$

The Figure 2.5 shows the quantities taken into account in this paragraph.

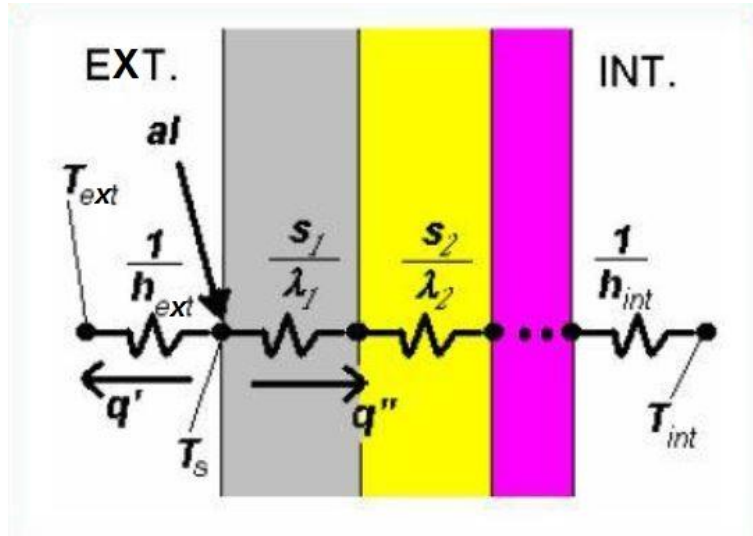


Figure 2.5: Thermal fluxes in a flat wall under solar radiation.

By entering equations 2.13 and 2.14 into the equation 2.11 it is possible to find the expression for  $T_s$ :

$$T_s = \frac{\alpha \cdot I + h_{ext} \cdot T_{ext} + B \cdot T_{int}}{h_{ext} + B} \quad (2.15)$$

By entering equation 2.15 into equation 2.13 the following equation is obtained:

$$q'' = B(T_s - T_{int}) = B \left( \frac{\alpha \cdot I + h_{ext} \cdot T_{ext} - h_{ext} T_{int}}{h_{ext} + B} \right) = B \cdot \frac{\alpha \cdot I + h_{ext} \cdot (T_{ext} - T_{int})}{h_{ext} + B} \quad (2.16)$$

## Section 1: Overview

By dividing numerator and denominator of 2.16 for  $B \cdot h_{\text{ext}}$  (remembering equation 2.14) the following equation is obtained:

$$q'' = \frac{\frac{\alpha \cdot I}{h_{\text{ext}}} + (T_{\text{ext}} - T_{\text{int}})}{\frac{1}{h_{\text{ext}}} + \frac{1}{B}} = K \cdot \left[ \frac{\alpha \cdot I}{h_{\text{ext}}} + (T_{\text{ext}} - T_{\text{int}}) \right] = K \cdot (T_{\text{as}} - T_{\text{int}}) \quad (2.17)$$

In this equation the term  $T_{\text{as}}$  represents the equivalent temperature air-sun. It takes into account the contribute of the solar load summing it to air temperature.

$$T_{\text{as}} = T_{\text{ext}} + \frac{\alpha \cdot I}{h_{\text{ext}}} \quad (2.18)$$

In other words, the thermal flux passing through the wall is expressed as a function of the difference between the internal temperature and this new fictitious or equivalent temperature which correspond to consider the effect of solar radiation as an increase in the temperature of the external environment. Therefore, under solar radiation, the thermal flux (calculated with 2.17) can actually be positive, facing the inside, not only when  $T_{\text{ext}} > T_{\text{int}}$  (e.g. during summer) but also when  $T_{\text{ext}} < T_{\text{int}}$  (e.g. during winter) as long as the effect of absorbed radiation by the wall, summarised in the term  $\frac{\alpha \cdot I}{h_{\text{ext}}}$  makes  $T_{\text{as}}$  greater than  $T_{\text{int}}$ .

## 2.5 Outline of Black Body Theory

In the universe all bodies have a temperature greater than 0 K and emit radiant energy. Hence a body emits radiant energy and then receives it from other bodies.

A radiative thermal flux is present whenever two or more bodies, having different temperatures, are found in the presence of each other, separated by a mean that is sufficiently transparent to radiation (such as vacuum or air). In contrast to what happened during conduction and convection, radiant energy can be transmitted even in the absence of matter, hence the study of heat transfer by radiation requires knowledge of the laws governing the emission and absorption of the bodies.

Solid state bodies have generally selective properties on energy. This means that they can emit it, reflect it, absorb it, or leave it may pass through, as a function of the wavelength.

Therefore, in order to characterise the behaviour of a body, it is not sufficient to know the extent of the radiant power globally emitted but it is necessary to know how it is distributed among the different wavelengths and in the different directions.

The following equations characterise the black body, a theoretical body with an absorption coefficient constant, whose value is equal to 1. From this equations the behaviours of the real bodies are derived. The three laws are:

1. Stefan-Boltzmann law;
2. Wien law;
3. Planck law.

The first one introduces the value  $J_G$ , the global emittance of a black body, namely the energy globally radiated:

$$J_G = \sigma T^4 \quad (2.19)$$

Where  $\sigma$  is the Stefan-Boltzmann constant =  $5.67 \cdot 10^{-8} \text{ [W /m}^2 \text{ K}^4]$ .

The second one, called *displacement law*, provides the wavelength value for which the monochromatic emittance is maximum:

## Section 1: Overview

$$\lambda_M = \frac{A}{T} \quad (2.20)$$

With  $A = 2898 \text{ } [\mu\text{m K}]$ .

The third one expresses the distribution of the monochromatic emittance of a black body.

$$J(\lambda) = \frac{2\pi \cdot h \cdot c^2}{\lambda^5 \cdot \left( e^{\frac{h \cdot c}{\lambda \cdot k \cdot T}} - 1 \right)} \quad (2.21)$$

having indicated with:

$c$ , the speed of light =  $3 \cdot 10^8 \text{ } [\text{m / s}]$ ;

$h$ , the Plank constant =  $6.6 \cdot 10^{-34} \text{ } [\text{J s}]$ ;

$k$ , the Boltzmann constant =  $1.4 \cdot 10^{-23} \text{ } [\text{J/K}]$ .

Referring to Figure 2.6, from the black body emission laws it can be derived that an increasing in temperature leads to:

- An increase of globally emitted power, proportionally to the fourth power of absolute temperature, based on the Stefan-Boltzmann law;
- The power increases even for every wavelength, based on the Plank law, the emission diagram moves totally towards higher values;
- The maximum emission value shifts towards smaller wavelengths.

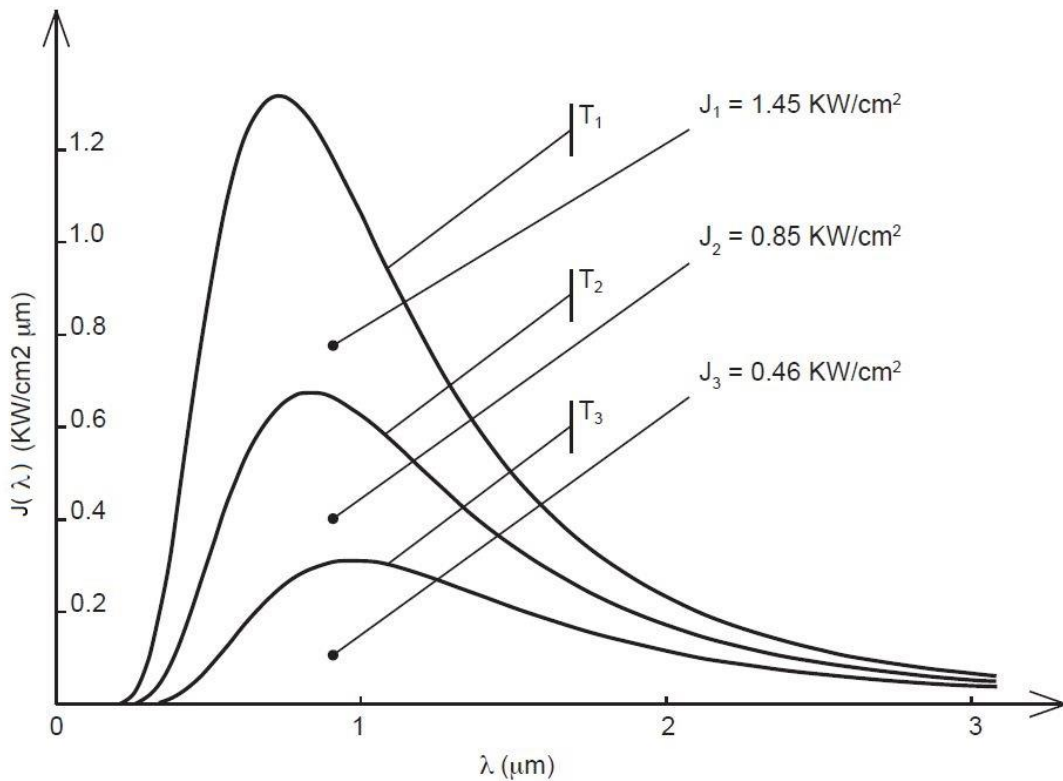


Figure 2.6: Specific emission of a black body at different temperatures:  $T_1 = 4000 \text{ K}$ ,  $T_2 = 3500 \text{ K}$ ,  $T_3 = 3000 \text{ K}$ .

In this way the black body behaviour has been characterised, but these considerations remain valid also for real bodies emitting temperature, although not black.

For them it is necessary to introduce a new quantity, the total emissivity  $\epsilon$  that is the ratio between the relevant body global emittance and that of the black body at the same temperature.

## Section 1: Overview

$$\varepsilon = \frac{J}{J_G} \quad (2.22)$$

Therefore, once the emissivity value of a real body is known, it is possible to easily calculate its fully radiative power, using the above formula.

The emissivity is another quantity that characterises the materials used as building coating. A material with a high emissivity is able to easily re-emit the heat accumulated, due to the solar loads.



## **Section 2: *Experimental and Numerical Analyses***

## 3. Instruments for solar and thermal characterisation of materials

---

### 3.1 Introduction

---

The reflectance and transmittance in solar, visible and NIR band together with the thermal emissivity are basic values to evaluate the performance of the materials used as building coatings.

Their measurements can be effectively performed by devices that return directly a broadband value such as reflectometers, but they can also be performed by more accurate instruments that have the ability to make a spectral analysis such as spectrophotometers. The spectral analysis allows to evaluate the behaviour of a material in the regions of the solar spectrum allowing to evaluate the selective ability of the material at a given wavelength.

The procedures contained in international standards used to calculate the broadband values of reflectance, transmittance and absorptance of materials in the solar, visible and NIR band start from the spectral data [3.1]. This suggests the importance of these measurements.

Apart from this consideration, a complete characterisation of radiometric / photometric material also requires the measurement of the spatial distribution of the light reflected / transmitted from the surface of the material when illuminated from different angles. In this case, an instrument exists to measure the luminance / radiance of a surface at different view angles: the gonio-photometer.

In this chapter the tools used for the solar and thermal characterisation of materials object of study in this thesis are presented. The principles of operation and the main constituent elements will be described in the following paragraphs.

## 3.2 Nomenclature

The following table reports the symbols used in this chapter.

Table 3.1: Chapter 3 nomenclature.

C	Certified reflectance value	[-]
D	Distance between light source and the sample (gonio - photometer)	[m]
E	Illuminance	[cd·sr/m <sup>2</sup> ]
G	Geometric parameter (Gonio - photometer)	[-]
I	Radiant Flux	[W/m <sup>2</sup> ]
k	Correction parameter for CCD readings (gonio - photometer)	[-]
L	Luminance	[cd/m <sup>2</sup> ]
S	Surface	[m <sup>2</sup> ]
T	Exposure time	[s]
q	Luminance coefficient	[1/sr]
ε	Angle between the perpendicular to the sample (z-axis) and a reference direction	[°]
φ	Angle between a reference axis (x-axis) and a reference plane	[°]
λ	Wavelength	[nm]
ρ	Reflectance	[-]
ω	Solid angle	[sr]
Subscript		
1	Incidence	
2	Reflection	
b	Light source	
B	Background	
r	Reflected	
R	Reference Sample	
S	Sample	

## 3.3 Spectrophotometer

A spectrophotometer is a photometer that can measure the intensity of light as a function of its wavelength. Single beam and double beam are the two major classes of spectrophotometers. Linear range of absorption and spectral bandwidth measurement are the important features of spectrophotometers. In Single Beam Spectrophotometers, all the light hits the sample. To measure the intensity of the incident light, the sample must be removed so that all the light can pass through towards the detector. This type of spectrometer is usually less expensive and less complicated. The single beam instruments are optically simpler and more compact and can also have a larger dynamic range. In a Double Beam Spectrophotometer, before it reaches the sample, the light source is split into two separate beams. One beam hits the sample and the second one is used for reference. This gives an advantage because the reference reading and sample reading can take place at the same time.

In transmission measurements, the spectrophotometer quantitatively compares the amount of light passing through the reference and test sample. For reflectance, it compares the amount of light reflecting from the test and reference sample. Many spectrophotometers must be calibrated before they start to analyse the sample and the procedure for calibrating spectrophotometer is known as "zeroing." Calibration is done by using the reference sample, and the reflectance or transmittance of all other samples are measured relative to the reference sample as a percentage value of the amount of light reflected / transmitted of the sample relative to the reference.

Every spectrophotometer is basically composed by the following elements:

## Section 2: *Experimental and Numerical Analyses*

- Light Source;
- Wavelength selector;
- Sample Holders;
- Detector.

Materials with rough surfaces present a difficulty during the measurements. For these materials the incident light beam is not fully reflected or transmitted at a predictable angle of reflection, but it will be diffuse in every direction. The detector will receive only a small percentage of the reflected light by altering significantly the measured value. To solve this problem a hemispherical cavity called "integrating sphere" covered with highly reflective material is used. The light beam after hitting the sample is reflected inside the sphere and the detector read the signal directly from this environment.

The law governing the measurements of the spectral quantities in a spectrophotometer is represented in the following equation 3.1, see Table 3.1 for used symbols.

$$\rho_S(\lambda) = \frac{I_{r,S}(\lambda) - I_B(\lambda)}{I_{r,R}(\lambda) - I_B(\lambda)} \cdot C(\lambda) \quad (3.1)$$

The first factor of the second member in equation 3.1 represent the ratio between the reflected flux from the sample (minus the background signal) and the reflected flux from the reference sample (minus the background signal).

Typically the sample reference is constituted by a material with a high reflection power in wavelengths of the solar band (solar reflectance broadband value ranging between 0.95 - 0.98). According to the reflectance definition given in the previous chapter, the ratio between the radiation reflected by a surface and the radiation incident on it (par. 2.32), the denominator should be constituted by the incident radiation flow, while it has been replaced by the flow reflected from the reference sample. Only in the case the reference reflectance value was 1 the two fluxes would coincide. To correct the measurement, the ratio is multiplied by  $C(\lambda)$ , which represents the certified reflectance value of the reference at the wavelength  $\lambda$ . In the case in which the measurements were performed with an instrument equipped with integrating sphere the total incident flux on samples and sphere found to be higher than the incoming flow (even of one order of magnitude) as a result of multiple reflections inside the cavity (sphere multiplier).

### 3.3.1 Commercial Spectrophotometer

The Perkin Elmer Lambda 950 is a double beam type commercial instrument made available by the UTTMAT laboratory (Unità Tecnica Tecnologie dei Materiali) of the ENEA Casaccia Research Centre, see Figure 3.1.



Figure 3.1: Spectrophotometer Perkin Elmer Lambda 950.

## Section 2: Experimental and Numerical Analyses

It can perform measures in reflectance, transmittance and absorbance modes from 200 to 3000 nm covering the whole solar spectrum with a minimum resolution of 1 nm. It can be equipped with a 150 mm Spectralon coated integrating sphere. Spectralon is a reference material with a high reflectivity (almost constant) at every wavelength of the solar spectrum. Figure 3.2 report the reflectance spectral response of Spectralon between 250 and 2500 nm.

Figure 3.3 shows the arrangement of the main elements that characterise the 150 mm integrating sphere mounted on Perkin Elmer. For reflectance measurements samples are mounted in the back sample holder. The front sample holder is used for transmittance measurements and it is removed during reflectance measurements in order to leave a free passage to the light beam through the input door of integrating sphere. The PMT / PbS detectors are placed at the bottom of the sphere. Figure 3.3 also shows the two light beams paths, the one incident on the sample (blue) and the one incident on the reference (violet). The spectrophotometer equipped with an integrating sphere has a measurement error of around  $\pm 0.01$  of units of the spectral quantity measured [3.2].

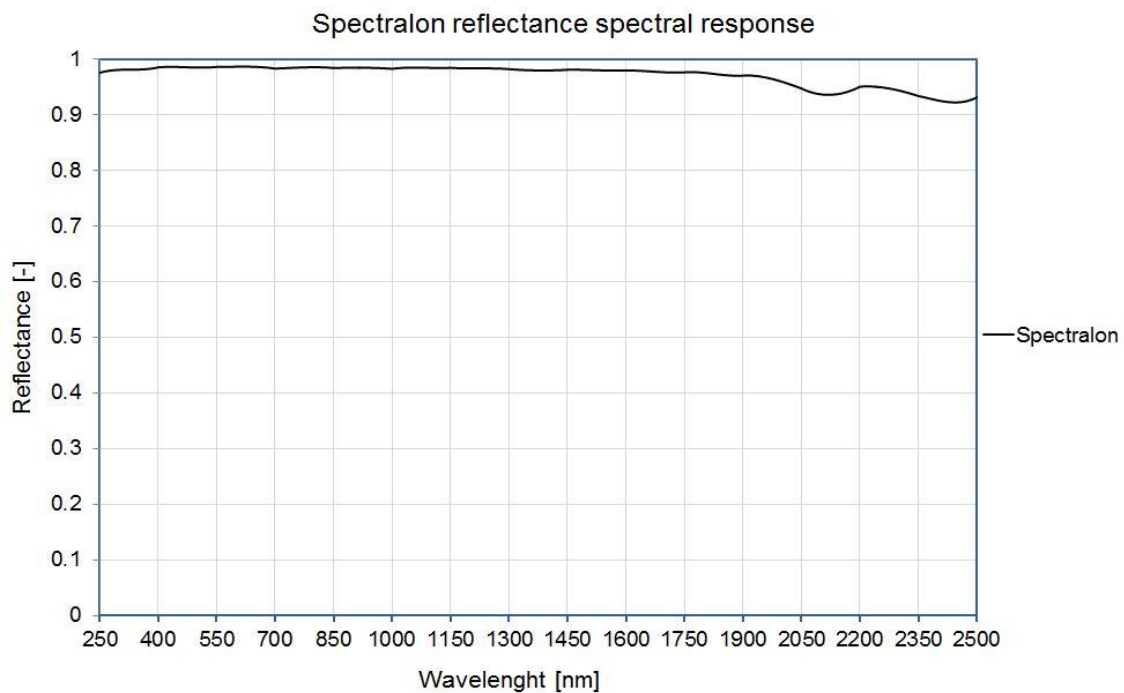


Figure 3.2: Spectral reflectance trend of Spectralon (from 250 nm to 2500 nm).

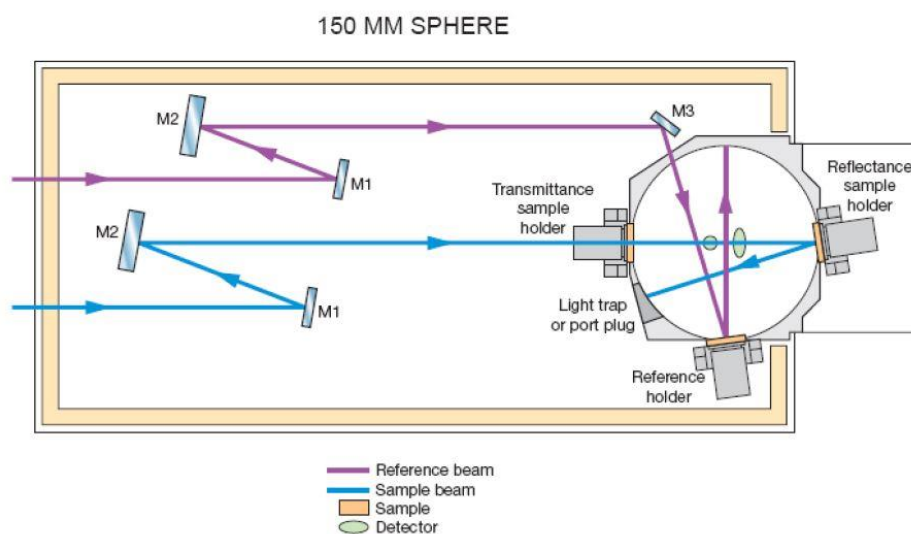


Figure 3.3: Integrating sphere optical scheme.

### 3.3.2 Experimental Facility

An experimental optical test bench equipped with a large integrating sphere was made available by UTEE (Unità Tecnica Efficienza Energetica) of the ENEA Casaccia Research Centre [3.3]. It is composed by the following elements:

- A tungsten halogen lamp with adjustable power, ranging from 250 up to 1000 Watt, see Figure 3.4. The collimated beam diameter can be modulated through a diaphragm according to the measurement requirements. Usual diameters range from 4 to 10 cm;
- An integrating sphere with a 75 cm diameter composed by an external aluminium shell, while the internal surface is made of Spectralon a material with a reflectivity greater than 95% in the whole solar range (300-2500 nm). The sphere is equipped with several ports; the layout of the facility can be adjusted in order to perform transmittance, reflectance and absorptance measurements;
- Detection system consisting of three array spectrometers and three detectors: NMOS for the 250-1000 nm range (dispersion 1.4 nm/pixel); InGaAs for the 900-1700 nm range (dispersion 3.125 nm/pixel); ExtInGaAs for the 1600-2500 nm range (dispersion 3.52 nm/pixel).

An optical characterisation which involves a variation of the angle of incidence of the beam on the sample is typically not feasible with commercial spectrophotometers. A large integrating sphere equipment is able to perform angular measurements on such materials. For reflectance measurements the sample is placed in a holder sited inside the sphere. The arm holder can rotate in order to vary the beam incidence angle. Figure 3.5 shows the setup.

For issues related to the shape of the measure instrument it was not possible to perform measures with an incidence angle greater than 75°. As shown in Figure 3.6, at 75° of incidence the light beam spot on the sample surface is very elongated going beyond the edges of the sample. To overcome this problem the lamp has to be translated and the dimension of the spot has to be sensibly decreased penalising the amount of incoming energy in the sphere and the accuracy of detectors. For this reason, for incidence angle greater than 75°, the problems related to the geometry of the configuration do not allow to perform the measurement.

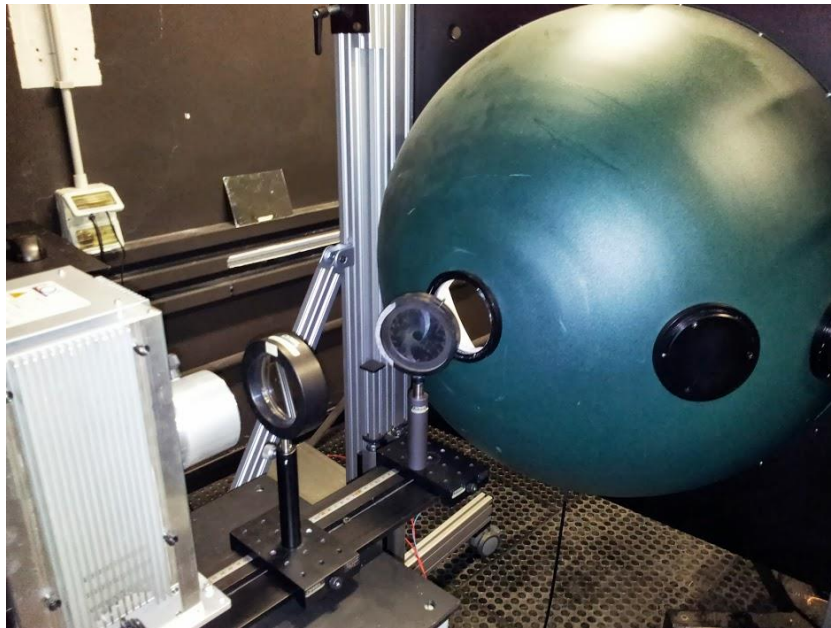


Figure 3.4: Lamp and input port.



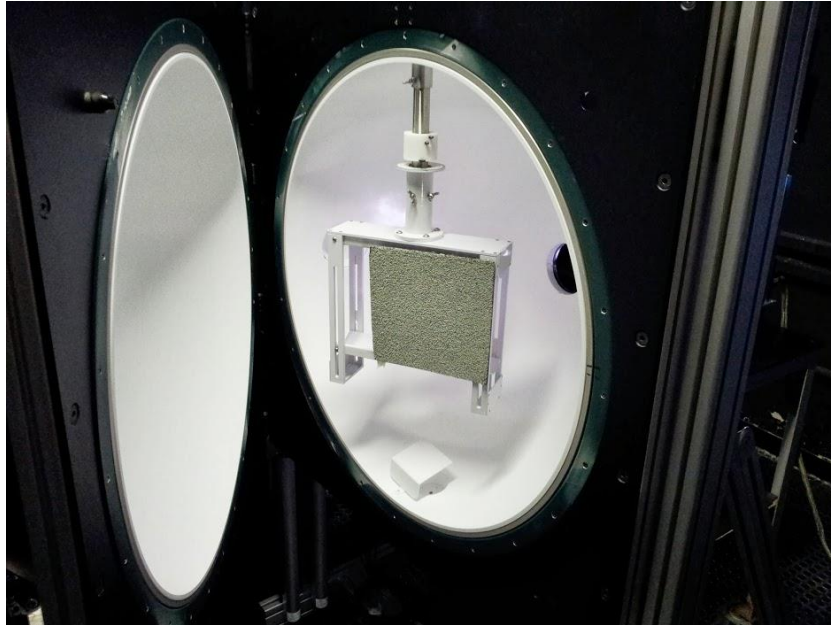


Figure 3.5: Inside the sphere and sample holder.

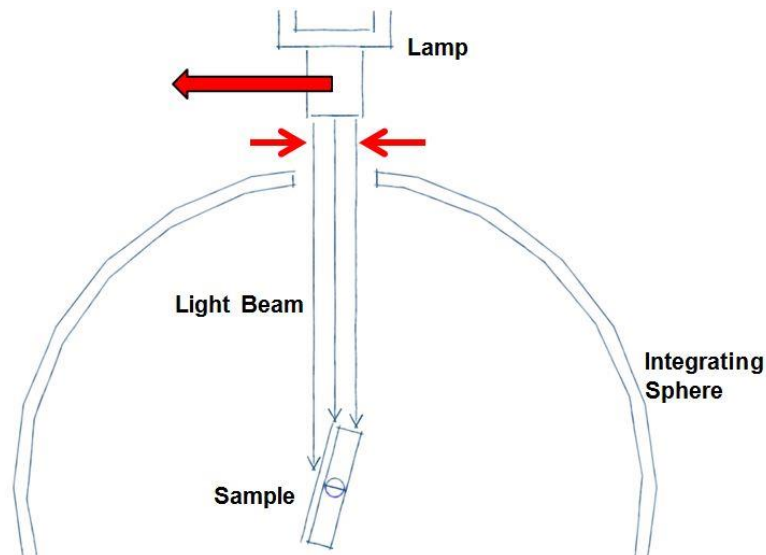


Figure 3.6: Measurement at 75° of incidence angle.

### 3.4 Gonio-Photometer

The calculation of the reflectance (global parameter) allows a first estimation of the illumination or irradiation levels due to the fraction of light or solar radiation reflected from the material. The presence of preferential directions of reflection requires, for more accurate calculations and simulations, a gonio-photometric characterisation of reflection, generally obtained through the measurement of the coefficient of luminance or radiance “q” often indicated with the acronym BRDF (bi-directional reflectance distribution function).

The gonio-photometer shown in Figure 3.7 was made available by the optics laboratory of INRIM (Istituto Nazionale di Ricerca Metrologica) of Turin.

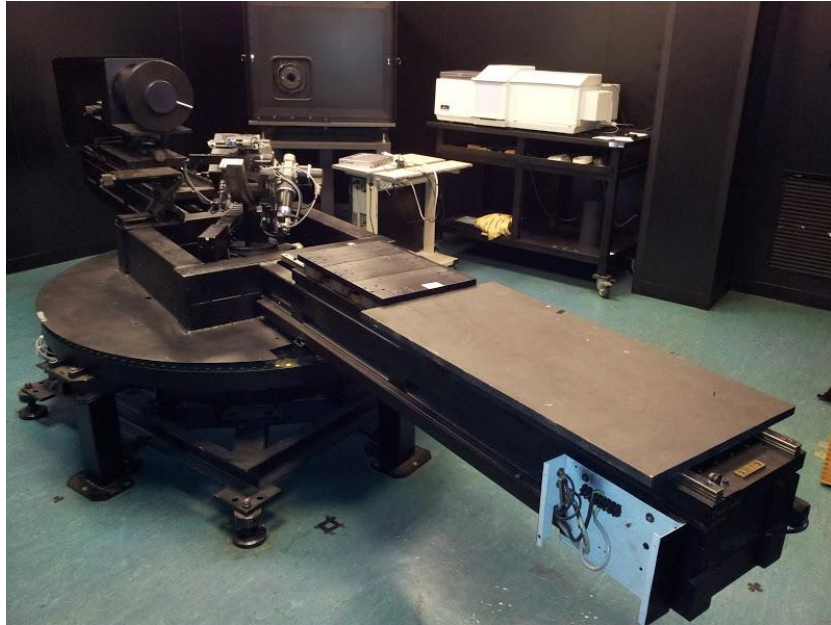


Figure 3.7: INRIM gonio-photometer.

The measurements geometry for the calculation of  $q$  is shown in Figure 3.8. To specify each direction, incident or scattered, it is necessary a pair of angles  $(\varepsilon, \varphi)$ . The polar angles  $\varepsilon_1$  and  $\varepsilon_2$  are the angles between the optical axis of the incident beam and the surface normal; the azimuth angle  $\varphi$  can instead be utilised to indicate the difference between the azimuth plane of incidence defined by  $\varphi_1$  and the plane of view defined by  $\varphi_2$  ( $\varphi = \varphi_2 - \varphi_1$ ).

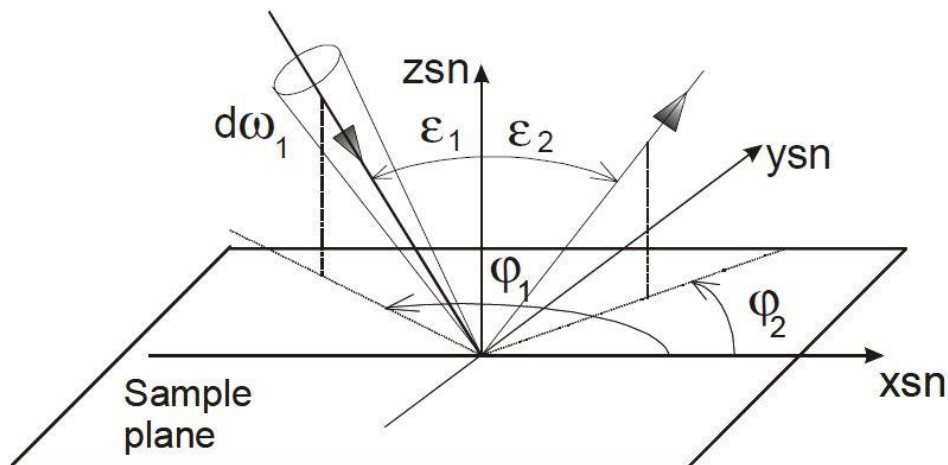


Figure 3.8: Reference angular system for incident and reflected light beam.

The instrument is composed by the following elements:

- A fixed luminous source;
- A detector (photometer or spectra-radiometer);
- A sample cradle rotator.

As a consequence, three axes which can have each orientation in the space, can specify the coordinates system used for measurements: the direction of the lighting beam, the view direction and the sample normal.



## Section 2: *Experimental and Numerical Analyses*

As shown in Figure 3.9, the light source hit the sample horizontally: The detector is installed on the horizontal plane containing it.

As shown in Figure 3.10 the detector can rotate around a vertical axis, which contains the centre of the cradle rotator setup supporting the sample that permits its orientation in any direction in the space. The cradle can also be lowered for permitting the measurement of the lighting beam luminance (or radiance) directly through the detector. The generality of the measurement system that means that it is possible to measure all geometrical configurations, is preserved if the sample normal can be rotate in any directions in the space. This requirement is satisfied only for the hemisphere facing the source, the one used for reflection measurements [3.4].

The sample is positioned in the centre of rotation O of a cradle rotator. This cradle (with a radius of 300 mm and a rotation range of  $100^\circ$ ) is mounted on a rotating unit and on two optical benches (on one is installed the photometric detector). The optical benches have dimensions 300 mm x 1500 mm and rotate horizontally.

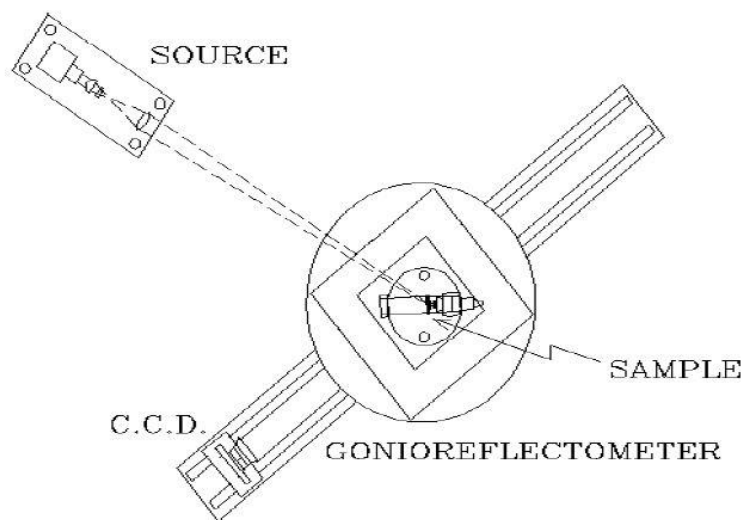


Figure 3.9: Gonio-photometer setup (horizontal plane).

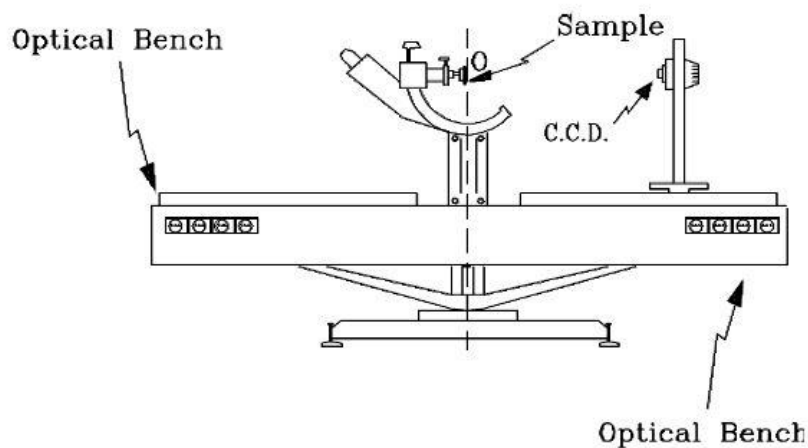


Figure 3.10: Gonio-photometer setup (vertical axis).

Figure 3.11 gives schematically a representation of the gonio-photometer movements: four linear (1, 2, 3, and 6) and four circular (0, 4, 5, and 7).

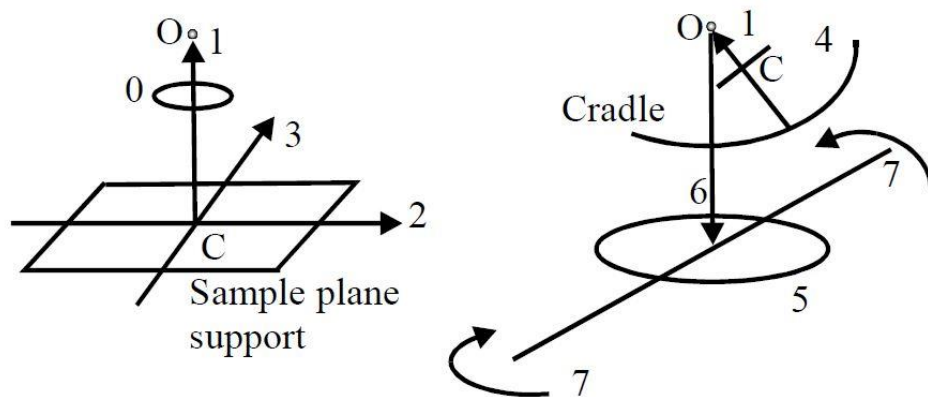


Figure 3.11: Linear (1, 2, 3, 6) and circular (0, 4, 5, 7) movements of gonio-photometer.

In particular:

- The movement 1 shifts the sample along its normal (axis  $z_{sn}$  in the sample reference of Figure 3.8): In order to obtain the coincidence between the sample surface height and the centre of cradle-rotator setup supporting it, the sample thickness has to be considered.
- The movements 2 and 3 shift the sample along two perpendicular axes on its plane (they could coincide with axes  $x_{sn}$  and  $y_{sn}$  of Figure 3.8): these movements permit to analyse different zones of the sample.
- The movement 6 permits to lift up and pull down the sample along the vertical: it is utilised only to commute between source ( $L_1$ ) and sample ( $L_2$ ) luminance / radiance measurements.
- The movement 0 permits to rotate the sample around its normal.
- The movement 4 is obtained by a guide that runs on the cradle: it permits each inclination between  $0^\circ$  and  $100^\circ$  of the sample normal respect to the horizontal plane.
- The movement 5 rotates the entire system cradle-sample around a vertical axis passing through the rotation centre  $O$  of the system.
- The movement 7 rotates horizontally the optical benches: on one of which is installed the detector.

From Figure 3.11 it can be observed that: if the central point of the sample analysed zone coincides with the centre of the cradle rotator  $O$ , this central point remains fixed while the guide run on the cradle (movement 4).

The linear and circular movements have respectively a mechanical precision of 0,01 mm and  $0.01^\circ$ . Globally it is possible to carry out radiometric / photometric measurements for any directions of incidence, any orientation of the reflection view axis (Figure 3.8) and almost all orientation of transmission viewing axis (Figure 3.2), with an uncertainty of  $0.1^\circ$ .

Once aligned the system by the movements 1, 2, 3, 6, it is possible to position the sample for each measurement configuration ( $\epsilon_1, \varphi_1; \epsilon_2, \varphi_2$ ) by the other movements 0, 4, 5, 7.

The detector mounted on the gonio-photometer is CCD (Charge Couple Device) luminance meter. It is a suitable devices able to evaluate the luminance of an acquired scene using digital technology. One of the advantages in the use of the CCD detector is its linearity associated with the possibility of varying the exposure time. In this way the calibration (incident illuminance measurement) is performed with the same detector by pointing directly the source.

The measurement of the luminance / radiance coefficient  $q$  is performed according to the following algorithm.

## Section 2: Experimental and Numerical Analyses

Indicating with “D” the distance between the light source and the sample in O (the centre of cradle rotator) and with  $\varepsilon_1$  the incidence angle, considered as a constant, for all the elements  $\Delta S_{bi}$  of the source (hypothesis certainly correct considering the small extension of this), the illuminance E in O can be written as:

$$E = \frac{\cos \varepsilon_1}{D^2} \cdot \sum_i L_{bi} \Delta S_{bi} \quad (3.2)$$

having indicated with  $L_{bi}$  the luminance of every element  $\Delta S_{bi}$ . The summation is extended to the entire source surface.

If the luminance of the source is uniform (a necessary condition, following the traditional measurement methodologies for gonio-photometers), all luminances  $L_{bi}$  are constant and the summation coincides with the luminance  $L_b$  of the source multiplied by its total area  $S_b$ . In this case this requirement is not necessary because, by means of the CCD detector, all values  $L_{bi}$  can be accurately measured.

In the context of material characterisations, the required accuracy is not comparable to that needed for the calibration samples. In this case, for practical reasons mainly related to the time of measurement, it is preferred to place the result of the summation equal to the average luminance of the source  $L_b$  multiplied by its total area  $S_b$ .

By introducing the geometric parameter G:

$$G = \left( \cos \varepsilon_1 \cdot \frac{S_b}{D^2} \right)^{-1} \quad (3.3)$$

The value of q can be obtained with the following equation 4:

$$q = G \cdot \frac{L_s}{L_b} \quad (3.4)$$

Knowing the measured luminance values of light source ( $L_b$ ) and sample ( $L_s$ ).

Unfortunately, also this type of measurement is not simple because of the relation between  $L_b$  and  $L_s$  that can exceed 4 orders of magnitude. The peculiar operation of the CCD detector allows to solve this problem through different exposure times: in fact, the output signal is proportional to the product of the luminance for the integration time. In the gonio-photometer the integration time is defined by a specially designed rotating shutter. By doing this it is possible to carry out the two measures under conditions of linearity of the detector.

The final equation is:

$$q = G \cdot \frac{T_s}{T_b} \cdot k \quad (3.5)$$

having indicated with  $T_b$  the exposure time used to measure the light source luminance, with  $T_s$  the exposure time used to measure the sample luminance and with k a correction parameter dependent on the readings of the CCD in the two measurement conditions.

### 3.5 Emissometer

The emissivity is the basic parameter to thermally characterise a material. It represents the capability of a body to emit the absorbed heat and it is a temperature function. The device proposed to measure the thermal emissivity is a Devices & Service emissometer, model AE 1, a very simple and cheap tool, based on the fact that the output quantity is a voltage value directly proportional to the emissivity value of the sample. It was made available by UTEE (Unità Tecnica Efficienza Energetica) of the ENEA Casaccia Research Centre.

It is capable of measuring the heat emission from a body in the wavelengths between 3 and 30 microns, and returns as output the broadband value in that band.

## Section 2: *Experimental and Numerical Analyses*

The main sensor is a thermocouple that measures the temperature change due to the heat emitted by the sample transducing it into a voltage signal.

The device needs to be calibrated. Two reference samples with known emissivity (one highly emissive and one low-emissive) are placed on a heat sink and measured by the detector once they have reached the equilibrium temperature. The reading on the voltmeter is adjusted so that it coincides with the value of reference samples emissivity. The calibration setup is shown in Figure 3.12.

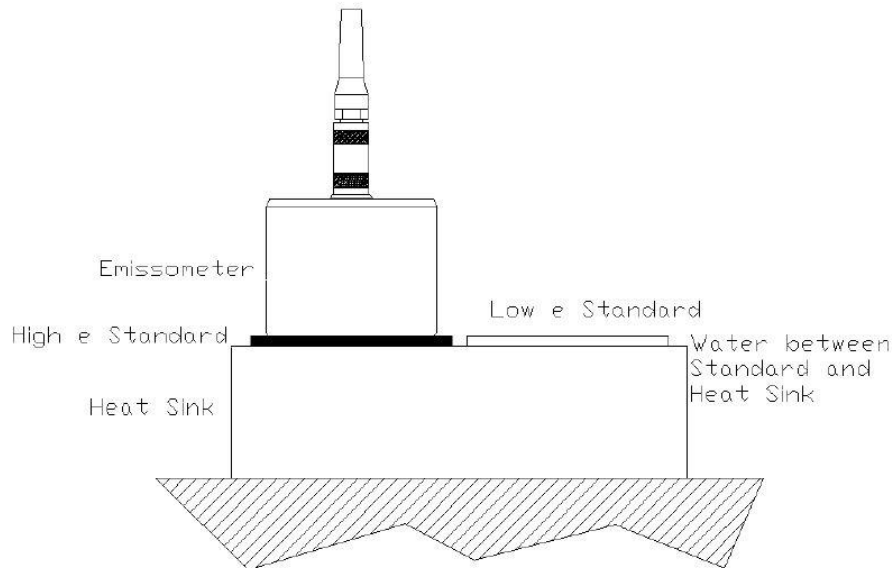


Figure 3.12: Emissometer: Calibration setup.

After the calibration the reference samples are replaced by samples to be measured. The repeatability of the measurement is subject to an error of  $\pm 0.01$  units of emissivity. This value is indicated in the data sheet of the instrument. During the measurement session was instead found an error that oscillates around the  $\pm 0.04$  units of emissivity.

## 3.6 References

- [3.1] ISO 9050. Glass in building-Determination of light transmittance, solar direct transmittance, total solar energy transmittance, ultraviolet transmittance and related glazing factors; 2003.
- [3.2] Rossi G, Iacomussi P. 'Fotometria e goniofotometria di materiali da costruzione opachi'. Ricerca di Sistema Elettrico. INRIM (Istituto Nazionale di Ricerca Metrologica); 2013.
- [3.3] Maccari A, Montecchi M, Treppo F, Zinzi M. 'CATRAM: an apparatus for the optical characterization of advanced transparent materials'. Applied Optics; 1998; 37: 5156 – 5161 (69 Suppl.) Nos. 1 - 6: 75 - 92.
- [3.4] Rossi G, Soardo P. 'A new gonioreflectometer'. CIE Proceeding 22nd Session, 59 - 60, Melbourne; 1991.

## 4. Cool Roofs

---

### 4.1 Topic

---

The topic of this chapter concerns experimental and numerical analyses related to a particular category of cool materials used as roof coatings: The cool roofs.

The activities will be reported as follow:

- An actual case concerning a cool roof application will be investigated in order to evaluate the influence of this material on comfort and energy performance of a building.
- The results of a measurement campaign concerning the decay of the reflection power of these materials will be discussed.
- After the performances evaluation of this technology an energy rating of these products will be proposed in order to fill a gap in the national energy policy.

### 4.2 Introduction

#### 4.2.1 Cool Roofing in General

---

Cool roofing materials can help address the issue of thermal discomfort in buildings and mitigate the problem of heat islands, which results in part from the combined heat of numerous individual hot roofs in a city or suburb. Cool roofing products are made of highly reflective and emissive materials that can remain cooler than traditional materials during especially peak summer weather, see Table 4.1.

## Section 2: Experimental and Numerical Analyses

Table 4.1: Comparison between roofing products “Hot” and Cool”.

FROM: HOT Roofs			TO: COOL Roofs		
Roof Type	Reflectance	Emissivity	Roof Type	Reflectance	Emissivity
Built - up Roof	0.08 - 0.15	0.80 - 0.90	Built - up Roof	0.50 - 0.70	0.80 - 0.90
With dark gravel			With off - white gravel and/or cementitious coating		
Single - Ply Membrane Black (PVC)	0.04 - 0.05	0.80 - 0.90	Single - Ply Membrane White (PVC)	0.70 - 0.78	0.80 - 0.90
Single - Ply Membrane Black (PVC)	0.04 - 0.05	0.80 - 0.90	Single - Ply Membrane Painted with coloured cool coating	0.30 - 0.80	0.80 - 0.90
Modified Bitumen			Modified Bitumen		
With mineral surface capsheet (SBS, APP)	0.10 - 0.20	0.80 - 0.90	White coating over a mineral surface (SBS, APP)	0.60 - 0.75	0.80 - 0.90
Concrete Tile			Cool Concrete Tile coloured	0.40 - 0.65	0.80 - 0.90
Dark color with conventional pigments	0.05 - 0.35	0.80 - 0.90			
Metal Roof			Metal Roof		
Unpainted, corrugated	0.30 - 0.50	0.05 - 0.30	painted with coloured cool coating	0.30 - 0.80	0.80 - 0.90

The most obvious advantage of this feature is lower energy use and, therefore, reduced utility bills. However cool roofs offer several additional benefits including:

- Increased life of the roof, thanks to decreased thermal stress on materials.
- Reduced HVAC system size, thanks to the smaller peak cooling loads.
- Increased comfort for building occupants.
- Diminished peak demand effects on the power grid.
- Reduced urban heat island effect, which in turn helps to minimise the formation of greenhouse gases and smog.

While providing a number of benefits, cool roofs do not pose a large additional cost when integrated into the design for new construction or renovation. Some cool roof options add no cost, for example, choosing a lighter colour shingle or tile. Other options, such as adding a cool roof coating over a built-up roof, may add to the cost of the project, but these options often increase the minimum the cost considering that added costs are offset quickly by lower utility bills and other benefits.

Cool roofs are beneficial even in locations with cold winters. Typically, the wintertime heat loss is less than generally thought because in winter months the sun is low in the sky, is less intense and shines for fewer hours each day.

### 4.2.2 Cool Roof Types

There are generally two categories of roofs: low-sloped and steep-sloped.

Low-sloped and steep-sloped roofs use different roofing materials. Traditionally, low-sloped roofs use built-up roofing or a membrane, and the primary cool roof options are coatings and single-ply membranes.

A low-sloped roof is essentially flat, with only enough incline to provide drainage. It is usually defined as having no more than 5 cm of vertical rise over 30 cm of horizontal run, or a 2:12 pitch. These roofs are found on the majority of commercial, industrial, warehouse, office, retail, and multi-family buildings, as well as some single-family houses.

Steep-sloped roofs have inclines greater than 5 cm rise over a 30 cm run. These roofs are found most often on residences and retail commercial buildings and are generally visible from the street. Most cool roofs focus on the low-sloped roofing sector, but cool roof options are becoming available for the steep-sloped sector as well. Asphalt shingles are the most common roofing materials used on steep-sloped roofs. Other products include metal roofing and tiles.

### 4.2.3 Main Cool Roof Products

The following section describes the different solutions of cool materials available on market or in research and development process. Various technologies are available in Italy and Europe.

#### White Cool Roofs

The white finishing is naturally the more reflective. Rather than the spectral response in the visible band, the spectral response in the NIR band determines a cool material. Figure 4.1 presents the different spectral patterns of two white elastomeric coating, with a different profile in the solar spectrum. On the market there are different white materials for roofs characterised by different properties and application technologies. A typical coating is made from white acrylic paints whose performance may be increased with the use of titanium dioxide pigments in a binder made of a transparent polymer. The solar reflectance of white coatings is often well above 0.8. The emissivity is generally between 0.83 and 0.89 [4.1]. Another type of material belonging to this category is a mineral, organic, eco-friendly paint made from milk and vinegar (solar reflectance = 0.85) [4.2].

Numerous experimental studies have shown that these coatings, when they are subjected to solar radiation, may increase their surface temperature of a few degrees (never more than 7 °C) than the air temperature. Conversely dark materials may have a surface temperature up to 30 °C higher than that of air.

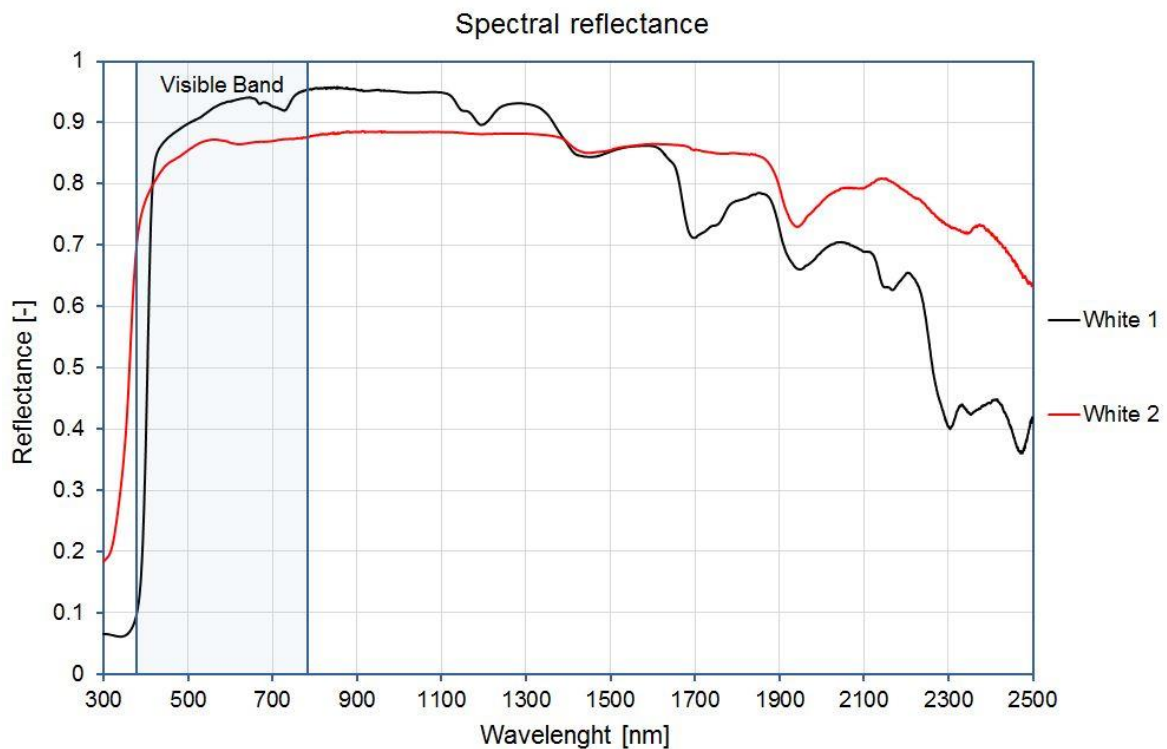


Figure 4.1: Spectral reflectance comparison between two white elastomeric coatings.

#### Metal Materials

The low-emissive metal surface are classified as cool materials only if associated with high values of solar reflectance. The aluminium pigments can be used on an asphalt layer with solar reflectance values of the order of 0.3 - 0.56. Also pigments applied on the building were taken into account. They gave better results, but they are not comparable to those of white materials due to the substrate, and to the silver - grey colour. Even the infrared emissivity is relatively low (0.25 - 0.68) reducing the possibility of radiative cooling of the roof surface during the night. Thermal



## Section 2: *Experimental and Numerical Analyses*

stress, however, has a lower impact on them by increasing the durability of the structure and its performance over time.

### *Cool Coloured Materials*

New materials of different colours are available on market offering a wide range of choices to meet the diverse needs of the designers. Among them reflective tiles, metal roofing, coatings in coloured stone, concrete and asphalt with very light colours aggregates can be mentioned. They present a reflection power medium-low in the visible band (so as to ensure the desired colour response) but a high reflection in the NIR band. This means that it is possible to achieve medium-dark coating having good levels of solar reflectance. The pigments used to impart high optical properties in these materials can be inorganic colorants such as titanium dioxide, iron oxide and organic selective dyes. Inorganic selective materials have also been developed through a combination of oxides of chrome and iron.

Some studies have led to the identification of a group of coloured pigments (white, yellow, brown / black, red / orange, blue / purple) with a reflectance in the NIR higher than 0.8 - 0.9 [4.3, 4.4]. Cool coloured coatings can be achieved with a single layer if the substrate is reflective in the NIR band, otherwise placing two layers. The solar reflectance of the coloured coatings was compared with that of conventional paints with the same colour gradations. Usually dark colours have a higher percentage increase in reflectance when treated with reflective pigments.

Ecological paints made from milk and vinegar achieved high levels of solar reflectance using mainly light colours [4.5].

### *Other Cool Materials*

Single-layer membranes prefabricated with sheets to be applied on ceilings are already available on market. The white membranes are characterised by a solar reflectance that ranges between 0.75 and 0.85. Innovative shingles were also created by the compression of stone granules in an asphalt matrix. Because of their composition (in particular the one of substrate that is very absorbent) even the best the shingles (white colour) hardly reach values of solar reflectance greater than 0.30.

### *Thermo-Chromic Materials*

They are materials composed by a dynamic casing able to adapt the physical properties as a function of climatic conditions. The thermo-chromic materials respond to external stimulation by changing their coloration and consequently their optical properties going from dark colours to lighter colours when temperature increase.

The change is reversible allowing the material to recover the initial colouring as temperature decreases. An attempt to produce thermo-chromic coatings for cool applications is described in a study [4.6]. The pigments appeared coloured on the initial state and translucent with the increasing in temperature (transition temperature = 30 °C). The maximum difference in solar reflectance of these green coloured materials (based on  $\text{TiO}_2$ ) between the enabled and disabled status reached 0.22. This technology, despite the potentialities are very promising, is not yet mature especially as regards the reliability of the performance over time.



### 4.3 Case study: Cool Roof Application in a Non-Residential Building

---

This study focuses on testing cool roof performances of an actual building in Rome. The experiment is composed of two phases:

- The first phase aims at assessing, based on field measurements, the possible modification of thermo-hygrometric conditions inside the building after the application of a cool material on a portion of the roof;
- The second phase required the creation of a building model equipped with a cool roof which is integrated in a simulation software. The goal is to evaluate the building energy performances in case some parameters could change: Insulation of the entire envelope, insulation of the ceiling, profiles of domestic employment, internal and external shading of windows.

#### 4.3.1 Building Description

---

The building is located in the outskirts of Rome and it is part of a structure assembly belonging to Roma Tre University. It was built in the 50s and partially restored in the 90s. During the experiment it hosted a cultural and recreational centre for elderly people run by the municipality of Rome. The guests frequently complained about problems of thermal discomfort during warm periods, despite the presence of a cooling system.

The building is a single unit covered by a low-sloped roof. It is an excellent test bench to verify the performance of the cool roof. This is due to the wide extension of the surfaces that during summer are subject to the higher solar load. The structure plan extends mainly in length and it has a surface of 275 m<sup>2</sup>. The internal layout of rooms is very simple: There are five rooms arranged in a row along the east-west axis and they are all characterised by a rectangular plant. The longer sides of the building are oriented south-north. Figure 4.2 shows the building plant.

Inside the building, the ceiling has a height of 3.80 m, except for the classroom and the relax room (see Figure 4.2) where there is a false ceiling in plasterboard at 3.10 m above the ground. Therefore, within these two environments the phenomena of heat exchange with the external environment show different properties compared to the other three rooms, due to the presence of an air gap of about 70 cm in the ceiling. For this reason they were excluded in the study.

The cool roof was applied on a portion of the roof of 133 m<sup>2</sup>, corresponding to the "Dance Hall" (shown in blue). The innovative material used for the covering is a membrane composed of milk and vinegar. This material is integrated into the database of cool materials, used as roofs coatings, of the European Cool Roofs Council (EU - CRC) [4.7]. Although it was not possible to know the exact thermal transmittance values of the building envelope, it was possible to access to a small sample of the wall and it could be identified the stratigraphy of vertical structures. Covering ceiling and floor layers were assumed according to the year of construction and to the subsequent retrofit. Table 4.2 shows the layers and thermal transmittance values used to modelling the opaque elements of the envelope.

The internal walls dividing the main rooms have the same stratigraphy of the external vertical walls. The partition walls are made of aired brick and plaster; they have a thickness of 21 cm and a transmittance of 1.6 W / m<sup>2</sup> K. The windows are made up of single glasses with a transmittance value of 2.8 W / m<sup>2</sup> K, mounted on a dark grey aluminium frame, for which it has been hypothesised a solar radiation absorptance of 0.85. The frame represents a very large percentage of the entire window, around 30% of the total area.

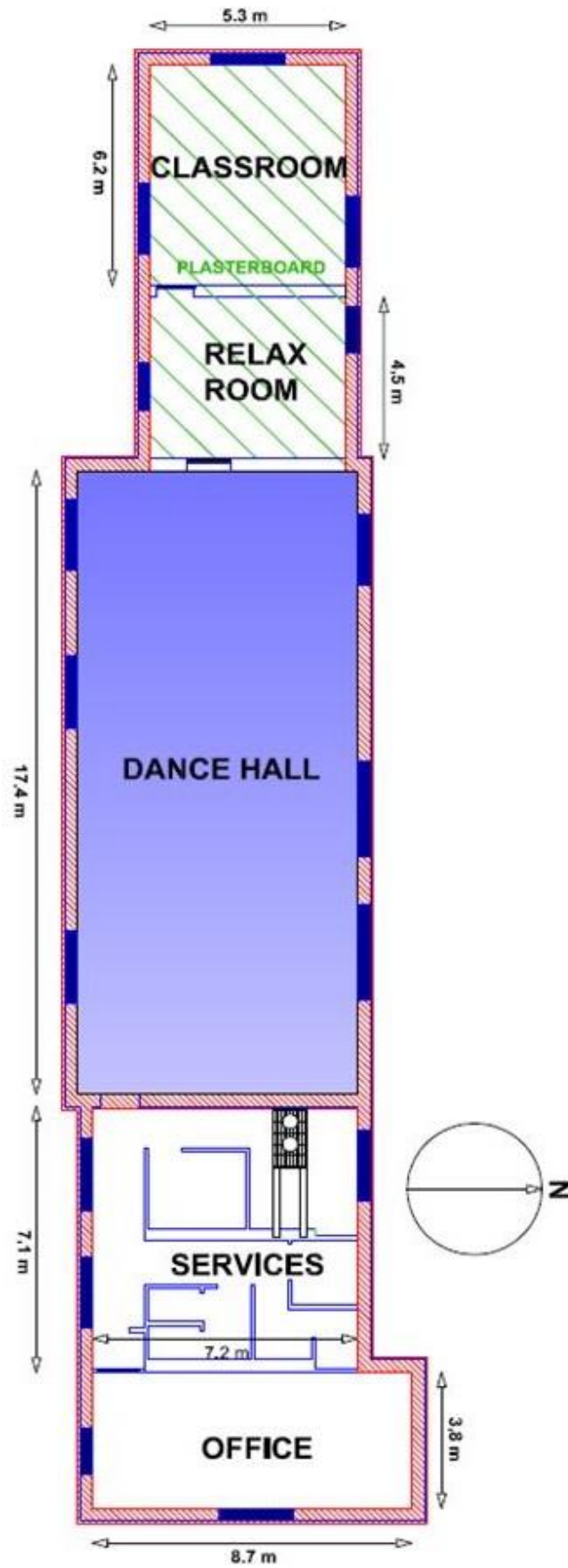


Figure 4.2: Reference building plant.

## Section 2: Experimental and Numerical Analyses

Table 4.2: Opaque elements characteristics.

	Vertical wall		Ceiling		Floor	
Thickness [m]	Plaster	0.005	Plaster	0.015	Tile	0.015
	Concrete	0.220	Aired Brick	0.120	Plaster	0.010
	Brick	0.120	Light Concrete	0.180	Conglomerate	0.460
	Plaster	0.005	Bitumen	0.005		
Total thickness [m]		0.350		0.310		0.475
Thermal transmittance [ $W/m^2 K$ ]		1.230		0.960		0.910

### 4.3.2 Cool roof application

The reflective mineral membrane was placed directly above the shingle using suitable adhesives. The application technique is quite similar to that used for wallpaper or other wall coverings, and it is called "Canadian Roof". The following Figure 4.3 shows the roof surface before and after the application of the heat reflective membrane.



Figure 4.3: Roof before and after the application of the reflective membrane.

### 4.3.3 Methodology

In the laboratory it was conducted an optical and thermal characterisation to compare the reflective mineral membrane and the shingle.

At the same time, a measurement campaign took place from June 17 2010 to August 31, 2010 to monitor the surface temperatures of the roof. In order to assess cool roof influence on thermo-hygrometric comfort of the building, indoor air temperatures were also monitored. The measurement campaign has been supported by weather observations during the relevant period by means of a device equipped with a thermo-hygrometer and a pyranometer. Data recorded from July 2 to July 6 and from August 9 to August 29 are particularly interesting, as during these time frames the building was closed to the public. Temperatures detectors, both for air and surface detection, were positioned on the innovative highly reflective material used to cover the original covering and directly on the last one. Internal temperatures were monitored both in rooms with the ceiling equipped with cool roof, and in rooms with the ceiling covered with the conventional shingle. This allowed a comparative analysis on both types of rooms. The measured data have also allowed to calibrate the next numerical analysis model to analyse different simulation scenarios.

### 4.3.4 Experimental

#### *Optical and Thermal Characterisation of Roof Coating Surfaces*

The original coating is a classic shingle. In order to compare the optical characteristics of the original material with those of the reflective membrane, two samples of these materials were

## Section 2: Experimental and Numerical Analyses

analysed with a commercial spectrophotometer (par. 3.3.1) in the laboratory of the UTTMAT (Unità Tecnica Tecnologie dei Materiali) ENEA Casaccia Research Centre. The measured spectral range goes from 300 to 2500 nm, corresponding to the solar spectrum. The spectral resolution was 5 nm.

The shingle presents a heterogeneous surface due to the presence of grains covering the layer of bitumen. For this reason, spectral analyses were carried out in three points. Figure 4.4 shows the comparison between the measured spectral reflectances.

It is possible to see the spectra of the three measurements carried out on the shingle. They are almost overlapping. Regardless the expected behaviour in the visible wavelength (the mineral membrane is white, the slate is dark grey), it can be observed that the cool material presents very interesting values also in the NIR with a reflectance value higher than 0.95 in a range that goes from 770 to 1100 nm. The reflectance of the slated shingle is constantly below 0.2 throughout the whole measuring range.

Spectral data allowed to obtain the broadband value of solar reflectance according to the procedure described in ISO 9050:2003 [4.8]. Shingle solar reflectance was found to be equal to 0.14 and it is the result of the average of the three values obtained with the three measurements. It seems to be very low compared to the value obtained for the mineral membrane which reached a value of 0.86.

In the laboratory of the UTEE (Unità Tecnica Efficienza Energetica) of ENEA Casaccia Research Centre, further tests were conducted to measure thermal emissivity of the reflective membrane. It was used Devices & Services Emissometer model AE 1 (par 3.5). The obtained broadband value of infrared emissivity is 0.88.

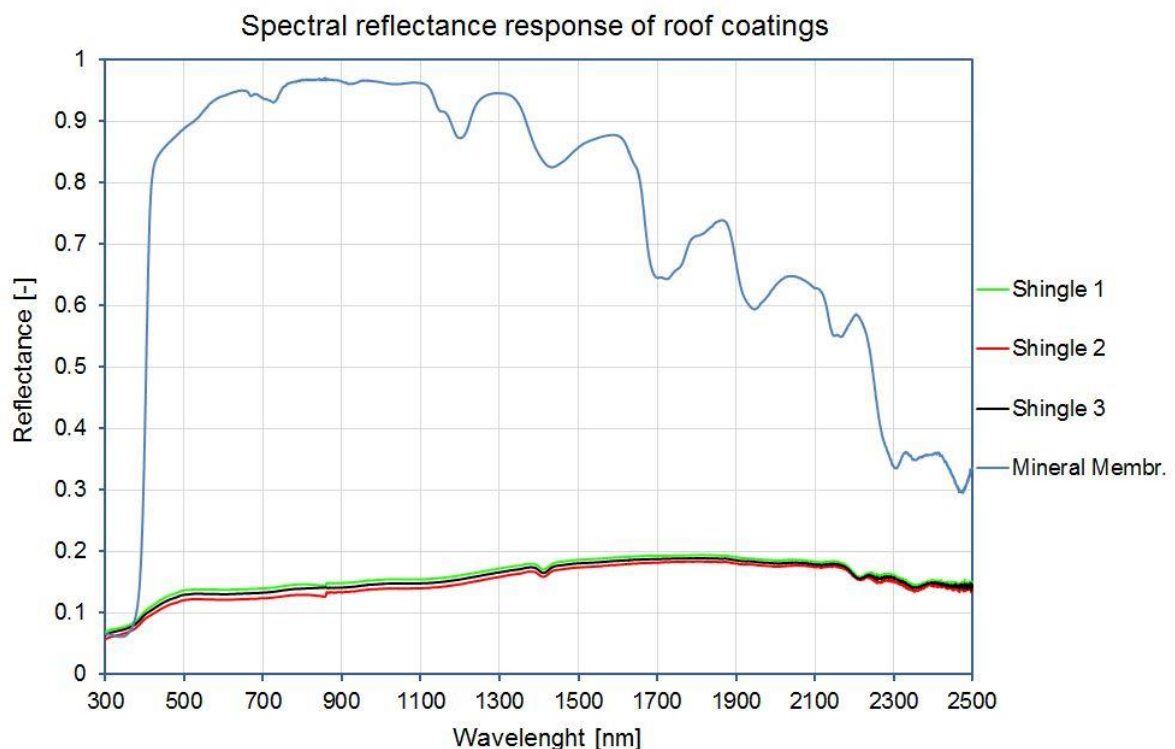


Figure 4.4: Spectral reflectance of mineral reflective membrane and shingle.

### Positioning of the Outdoor Equipment

The equipment for detecting local climate data and monitoring temperature and humidity needed in this study were provided by UTEE (Unità Tecnica Efficienza Energetica) of ENEA Casaccia Research Centre. Figure 4.5 shows the sensors positioning points inside and outside the building. The equipment is composed of:

## Section 2: *Experimental and Numerical Analyses*

- Thermo-resistances for detecting internal surface temperature (green dots in Figure 4.5);
- Thermo-resistances for detecting external surface temperature (red dots in Figure 4.5);
- Pyranometer for measuring incident solar radiation (yellow dot in Figure 4.5);
- External thermo-hygrometer (black dot in Figure 4.5);
- Internal thermo-hygrometers (purple squares in Figure 4.5).

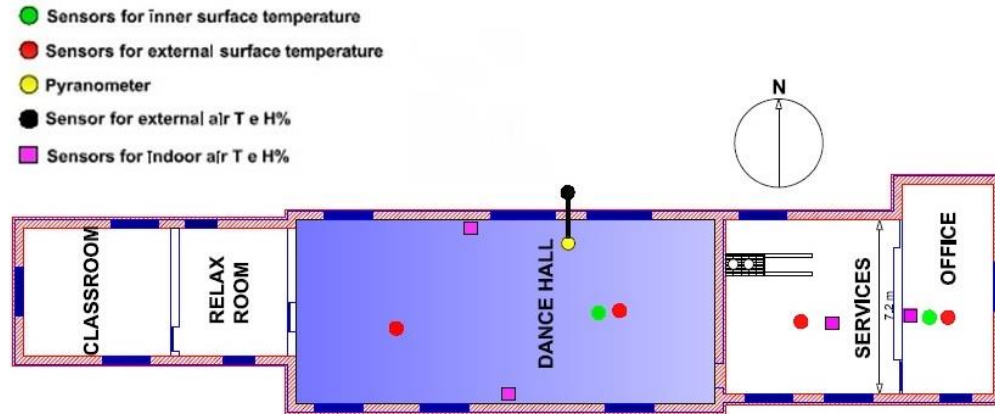


Figure 4.5: Sensors positions in the building plant.

Thermo-resistances have been positioned in order to monitor roof temperature either on the surface covered by the reflective membrane and on the original shingle. In a similar way, in correspondence of the two types of roof external coating other temperature sensors were placed on the internal surfaces.

### *A Drawback for the Membrane*

Cool roof installation was completed on July 20<sup>th</sup>. On August 12<sup>th</sup>, after a routine check of membrane conditions, it was found a substantial layer of dust and soil on its surface probably caused by the presence of a construction site near the building object of the study, as shown in Figure 4.6. This issue caused the deterioration of cool material surface properties and compromised its efficiency in part. The decay of reflectance value due to soiling and ageing will be investigated in paragraph 4.4.



Figure 4.6: Dust and soil effects on mineral membrane.



### Comparative Analysis of Measured Data

#### Surface Temperature Profiles

Through the data stored by surface temperature sensors, it was possible to create temperature daily profiles of the covering ceiling external and internal surfaces. Figure 4.7, Figure 4.8, and Figure 4.9 show the comparison between temperature profiles of the "Dance Hall", where it was applied the high reflectance membrane (black), and temperature profiles of the area called "Office" (see Figure 4.2) characterised by the shingle coating (red). The comparisons, shown in the following figures, refer to different days of August. Cool roof surface temperature was in average 20° lower than the shingle one. On the other hand, internal surface temperatures are much closer. Temperature difference during solar radiation peak between external and internal surface for a cool roof is about 10 °C, while for the shingle is higher than 20 °C. This means that the dispersed heat flux entering in the building in the central part of the day during summer is almost halved due to the use of the reflective membrane.

The difference between the two external surfaces with a different reflectance decreases during night and then increases sharply near the middle of the day characterised by the incident solar radiation peak where the cool roof gives the maximum efficiency.

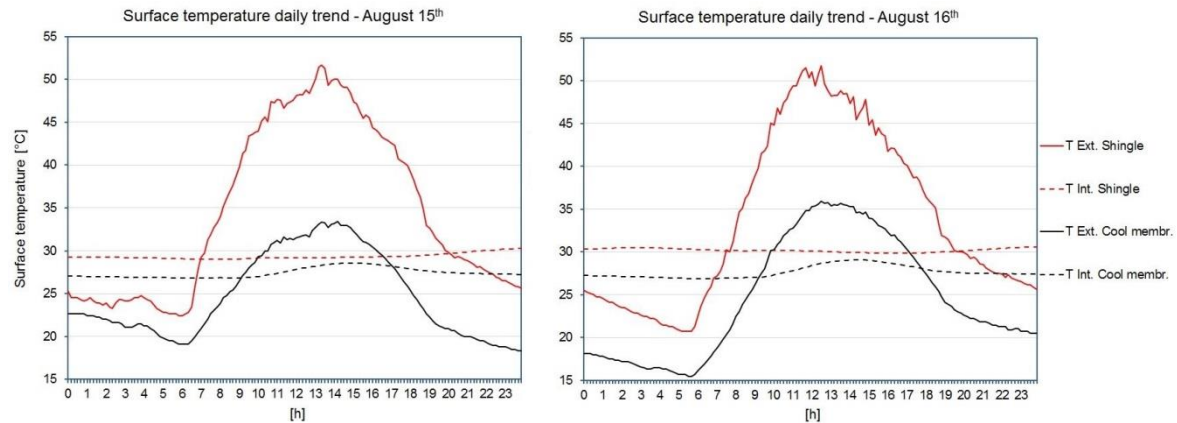


Figure 4.7: Comparison of surface temperature daily trend for cool membrane and conventional shingle (August 15<sup>th</sup> and August 16<sup>th</sup>).

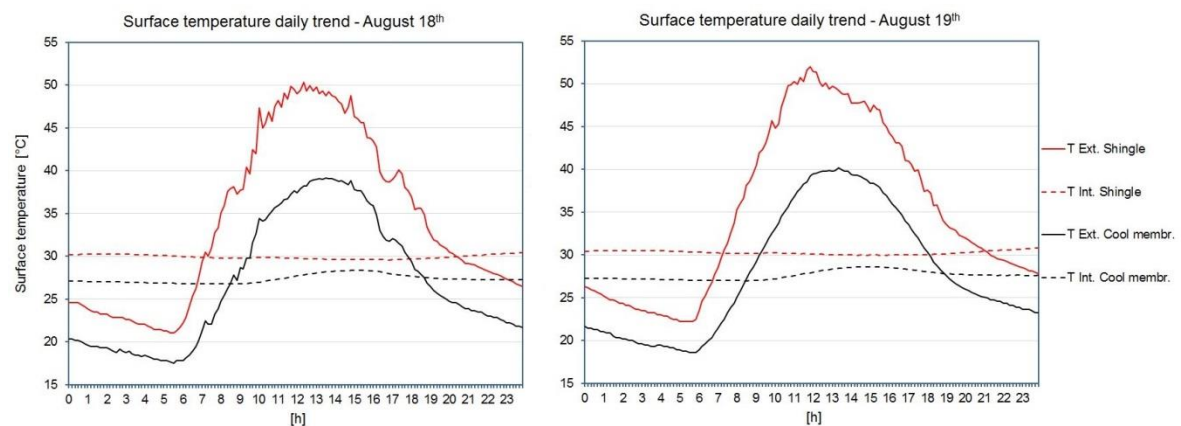


Figure 4.8: Comparison of surface temperature daily trend for cool membrane and conventional shingle (August 18<sup>th</sup> and August 19<sup>th</sup>).

## Section 2: Experimental and Numerical Analyses

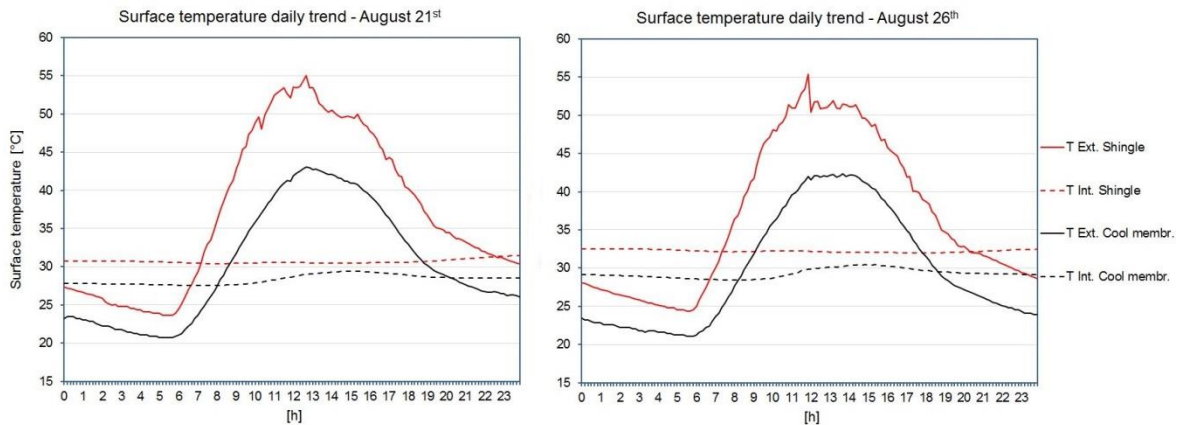


Figure 4.9: Comparison of surface temperature daily trend for cool membrane and conventional shingle (August 21<sup>st</sup> and August 26<sup>th</sup>).

These results are even more significant taking into account that the comparisons were made with data registered few days after the soiling of the mineral membrane.

### Comparison Between Indoor Temperatures

It was not possible to monitor directly and simultaneously the difference between indoor temperatures induced by the reflective membrane and the original covering in the same thermal zone. For this reason two periods of two days were chosen, corresponding to the beginning of two heat waves in July 2 and August 15. In the first period the cool roof was not applied yet. The choice fell on these two periods because of their global solar radiation on the horizontal surface and the outdoor temperatures were almost overlapping. Figure 4.10 shows the global solar radiation trend referred to these two periods.

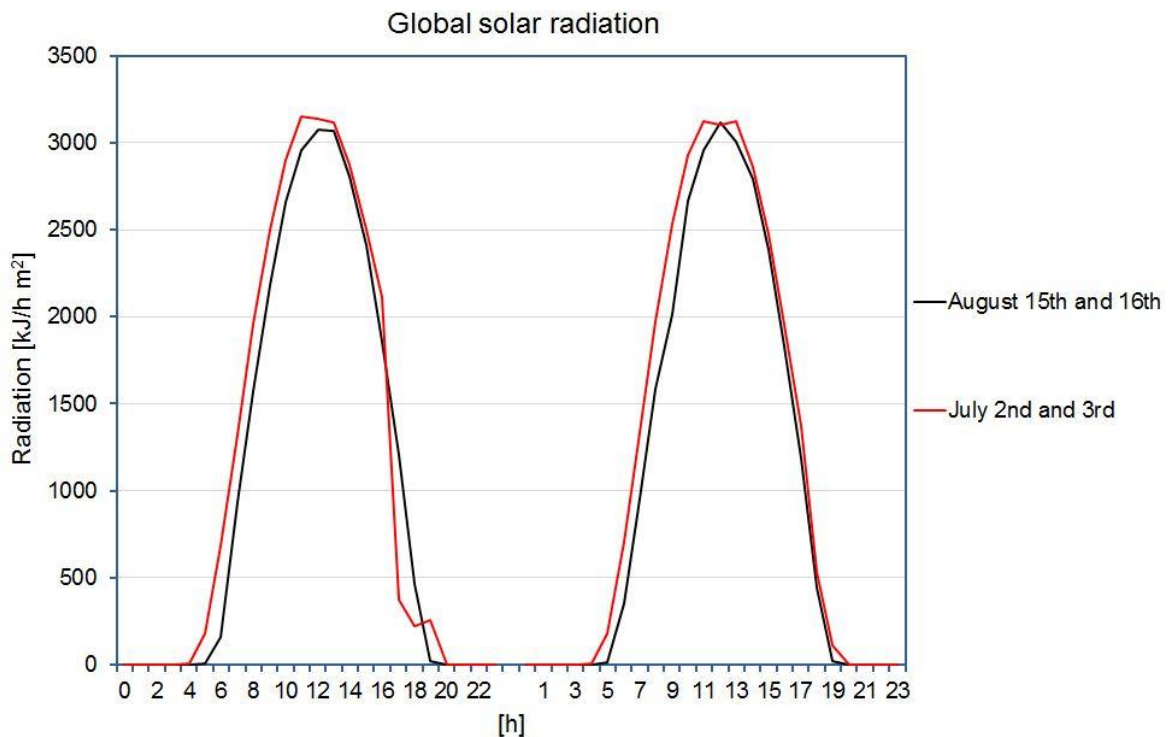


Figure 4.10: Comparison between the global solar radiation on horizontal plane referred to July 2nd and July 3rd period and August 15th and August 16th period.

## Section 2: Experimental and Numerical Analyses

Through this procedure, it was possible to compare the temperatures in the same thermal zone before and after the cool roof application, with the same solar gains, circulating air volumes and without air conditioning systems. Figure 4.11 shows the comparison between air temperatures of the "Dance Hall" recorded on July 2 and July 3 without a cool roof applied on the ceiling and on August 15 and August 16 when the cool roof was applied (and it was already dirty with dust and soil brought from the neighbouring yard). The air temperature trend obtained with the cool roof is shifted down to 2.5 °C, highlighting how this passive technique significantly affects the building internal temperatures.

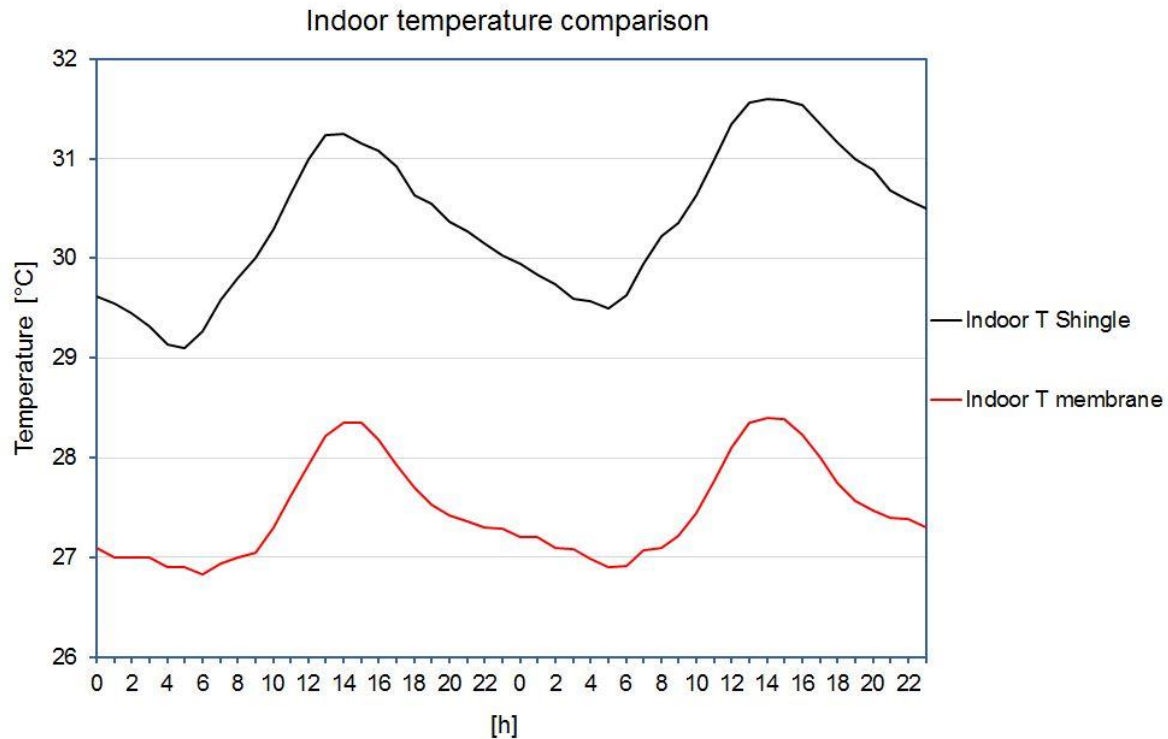


Figure 4.11: Indoor temperature comparison induced by the shingle (black) and the mineral membrane (red).

### 4.3.5 Numerical Analyses

#### The Software

The energetic analysis software used in this study is the TRNSYS. It is a well-known and calibrated calculation model based on a series of components linked each other making easier the modelling of the problem. The functional blocks are called "types" and are written in Fortran language. They consist of mathematical elements that model the performance of one part of the system. "Types" can be linked together to compose the main structure of the project. Ultimately TRNSYS is a collection of energetic components models grouped around a simulation engine. A section called TRNBuild allows to design the building envelope with its thermo-physical properties. By linking it at weather data "types", TRNSYS is able to calculate the heat fluxes which affect the structure [4.9].

#### The Model

The model integrated in the TRNSYS simulation software has been designed first considering the actual building envelope transmittance and respecting building thermo-physics as close as possible to reality. The model was calibrated based on the indoor air temperature and on the primary roof external surface temperature data gathered from July 3 to July 5. Figure 4.12 and



## Section 2: Experimental and Numerical Analyses

Figure 4.13 show the comparison graphs between the real temperature data and the data obtained from the calibrated model. Referring to the indoor air temperature concerning the “Dance Hall” (Figure 4.12), the maximum difference obtained was 0.3 °C. The maximum difference obtained between the measured shingle surface temperatures and those obtained from the model is 6.4 °C (Figure 4.13). If temperature peaks are considered, this last temperature difference decreases to 1.1 °C.

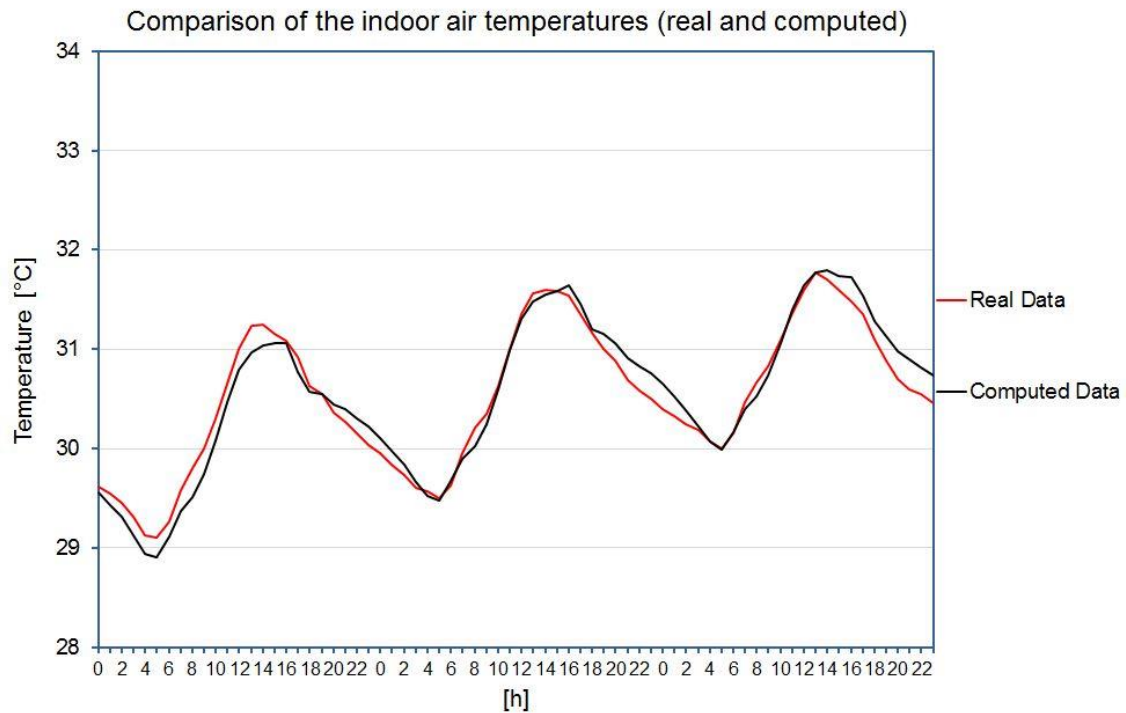


Figure 4.12: Model calibration: Comparison between real and computed indoor air temperature of “Dance Hall” thermal zone.

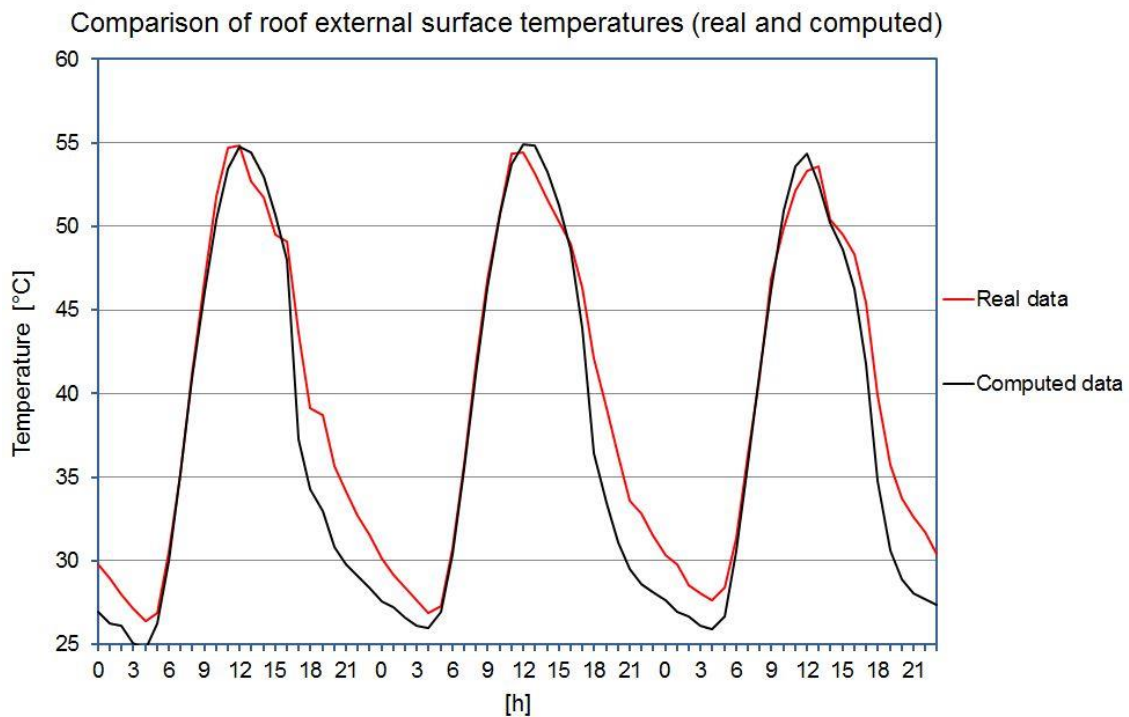


Figure 4.13: Model calibration: Comparison between real and computed surface temperatures of the primary roof equipped with shingle.

## Section 2: Experimental and Numerical Analyses

To achieve the optimum calibration, it was made an intervention on the air infiltration parameters and on internal and external shading factors of transparent surfaces.

*The simulation software used in this study was useful to derive the new mineral membrane reflectance value reached in the points most affected by the deposit of dust and soil. In fact, comparing the surface temperature values measured with thermo-resistances located on the cool roof with the results extracted from the simulations, it was possible to vary the roof reflectance value in the model to obtain an external temperatures trend calibrated with the measured one. Performing the above procedure, the new solar reflectance value obtained is equal to 0.68.*

Once established the effectiveness of the model, three configurations of thermal insulation of the building envelope were created:

- Actual thermal transmittance values of the envelope;
- Ceiling transmittance value in compliance with Italian Legislative Decree, zone D ( $0.32 \text{ W/m}^2\text{K}$ ) [4.10];
- Insulation of the entire envelope in compliance with Italian Legislative Decree, zone D (vertical wall =  $0.36 \text{ W / m}^2 \text{ K}$ , ceiling =  $0.32 \text{ W / m}^2 \text{ K}$ , floor =  $0.36 \text{ W / m}^2 \text{ K}$ , window =  $1.9 \text{ W / m}^2 \text{ K}$ , window including frame  $2.4 \text{ W / m}^2 \text{ K}$ ) [4.10].

For each of these configurations three further configurations were adopted relating to solar reflectance value associated to the roof:

- 0.14 to simulate the original covering (shingle);
- 0.68 to simulate the reflective membrane covered by dust and soil;
- 0.86 to simulate the clean reflective membrane.

### Simulations Results: Operative Temperatures

The operative temperature of a thermal zone is the temperature considering both internal air temperature and the average temperature of structure internal surfaces, multiplied by appropriate coefficients. In this case, the chosen coefficients allow the operative temperature to represent the arithmetic average of the two temperatures.

In this simulation group it was conducted an analysis on operative temperatures obtained for the three thermal insulation levels and for the three roof solar reflectance values. Simulations were conducted under free floating conditions thus without cooling systems affecting air temperature.

Figure 4.14, Figure 4.15 and Figure 4.16 report the cumulative distribution in the examined period, from June 17 to September 1, of the hours in which the operative temperature exceeds the given range:  $26^\circ\text{C}$ ,  $27^\circ\text{C}$ ,  $28^\circ\text{C}$ ,  $29^\circ\text{C}$  and  $30^\circ\text{C}$ . The graphs show the results obtained for the "Dance Hall". It is possible to note that the increase in the reflection power of the external ceiling surface causes a decrease of hours of thermal discomfort. This trend occurs in all three insulation levels of the structure, although the influence of the cool roof is less effective in the more thermally insulated building configuration where also the highest hourly cumulative distributions are found (Figure 4.16). In fact, in the latitudes of Rome, most of summer cooling load is determined by the solar gains through transparent surfaces and an increase in the structure insulation complicates the night disposal of heat accumulated during the day.

The configuration that implies the actual thermal transmittance value for vertical walls, together with a roof transmittance according to the reference standard (Figure 4.15) does not present the drawback mentioned above. In fact, operative temperatures take values averagely lower than the other two treated configurations: A possible roof retrofit that would result in the dual intervention on thermal transmittance and solar reflectance would increase significantly the thermal comfort in a building similar to the examined one.

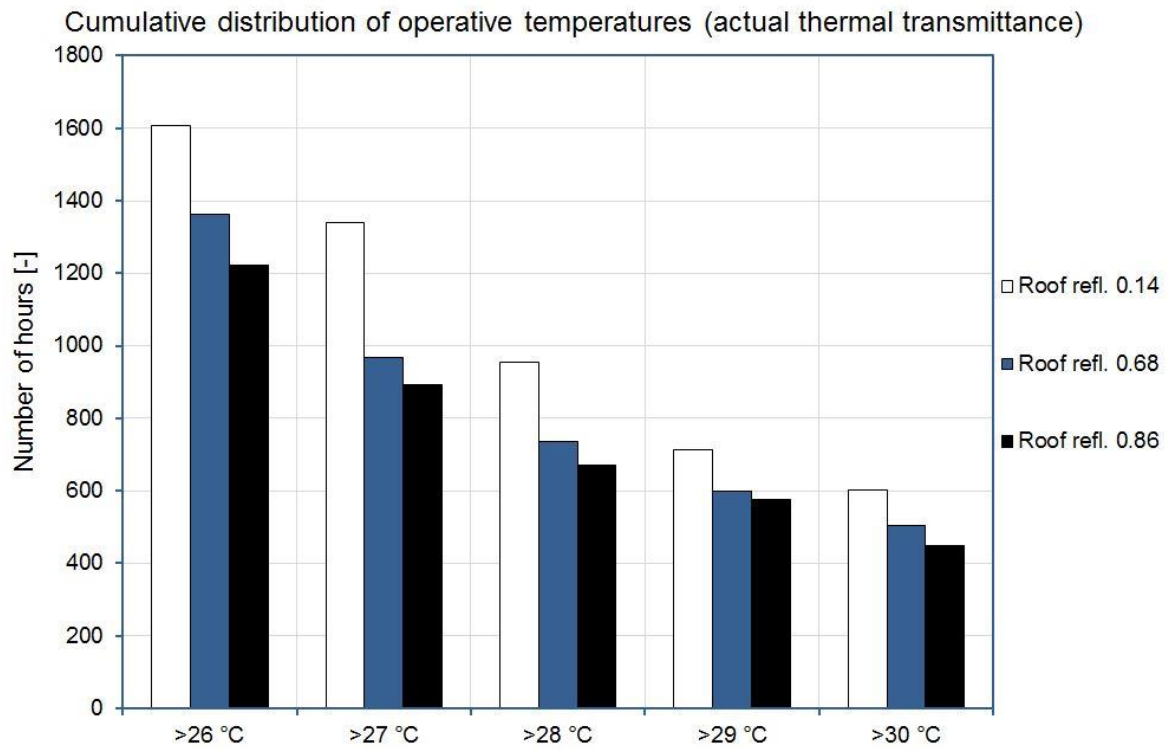


Figure 4.14: Cumulative distribution of operative temperature for the building with the actual thermal transmittance of the envelope.

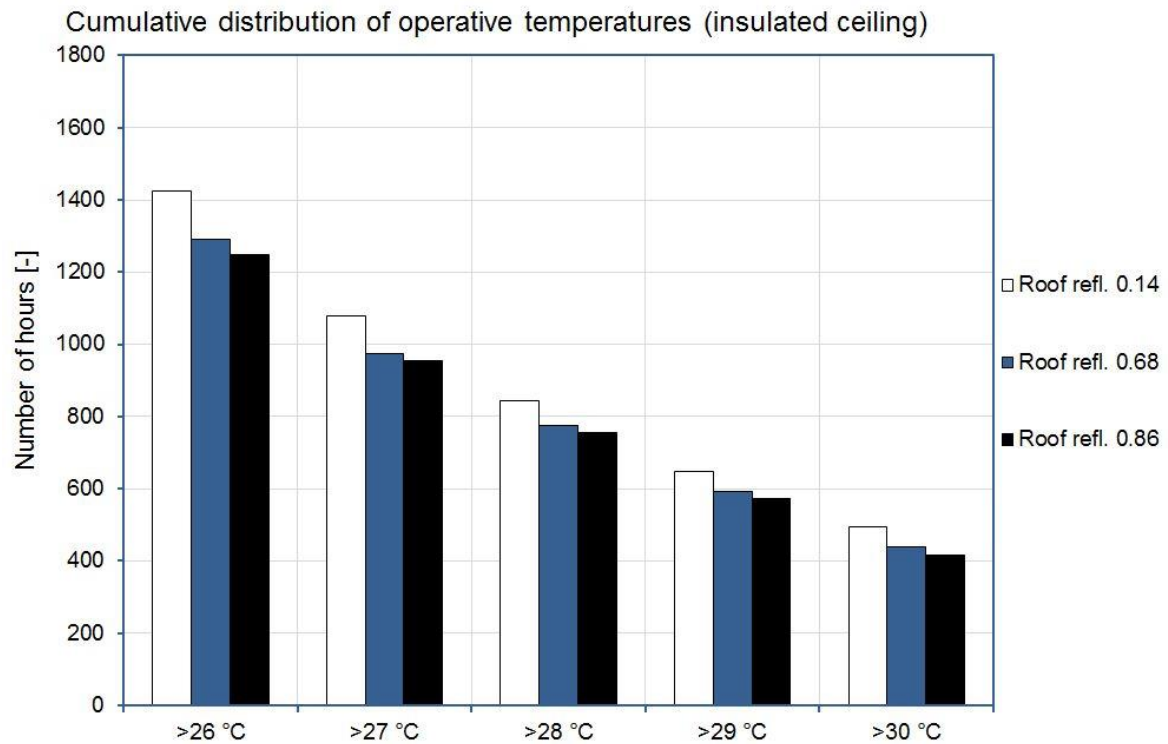


Figure 4.15: Cumulative distribution of operative temperature for the building with roof insulation according to the Italian reference standard.

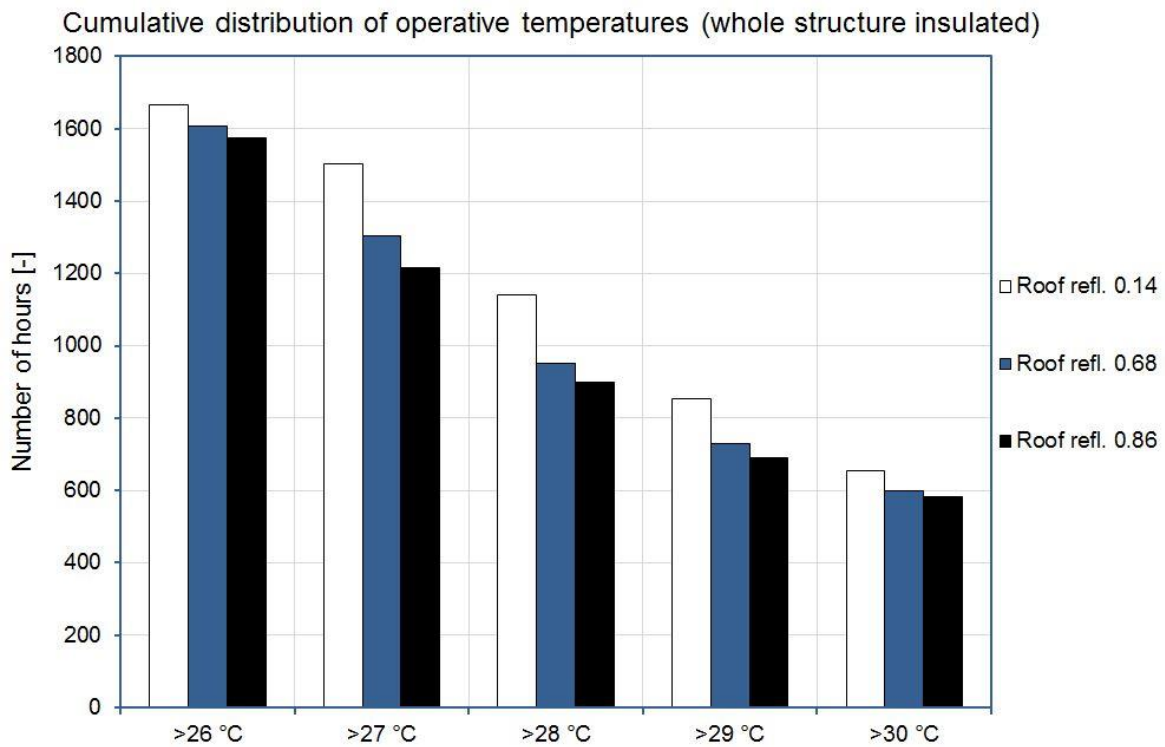


Figure 4.16: Cumulative distribution of operative temperature for the building with whole building insulation according to the Italian reference standard.

### *Simulations Results: Cooling Energy Demands*

In the simulations group considered in this paragraph, it was calculated the building cooling energy demand during the period from June 17 to September 1. Simulations aim at evaluating the influence of an increase in roof solar reflectance on energy performances of the building envelope.

Figure 4.17 shows the variation of cooling energy demand of the "Dance Hall" achieved by changing roof reflectance from 0.14 to 0.68 and similarly from 0.14 to 0.86. As it can be observed in the figure and as it was already been pointed out in the previous section, a higher level of insulation makes the structure less sensitive to the benefits induced by a high reflectance roof.

Considering the actual case, a decreasing in cooling energy demand of about 8 kWh / m<sup>2</sup> was obtained considering the clean and reflective membrane with a percentage variation of 32.3%, and slightly lower than 6 kWh / m<sup>2</sup> considering the dirty membrane with a percentage variation of 24.5%.

For the configuration with an insulation level according to Italian standard reference, a maximum variations of 2.2 kWh / m<sup>2</sup> was found for the structure corresponding to a percentage variation of 14% for the dirty membrane, the maximum decreasing in energy demand obtained is slightly lower than 3 kWh / m<sup>2</sup> in the case of the clean membrane with a percentage change of 18.8%.

Increasing only the roof insulation level determined smaller energy demand variations than the previous cases: 1.8 kWh / m<sup>2</sup> passing from a conventional shingle to the dirty membrane with a percentage variation of 10.1% and 2.3 kWh / m<sup>2</sup> considering the clean membrane corresponding to a percentage variation of 13.6%.

Considering a period covering the entire warm season, including entirely May and September, energy savings would be undeniable and even more if a cool roof was applied on the whole ceiling considering the entire structure energy demands.

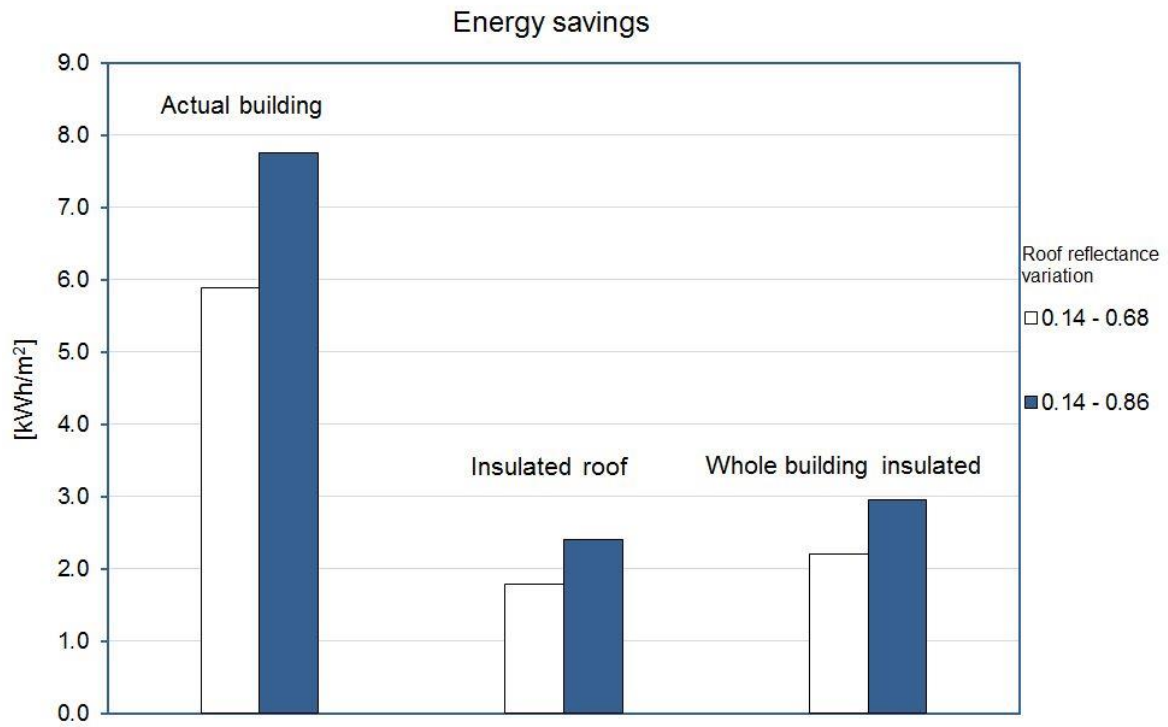


Figure 4.17: Energy savings in summer associated to an increasing in roof solar reflectance for the three considered insulation levels.

## 4.4 Effects of Ageing and Soiling on Solar Reflectance of Roofing Membranes

The benefits derived from properties of high reflectance materials used in construction as a passive technique for house energy saving decrease if those materials get dirty. In fact, the reduction of their reflection power leads to an increase of surface temperature with a consequent increase of the heat flow entering the building envelope during summer. A study confirmed these statements, highlighting that there is a decrease higher than 20% in energy savings achieved by cool materials application, when compared with the saving obtained in the first year of application on residential buildings [4.11 - 4.14]. Although there are cleaning techniques to bring the reflectance to the initial values, their cost is high and not eco-friendly. In literature there are several studies focused on temporal evolution evaluation of building materials solar reflectance. In addition, many data can be retrieved from the databases provided by the US Environmental Protection Agency (US EPA) and Cool Roofing Rating Council (CRRC) of United States that report solar reflectance and thermal emissivity values of clean and aged materials (three years of natural exposure). More in detail, the CRRC manages the natural exposure of more than 2500 products for roofing in three sites in the United States: one in a sub-urban tempered environment in Ohio with moderate air pollution outside the city centre, one in an extra-urban hot dry climate in Arizona and one in an extra-urban hot and wet context in Florida [4.15]. It is interesting to note that none of the exposure fields is located within a urban area due to the space needed for the exposure structures and for the cost of land use. Within the CRRC exposure sites, excluding roofing materials with initial solar reflectance lower than 0.20, all exposed products have an impoverishment of the surface optical and solar features over time. For example, for materials with a reflectance higher than 0.80 after three years there has been an average decrease of about 20% of this property with respect to the initial value. With reference to the thermal emissivity, products tested by Cool Roofing Rating Council during three years presented maximum variations of 10% and for 90% of samples variation was lower than 5% with a mean value of 1.15%. These databases rarely show spectral data that would prove useful for understanding the causes of changes in surface properties due to aging and soiling and in any case they refer only to sites in North America.

A study, carried out by testing a series of roofing membranes, indicates that the particles of soot that lay down on buildings surfaces are the main agent producing the reflection variation. It was also noted that the soot absorbs more at low wavelengths than in the NIR, resulting in a yellowing of surfaces [4.16].

There are no similar data for the Italian territory. For this reason, an experimental campaign was conducted by monitoring reflectivity evolution over time in two Italian cities: Rome and Milan.

### 4.4.1 Nomenclature

Table 4.3: Nomenclature of paragraph 4.4.

$\rho$	Reflectance	[-]
Subscript		
0	Clean sample at time 0	
24	Title 24	
e	Solar	
NIR	Near Infra Red	
sl	Opaque soil layer	
T	Time	
Vis	Visible	



### 4.4.2 Selected Materials

Fourteen samples (10 x 10 cm) of easily available membranes used as covering for roofs were selected. They differ based on colour and surface finish. In addition, for some product classes, standard samples and their corresponding "cool" samples were chosen (higher reflectance values in the NIR band, but same colour rendering).

The sample list can be found in Table 4.4, where it was added the classification code, the product class and the solar reflectance at time 0 ( $\rho_{eT0}$ ).

Table 4.4: Selected materials.

Code	Description	Color	Surface finishing	$\rho_{eT0}$
m1	flexible polyolefin	Grey	Matte and with anti-slip surface	0.26
m2	flexible polyolefin with white factory applied elastomeric coating	White	Glossy	0.85
m3	flexible polyolefin	White	Matte and with anti-slip surface	0.76
m4	thermoplastic polyolefin	White	Glossy	0.82
m5	PVC membrane	Grey	Glossy	0.46
m6	PVC membrane	White	Matte	0.84
m7	Cool thermo - plastic polyolefin	Beige	Matte	0.59
m8	Polymer - bitumen with extra white field applied elastomeric coating	White	Matte	0.81
m9	Polyme - bitumen with white field applied elastomeric coating	White	Glossy	0.73
m10	Polymer - bitumen with white $TiO_2$ photoactive field applied coating	White	Matte	0.77
m11	Polymer - bitumen with white field applied elastomeric coating type B	White	Glossy	0.72
m12	Polymer - bitumen with cool coloured elastomeric field applied coating	Grey	Matte	0.39
m13	Photoactive asphalt shingle	Dark Grey	Rough	0.28
m14	Standard asphalt shingle	Dark Grey	Rough	0.23

### 4.4.3 Exposure Sites and Sample Positioning

Reflectance decrease due to air pollution and aging parameters was tested by placing the samples simultaneously in two urban sites:

- Rome (41.93 N; 12.47 E; 35 m AMSL), roof of ENEA headquarters, Lungotevere Thaon di Revel 76;
- Milan (45.48 N; 8.23 E; 123 m AMSL), roof of ABC department of Politecnico di Milano, Via G. Ponzio 31.

The selected sites provide a climatic and concentration differentiation of pollutants. Buildings are located in areas equidistant from the city centre and the suburbs, away from factories or plants for electrical power production, which would have resulted in a higher concentration of pollutants and would have altered the experimental analysis. Both in Rome and in Milan, samples were exposed with a slight inclination: 1.5% based on the Italian code practices [4.17] and the Swiss standard [4.18]. On Milan site, samples were also positioned with an inclination of 45° and south oriented.

### 4.4.4 Methodology

Samples spectral reflectance measurements were carried out at time 0, after 3 months, 6 months, 12 months and 18 months starting from April 18, 2012. During each measurement session, samples were taken from the exposure site and measured with a commercial spectrophotometer (par 3.3.1) and thus repositioned. Measurements were carried out at UTTMAT laboratory (Unità Tecnica Tecnologie dei Materiali) of the ENEA Casaccia Research Centre. The analysed spectrum corresponds to the solar spectrum (300 - 2500 nm), while the spectral resolution was set to 5 nm. The broadband reflectance values were obtained by spectral data by means of a weighted average compliant with the distribution of the solar spectrum in accordance with ISO 9050:2003 [4.8].

#### 4.4.5 Experimental Results

This section presents the values of the experimental measurements from time 0 to 18 months of exposure in the two selected sites. Table 4.5 shows the time evolution of solar reflectance for samples subjected to natural aging and soiling.

Table 4.5: Reflectance evolution over time of materials due to ageing and soiling.

		Solar reflectance							
		Milan				Rome			
	T0	T3	T6	T12	T18	T3	T6	T12	T18
m1	0.26	0.23	0.22	0.22	0.21	0.24	0.24	0.23	0.23
m2	0.85	0.72	0.70	0.62	0.62	0.74	0.75	0.70	0.68
m3	0.77	0.64	0.60	0.52	0.50	0.64	0.65	0.62	0.58
m4	0.84	0.70	0.68	0.59	0.60	0.71	0.72	0.67	0.62
m5	0.47	0.41	0.38	0.35	0.31	0.43	0.42	0.41	0.37
m6	0.87	0.68	0.63	0.63	0.60	0.74	0.76	0.73	0.75
m7	0.61	0.55	0.52	0.43	0.44	0.54	0.54	0.50	0.46
m8	0.82	0.69	0.66	0.59	0.58	0.69	0.69	0.67	0.67
m9	0.74	0.65	0.61	0.52	0.49	0.62	0.64	0.61	0.59
m10	0.78	0.76	0.71	0.57	0.61	0.73	0.72	0.71	0.68
m11	0.74	0.58	0.50	0.46	0.46	0.63	0.66	0.63	0.64
m12	0.40	0.38	0.36	0.35	0.34	0.37	0.37	0.37	0.36
m13	0.28	0.28	0.27	0.27	0.27	0.28	0.28	0.28	0.28
m14	0.24	0.24	0.24	0.23	0.23	0.23	0.24	0.23	0.23

Both in Milan and in Rome sensitive decreases in values of solar reflectance were observed after 3 months of exposure (July 2012). For more reflective membranes with initial solar reflectance greater than 0.8, in this period of time it was recorded a decrease in the average reflectance of 0.13 (16% compared to the initial reflectance) for both exposure sites. However after 6 months (mid-late October), both in Rome and in Milan the extent of solar reflectance reduced and it reached around 1-3% in Rome and 3-5% in Milan. Between 6 and 12 months of exposure, coinciding with fall and winter 2012 (October-April 2012) there was again an increase in the variation of solar reflectance of 6-8%, probably due to discharges of heating systems. To conclude, it is to be noted an adjustment of reflection values after 18 months of exposure with a lowering of reflectance that is between 1 and 3%.

By analysing the entire exposure period, it was recorded a maximum decrease in solar reflectance of 0.20 (mean value between Rome and Milan) for samples with initial reflectance between values greater than 0.8 up to values of about 0.6, corresponding to variations between 24 and 27%. Interesting values differences between the two exposure sites emerge during winter. The most severe winter of Milan led to a bigger concentration of pollutants in the air caused by heating systems in buildings. For samples that showed a solar reflectance higher than 0.6 (m2, m3, m4, m6, m8, m9, m10 and m11), the difference between the values obtained in the two sites is around 0.08 which is equivalent to about 10% compared to the initial value.

The greater reflectance decreases detected are about 0.25 and they are recognised as equivalent to 33% of initial values after 18 months of natural exposure. From the data obtained from the CRRC in their exposure sites after 3 years, for membranes with initial solar reflectance greater than 0.8, it results an average decrease of this magnitude of 0.16, that is 18% of the initial value and only for the exposure site in Florida the decrease is around 0.24, that is 30% of the initial value [4.19]. The mismatch of these results does not depend on the tested materials type that appear to be quite similar to those exposed in the sites of CRRC. The reflectances measured in Milan are much lower than those that would be obtained according to the formula proposed by DOE and California Title 24 [4.20].

On the contrary, results obtained in Rome are similar to those provided by the equation 4.1. Refer to Table 4.3 for used symbols.

$$\rho_{24} = \rho_{sl} + 0.70 \cdot (\rho_{eT0} - 0.20) \quad (4.1)$$



## Section 2: Experimental and Numerical Analyses

Membranes with initial solar reflectance between 0.2 and 0.3 (m1, m11 and m12) have limited reflectance variations over time and they range from 0.02 to 0.05. Membrane m1 has a gradual solar reflectance decrease (monotonic), while values recorded for shingles (m11 and m12) fluctuate around the initial reflectance value, since the layer of modified bitumen under gravel coating is veiled with soot, a dark hydrophilic substances that is removed when it rains, or in dry climates, transported by dew [4.21]. Considering the limited changes in reflectance especially for sample m1 (initial solar reflectance equal to 0.26) it can be inferred that soot solar reflectance in Rome and Milan ranges from 0.20 to 0.25.

No significant differences between samples exposed almost horizontally and samples inclined at 45° were detected, with the exception of the shiny membranes m2 and m9.

In general in Milan after 18 months, solar reflectance for all exposed membranes converges to a stable value (with variations of around 0.01), while in Rome they are still detectable more sensitive reflectance changes with decreases ranging from 0.02 to 0.04 for membranes with initial solar reflectance greater than 0.6. While considering surface roughness, it was noted that samples with smoother or moderately porous surfaces (m2, m4 and m6) have a less pronounced tendency to reflectance decrease (mean change for Rome and Milan of about 24% of the initial value) compared to membranes which have anti-slip surfaces (m3, for which the percentage change reaches about 29%) and compared to the white field applied coatings (m8, for which the percentage change reaches about 27%). This is due to the high porosity (presence of micro-pores on the surface) in which it is deposited dirt, offering high resistance to removal through the rains.

Figure 4.18, Figure 4.19, Figure 4.20 and Figure 4.21 show the evolution over time of spectral values for Rome and Milan related to four selected samples (m2, m7, m12 and m14) which have the most significant spectral variations due to ageing and soiling that summarise the behaviour of the other samples.

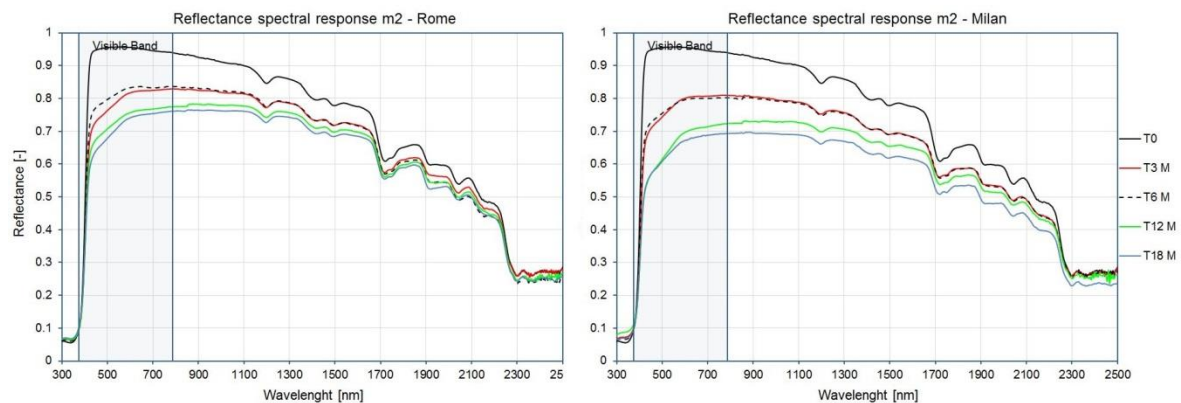


Figure 4.18: Spectral reflectance evolution over time for Rome and Milan - sample m2.

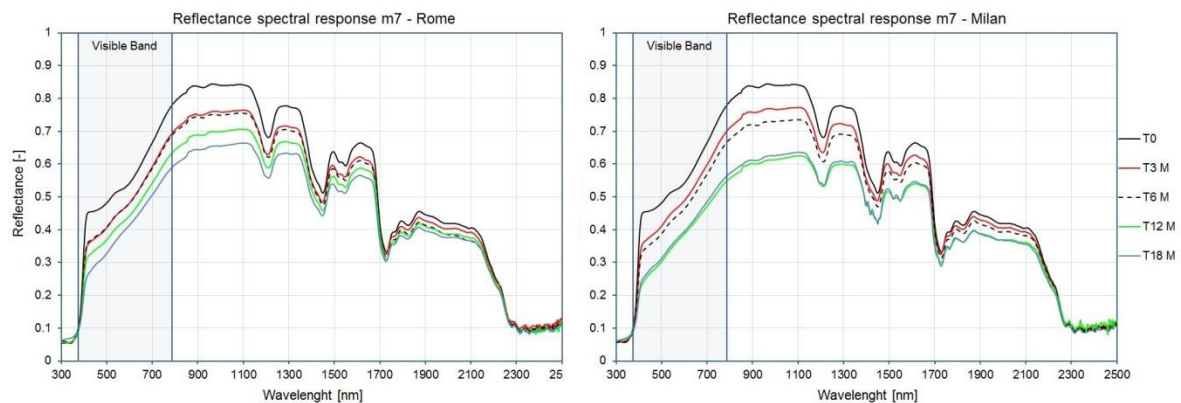


Figure 4.19: Spectral reflectance evolution over time for Rome and Milan - sample m7.

## Section 2: *Experimental and Numerical Analyses*

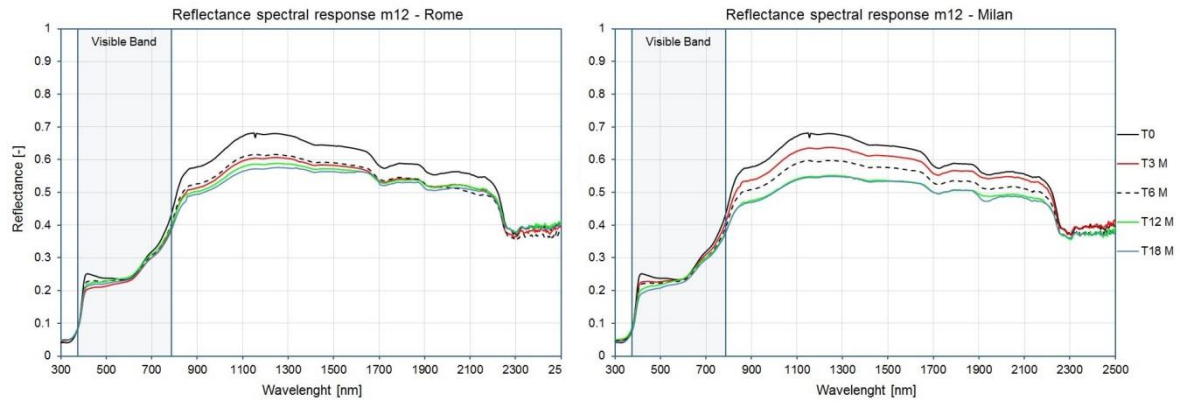


Figure 4.20: Spectral reflectance evolution over time for Rome and Milan - sample m12.

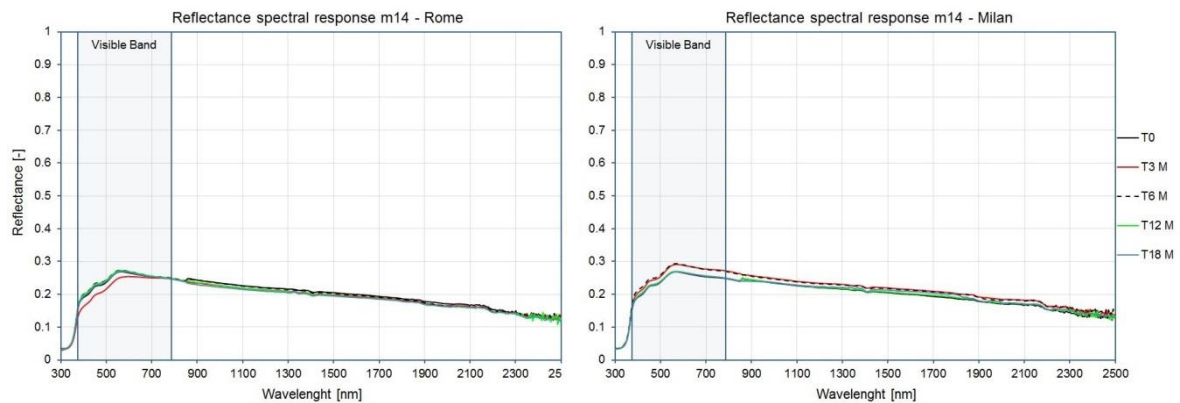


Figure 4.21: Spectral reflectance evolution over time for Rome and Milan - sample m14.

Spectral responses reported in figures above for Rome and Milan are similar.

Sample m2 (Figure 4.18), the white glossy polyolefin membrane shows a changing in trend in the visible band after 3 months. The trend continues to maintain that shape in the visible band during the subsequent measurements.

Sample m7 (Figure 4.19), the beige thermo-plastic polyolefin, presents a shifted evolution over time of the spectral data from 300 to about 2100 nm. The trends are overlapped in the rest of spectrum.

Sample m12 (Figure 4.20), the cool coloured coating shows a decreasing in spectral response limited to NIR band, while the visible band stay almost constant over time.

Sample m14 (Figure 4.21) is a shingle. The spectral trend is almost constant over time.

Figure 4.22, Figure 4.23, Figure 4.24 and Figure 4.25 show the evolution over time of the broadband reflectance values obtained through the ISO 9050:2003 in the solar, visible and near infra-red bands after 18 months of measurement, for samples m2, m7, m12 and m14.

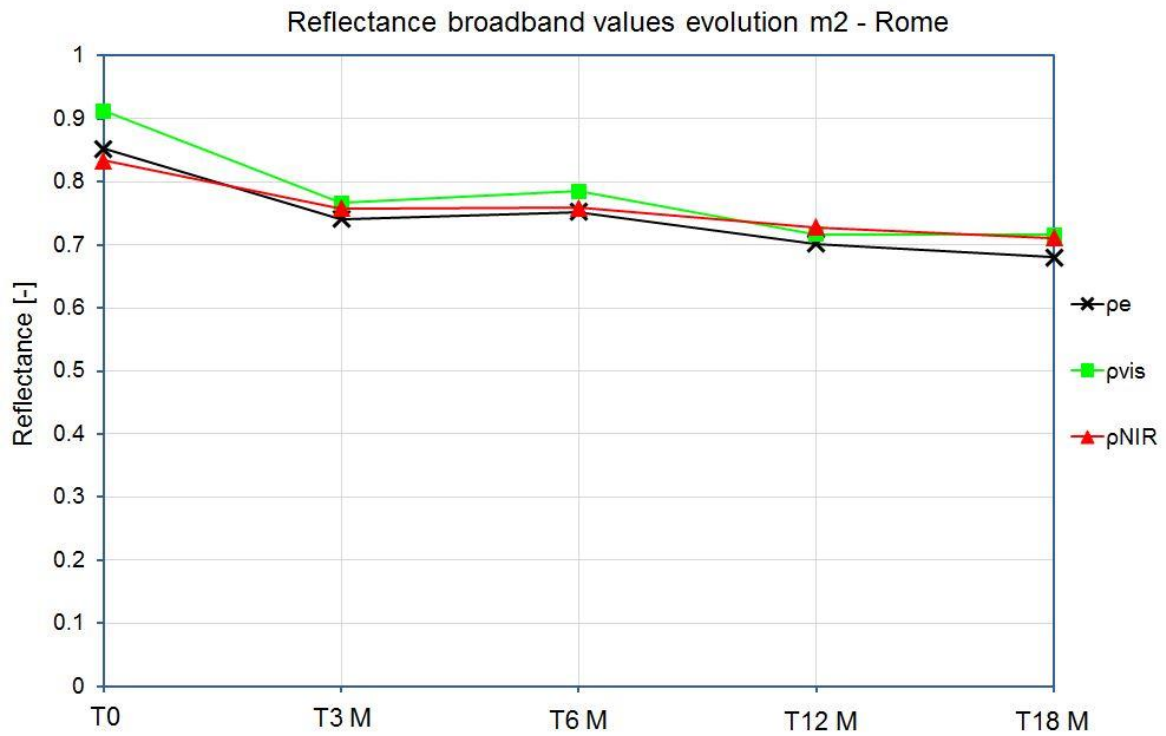


Figure 4.22: Reflectance broadband values evolution over time in solar, visible and NIR bands due to ageing and soiling for Rome - m2.

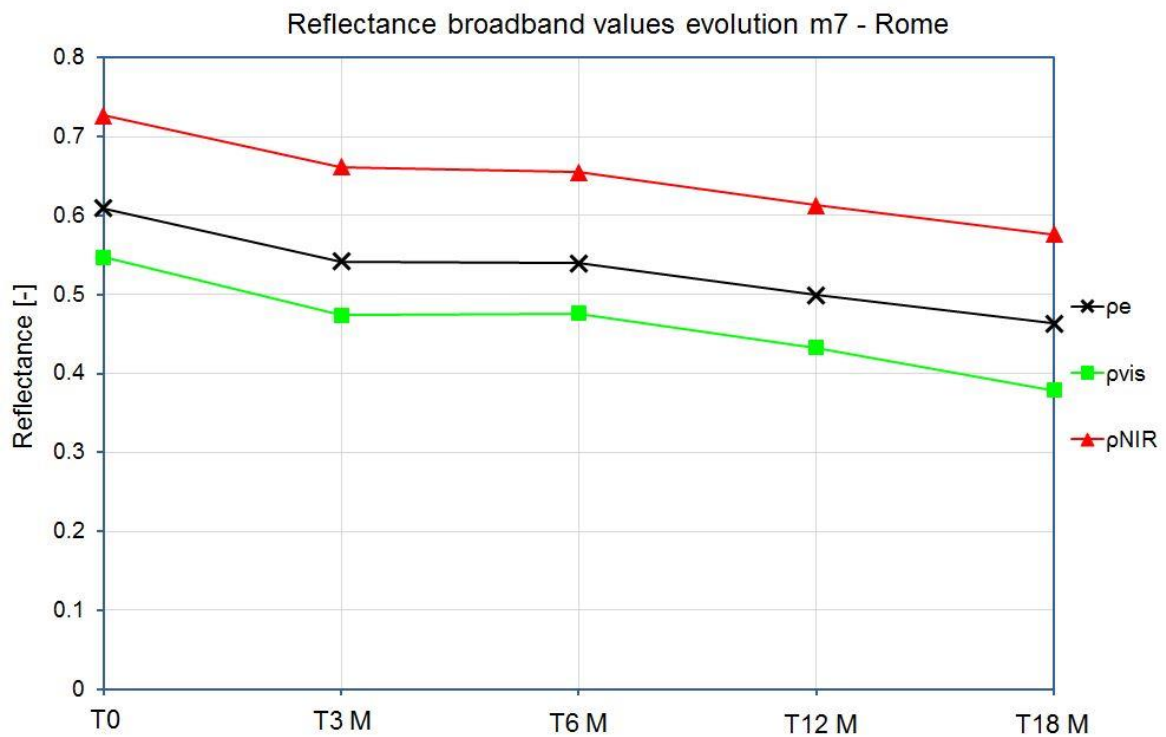


Figure 4.23: Reflectance broadband values evolution over time in solar, visible and NIR bands due to ageing and soiling for Rome - m7.

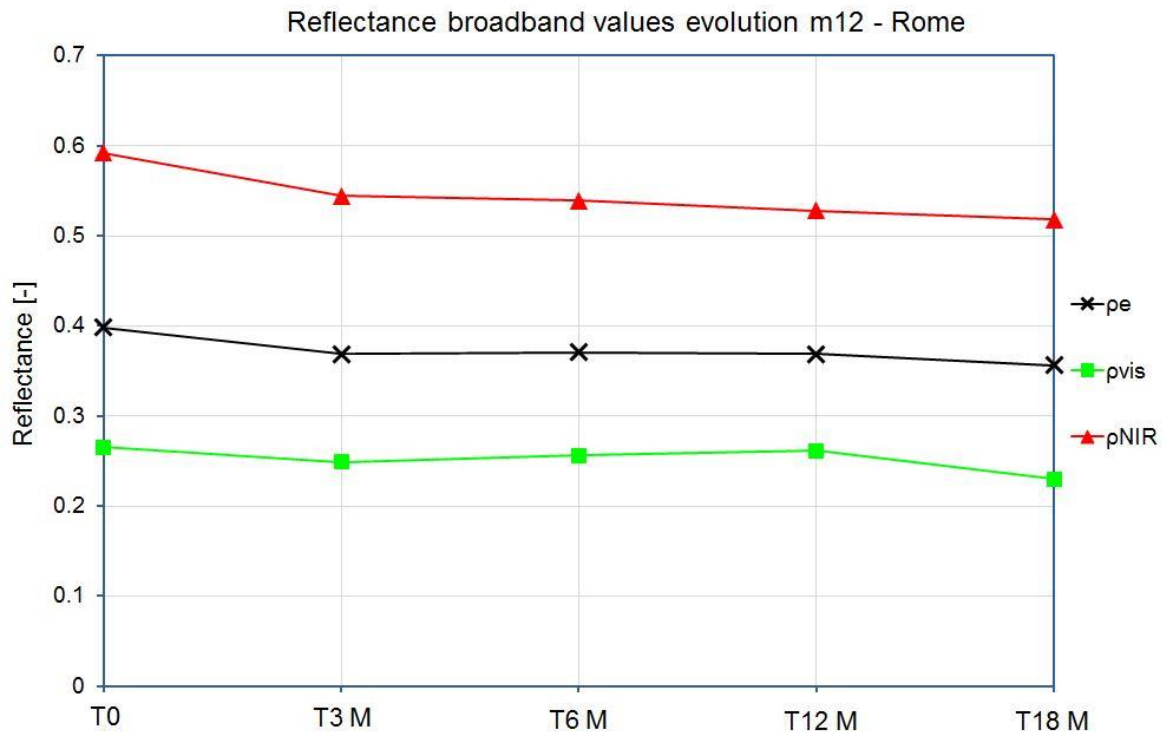


Figure 4.24: Reflectance broadband values evolution over time in solar, visible and NIR bands due to ageing and soiling for Rome - m12.

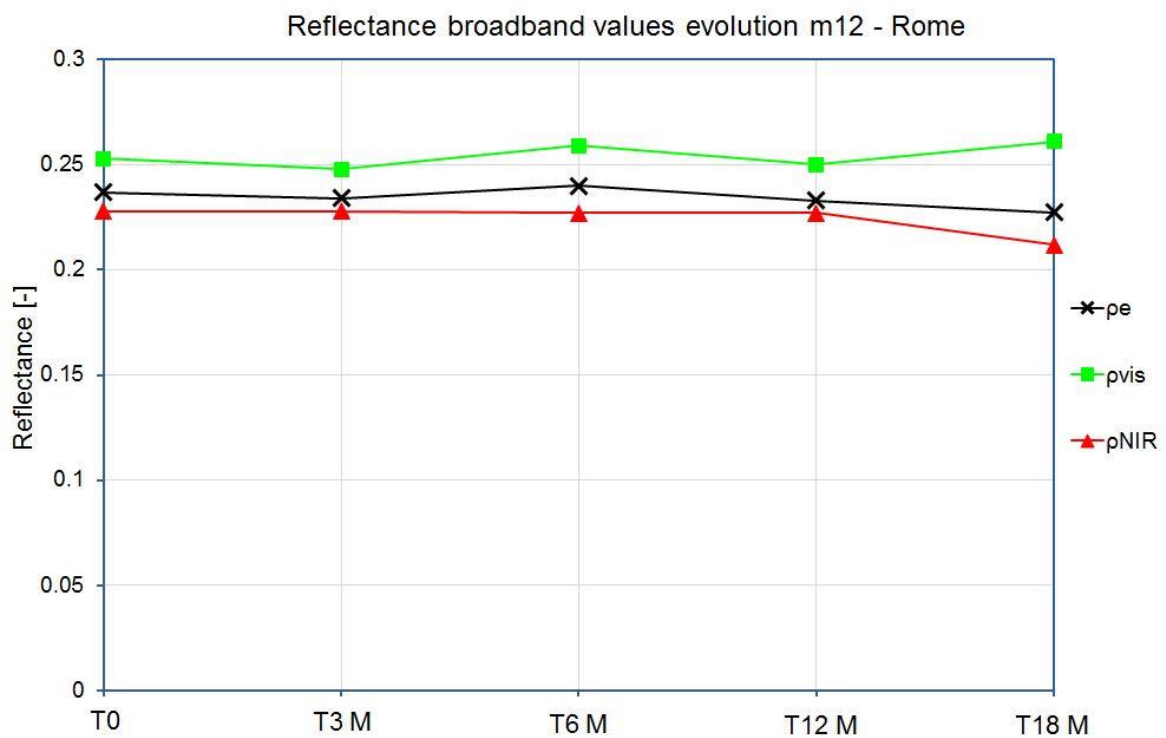


Figure 4.25: Reflectance broadband values evolution over time in solar, visible and NIR bands due to ageing and soiling for Rome - m14.

## Section 2: *Experimental and Numerical Analyses*

The considerations made for the spectral reflectance are even more evident for the broadband values.

In Figure 4.22 the sample m2 presents almost similar trends for the three broadband values, being the trend in the visible band the one with the higher variations.

In Figure 4.23 the trends of the three broad band values, for sample m7, are parallel putting in evidence similar variation as expected by the spectral data analysis.

The broadband values evolution for sample m12 in Figure 4.24 is interesting. While the solar and NIR broadband values decrease over time, the luminous reflectance fluctuates with small variations.

The behaviour of sample m14, in Figure 4.25, puts in evidence the variations in broadband values of luminous reflectance due to the soot depositing on the bituminous substrate of the shingle. Weather effects as rain carry away the layers of the hydrophilic soot cleaning the surface and inducing a small increasing in reflectance, as reported in a study previously cited [4.21].

## 4.5 Cool Roofs Energy Rating System Proposal

---

Improving the energy efficiency in the building sector is one of the key issues to achieve at national and EU levels, as communicated by the EU in the 2011 Energy Efficiency Plan and the 2020 Strategy, as well as in the 2011 Italian Energy Efficiency Plan. Even if characterised by a wide variety of climatic conditions, Italy energy policies were aimed at reducing the energy consumption related to space heating in buildings, neglecting other relevant energy uses (i.e. space cooling), which dramatically increased in the past years [4.22]. Similar trends can be observed in other countries for residential and commercial buildings. What is highly relevant, in this sense, are the requirements set by the EPBD 2010/21 / EU regarding the energy quality of buildings to be assessed by taking into account all the relevant energy uses.

Improving the energy performances on yearly basis requires the implementation of cooling efficient technologies in new and existing buildings.

Even if the cool roof technology is now a well-established technology, the market penetration is not yet effective. Policy instruments, as those developed in some countries, support the exploitation of the technology but the phenomenon remains limited to few examples, without adequately awarding the technology potentialities [4.23]. If energy policies or financial schemes do not support energy efficient measures, other solutions are needed. An exemplary case is the energy rating and labelling for window, implemented as a voluntary scheme, in several countries: Australia, Canada, Denmark, Sweden, United Kingdom, and USA. The rating is based on window performances related to heating, cooling, lighting and it can also be expressed using a global performance indicator. A preliminary study was carried out in Italy and similar activities are on-going in several EU countries, as well as at European level [4.24]. Where implemented, this instrument resulted to be an important wheel in driving the market towards more efficient energy related products. These instruments, moreover, are of relevance in the EU framework, as a matter of fact the Ecodesign Directive 2009/125/EU and the Energy Labelling Directive 2010/30/EU are extending the requirements not only to energy consuming products (e.g. light bulbs, refrigerators, washing machine, etc.) but also to energy related products. The latter including envelope products related to the energy performance of buildings, as: windows and insulating materials. The new framework is expected and will have a strong impact on the market in the next few years.

Even if the cool roof technology is not a priority among the different scheduled technologies according to the EU framework, the energy rating scheme for cool roof can be intended, at last, as a tool useful to facilitate the market penetration. The energy rating, moreover, allows to properly inform the end users about energy efficient solutions and to set the boundaries for the implementation of EU Directives in the coming years. Unlike products that directly use energy, the definition of a rating scheme for cool roof requires very in-depth analyses in order to take into account all the variables affecting the performance of the product and of the building it will be installed on.

### 4.5.1 Methodology

---

The building energy performances depend on several parameters: climatic conditions; building geometry and use; thermal and solar properties of the building envelope. At the same time, a successful energy rating scheme should be simple and general. Based on the experience of the existing windows energy rating and the findings of a related EU Project (Project EU-SAVE, 2000), the energy rating of an energy related products can be defined at four different levels:

1. Rating based on the relevant thermo-physical properties of the product;
2. Rating based on the energy balance of the product;
3. Rating based on the energy performance of the reference building equipped with the products;
4. Rating based on the energy performance of the actual building equipped with the product.



Level 1 and 2 do not provide any correlation between the product properties and the building performances. On the contrary, level 4 required too detailed data related to the building. To achieve the above mentioned objectives, the development of the energy rating method for cool materials was aimed at level 3, based on the effort to establish a direct relation between the energy performances of the building and its surface thermo-physical properties, without taking into account variables that are specifically building-dependent.

Cooling and heating energy calculations were performed in order to assess how different parameters affect the building and roof thermal response, taking into account all the parameters affecting the energy performance. The calculation results also provided the data set necessary to implement the mathematical functions and regressions, the energy rating should be based on. The variables analysed in the study are described below.

### 4.5.2 Climatic Conditions

The regulatory framework for the heating season is implemented since more than two decades, with small adjustments through the years (Decree DPR 412/93, 1993). The Italian territory is divided in six climatic zones as a function of the heating degree days, counted in base 20 °C. The zones range from A (degree days lower than 700) up to F (degree days higher than 3000). No legislative or technical standard officially exist yet for the cooling season. Nevertheless, a relevant technical pre-normative work has been carried out with the introduction of a climate severity index based on cumulative values of air temperature, specific humidity and solar irradiation during summer [4.25]. The index ranges from A (coolest zone in summer) to G (hottest zone in summer). Even if the summer zoning is not yet implemented, the data are useful for the selection of the reference localities. Three exemplary cities were selected: Palermo, with hot summer and mild winter; Rome, mild summer and mild winter; Perugia, mild summer and cold winter. The reference climatic data are reported in Table 4.6. The choice of Perugia as cold city depended on the focus given to the Mediterranean area of the country, where the cool roof technology has a major chance of market penetration, without considering the alpine and sub-alpine areas.

Table 4.6: Climatic parameters of the reference localities.

City	Winter climatic zone	Winter degree days	Summer climatic zone	Summer climate severity index
Palermo	B	720	F	2014
Rome	D	1440	E	1758
Perugia	E	2289	B	1536

### 4.5.3 The Reference Buildings

The main choice for the reference buildings was to consider a single flat instead of the whole structure, since most of the new and existing buildings use ambient regulation controls for heating and cooling systems. The following typical apartments were selected:

- Flat with two exposures, typical configuration of large and tower apartment blocks, see apartment highlighted in red (Figure 4.26 A);
- Flat with three exposures, typical configuration of small apartment blocks, see apartment highlighted in red (Figure 4.26 B);
- Flat with four exposures, typical configuration of detached houses (Figure 4.26 C).

The three building configurations differ in the extension of surfaces exposed to the outside and thus in the amount of thermal dispersion. Moreover the apartment characterised by four exposures is also directly in contact with the ground, further increasing the dispersion area. Higher surfaces of dispersion generally induce higher heating demands, but on the other hand, in summer

## Section 2: Experimental and Numerical Analyses

season facilitate dissipation of the heat stored in the building during the night. The base floor and the internal walls are adiabatic for the other two configurations; the roof is flat. The geometrical characteristics were summarised in Table 4.7.

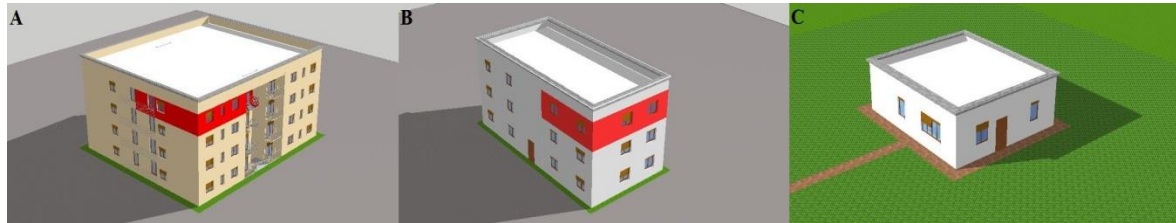


Figure 4.26: Apartments selected: (A) two external walls, (B) three external walls, (C) four external walls.

Table 4.7: Geometric characteristics of chosen reference buildings.

	2 External walls	3 External walls	4 External walls
Net floor area [m <sup>2</sup> ]	87	76.5	99.5
Gross Volume [m <sup>3</sup> ]	267.3	245.7	302.4
S/V Ratio [m <sup>-1</sup> ]	0.53	0.59	0.68
Internal Height [m]	2.7	2.7	2.7

Each building was created considering two insulation levels. The not insulated envelope was characterised by elements with the following thermal transmittances: 1.15 W / m<sup>2</sup> K for the external vertical walls, 1.13 W / m<sup>2</sup> K for the roof, 3.5 W / m<sup>2</sup> K for the window glass, and 3.48 W / m<sup>2</sup> K for the window frame.

The insulated envelope configuration, instead, presents an external wall thermal transmittance of 0.45 W / m<sup>2</sup> K, a roof thermal transmittance of 0.47 W / m<sup>2</sup> K, and window transmittance values of 2.42 W / m<sup>2</sup> K for the glass and 2.15 W / m<sup>2</sup> K for the frame.

Other settings, common to all the three considered building models, both non-insulated and insulated, were chosen according to the Italian standard reference for residential structures [4.26]. Internal gains were set to 4 W / m<sup>2</sup> (0.8 of radiative fraction) with a constant occupancy density of 0.04 persons / m<sup>2</sup>, metabolic rate: Seated, light work, according to standard reference [4.27]. Air change value was set to 0.3 volumes / h. Net energy demands were calculated considering a temperature set-point of 20 °C during winter and a temperature set-point of 26 °C and a relative humidity set-point of 60% during summer. The heating and cooling systems were maintained continuously turned on. Windows were equipped with low reflective shading slats horizontally tilted. The solar reflection and thermal emissivity of slats were set, respectively, to 0.2 and 0.9. The shading factor was controlled with a solar set-point: During summer the shading devices were enabled whenever the solar radiation value exceeded 150 W / m<sup>2</sup> and were always disabled during winter.

In order to evaluate the energy performances of cool materials, characterised by high solar reflectance and high infrared emissivity, used as roof covers, the reference buildings were analysed assigning three different values of roof solar reflectance, 0.2, 0.5 and 0.8, combined with three different values of thermal emissivity, 0.3, 0.6 and 0.9. Nine different pairs of roof radiative properties were hence considered in the calculation set.

### 4.5.4 Numerical Analysis

#### Software

A numerical analysis was performed using Design Builder in order to investigate the energy performances of a cool roof application. Design Builder is a graphical interface developed to make Energy Plus software more user-friendly [4.28]. The latter is a stand-alone software for thermal simulation in a dynamic regime of building-plant systems and returns outputs in energy



## Section 2: Experimental and Numerical Analyses

consumption, temperatures, and heat flows. In essence, Design Builder combines a calculation engine for energy simulations with dynamic modelling tools including also a simulation module for natural lighting and a CFD (Computational Fluid Dynamics) engine calculation. Moreover it provides the use of a solid modeller that allows assembling buildings models through the positioning, the stretch, and the blocks cut in three-dimensional space. Realistic three-dimensional elements determine a visual feedback of the element thickness and internal areas and volumes. Several geometric forms can be modelled as well as the optical and thermal properties of the surfaces. The templates allows loading into data projects the most common settings, activities, and HVAC (Heating, Ventilation and Air Conditioning) and lighting systems of buildings by simply selecting this feature from the drop-down lists. It is also possible to add or create customised templates. The choice of using this software is due to the necessity of obtaining energy demands pertaining to a whole year and especially the summer season. For this reason software capable of drawing up the thermo-physical phenomena hourly was necessary. As a matter of fact thermal analysis strictly limited to the winter period would be sufficiently accurate even using stationary calculation methods that process and return as results monthly average data. The same is not achieved in an analysis that covers a whole year since the stationary methods in this case are less accurate and have no general validity for the summer season yet.

### Numerical Analysis Results

More than 600 simulations were carried out, taking into account climate, building type and orientation, insulation level, and roof surface properties. The first screening to reduce the number of calculations was to assess the influence of the apartment orientation. A set of simulations was performed for the eight cardinal orientations, being the apartment configured with typical values of insulation and roof properties. The orientation, which emerged as the closest to the average of the eight orientations for the cooling and heating demand, was chosen as the reference, reducing to 162 the final number of simulations.

Explanatory histograms show the annual cooling, heating, and total (the sum of the first two) demands in Rome as a function of the building models under study, see Figure 4.27. It is important to notice that the increase in insulation affects especially the heating demands, also by decreasing the cooling ones even if in smaller amounts. The building with four exposures presents a higher heating demand and a lower cooling demand during the year for both insulation levels because of the larger dispersion surface. It is to be noted that the building with four orientations is the most energy-consuming for the non-insulated configuration, while the three-external-façade building has the highest energy consumption for the insulated configuration. Moreover it is to be noted that, in any case, the total energy demand is similar for the three configurations, since the energy performances of each building differ from the average value by less than 10%.

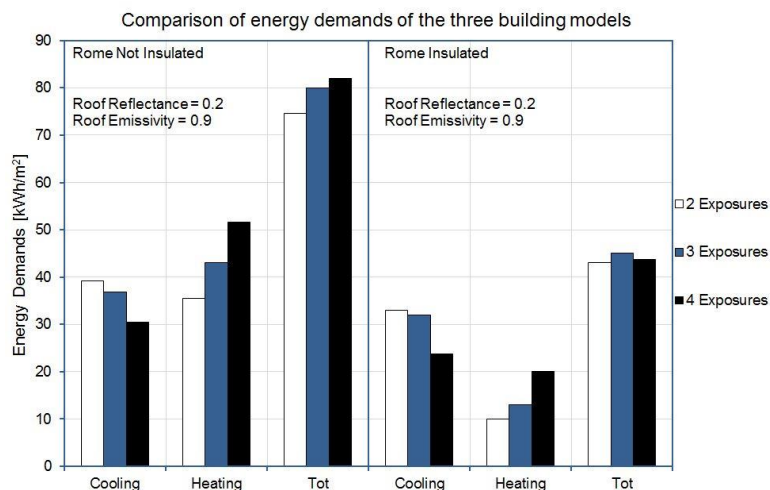


Figure 4.27: Annual energy demands for Rome, roof solar reflectance 0.2, roof emissivity 0.9.

## Section 2: Experimental and Numerical Analyses

Figure 4.28 shows the energy savings for the three building configurations. They were obtained by subtracting the global energy demands of a building with a roof reflectance of 0.8 from the global energy demands obtained for a building with a roof reflectance of 0.2. The thermal emissivity was maintained constant at a value of 0.9. As shown in the figure, the higher energy savings is related to the building configuration with two exposures. A negative value of energy savings was registered only for the four exposures of a non-insulated building, in Perugia. As a matter of fact, the building with four exposures is the most penalised during the cold season due to the dispersions.

In a similar way, in Figure 4.29, energy savings were obtained by subtracting the global energy demands of a building with a roof emissivity of 0.9 from the global energy demands obtained for a building with a roof thermal emissivity of 0.3, keeping the roof reflectance constant at a value of 0.5. Lower energy savings were obtained for all configurations when compared with the previous case. Negative energy savings were registered only in the non-insulated buildings mainly in Perugia for the three and four exposure buildings. A slightly negative value of energy savings was found also in Rome for the four exposure building.

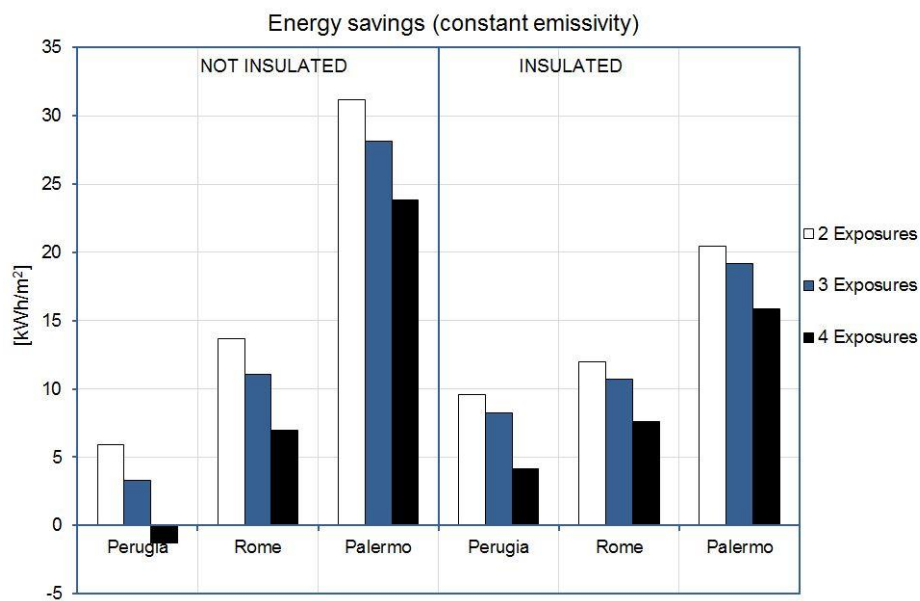


Figure 4.28: Difference in global energy demand changing roof reflectance from 0.2 to 0.8 (thermal emissivity = 0.9)

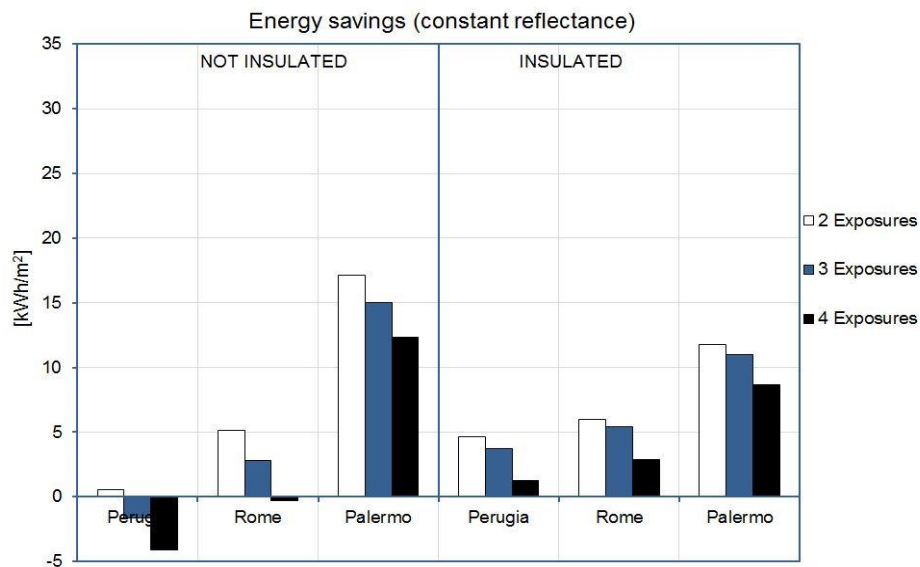


Figure 4.29: Difference in global energy demand changing roof emissivity from 0.3 to 0.9 (solar reflectance = 0.5)

## Section 2: Experimental and Numerical Analyses

In order to assess the large number of simulation results in a more simple and general way, from this point of the text it was decided to report only the average values of annual demands obtained for the three structure type, see Table 4.8. In Table 4.8 are reported the cooling, heating and total energy demands in kWh / m<sup>2</sup> as a function of solar reflectance ( $\rho_e$ ) and thermal emissivity ( $\epsilon$ ). The percentage variations of total energy demand were calculated relative to the configuration with roof reflectance 0.2 being equal the thermal emissivity. In cells reporting two values, the second one is the percentage variation relative to a roof with reflectance 0.2 and emissivity 0.3.

As shown in Figure 4.30 and Figure 4.31, an increase in both roof reflectance and roof emissivity can induce, during a year, a reduction in cooling demands and an increase in heating demands depending on climatic zone. These results were obtained by changing roof solar reflectance being equal infrared emissivity (Figure 4.30) and by changing roof emissivity being equal solar reflectance (Figure 4.31). Hence, in all cases an increase in solar reflectance and infrared emissivity of a roof induces savings during summer and energy losses during winter. However this last issue can be limited by increasing the insulation level of the building as shown in the figures by comparing the non-insulated case with the insulated one. In warmer climates the improvement of the energy performance of a building, due to an increase in reflectance and in emissivity, determines the most efficient results. In fact, the losses during winter may be limited near to zero by increasing the level of insulation of the building (i.e. the case of Palermo in Figure 4.30 and Figure 4.31).

Table 4.8: Design Builder results: Energy demands in kWh/m<sup>2</sup> as a function of solar reflectance ( $\rho_e$ ) and thermal emissivity ( $\epsilon$ ).

	$\rho_e$	$\epsilon$	Insulated [kWh/m <sup>2</sup> ]			Total Variation [%]	Not Insulated [kWh/m <sup>2</sup> ]			Total Variation [%]
			Cooling	Heating	Total		Cooling	Heating	Total	
Perugia	0.2	0.3	35.4	21.2	56.6	-	52.5	54.6	107.2	-
	0.5	0.3	25	24	49	13.4	31	63.1	94.1	12.2
	0.8	0.3	14.7	27.4	42.1	25.6	12.2	74.5	86.7	19.1
	0.2	0.6	27.7	24.7	52.4	-	37	64.4	101.4	-
	0.5	0.6	19.5	27.3	46.8	10.7	20.8	73.2	94	7.3
	0.8	0.6	11.4	30.8	42.2	19.5 - 25.4	7.9	84.1	92	9.3 - 14.2
	0.2	0.9	22.7	27.3	50	-	27.1	72.6	99.7	-
	0.5	0.9	16	29.8	45.8	8.4	14.6	81.2	95.8	3.9
	0.8	0.9	9.5	33.1	42.7	14.6 - 24.6	5.6	91.4	97.1	2.6 - 9.4
Rome	0.2	0.3	42.5	9.8	52.3	-	61.4	29.4	90.8	-
	0.5	0.3	31.4	11.9	43.3	17.2	38.7	35.7	74.5	18.0
	0.8	0.3	20.5	14.6	35.1	32.9	18.8	44.3	63.2	30.4
	0.2	0.6	34.7	12.3	47	-	45.7	37	82.7	-
	0.5	0.6	25.8	14.4	40.2	14.5	28.4	43.6	71.9	13.1
	0.8	0.6	17.2	16.9	34.1	27.4 - 34.8	13.5	52.2	65.7	20.6 - 27.6
	0.2	0.9	29.6	14.4	44	-	35.5	43.4	78.9	-
	0.5	0.9	22.2	16.3	38.6	12.3	21.8	50.1	71.9	8.9
	0.8	0.9	15.2	18.7	33.9	23.0 - 35.2	10.1	58.2	68.3	13.4 - 24.8
Palermo	0.2	0.3	62.8	0.4	63.1	-	90	5.2	95.2	-
	0.5	0.3	49.3	0.7	49.9	20.9	62.3	8.4	70.6	25.8
	0.8	0.3	35	1.2	36.2	42.6	35	13.2	48.2	49.4
	0.2	0.6	53.7	0.7	54.4	-	72	8.3	80.3	-
	0.5	0.6	42.5	1.1	43.6	19.9	49.3	12.1	61.4	23.5
	0.8	0.6	30.7	1.8	32.5	40.3 - 48.5	27.4	17.2	44.6	44.5 - 53.2
	0.2	0.9	47.6	1.1	48.7	-	59.5	11.4	70.9	-
	0.5	0.9	37.9	1.5	39.5	18.9	40.6	15.3	55.8	21.3
	0.8	0.9	27.9	2.3	30.2	38.0 - 52.1	22.6	20.5	43.1	39.2 - 54.7

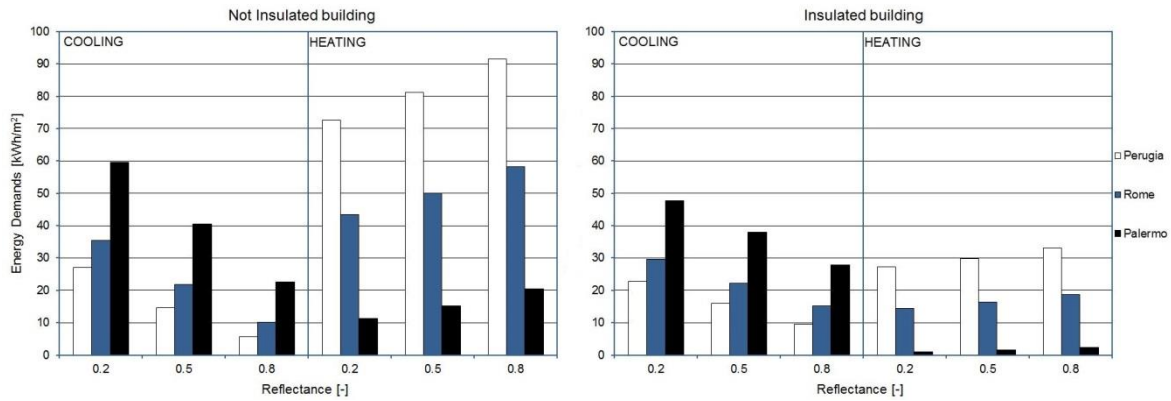


Figure 4.30: Impact of increasing roof reflectance on cooling and heating demands (emissivity = 0.9).

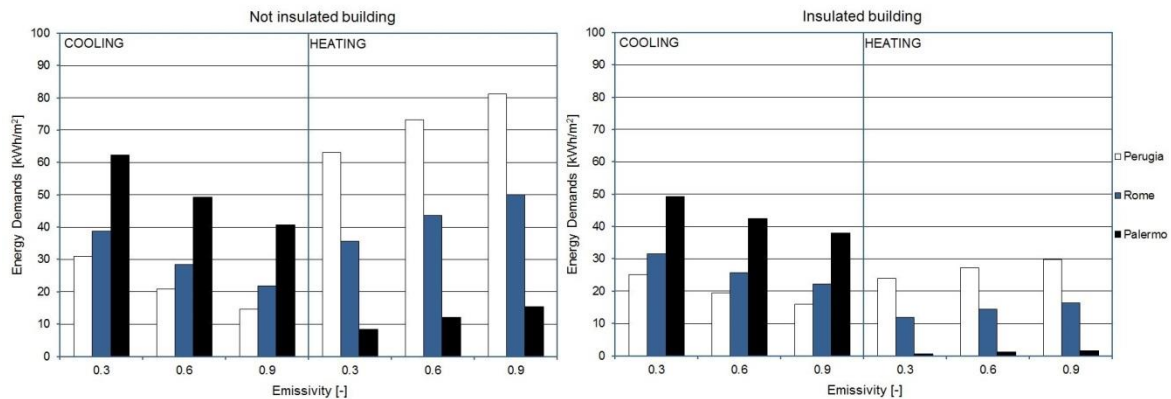


Figure 4.31: Impact of increasing roof thermal emissivity on cooling and heating demands (reflectance = 0.5).

### 4.5.5 The Rating Procedure

The simulation results were used to develop the regressions the energy rating should be based on. Observing the data, it can be inferred that heating and cooling demands affect the global demand in a different way as a function of the roof surface properties in the various climatic zones. Moreover the share of cooling and heating demand respect to the global energy demand dramatically depends on the insulation level for the three cities. Following the above considerations, a double track for the cool roof rating definition was implemented and it is presented in the next sub-chapters.

In the framework of the coming nearly-zero energy buildings and in order to skip the dependence on energy system efficiencies, the analyses are carried out considering on the net energy demand as provided by the simulations.

#### *Climate Dependent Energy Rating*

Three rating algorithms were implemented for the three selected climatic zones. A first analysis was carried out to check the impact of cool roof technologies on the global energy performances. The absolute value of the global energy demand in kWh / m<sup>2</sup> is strongly dependent on the insulation level, check Table 4.8. The results can be also be presented as energy savings normalised respect to the maximum energy demand (calculated for emissivity 0.3 and solar reflectance 0.2) for each climatic zone.

Figure 4.32 reports the normalised energy savings for the two configurations and it can be inferred that trend and figures are similar for the two insulation levels, for the Rome case. Similar results were obtained for Palermo and Perugia, for the latter small differences of global energy demand were calculated for the not insulated configuration and for the roof properties but the trend

## Section 2: Experimental and Numerical Analyses

was confirmed. For this reason the regressions were calculated starting from the global energy demand values obtained for the insulated configuration. This choice is also in accordance with the requirements of actual building codes in Italy.

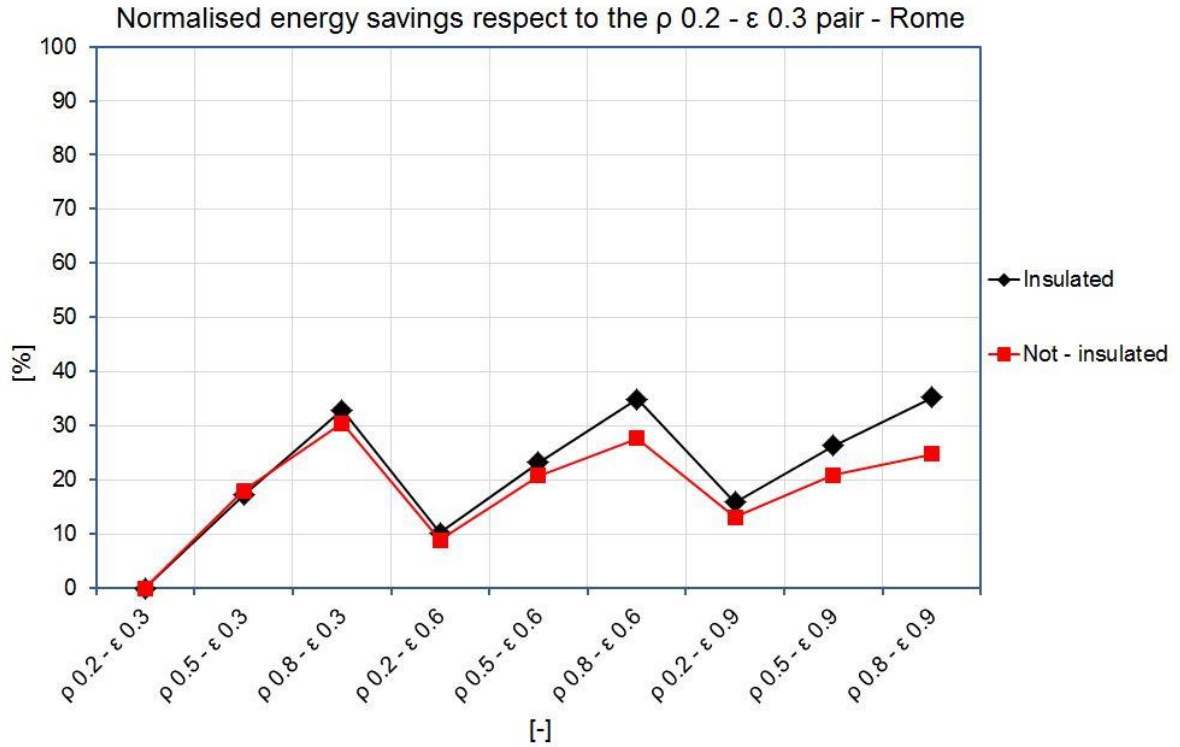


Figure 4.32: Comparison of the normalised global energy savings for Rome buildings.

Nine pairs of emissivity and solar reflectance values of the roof were considered in total. A linear regression for heating and one for cooling were calculated, and then combined together in a single equation for each climatic zone. The equations for the three climatic zone are (having indicated with  $\rho_e$  the solar reflectance and with  $\epsilon$  the emissivity):

$$\begin{cases} E_{H,i} = \beta_{0,i} + \beta_{1,i}\rho_e + \beta_{2,i}\epsilon + z_{1,i} \\ E_{C,i} = \beta_{3,i} + \beta_{4,i}\rho_e + \beta_{5,i}\epsilon + z_{2,i} \\ E_{TOT,i} = E_{H,i} + E_{C,i} \end{cases} \quad (4.2)$$

where  $i$  = Perugia, Rome, Palermo.

The estimation results were derived through the econometric software STATA 11 [4.29] and present excellent r-square values for each equation, ranging from 0.964 for the heating season in Perugia to 0.995 for the cooling season in Rome. Very high values for the  $\chi$ -square statistics ensure the statistical significance of each equation as a whole as well as the very good values of the standard errors for the single parameters within each of them. Combining them together in a single equation for each climatic zone, the equations are:

$$E_{TOT,Perugia} = 59.66 - 17.53 \cdot \rho_e - 5.65 \cdot \epsilon \quad (4.3)$$

$$E_{TOT,Rome} = 56.87 - 22.32 \cdot \rho_e - 7.96 \cdot \epsilon \quad (4.4)$$

$$E_{TOT,Rome} = 73.00 - 38.33 \cdot \rho_e - 16.00 \cdot \epsilon \quad (4.5)$$



### Climate Independent Cooling Energy Rating

Figure 4.33 shows the specific cooling demand (the crosses) for the three localities and for the insulated configuration. The results depend on the climatic zones, since significant differences can be found for the three cities and, in particular, between Palermo and the other two localities. The same results can be normalised respect to a climatic indicator as shown in Figure 4.33, secondary Y-axis (red dots). Normalising the specific cooling demand to the Cooling Degree Days, calculated with base 10°C, a more uniform trend was obtained for the three data sets. The Degree Days are an output of the Design Builder.

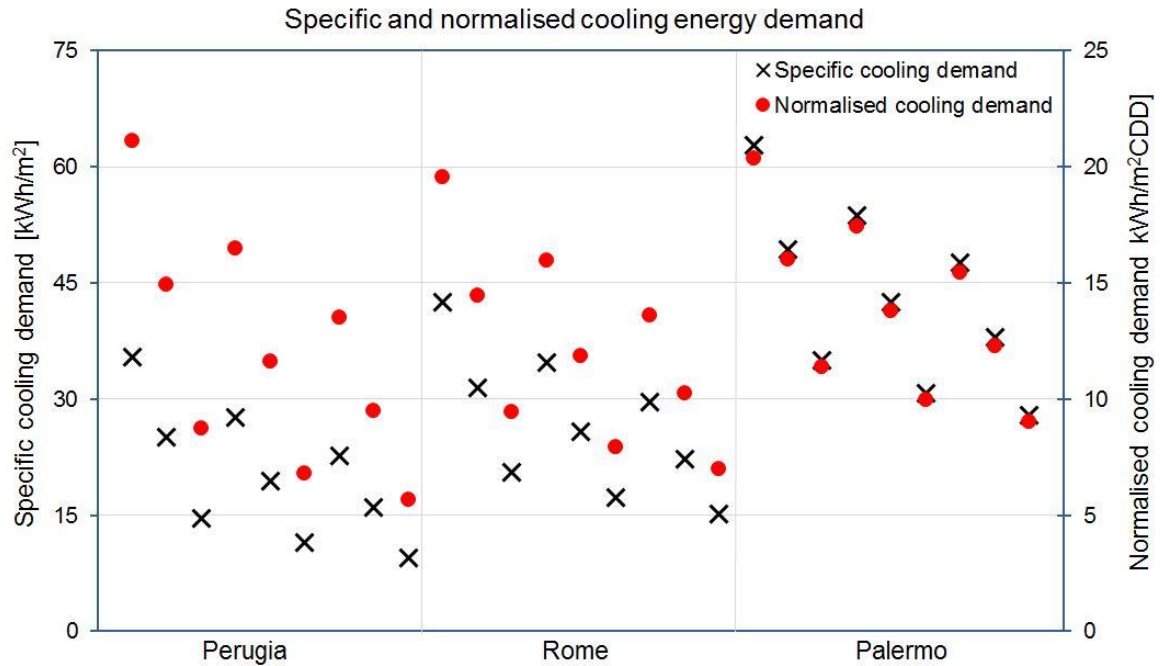


Figure 4.33: Effect of the cooling degree days normalisation on the climate dependence of the energy performances.

The normalised 27 points (9 pairs of emissivity and solar reflectance values for 3 cities) were used to derive a three-stage least squares estimation of the following structural linear equation:

$$NEP_{cool} = \beta_0 + \beta_1 \rho_e + \beta_2 \varepsilon + \beta_3 \rho_e \varepsilon + z \quad (4.6)$$

where the indicator, expressing the net energy performance of the cool roof product in Italy for the cooling season ( $NEP_{cool}$ ), is a function of thermal emissivity ( $\varepsilon$ ), solar reflectance ( $\rho_e$ ), and the interaction term ( $\rho_e \varepsilon$ ) between the two aforementioned variables.

Several regression models were tested, including different powers for reflectance and emissivity; the best result was obtained with the following equation which includes the aforementioned interaction between the two physical properties:

$$NEP_{cool} = 27.32 - 20.35 \cdot \rho_e - 12.35 \cdot \varepsilon + 10 \cdot \rho_e \varepsilon \quad (4.7)$$

The r-square value of the regression is 0.94, which can be considered satisfactory according to the simplicity of the model. The relative error between the simulation and regression values is lower than 15% in 24 of 27 points, see Figure 4.34. Higher discrepancies are generally found for high solar reflectance values, being lower the global energy demand.

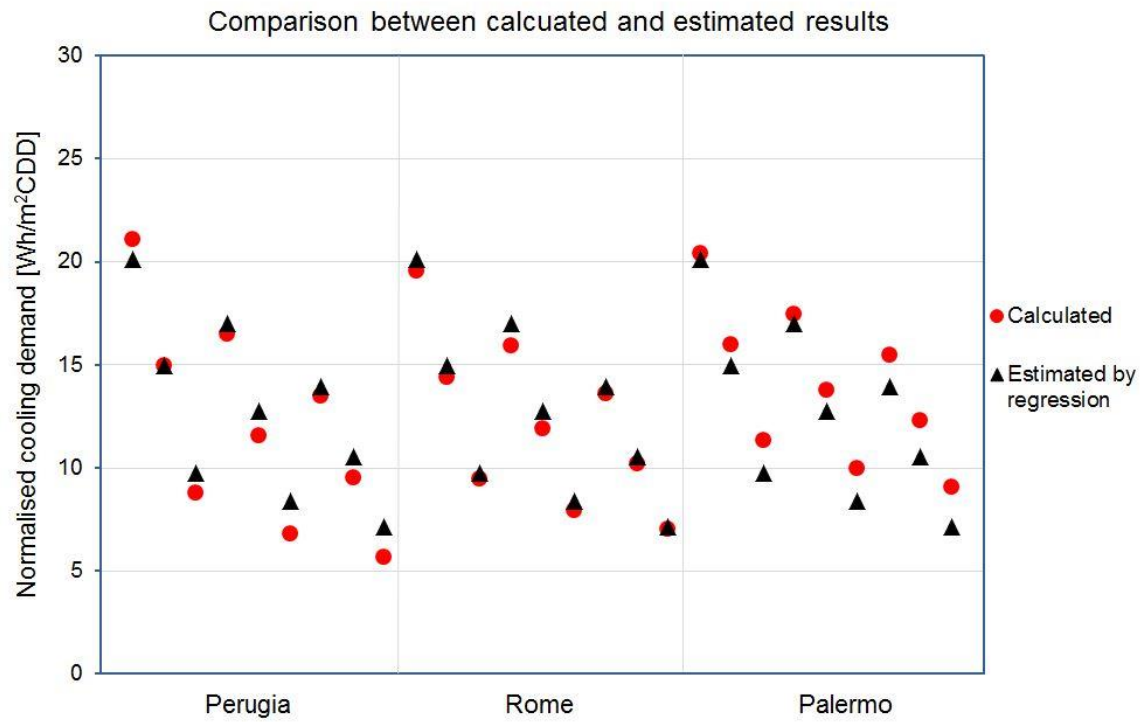


Figure 4.34: Comparison of the normalised cooling demand as obtained by simulations and as estimated by regression.



## 4.6 Chapter Conclusions

---

The findings reported in this chapter demonstrate the potentialities of cool roofs as an effective passive technique to increase the comfort levels and decrease the energy demands in residential buildings.

The tests carried out on the case study were very exhaustive. The surface temperatures of the cool membrane is in average 20 °C lower than the primary shingle surface temperature during solar peak inducing a decrease in the dispersed heat flux entering in the building through the roof leading to a sensible decrease of the indoor environment temperature in average of 2.5 °C.

The numerical analyses performed on the case study have reported that insulated building are less sensible to the benefits due to a roof reflectance increasing.

However extending the energy calculation to the whole year considering also winter, an increase in insulation level leads to lower heat losses due to an increased roof reflectance. Further numerical analysis on typical residential building have resulted in positive global annual energy savings mainly depending on latitude. In warm climates the found percentage decreasing in energy demands reached values higher than 50% for insulated and not insulated buildings increasing both solar reflectance and thermal emissivity of roofs.

One of the main flaws of this technology is its durability over time. The experimental campaign, carried out in two exposures Italian sites aimed at evaluating the influence of natural ageing and soiling on decay of solar reflectance of roofing materials, highlighted how this decay affects mainly the membranes with an initial solar reflectance higher than 0.8. Nonetheless in many cases spectral data measured after 12 and 18 months demonstrate a convergence trend with broadband values however higher than that of conventional materials. A numerical analysis demonstrated that the decrease effect of the reflection power of these materials for building coating affects over time their surface temperature increase, boosting the cooling energy demand and power supply peaks during summer [4.30].

The national energy policy shows a lack in the energy rating of these materials used as roof coatings. For this reason a rating system was proposed and developed starting from the results of numerical analysis on three reference buildings. According to the available data two options were proposed: a climate dependent rating, assessing the performance of cool roof throughout the whole year; an independent climate rating, actually developed for the cooling season only. The regressions are hence suitable for rating the cool roof products and define the efficiency classes in case of energy labelling. First results of the study were promising and the research is ongoing, aimed at refining the actual algorithms as a function of more populated data sets and other more accurate normalisation procedures.

## 4.7 References

---

- [4.1] Synnefa A, Santamouris M, Livada I. 'A study of the thermal performance and of reflective coatings for the urban environment'. *Solar Energy*; 2006; 80: 968 - 981.
- [4.2] Zinzi M, Fasano G. 'Properties and performance of advanced reflective paints to reduce the cooling loads in buildings and mitigate the heat island effect in urban areas'. *International Journal of Sustainable Energy*; 2009; 28 (1): 123 - 139.
- [4.3] Levinson R, Berdahl P, Akbari H. 'Spectral solar optical properties of pigments Part I: model for deriving scattering and absorption coefficients from transmittance and reflectance measurements'. *Solar Energy Materials and Solar Cells*; 2005; 89: 319 - 349.
- [4.4] Levinson R, Berdahl P, Akbari H. 'Spectral solar optical properties of pigments Part II: Survey of common colorants'. *Solar Energy Materials and Solar Cells*; 2005; 89: 351 - 389.
- [4.5] Zinzi M, Daneo A, Fanchiotti A, Trillò A. 'Optical properties and influence of reflective coatings on the energy demand and thermal comfort in dwellings at Mediterranean latitudes'. *Proceedings of PLEA 2008; 25th Conference on Passive and Low Energy Architecture*, Dublin, Ireland; 2008.
- [4.6] Karlessi T, Santamouris M, Apostolakis K, Synnefa A, Livada I. 'Development and testing of thermochromic coatings for buildings and urban structures'. *Solar Energy*; 2009; 83: 538 - 551.

## Section 2: *Experimental and Numerical Analyses*

- [4.7] EUROPEAN COOL ROOF COUNCIL. <http://coolroofcouncil.eu>; available online at.
- [4.8] ISO 9050. Glass in building-Determination of light transmittance, solar direct transmittance, total solar energy transmittance, ultraviolet transmittance and related glazing factors; 2003.
- [4.9] TRNSYS 16. <http://www.trnsys.com>; available online at.
- [4.10] Decreto Legislativo 19 Agosto 2005, n.192. Attuazione della direttiva 2002/91/CE relativa al rendimento energetico nell'edilizia.
- [4.11] Rosenfeld AH, Akbari H, Romm JJ, Pomerantz M. 'Cool communities: strategies for heat island mitigation and smog reduction'. Energy and Buildings; 1998; 28: 51 - 62.
- [4.12] Levinson R, Akbari H, Konopacki S, Bretz S. 'Inclusion of Cool Roofs in non – residential. Title 24 Prescriptive Requirements'. Energy Policy; 2005; 33: 151 - 170.
- [4.13] Synnefa A, Santamouris M, Akbari H. 'Estimating the effect of using cool coatings on energy loads and thermal comfort in residential buildings in various climatic conditions'. Energy and Buildings; 2007; 39: 1167 - 1174
- [4.14] Zinzi M. 'Cool materials and cool roofs: Potentialities in Mediterranean buildings'. Advances in Building Energy Research; 2010; 4: 201 - 266.
- [4.15] Moise N, Rogers M, Rush J, Shah P. 'Cleveland Department of Public Health, Annual Air Quality Monitoring Report'. City of Cleveland: Department of Public Health, Division of Air Quality. [http://www.clevelandhealth.org/assets/documents/health/communicable\\_disease/air\\_quality\\_report\\_2010\\_final\\_draft.pdf](http://www.clevelandhealth.org/assets/documents/health/communicable_disease/air_quality_report_2010_final_draft.pdf); available on line at; 2010.
- [4.16] Berdahl P, Akbari H, Rose LS. 'Aging of reflective roofs: soot deposition'. Applied Optics; 2002; 41(12): 2355 - 2360.
- [4.17] IGLAE. Codice di pratica delle impermeabilizzazioni (Practice code for waterproofing. In Italian). Istituto per la Garanzia dei Lavori Affini all'Edilizia. <http://www.iglae.org>; available online at; 2012.
- [4.18] SIA, SIA 271. 2007. Waterproofing for buildings. Swiss Society of Architects and Engineers. Zurich (CH).
- [4.19] Sleiman M, Ban - Weiss G, Gilbert HE, Francois D, Berdahl P, Kirchstetter TW, Destailats H, Levinson R. 'Soiling of building envelope surfaces and its effect on solar reflectance - Part I: Analysis of roofing product databases'. Solar Energy Materials and Solar Cells; 2011; 95: 3385 - 3399.
- [4.20] California Energy Commission, Building Energy Efficiency Standards for Residential and Non-residential Buildings. <http://www.energy.ca.gov/2008publications/CEC-400-2008-001/CEC-400-2008-001-CMF.PDFS>; available online at; 2009.
- [4.21] Berdahl P, Akbari H, Levinson R, Jacobs J, Klink F, Everman R. 'Three-year weathering tests on asphalt shingles: Solar reflectance'. Solar Energy Materials and Solar Cells; 2012; 99(special issue): 277 - 281.
- [4.22] Rapporto Energia e Ambiente, ENEA; 2012.
- [4.23] California code of regulation, Vol. 15, Title 11.
- [4.24] Maccari A, Zinzi M. 'Simplified algorithms for the Italian energy rating scheme for fenestration in residential buildings'. Solar Energy; 2002; (69 Suppl.): Nos. 1 - 6, 75 - 92.
- [4.25] Iatauro D, Federici A, Signoretti P, Terrinoni L, Romeo C. 'Climatic Severity Index: Definition of summer climatic zones in Italy through the assessment of air conditioning energy need in buildings'. 2013.
- [4.26] UNI TS 11300 – 1. Determinazione del fabbisogno di energia termica dell'edificio per la climatizzazione estiva ed invernale; 2008.
- [4.27] UNI EN ISO 7730. Ergonomia degli ambienti termici - Determinazione analitica e interpretazione del benessere termico mediante il calcolo degli indici PMV e PPD e dei criteri di benessere termico locale; 2006.
- [4.28] Design Builder – Energy Plus. [www.designbuilder.co.uk](http://www.designbuilder.co.uk); available online at.
- [4.29] STATA11. StataCorp. [www.stata.com](http://www.stata.com); available online at; 2009.
- [4.30] Paolini R, Zinzi M, Poli T, Carnielo E, Fiori M, Mainini AG. 'Evolution over time of UV-VIS-NIR reflectance of cool roofing materials in urban environments'. In: 34th AIVC Conference, Athens, Greece; 2013.

## 5. Cool Paving

---

### 5.1 Topic

---

This chapter is aimed at evaluating the potentialities of cool paving on mitigation of urban heat island effect. The experimental and numerical analyses were presented as follow:

- First of all, the UHI (Urban Heat Island Intensity) was monitored by means of an outdoor experimental campaign on summer temperature values in several sites of the city of Rome.
- Optical and solar characterisations were carried out on tints used as asphalt and concrete paving coatings.
- The experimental results were integrated in numerical models to evaluate the influence of these materials on the urban environment temperatures.

### 5.2 Introduction

---

Paving plays an important role in the overall energy balance of an urban area because they represent a significant portion of the built-up surfaces. Based on a survey conducted in several cities in the United States, the percentage of paving ranges between 29 and 45% [5.1]. Streets, pavement, parking lots and pedestrian areas are generally composed by cement and asphalt, and sometimes by aggregate stone. The solar reflectance of this wide variety of materials ranges from 5% to 45%, even if the default values are: 5% for new asphalt (the black tar covers uniformly the aggregate), 15% for "aged" asphalt (the aggregate emerges on the asphalt surface), 25% for concrete.

## Section 2: *Experimental and Numerical Analyses*

While cool materials used as roof coatings (cool roofs) are now a proven technology, this cannot yet be said for cool paving, designed for applications on the urban fabric. This depends on the fact that the development of this technology in the latter case seems to be more complex. Moreover there are three factors to consider:

- Urban activities (general massive use of a road surface, both for pedestrians and for cars), require a more extensive thermo-physical study of surfaces related to wear phenomena; convective motions considering the presence of moving objects; shading effects conditioned by the number of people, road traffic and buildings shape;
- Surface temperatures of asphalts and concretes used for paving are affected by thermal and radiative characteristics and, unlike the case of a cool roof, the radiative properties are the most relevant;
- Road paving must meet different functionalities within an urban area. Their use ranges from trails to busy motorways, while the cool roofs have the same function and generally do not require specific mechanical properties.

However cool pavements present high potentialities linked to the reduction of power consumption resulting from cooling systems and quality air improvement [5.2 - 5.8]. They can be designed as tints to be applied directly on the existing asphalt or as materials composed of concrete which present a high reflectance, higher to that of conventional asphalt, and a permeable structure [5.9]. In fact, although originally designed for the control of storm waters, draining surfaces are emerging as potential "cool materials". Draining surfaces can be classified as follows: porous asphalts, drain concretes and some special paving for sidewalks. Given that the main goals are permeability and structural requirements related to the type of traffic expected, these paving must be supported both by an efficient design and by a suitable installation [5.10].

These surfaces allow to store wet air and water in their interstices. During particular climatic conditions, they allow to limit the raising of their surface temperature, due to solar loads, through evaporation. In fact the water stored during rains inside the cavities and porosities of their structure serves as a reservoir of latent heat. The irradiated solar energy is employed in the water vaporisation and only a minor fraction remains to warm the surfaces. This phenomenon is quite similar to evapotranspiration operated by vegetation. For this reason, there are some draining paving systems which are integrated with grass or bush vegetation.

The surface conformation of these products can also affect the values of environmental temperature. In fact, a high number of cavities lead to an increase in the shadows over a wide area. These conditions may limit the processes of heat transfer to the substrate, subjecting in any case the outer surface to the heating caused by solar radiation, but reducing the accumulation of heat and the consequent release during the night hours.

The phenomenon of night heat release is one of the most significant contributions that lead to the urban heat island. On this topic, there are several studies of universities and research institutes which are focused to assess the real benefits associated with the use of permeable materials on the urban scale [5.11, 5.12].

The surface temperature of a road pavement depends on many factors. Reflective surfaces would limit solar gains and permeable materials would allow to exploit the evaporation of the accumulated water to keep cool, as mentioned earlier. However, beyond solar reflectance, thermal emissivity and drain power there are multiple thermo-physical factors that affect the properties of materials used for the coverage of the road surface: thermal conductivity, thickness of layers, heat capacity and convection. In particular the last one depends on the air speed, on its temperature near the surface and on roughness. Some draining paving have much rougher surfaces than conventional paving and this causes an increase of the effective area and turbulence, leading to a more efficient convective thermal exchange. However the roughness and the presence of voids tend to reduce the reflection power.

### 5.3 The Urban Heat Island effect

The indiscriminate development of urban areas and the proportion between built-up areas and green areas within urban texture play a crucial role in relation to cities climate change. Within the scope of the definition of new sustainable models, it is necessary to take into account urban density and built-up environment design. Based on the studies carried out by a major energy agency [5.13], in 2030 over 80% of the world's population will reside in urban areas. For this reason, energy studies focused on energy saving and public and environmental health must be conducted at urban scale. The problem is recurrent as climate changes and, in particular, global warming directly affects the temperatures of urban areas through more frequent and longer heat waves. This phenomenon induces a size increase together with an enhanced use of air conditioning systems and it results in an energy consumption increase for final electric uses and in the increase of greenhouse gas emissions into the atmosphere.

The Urban Heat Island (UHI) is a particular phenomenon that can be found within cities with an intensity which is proportional to the density of population. It can be described as the increase in air temperature in urban areas compared to rural areas characterised by lower temperature profiles. Essentially it is an environment modification caused by human actions. UHI intensity (UHII) is defined as the maximum difference between the hourly dry bulb air temperatures measured contemporarily in an urban area and in a reference rural area, as shown in equation 5.1.

$$UHII = (T_U - T_{RR})_{MAX} \quad (5.1)$$

having indicate with  $T_U$  the temperature of the urbanised site, while with  $T_{RR}$  the temperature of the rural reference site.

Obviously UHI is not constant throughout the year and it depends on several parameters: climatic conditions, concentrations of pollutants, population density, etc. The first studies on this subject date back to the XIX century with Luke Howard [5.14], even if most of the currently available literature dates back to more recent times demonstrating that daytime and daily urban heat islands range between 2 °C and 6 °C [5.15 - 5.21]. The heat island is determined by various caused that can be summarised as follows:

- Lack of evapotranspirative surfaces (i.e. vegetation): the built-up surfaces do not allow the water storage limiting the quantity of solar energy used for the evaporation. This facilitates an accumulation of heat;
- Minor effects related to the wind: this is due to the presence of tall and massive structures that act as a wind barrier increasing the turbulence and decreasing the speed;
- Urban surfaces have a high power of absorption of solar radiation (absorptance between 0.7 and 0.9). The high thermal emissivity helps the re-emission of the heat accumulated during the day leading to a rise of air temperature;
- Urban canyons: the proximity of vertical surfaces to other vertical surfaces caused phenomena of multiple reflections and the absorbed radiation is re-emitted with an high wavelength but it is trapped inside the canyon due to the low view factor of the sky;
- HVAC systems: the high temperature induces the increasing of use profiles of cooling systems. The outdoor units of these systems pump in hot air into the atmosphere.

The air temperature rise is certainly the main effect of the urban heat island, but it is not the only one. Its influence on the urban microclimate can be found also observing other factors: relative humidity decrease, greater difficulty in dispersing pollutants in the atmosphere, slight increase in rainfalls, and increase of the number of freeze and thaw cycles in cold climates that have a bad impact on the life of building components.

## Section 2: *Experimental and Numerical Analyses*

The discomfort increase for the population implies also a series of problems related to energy management at building and urban scale:

- Energy consumption increase for summer air conditioning of buildings;
- Rise of peak demand for summer air conditioning and, therefore, the size increase of refrigerating systems to install;
- Consequent increase in energy costs;
- Risks to the energy supply at a large scale during peak loads;
- Reduction of the effectiveness of passive cooling strategies that would allow to reach higher indoor comfort levels without recurring to mechanical systems.

The critical nature of this phenomenon is demonstrated in RAEE (Rapporto Annuale Efficienza Energetica) drawn up by ENEA from data provided by MSE (Ministero dello Sviluppo Economico). It shows a sensible increasing trend in electricity consumption in the civil sector in the last two decades [5.22]. The constant increase in sales of compact units for air conditioning of residential environments is a further sign of this problem, as well as the widespread and growing demand for comfort from the growing population.

Several strategies and techniques for the mitigation of UHI have been proposed. Among all of them, the mostly reported are:

- Increase in reflectivity of surfaces (this technique is the object of the following chapter) [5.23 - 5.27];
- Increase in green areas (green roofs, green vertical building envelopes, increase of number of trees, urban parks) [5.28 - 5.36];
- Improvement of urban design [5.37, 5.38];
- Urban shadings [5.39];
- Reduction of energy demand for air conditioning [5.40].

### 5.3.1 Measurement of the Intensity of the Urban Heat Island in the City of Rome

---

The intensity of the heat island in the city of Rome was monitored in 2011 during the summer season. The temperature data were obtained by means of seven units composed by a thermo-hygrometric sensor and a data reader housed in a waterproof container. The equipment was provided by the UTEE (Unità Tecnica Efficienza Energetica) of the ENEA Casaccia Research Centre.

One of the devices was located in a rural area in the north of Rome, while the others were all located in densely urbanised areas within the city. Figure 5.1 shows the city of Rome and the positioning of the seven thermo-hygrometers. The yellow circle highlights the most densely urbanised area.

Table 5.1 shows the operating ranges of data reader devices. The detected values of temperature and humidity were compared in the period from July 13 to August 13. This choice was an obligatory choice and this is due to two reasons: In site n.3 (Monte Verde) it was possible to place the thermo-hygrometer only on July 12; the data reader device n. 1 (ENEA Casaccia Research Centre) corresponding to the rural reference site broke on August 14 and this problem has not allowed to compare the data with the urban sites ones for a longer period.

Table 5.2 shows the maximum temperatures detected by the sensors with an acquisition time of ten minutes, the hour and the day of acquisition.



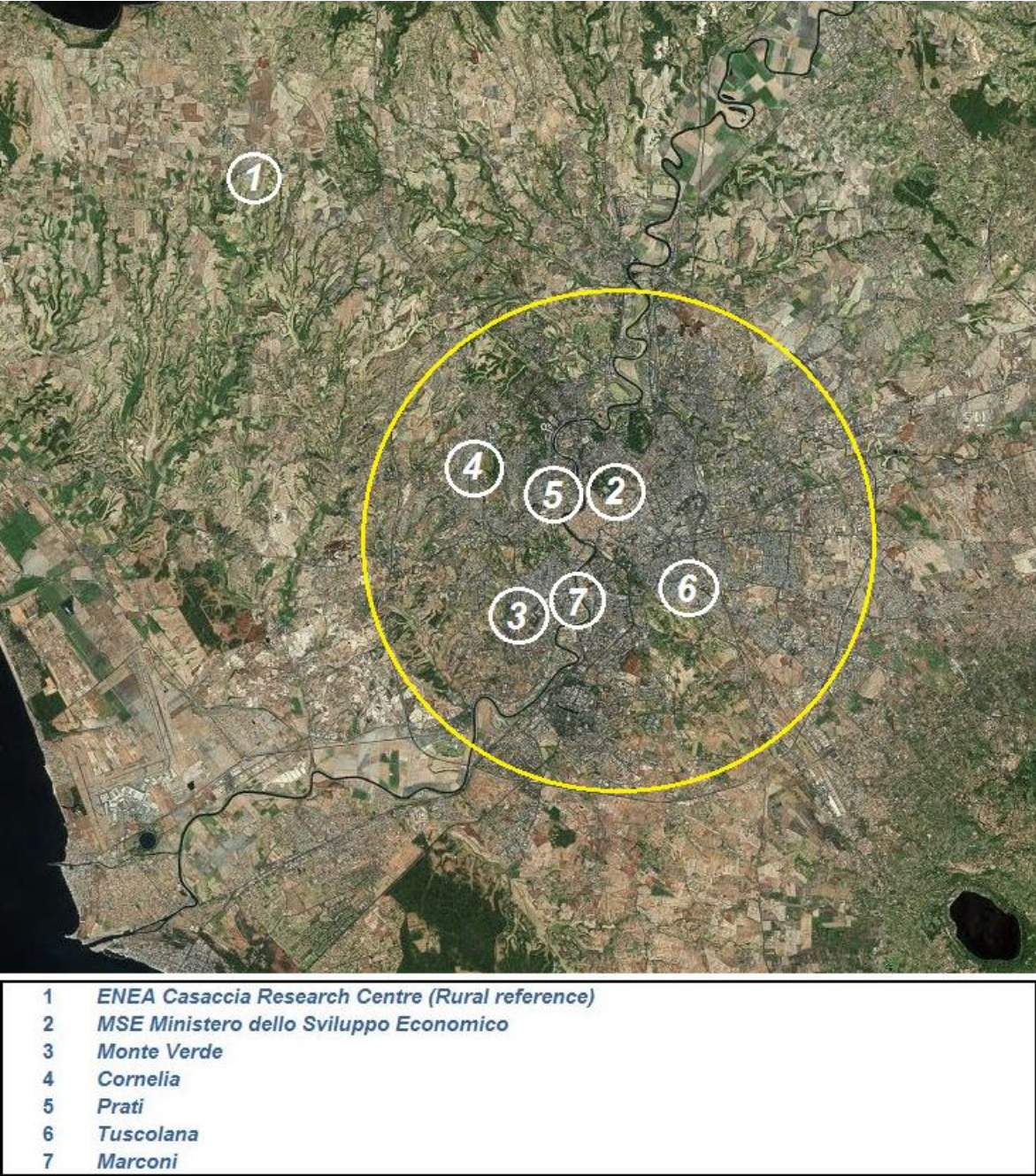


Figure 5.1: Thermo-hygrometric sensors positions in the Rome urban area.

Table 5.1: Data reader operating ranges.

N.	Position	Hour	Start		Hour	End	
			Day	Month		Day	Month
1	ENEA Casaccia Research Centre	19:20	16	6	10:30	13	9
2	MSE Ministero dello Sviluppo Economico	14:30	1	7	19:20	13	9
3	Monte Verde	17:40	12	7	16:40	10	11
4	Cornelia	15:00	17	6	22:00	11	11
5	Prati	17:30	16	6	20:10	30	11
6	Tuscolana	19:00	25	6	09:50	16	11
7	Marconi	15:00	17	6	16:40	21	11



## Section 2: Experimental and Numerical Analyses

Table 5.2: Maximum temperature detected.

N.	Position	Maximum Temperature [°C]	Hour	Day	Month
1	ENEA Casaccia Research Centre	35.4	15:40	13	7
2	MSE Ministero dello Sviluppo Economico	39.6	14:20	22	8
3	Monte Verde	38.8	11:20	23	8
4	Cornelia	37.2	15:30	13	7
5	Prati	41.1	12:40	23	8
6	Tuscolana	39.1	14:00	22	8
7	Marconi	39.3	15:30	13	7

Through the analysis of the measured data it was possible to construct a diagram, shown in Figure 5.2, which represents the cumulative percentage distribution of temperatures in the different sites of interest. It was counted the number of hours in the period in which the temperature is equal or exceeds a predetermined value. Then it has been calculated the percentage that the number of hours represents if compared to the monitoring period considered.

The substantial difference between the reference rural site n.1 (ENEA Casaccia Research Centre) and urban sites is clearly visible. In particular, it can be found that in site n.1 the temperature never exceeds 36 °C, which is the case for all other sites. The most critical site is n.5 (Prati) in which for the 32% of the time the temperature is higher than 28 °C. Furthermore, for more than 18% of the monitoring period, temperature stayed above 30 °C. Site n. 4 (Cornelia) has the lowest percentages among urban areas and this is justified by the presence of a broad pine forest adjacent to the site of placement of the device.

The difference between the average daily temperatures of urban sites and the ones of the reference site 1 has been reported in Figure 5.3. Site n. 5 (Prati) turns out to be the most critical area. In fact it records the highest average daily temperature difference, which is 4.7 °C on August 7. It is followed by: Sites n. 2 (MSE) and n. 3 (Monte Verde), with a value of 4.2 °C recorded respectively on July 14 and on August 7; site n. 6 (Tuscolana) with 4 °C on July 18 and August 7; and finally sites n. 4 (Cornelia) and n. 7 (Marconi) with peak values very close to 3.5 °C. The figure shows also how site n. 4 is the area where the smaller differences were found compared to the rural site reference, always due to the favourable effect of mitigation of temperatures which is linked to the massive presence of vegetation in that area.

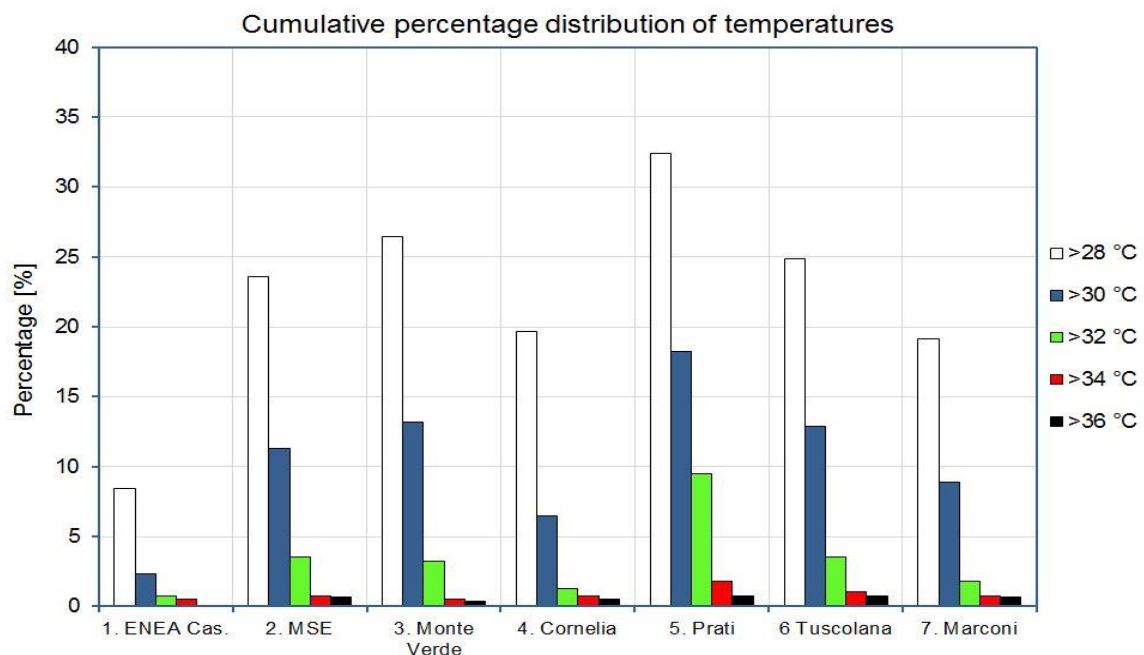


Figure 5.2: Cumulative percentage distribution for the investigated sites.

## Section 2: Experimental and Numerical Analyses

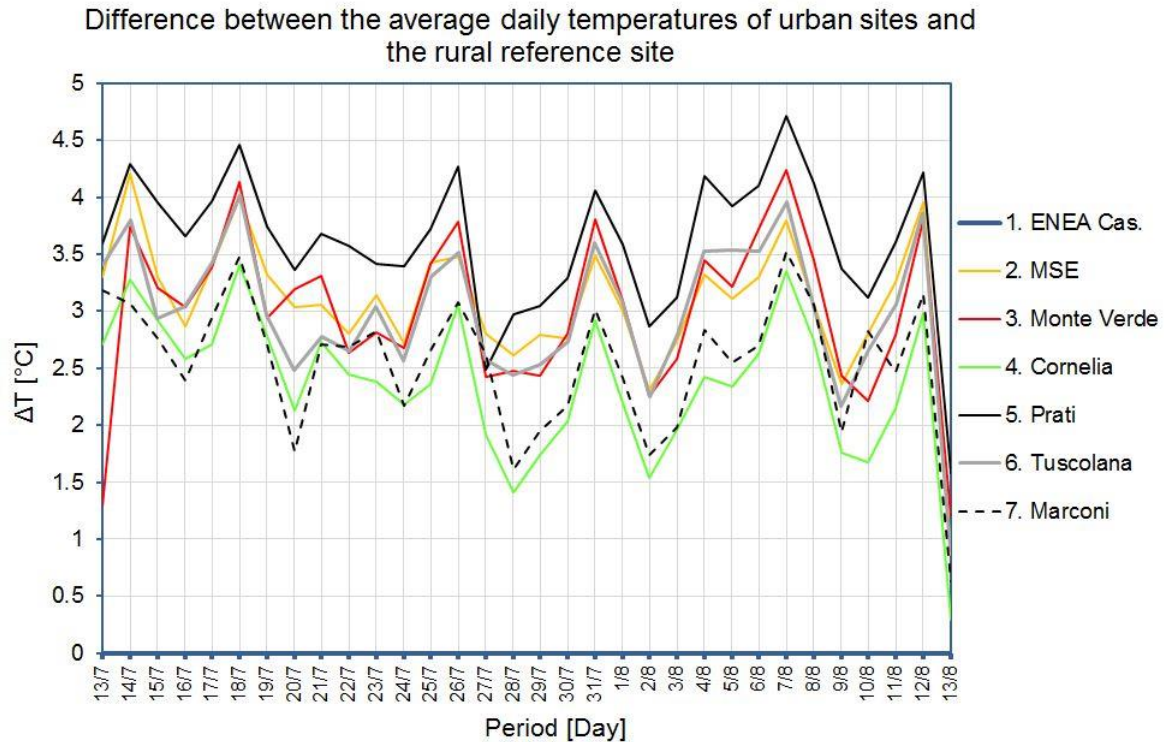


Figure 5.3: Daily temperature differences between urban sites and reference site n.1 (Enea Casaccia Research Centre).

Finally, in Table 5.3 it has been reported the numerical value of the intensity of the urban heat island which has been calculated with the equation 1 applied to hourly temperatures.

Table 5.3: UHII (Urban heat island intensity).

N.	Position	UHII [°C]	Hour	Day	Month
1	ENEA Casaccia Research Centre	-	-	-	-
2	MSE Ministero dello Sviluppo Economico	7.0	02:00	21	7
3	Monte Verde	6.7	03:00	21	7
4	Cornelia	6.1	02:00	21	7
5	Prati	6.9	02:00	25	7
6	Tuscolana	6.9	03:00	25	7
7	Marconi	5.9	01:00	25	7

The intensity of heat island varies from 5.9 °C to 7 °C and it occurs in times far away from the peak temperatures, as shown in Figure 5.4, where, by way of example, it is reported the daily trend of the temperatures for site n. 2 and for rural site n. 1. Figure 5.4 reported also the difference in temperature between the first one and the second one. Temperature of site n. 2 differs less than the reference site one in the central part of the day and it increases significantly in the initial hours. This behaviour is linked to phenomena of heat accumulation in the built-up environment during the peak hours of irradiation with a consequent heat release in the following hours, due to the high solar absorptance of building materials.

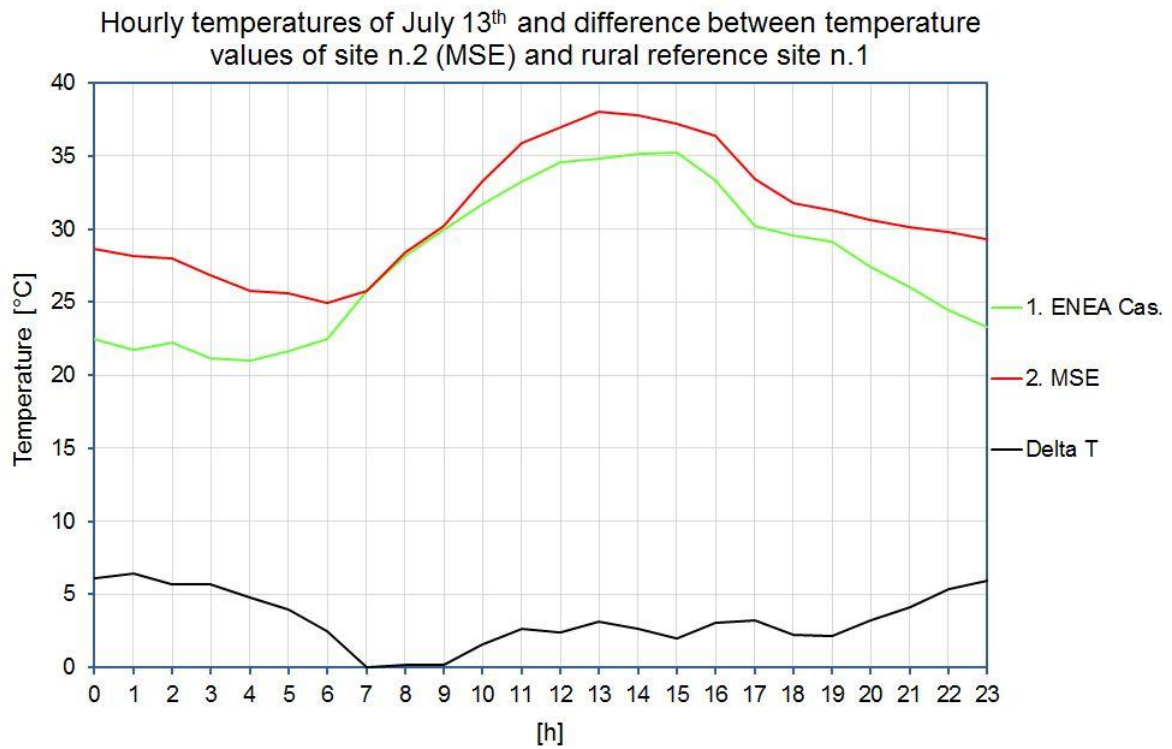


Figure 5.4: Daily temperature trend for sites n. 1 (ENEA Casaccia Research Centre) and n. 2 (MSE). Temperature variation (in black trend) obtained by subtracting the values detected in rural reference site n. 1 to the values detected in site n. 2.

## 5.4 Photo-Catalytic Tints for Asphalts

### 5.4.1 Samples Description

Photo-catalytic tints for asphalts are premixed powder products composed of photo-catalytic cement (made of titanium dioxide), selected aggregates of special sizes and patented additives. Different types of pigments can be added to give the desired colour to the product. The product acts as a coating to be laid on the existing asphalt and covers holes and cavities. The product, which is already on market, was not originally developed as a cool material but as material with photo-catalytic properties (not considered in this work). The mitigation potentialities of the urban temperature have to be tested. For this reason, both solar characterisation in laboratory and outdoor tests on surface temperatures are required to totally assess its quality. Five reference colours were selected: off-white, grey, green, red and blue.

### 5.4.2 Methodology

With each colour it was painted a 15 x 15 cm support prepared for solar characterisation. Portions of asphalt of approximately 2 x 2 m were treated with photo-catalytic tints and applied on a pedestrian street in the ENEA Casaccia Research Centre in order to monitoring continuously the surface temperature of the five selected colours. The outdoor tests on these materials were carried out during the summer of 2011, from August 11 to August 30. Even if this period is not the most intense in terms of solar radiation, the monitoring was implemented to control the response of materials under real conditions. The tints were applied on a substrate of aged asphalt, which is the reference material for comparison. The surface temperature was monitored with thermo-resistance placed at the centre of the different colour samples and were shielded from solar radiation through a thin layer of sample tint on the top of the sensor. The equipment was made available by UTEE (Unità Tecnica Efficienza Energetica) of ENEA Casaccia Research Centre.

### 5.4.3 Experimental

#### *Thermo-Graphic Analysis*

Photo-catalytic tints samples, arranged on 15 x 15 cm supports, were subjected to thermo-graphic analysis when affected by solar radiation. The device used is the thermal imaging camera NEC TH 9100 ML 320 x 240 and it has been made available by LIFT (Laboratorio Interdisciplinare di Fisica Tecnica) of the University of Roma Tre. Figure 5.5 shows the images in the infrared range and in the visible range.

The surveys were conducted at the following operative conditions:

- Outside air temperature: 31 °C (August 5, 2011, 12:00 a.m.);
- Samples emissivity: Experimental tests estimate an average value of 0.9 [5.9].

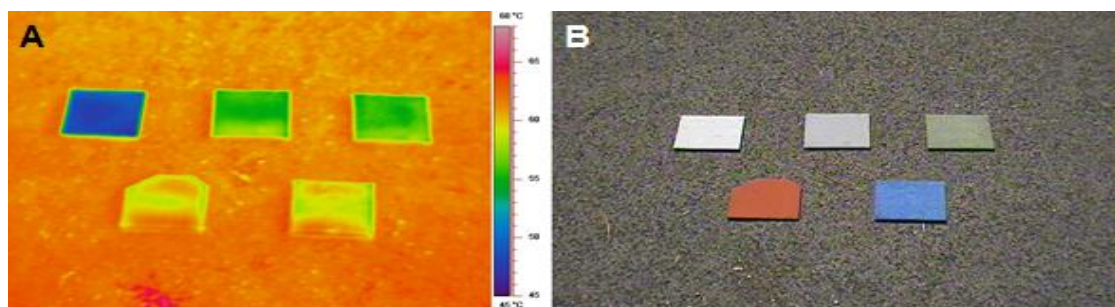


Figure 5.5: Images of photo-catalytic tints in infrared range (A) and in visible (B) range.

## Section 2: Experimental and Numerical Analyses

Table 5.4 shows the maximum and minimum temperature values obtained through a thermal imaging processing software: the Multi Thermal Image Processing. Table 5.4 reports also average values and temperature differences compared to the average temperature of the asphalt always detected by the thermal camera. Despite the temperature resolution of this device is declared to be 0.08 °C, the performed thermo-graphic analysis is valid only for comparison and the temperatures shown in the table were obtained processing on the thermal image. More detailed analyses are needed to evaluate the real performance of materials.

Table 5.4: Processed surface temperatures of the photo-catalytic tints.

	White	Green	Grey	Red	Blue	Asphalt
$T_{min}$ [°C]	46.6	54.7	54.9	58.6	58.9	-
$T_{max}$ [°C]	48.8	57.8	58.1	62.3	62.0	-
$T_{ave}$ [°C]	47.7	56.3	56.5	60.5	60.5	63.5
$\Delta T_{asphalt - sample\ ave}$ [°C]	15.8	7.3	7.0	3.1	3.1	-

### Solar and Optical Characterisation

The reflectance measurements were performed with a commercial spectrophotometer equipped with an integrating sphere of 15 cm, made available by the UTTMAT laboratory (Unità Tecnica Tecnologie dei Materiali) of the ENEA Casaccia Research Centre (par. 3.3.1). The integrating sphere is strictly necessary during testing on diffusing materials, such as those under consideration. The measurements were carried out between 300 and 2500 nm, with a spectral resolution of 5 nm. Because of samples roughness and source light beam geometry (about 1.5 cm), three measurements were conducted on each sample. For comparison purposes, two types of traditional asphalt were also tested:

- new asphalt (bitumen covers completely the aggregates);
- aged asphalt (bitumen does not entirely cover the aggregates and the surface colour is grey).

Figure 5.6 presents the spectral values of reflectance of the tested materials obtained by operating an average of the three mentioned measurements.

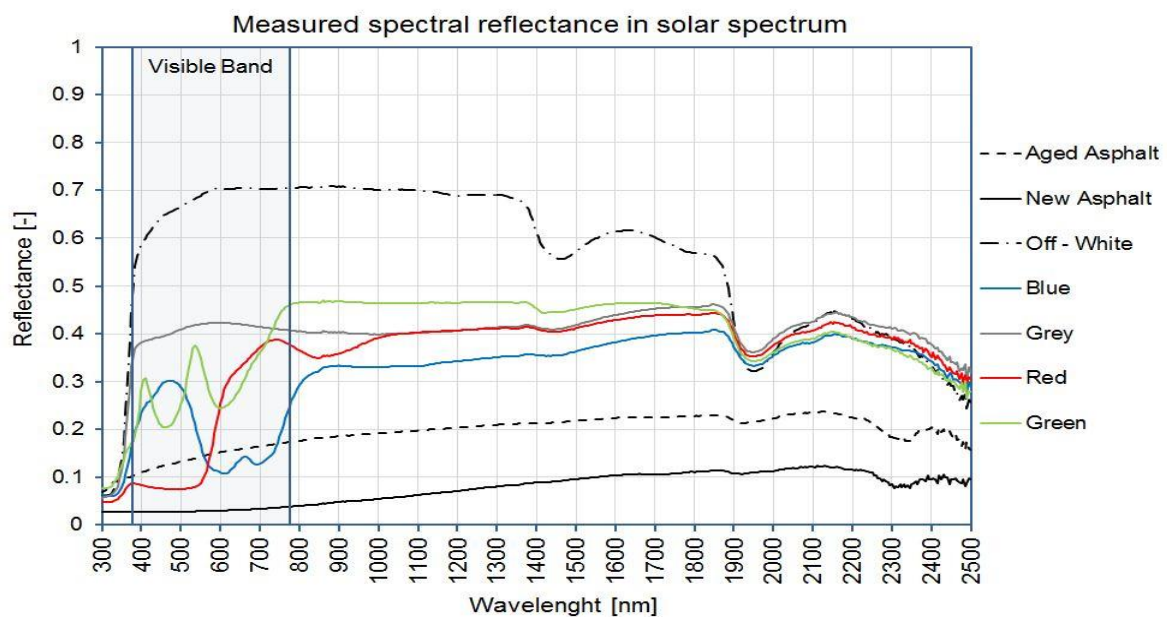


Figure 5.6: Photo-catalytic and conventional asphalts spectral reflectance.



## Section 2: Experimental and Numerical Analyses

The broadband reflectance values in the solar range ( $\rho_e$ ) in the visible range ( $\rho_v$ ) and in NIR range ( $\rho_{NIR}$ ) were calculated starting from spectral measurements in accordance with the procedures and weighting curves defined in the standard reference ISO 9050:2003 [5.41]. Table 5.5 shows the results obtained.

Table 5.5: Broadband reflectance values of photo-catalytic tints and conventional asphalts.

	$\rho_e$ [-]	$\rho_v$ [-]	$\rho_{NIR}$ [-]
Aged Asphat	0.16	0.14	0.20
New Asphalt	0.05	0.03	0.07
Off - White	0.66	0.69	0.66
Blue	0.25	0.18	0.34
Grey	0.40	0.42	0.41
Red	0.28	0.14	0.39
Green	0.36	0.30	0.46

The measurements results show that coloured asphalts have a higher solar reflectance compared to conventional asphalts. This is the main feature to keep the surface cold under solar radiation. New asphalt has a much lower reflectance than the aged asphalt in the entire solar spectrum: in the visible spectrum the dark colour of the first results in a visible reflectance almost 5 times lower than the second one. Besides the reflectance values in the NIR band and solar band are also much lower, respectively, 4 and 3 times approximately.

As it can be seen from the smooth curves in Figure 5.6 and from the values in Table 5.5, it is interesting to note that off-white and grey do not show significant selective properties: the values of reflectance in the visible and NIR bands are very near for both materials. The same situation does not occur for coloured samples, for which there is always an increase in reflectance in the NIR than in the visible band. The difference in reflectance between the NIR and visible bands ranges between 0.16 (green) and 0.25 (red). In relative terms, this means that the reflectance in NIR is higher than the visible reflectance from 1.5 to 3 times. The difference between the reflectance in NIR and solar reflectance is, of course, lower and it varies from 0.09 (blue) to 0.11 (red).

Finally a study carried out on these tints estimated their thermal emissivity obtaining an average value of 0.9 very similar to the asphalt one. This finding demonstrate that these materials do not affect the thermal behaviour of asphalt [5.9].

### Surface Temperatures Analysis

Figure 5.7 shows the tested portions of asphalt treated with tints.



Figure 5.7: Site of application of the photo-catalytic tints.

## Section 2: Experimental and Numerical Analyses

Figure 5.8 and Figure 5.9 report the surface temperature profiles of the monitored area for eleven days in August. The air temperature is also reported. The conventional asphalt has reached a temperature of 58 °C during the radiation peak, while the off-white coating has reached a maximum value of 39 °C. The coloured samples show intermediate performance, keeping the surface of the asphalt to a temperature of at least 5 °C lower than the one of the conventional asphalt during solar radiation peaks. Temperature differences compared to the asphalt ones decrease significantly during the night period.

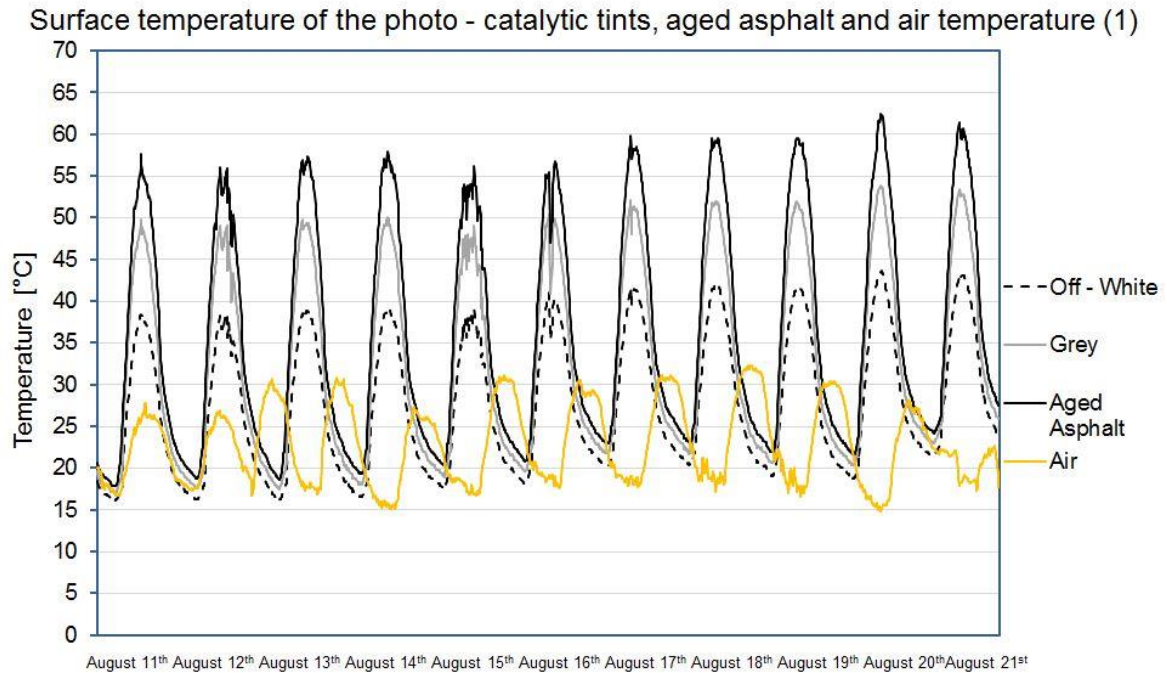


Figure 5.8: Monitored surface temperatures of the following samples: Off-white, grey and aged asphalt.

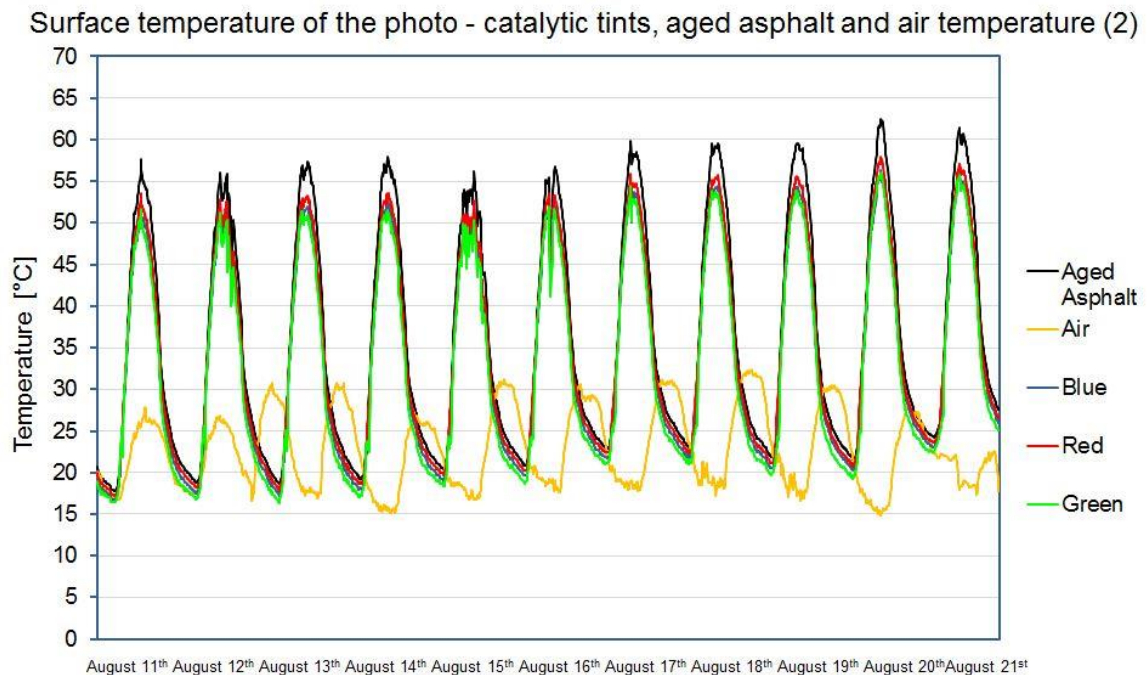


Figure 5.9: Monitored surface temperatures of the following samples: Blue, red, green and aged asphalt.



## Section 2: Experimental and Numerical Analyses

The maximum surface temperatures and the respective average values recorded during monitoring are shown in Table 5.6. It also includes the maximum ( $\Delta T_{\max}$ ) and the mean deviation ( $\Delta T_{\text{ave}}$ ) between conventional aged asphalt surface temperature and the colourful tints one.

Table 5.6: Maximum temperature values detected and maximum and average deviation from the conventional aged asphalt.

	$T_{\max}$ [°C]	$T_{\text{ave}}$ [°C]	$\Delta T_{\max}$ [°C]	$\Delta T_{\text{ave}}$ [°C]
Aged Asphalt	62.4	36.4	-	-
Off - White	43.9	28.1	19.3	8.2
Blue	56.3	33.6	7.9	2.7
Grey	53.9	32.5	10.0	3.8
Red	57.9	34.5	6.2	1.8
Green	56.1	32.8	7.8	3.5

The results show the high qualities of the off-white coating and coloured coatings in order to improve the thermal response of the asphalt, especially during peak hours, when the maximum values of temperature are reached.

Additional results were obtained by the cumulative distribution of the difference between the surface temperatures of conventional aged asphalt and the temperatures of the colourful photo-catalytic tints. These data are summarised in Figure 5.10.

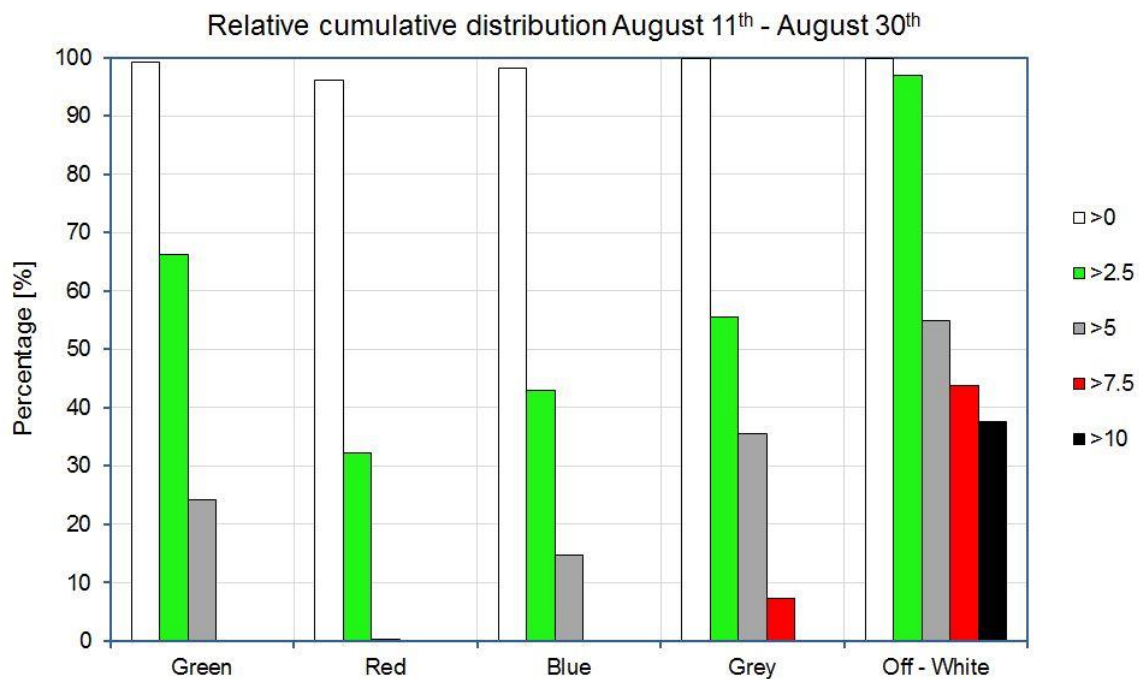


Figure 5.10: Percentage cumulative distribution of the difference between the surface temperature of the aged asphalt and the five photo-catalytic tints.

According to the data obtained, all samples showed a temperature lower than the asphalt one during the entire period, excluding rare exceptions during the night.

The most interesting results concern once again the off-white, which stayed colder of at least 5 °C for 55% of the time and 10 °C for 37%. The grey tint was colder than the conventional asphalt of 2.5 °C for half of the period and of 7.5 °C during the 7% of the time. Green and blue have surface temperatures lower than 5 °C, respectively for 24% and 15% of the period. The worst results were obtained for the red sample. It almost never reached temperature differences higher than 5 °C.

## 5.5 Porous Concrete Draining Paving

### 5.5.1 Selected Materials

---

Porous concrete materials used as a surface coating for roads and sidewalks were tested. This material presents a water drain power much higher than the natural soil. The binder of the cement has been coloured with three different shades of grey.

The water storage power, used to limit the increase of the surface temperature through evaporation, is not a phenomenon taken into account in these tests. It was analysed how the size of the grains, and thus the voids, affects the value of solar reflectance.

The selected samples are shown in Figure 5.11:



Figure 5.11: Porous concrete samples selected: White Grain Size 6 mm (1), White Grain Size 12 mm (2), Light Grey Grain Size 12 mm (3), Dark Grey Grain Size 12 mm (4).

### 5.5.2 Experimental

---

Also in this case, the optical characterisation was carried out through the commercial spectrophotometer made available by UTTMAT laboratories (Unità Tecnica Tecnologie dei Materiali) of the ENEA Casaccia Research Centre (par. 3.3.1). The samples were examined in five different points due to the high surface irregularities. As in the previous case, the samples were compared with the spectra obtained from analyses on new and aged asphalt samples.

Figure 5.12 shows the spectral response of the four selected samples in the entire solar spectrum, while Table 5.7 shows the broadband values in the relevant spectra (visible, N.I.R. and solar). The spectral responses were obtained by an average of the five measurements taken in

## Section 2: Experimental and Numerical Analyses

different points of incidence of the light beam generated by spectrophotometer lamp. The results highlight how analysed concrete pavements present advanced solar performance when compared with conventional materials.

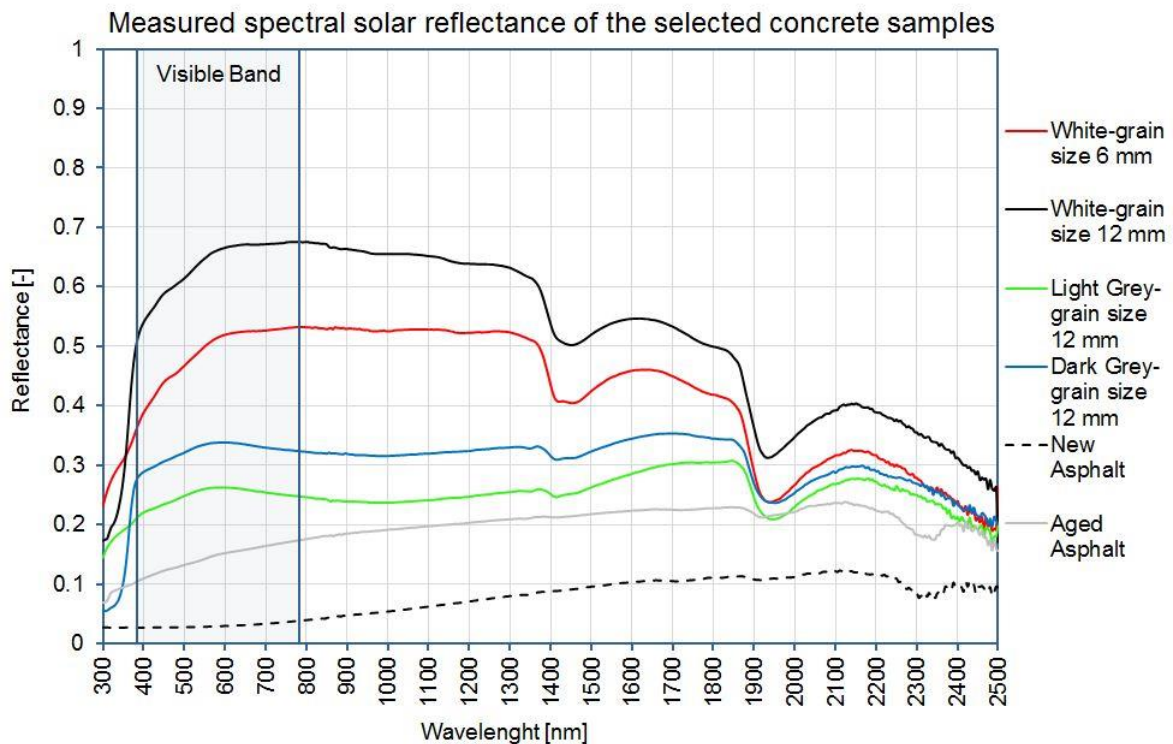


Figure 5.12: Porous concrete and conventional asphalts spectral reflectance.

Table 5.7: Broadband spectral values of porous concrete pavements and conventional asphalts.

	Grain size [mm]	$\rho_e$ [-]	$\rho_v$ [-]	$\rho_{NIR}$ [-]	$\rho_e - \rho_{e \text{ new asphalt}}$	$\rho_e - \rho_{e \text{ aged asphalt}}$
Aged Asphat	-	0.16	0.14	0.20	-	-
New Asphalt	-	0.05	0.03	0.07	-	-
White	6	0.45	0.46	0.46	0.40	0.29
White	12	0.56	0.57	0.56	0.51	0.39
Light Grey	12	0.30	0.31	0.31	0.25	0.14
Dark Grey	12	0.22	0.23	0.23	0.17	0.06

Referring to Table 5.7, the white colour sample with a grain size of 12 mm, showed the higher solar reflectance. Not surprisingly, the smaller value of solar reflectance was obtained from the dark grey sample. The differences in solar reflectance obtained by the comparison between the porous concrete samples and the new asphalt range between 0.17 and 0.51 (Table 5.7, column 6), while for the aged asphalt range between 0.06 and 0.39 (Table 5.7, column 7).

If the high solar reflectance is an important step, the results also show the possibility of a significant improvement. In fact, according to the graph and the table, it can be seen that the reflectance in the NIR presents almost the same value as in the visible band. This means that the products are not spectrally selective in the NIR region. A further increase in solar reflectance could be achieved by aiming at increasing the reflectance in the NIR band without altering the colour render.

## 5.6 Calculation of Urban Environment Temperatures: Numerical Analysis

The impact that coatings with high solar reflectance may have on air temperature in an urban area has been the subject of several numerical analyses reported in this paragraph.

### 5.6.1 Description of the Calculation Software: ENVI-met

The tool used for the numerical analysis is the ENVI-met software. It uses a deterministic calculation method called SVAT (Soil, Vegetation and Atmosphere Transfer) and it has been designed by an environmental modelling group of the University Johannes Gutenberg of Mainz [5.42]. This tool operates at micro-scale level and it is able to simulate the temporal evolution of various thermo-fluid-dynamic parameters within a three-dimensional grid. Using this grid, it is possible to recreate the portion of an urban area with buildings and roads, as well as to modify the thermal and optical factors such as the temperature inside buildings, the thermal transmittance and surface reflectance. Within the urban texture it is possible to implement also the distribution and characteristics of the vegetation. Climatic variables to be set in input are: Potential air temperature and specific humidity at 2500 m above the ground; relative humidity at 2 m above the ground; speed and wind direction at 10 m above the ground. After the initialisation, it is created a vertical profile from 0 to 2500 m of these variables and it is used as input condition to the one-dimensional boundary applied to the edge of the three-dimensional model. Although ENVI-met has been considered in many scientific articles [5.43 - 5.46], the models created with this software need to be calibrated, since for now only trial versions are available. Figure 5.13 shows the diagram of the three-dimensional model used in ENVI-met.

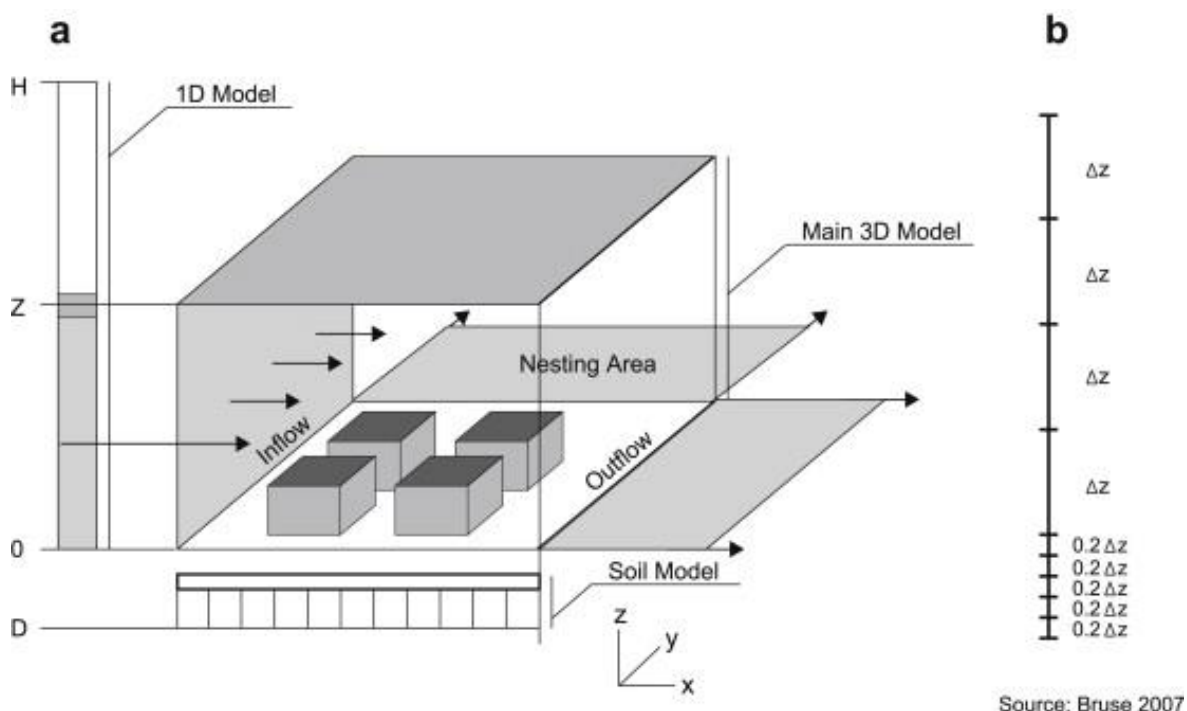


Figure 5.13: Diagram of the model used in ENVI-met.

### 5.6.2 ENVI-met Model of a Neighbourhood of Rome: Prati

The chosen area is a portion of Prati district, a densely urbanised area of about 580.000 m<sup>2</sup> in the centre of Rome. This area has been inserted into the ENVI-met tool in order to recreate the



## Section 2: *Experimental and Numerical Analyses*

three-dimensional distribution of structures, road paving and vegetation. The dimensions of the computational grid are set to 755 (x) × 770 (y) × 58.5 (z) m by dividing each axis into a number of cells, respectively, equal to 151 × 154 × 20. To limit the problems of transient on structures and areas located near the periphery of the domain, due to the values of the one-dimensional boundary conditions, two additional nesting grids were added around the main grid. The method chosen for the calculation of the variation of the lateral boundary conditions of temperature and humidity is a method known as "open." This means that the values of the internal points of the mesh were copied on the edge of the input side. This allows to minimise the edge effect of the model on the inner parts of the domain. The variation of the side boundary conditions of kinetic energy of the incoming air mass was instead calculated with the "cyclic" method, in which the out coming values from the model are copied on the incoming boundary: The grid is designed within a large urban area and for this reason, confining with similar building structures, the profile of the incoming air is hypothetically similar to the out coming profile.

Five "receptors" were positioned within the model in order to detect the variation of several thermo-physical parameters, at different heights from the ground, during the simulation. In this way, it was possible to obtain a vertical profile of air temperature in some relevant points. Figure 5.14 shows the positions of receptors within the considered area: the position of the receptor 1 was chosen close to a green area while the other receptors have been positioned progressively more distant from the first one in most thermally critical areas without vegetation.



Figure 5.14: Selected area and positions of the five receptors (from 1 to 5).

## Section 2: Experimental and Numerical Analyses

Figure 5.15 is the 3D image of the examined area represented through the ENVI-met interface. It is possible to notice also the vegetation distribution. The latter can be modelled within the tool according to the plant type.

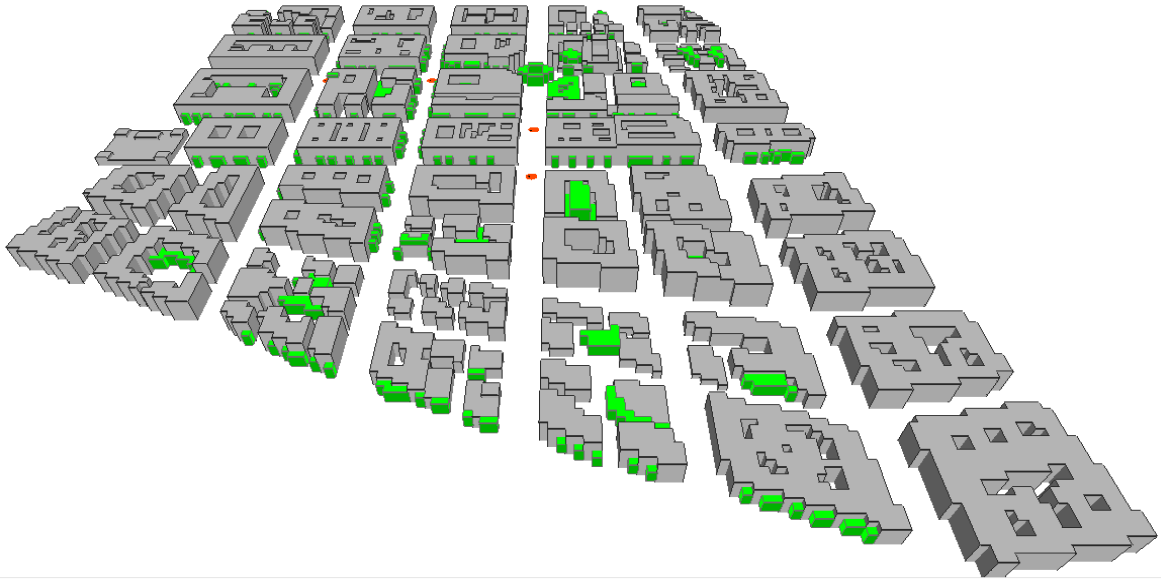


Figure 5.15: 3D Image of the urban area recreated in the calculation domain.

Figure 5.16 shows the input data set for the simulations. The values entered in the MAIN-DATA BLOCK are parameters used by the tool to create the mentioned one-dimensional vertical distribution of local climatic variables to be directly applied to the periphery of the computational domain. The BUILDING section allows to enter the optical and thermal parameters of the structures.

```
% ---- Basic Configuration File for ENVI-met Version 3 ----
% ---- MAIN-DATA Block ----
Name for Simulation (Text):                = Zona Cola Di Rienzo Conf Orig P
Input file Model Area                      =[INPUT]\Cola_Rienzo_Estesa.in
Filebase name for Output (Text):           =Cola_Rienzo_Output_B_Conf_Orig_P
Output Directory:                         =[OUTPUT]\ColaRienzoConfOrigP
Start Simulation at Day (DD.MM.YYYY):      =20.07.2010
Start Simulation at Time (HH:MM:SS):       =00:00:00
Total Simulation Time in Hours:            =72
Save Model State each ? min               =60
Wind Speed in 10 m ab. Ground [m/s]       =1.5
Wind Direction (0:N..90:E..180:S..270:W..) =225
Roughness Length z0 at Reference Point     =0.1
Initial Temperature Atmosphere [K]         =300
Specific Humidity in 2500 m [g Water/kg air] =7
Relative Humidity in 2m [%]                =71
Database Plants                           =[input]\Plants.dat

( -- End of Basic Data --)
( -- Following: Optional data. The order of sections is free. --)
( -- Missing Sections will keep default data. --)
( Use "Add Section" in ConfigEditor to add more sections )
( Only use "=" in front of the final value, not in the description)
( This file is created for ENVI-met V3.0 or better )

[BUILDING]                               Building properties
Inside Temperature [K]                   = 299
Heat Transmission Walls [W/m²K]           =1
Heat Transmission Roofs [W/m²K]           =1.2
Albedo Walls                             =0.45
Albedo Roofs                             =0.25
```

Figure 5.16: Configuration tool for input data of ENVI-met.



## Section 2: Experimental and Numerical Analyses

In order to verify the reliability of the results produced by the simulations, it was carried out a preliminary calibration of the model. The temperature profile generated by ENVI-met in an entire summer day (July 21) at 45 m of height was compared to real values provided by the Torre Calandrelli weather observatory of Rome, always at 45 m above the road surface, as shown in Figure 5.17.

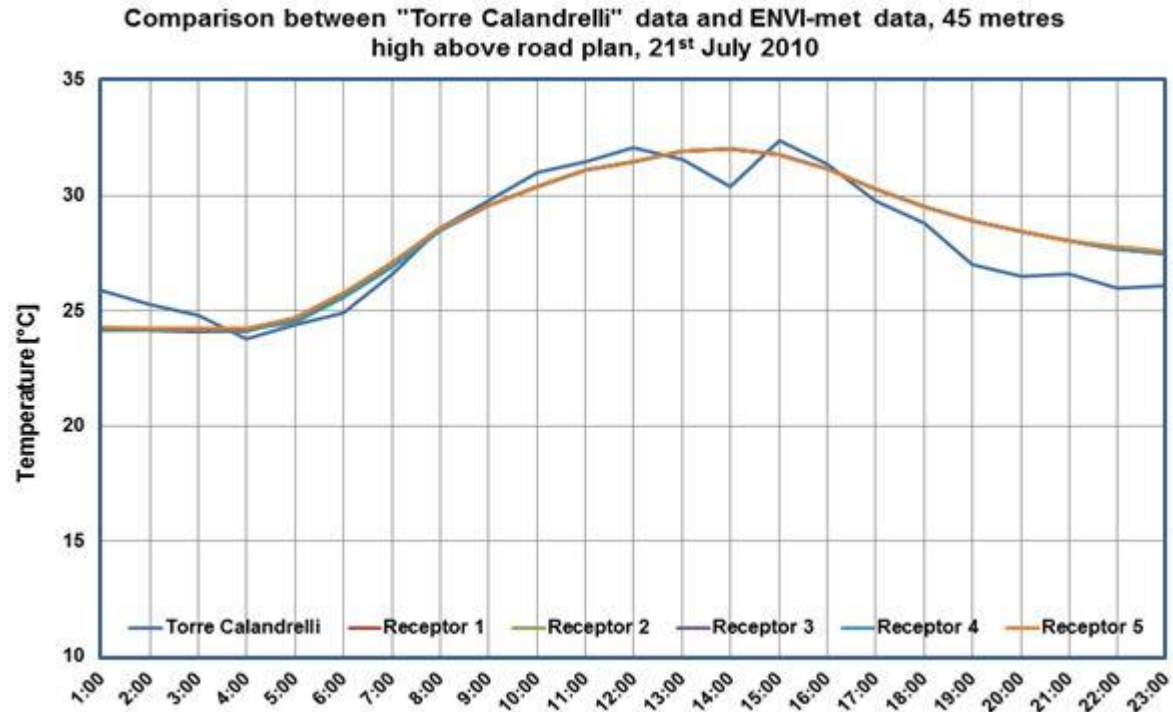


Figure 5.17: Comparison between Torre Calandrelli data and ENVI-met data.

Although they are related to two different areas of Rome (both belonging to the old town), it is possible to make a comparison between these values because, as mentioned earlier, they are representative of a situation above the average height of the buildings (over the canopy). Inside the model the five receptors record, at 45 m high, a temperature trend almost perfectly superimposed and this is due precisely to the level at which the data were taken. In fact, at this height from the ground, the mitigating effects of temperature related to green areas become completely negligible. It is interesting to note as the trend generated by the actual data (in blue) is very similar to that obtained through the simulation, both for the shape and for the peaks. This represents a first assessment of the reliability of the results of the simulations also considering the fact that they were obtained with values of solar radiation as a result of statistical calculations that do not reflect the real sunshine duration of the area object of study.

Through the model described above, it was possible to perform several simulations that have as purpose to examine the influence that cool materials have on the urban area air temperature. These simulations have been classified into three groups: In the first group, the reflection parameters of vertical and horizontal surfaces of buildings and, in a less sensitive way, of road paving have been changed according to three different configurations. In the second group it has been altered only the reflectivity power of the road surface, but in a more sensitive way than the previous case and using reflectance values in accordance with the experimental data obtained for the photo-catalytic tints. The third group is similar to the second group but using the reflectance values obtained from the experimental analysis on the concrete draining paving samples.



### 5.6.3 Simulations Result

#### *Buildings and Asphalt Surfaces*

The reflectance of the model surfaces has been changed as shown in Table 5.8, allowing to create three configurations: In the first one conventional reflectance values were recreated, in the second it has been changed the reflectivity power of horizontal surfaces and asphalts (henceforth called cool 1), while in the third one it is hypothesised an intervention with an higher impact on the performance of the build-up surfaces (henceforth called cool 2). The emissivity has been set to 0.9 for all the three configurations.

Table 5.8: Reflectance and emissivity values chosen for the three configurations.

	Solar Reflectance [-]			Emissivity [-]		
	Conventional	Cool 1	Cool 2	Conventional	Cool 1	Cool 2
Roof Surf.	0.25	0.50	0.70	0.90	0.90	0.90
Vertical Surf.	0.45	0.45	0.60	0.90	0.90	0.90
Road paving	0.13	0.25	0.35	0.90	0.90	0.90

The simulations cover two summer days in order to limit the effect of the initial transient related to the convergence of the input variables. Figure 5.18, Figure 5.19 and Figure 5.20 show the horizontal distribution of the potential air temperatures at 3 m above the ground, at 15:00 (GMT +1) on July 21. The temperature potential of a fluid particle at a pressure “p” is the temperature that the particle would have if it were brought adiabatically to a pressure reference standard  $p_0$ , generally 0.1 MPa. Therefore, at a height of 3 meters above the ground, it can be considered to be coincident with the dry bulb absolute temperature. In following figures the buildings are shown in black, vegetation in green.

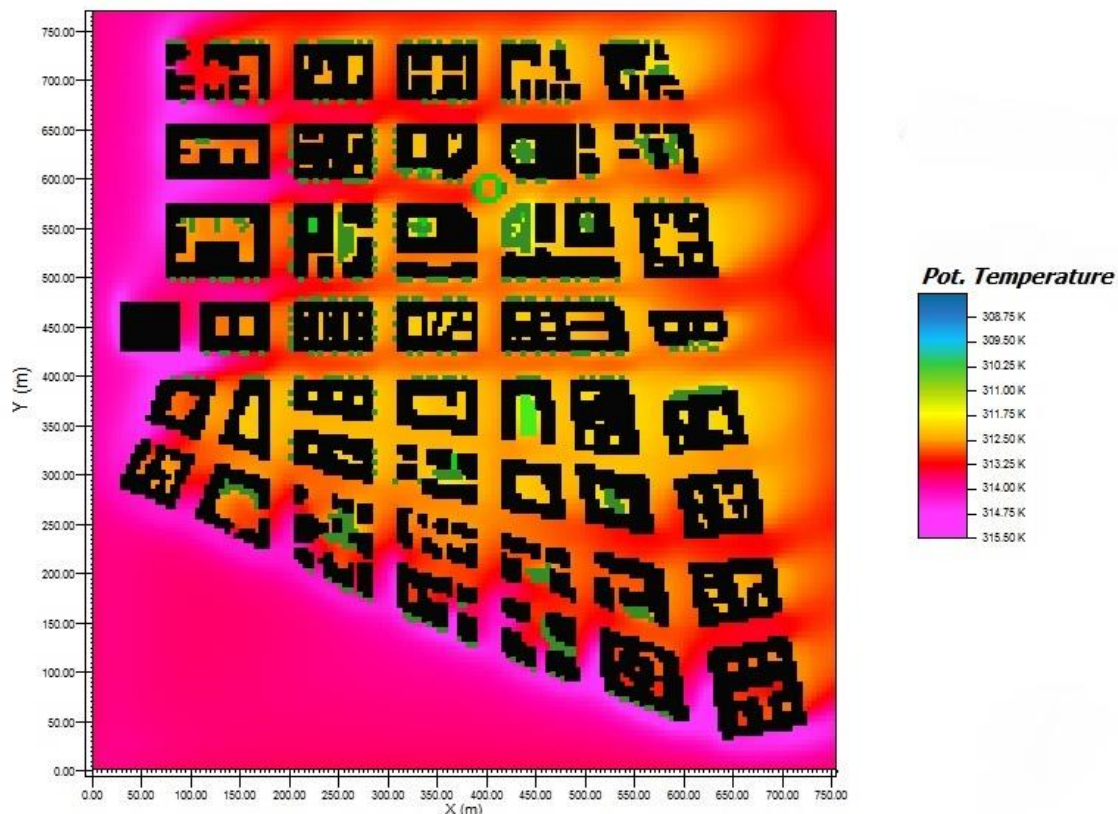


Figure 5.18: Horizontal distribution of potential temperature - Conventional configuration.

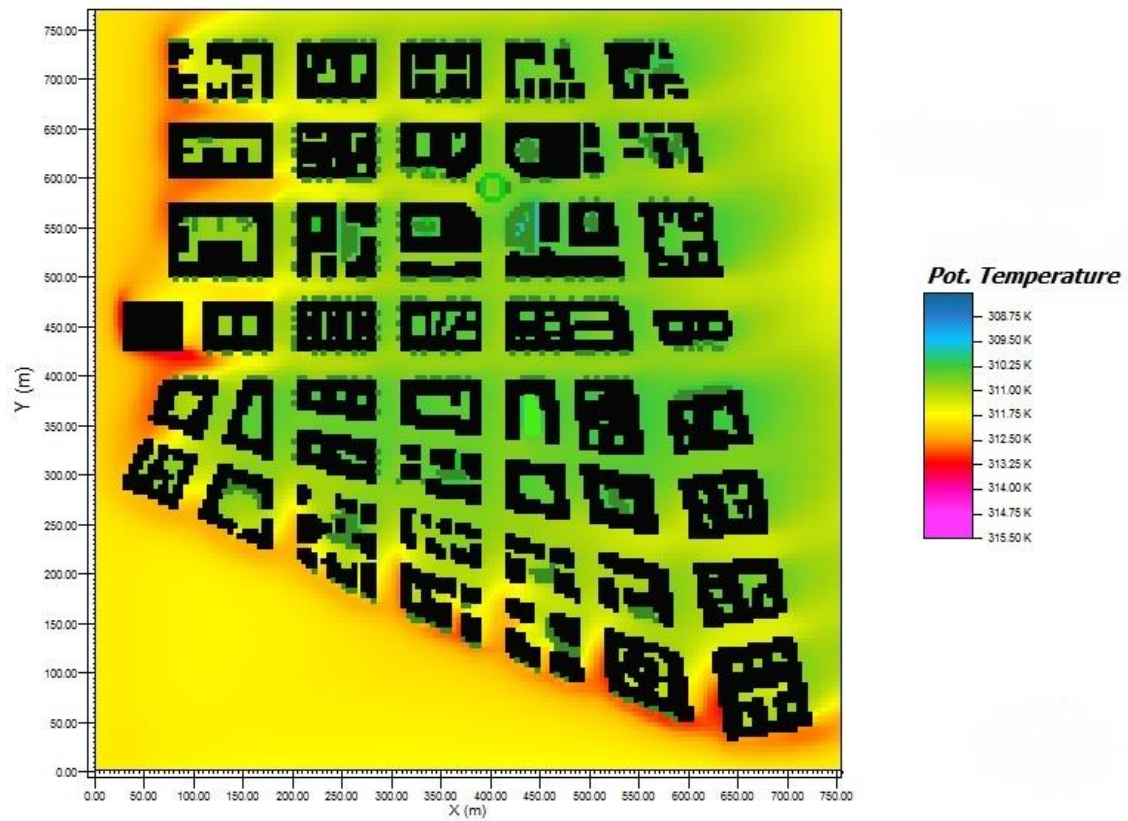


Figure 5.19: Horizontal distribution of potential temperature - Cool 1.

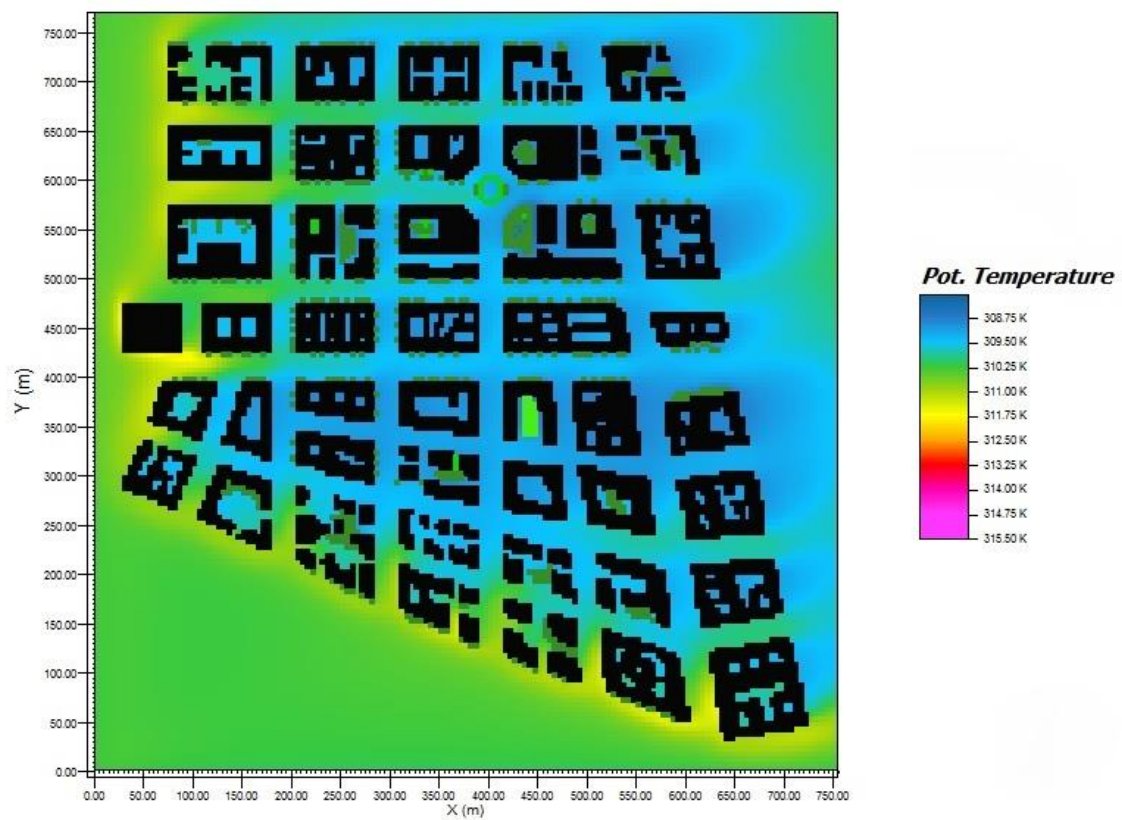


Figure 5.20: Horizontal distribution of potential temperature - Cool 2.



## Section 2: Experimental and Numerical Analyses

The temperature decreases with an average of 2 °C by analysing the values obtained in the configuration “cool1” (Figure 5.19) compared to the conventional configuration (Figure 5.18). Considering the configuration “cool 2” (Figure 5.20), the temperature decreases by 3.5 °C in comparison to the conventional configuration (Figure 5.18). The temperature values obtained are more reliable in points further away from the domain boundary. This is because the layout of the urban area is limited to an area of about 580.000 m<sup>2</sup> beyond which buildings have not been represented, and this is a factor that alters the boundary conditions of points belonging to the periphery of area. This problem can be found in the left part of the three figures where the air temperature presents much higher values.

The dry bulb air temperatures recorded by the five receptors at about 4.5 meters above the ground are shown in the following Table 5.9. The difference in temperature between the cool configurations and the conventional one ( $\Delta T_1$  and  $\Delta T_2$ ) are also reported in Table 5.9.

Table 5.9: Hourly temperatures recorded by the five receptors for the three configurations - Temperature changes compared to the conventional configuration.

		Hours [h]																							
		0	1	2	3	4	5	6	7	8	9	10	11	12	13	14	15	16	17	18	19	20	21	22	23
R 1	T Conventional [°C]	29	29	29	28	28	28	28	29	30	32	33	35	36	37	38	39	38	38	37	35	34	33	32	32
	T Cool 1 [°C]	28	28	28	28	27	27	27	29	30	31	32	33	35	36	36	37	37	36	35	34	33	32	31	31
	T Cool 2 [°C]	28	28	27	27	27	27	27	28	29	30	31	32	34	34	35	35	35	35	34	33	32	31	30	30
	ΔT <sub>1</sub> [°C]	0.7	0.7	0.6	0.6	0.6	0.6	0.6	0.7	0.8	0.9	1.1	1.3	1.5	1.7	1.8	1.8	1.8	1.7	1.6	1.4	1.2	1.1	1.1	1
	ΔT <sub>2</sub> [°C]	1.3	1.2	1.1	1.1	1.1	1	0.9	1.1	1.3	1.5	1.8	2.2	2.6	2.9	3	3.1	3.1	3	2.8	2.4	2.2	2	1.9	1.8
R 2	T Conventional [°C]	30	30	30	29	29	29	29	30	31	32	34	36	37	38	39	40	39	39	38	36	35	34	34	33
	T Cool 1 [°C]	30	29	29	29	28	28	28	29	30	31	33	34	36	37	37	38	38	37	36	35	34	33	33	32
	T Cool 2 [°C]	29	29	28	28	28	28	28	29	30	31	32	33	34	35	36	36	36	36	35	34	33	32	32	31
	ΔT <sub>1</sub> [°C]	0.8	0.7	0.7	0.6	0.6	0.6	0.6	0.7	0.8	1	1.2	1.4	1.6	1.7	1.8	1.9	1.8	1.8	1.6	1.4	1.3	1.2	1.1	1.1
	ΔT <sub>2</sub> [°C]	1.4	1.3	1.2	1.2	1.1	1	1	1.2	1.4	1.7	2	2.4	2.8	3	3.2	3.3	3.2	3.1	2.8	2.5	2.3	2.1	2	1.9
R 3	T Conventional [°C]	31	30	30	30	29	29	29	30	31	32	34	36	37	38	39	40	39	39	38	36	35	34	34	33
	T Cool 1 [°C]	30	29	29	29	29	29	29	29	30	31	33	34	36	37	37	38	38	37	36	35	34	33	33	32
	T Cool 2 [°C]	29	29	29	28	28	28	28	29	30	31	32	33	34	35	36	36	36	36	35	34	33	32	32	31
	ΔT <sub>1</sub> [°C]	0.8	0.7	0.7	0.6	0.6	0.6	0.6	0.7	0.8	1	1.1	1.4	1.6	1.7	1.8	1.9	1.8	1.8	1.6	1.4	1.3	1.2	1.1	1
	ΔT <sub>2</sub> [°C]	1.4	1.3	1.2	1.2	1.1	1.1	1	1.2	1.4	1.7	2	2.4	2.8	3	3.2	3.3	3.2	3.1	2.8	2.5	2.3	2.1	2	1.9
R 4	T Conventional [°C]	30	30	30	29	29	29	29	30	31	33	34	36	37	39	40	40	40	39	38	37	35	34	34	33
	T Cool 1 [°C]	30	29	29	29	29	29	29	29	31	32	33	35	36	37	38	38	38	37	36	35	34	33	33	32
	T Cool 2 [°C]	29	29	29	28	28	28	28	29	30	31	32	34	35	36	36	37	37	36	35	34	33	32	32	31
	ΔT <sub>1</sub> [°C]	0.8	0.7	0.7	0.7	0.6	0.6	0.6	0.7	0.8	1	1.2	1.4	1.6	1.7	1.8	1.9	1.9	1.8	1.6	1.4	1.3	1.2	1.1	1.1
	ΔT <sub>2</sub> [°C]	1.4	1.3	1.3	1.2	1.1	1.1	1.1	1.2	1.4	1.7	2	2.4	2.7	3	3.2	3.3	3.3	3.1	2.8	2.5	2.3	2.1	2	1.9
R 5	T Conventional [°C]	31	31	30	30	30	30	30	31	32	33	35	37	38	39	40	41	41	40	39	37	36	35	34	34
	T Cool 1 [°C]	30	30	30	29	29	29	29	30	31	32	34	35	36	38	38	39	39	38	37	36	35	34	33	33
	T Cool 2 [°C]	30	29	29	29	29	28	28	29	30	31	33	34	35	36	37	37	37	37	36	35	34	33	32	31
	ΔT <sub>1</sub> [°C]	0.8	0.8	0.7	0.7	0.6	0.6	0.6	0.7	0.8	1	1.2	1.4	1.6	1.8	1.9	1.9	1.9	1.8	1.6	1.5	1.3	1.2	1.1	1.1
	ΔT <sub>2</sub> [°C]	1.4	1.4	1.3	1.2	1.2	1.1	1.1	1.2	1.4	1.7	2.1	2.5	2.8	3.1	3.3	3.4	3.3	3.1	2.9	2.6	2.3	2.2	2	1.9

The maximum temperatures occur at 15:00. The values of the receptors 2, 3 and 4 are very similar in every hour of the day. In the conventional configuration, the peak temperature of the receptor 1, positioned in the green area, is 1.1 °C lower if compared to the one of receptor 2 and 2.1 °C lower if compared to the one of receptor 5. The latter recorded the higher temperature values. However this receptor is closer to the edge of the domain and it is affected by the problem stated above concerning the boundary conditions. The temperature of the receptor 1 highlights the importance of vegetation as an additional mitigation technique of temperatures for the densely urbanised areas. The comparison between the temperature trends of receptor 1 with another receptor placed in a crossroad, the receptor 2, is reported in the following Figure 5.21.

The maximum temperature difference between the conventional configuration of reflectance and the cool 1 configuration (medium impact cool materials application) is 1.8 °C for receptor 1 and 1.9 °C for the other receptors. If the conventional configuration is compared with the cool 2 configuration (high impact cool materials application), the difference rises to 3.1 °C for receptor 1, to 3.3 °C for receptors 2, 3 and to 4 and 3.4 °C for receptor 5.

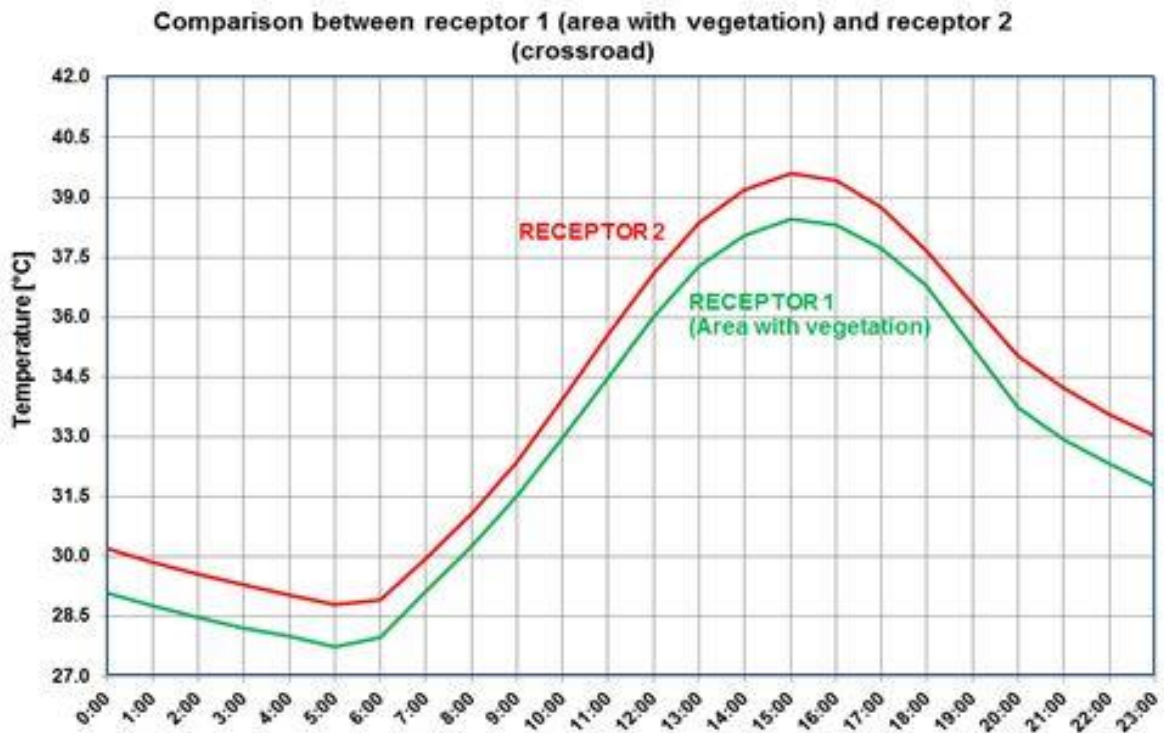


Figure 5.21: Comparison between receptor 1 (vegetation) and 2 (crossroad), conventional configuration.

Figure 5.22 shows the daily trend of temperature variation calculated between the conventional configuration of reflectance and the two cool materials configurations for the receptor 2 in July 21. It is possible to observe a significant increase in  $\Delta T$  in the central part of the day, with a maximum peak at 15:00. Cool materials generate a surface temperature profile with lower values if compared to a conventional materials and this difference is accentuated with the increase of the incident solar radiation intensity.

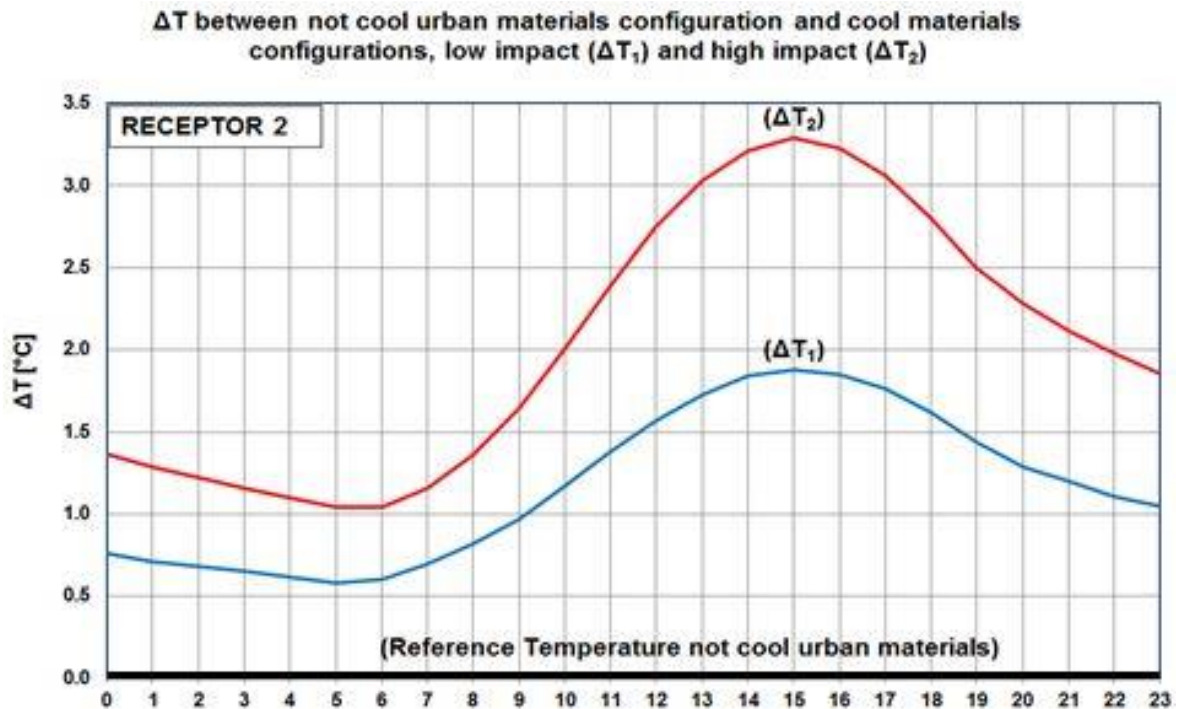


Figure 5.22: Difference in temperature between cool1 ( $\Delta T_1$ ) and cool 2 ( $\Delta T_2$ ) configurations and conventional configuration.

### Asphalt Surfaces: Photo-Catalytic Tints

The aim of this study was to verify the possible reduction of the external temperature at a local scale due to the use of cool materials applied only on the road paving. For this purpose, three simulations were performed during a summer day, July 20, with three different configurations of solar reflectance for asphalt: 0.10 to simulate a conventional asphalt, 0.40 and 0.65 to simulate respectively a cool grey asphalt tint and cool off-white asphalt tint.

The chosen reflectance values reflect the solar reflectance values measured experimentally in the optical characterisation of the asphalt photo-catalytic tints previously discussed.

Figure 5.23, Figure 5.24 and Figure 5.25 present an ENVI-met overview on a horizontal distribution of potential temperatures at about 3 m above the ground, for the considered area and for the three reflectance configurations of asphalts, assessed through a chromatic scale. Also in this case the buildings are highlighted in black while vegetation in green. The figures represent a "snapshot" at 15:00 (GMT +1), corresponding to the peak temperature of July 20.

Comparing the results of the three simulations, it is evident as the air temperature decreases in average of about 3 °C, from an urban area equipped with conventional asphalts (Figure 5.23) to an area in which the asphalt is stained with cool grey tint (Figure 5.24). Considering the application of a cool off-white tint on asphalt (Figure 5.25), the temperature decreases further, with an average difference of 5.5 °C. This is due to the fact that the surface equipped with cool tints, because of its high solar reflectance, stays cooler if subjected to solar radiation than a conventional asphalt surface, as previously verified experimentally.

A cooler surface determines a lower convective and radiative heat transfer to the air of the urban environment and consequently its temperature tends to reach lower values.

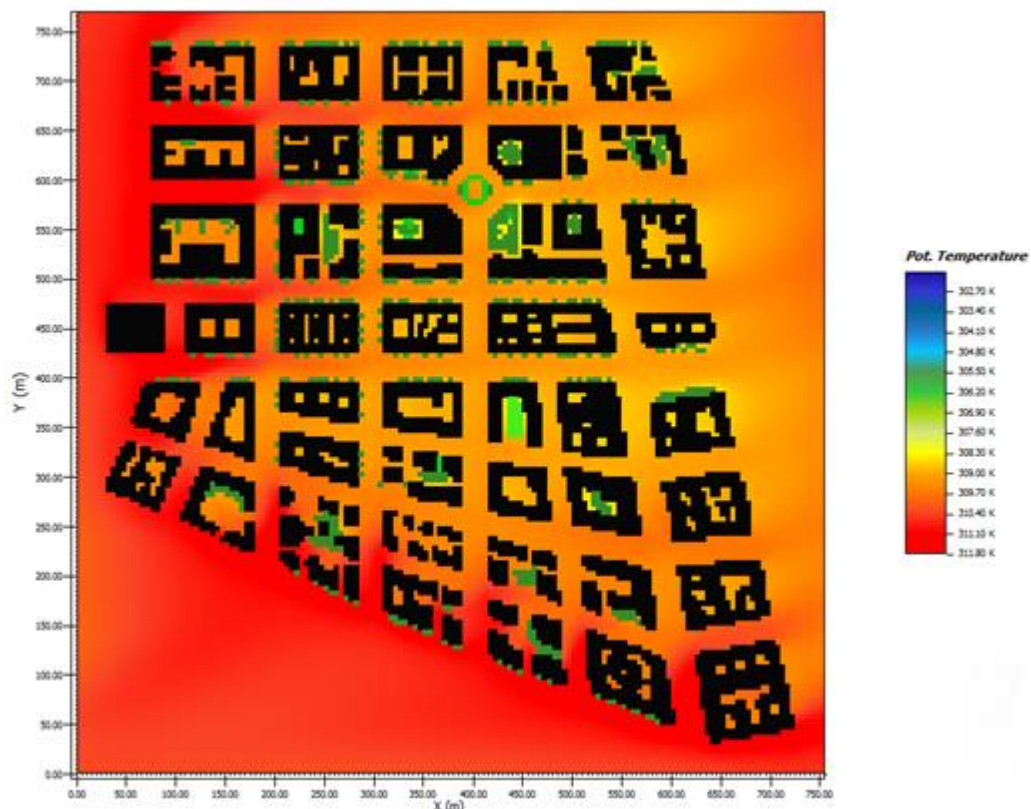


Figure 5.23: Horizontal distribution of potential temperature: Asphalt reflectance 0.10.



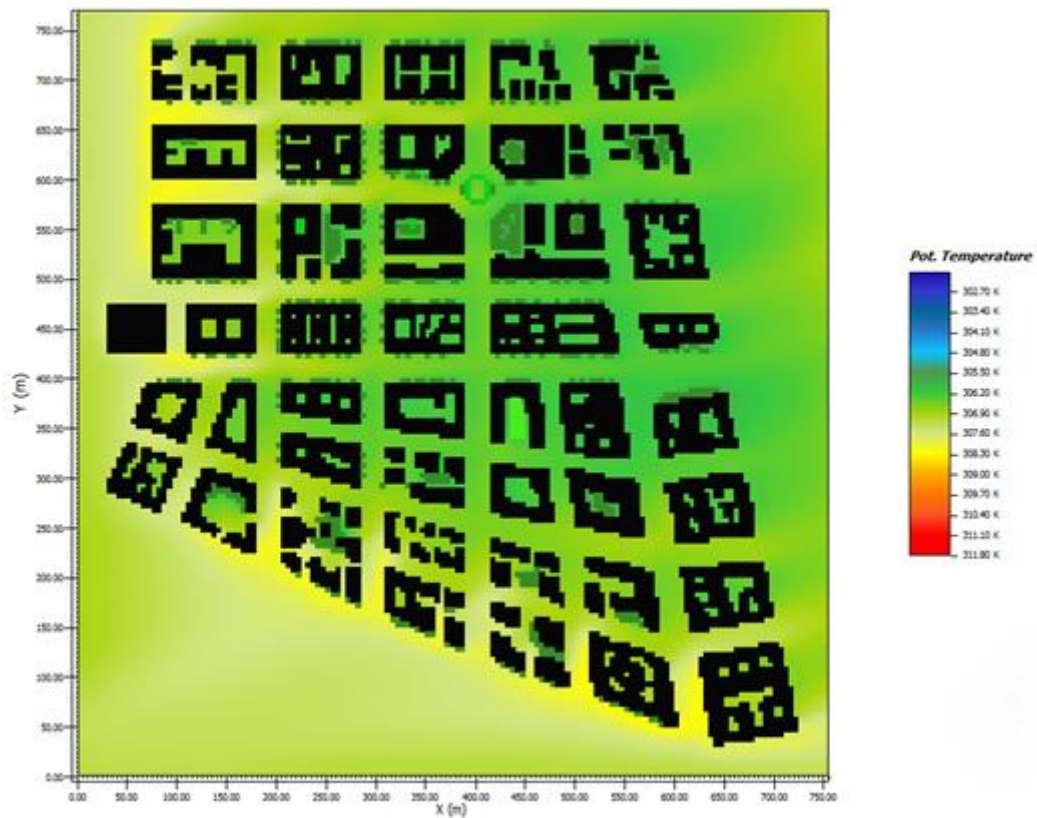


Figure 5.24: Horizontal distribution of potential temperature: Asphalt reflectance 0.40.

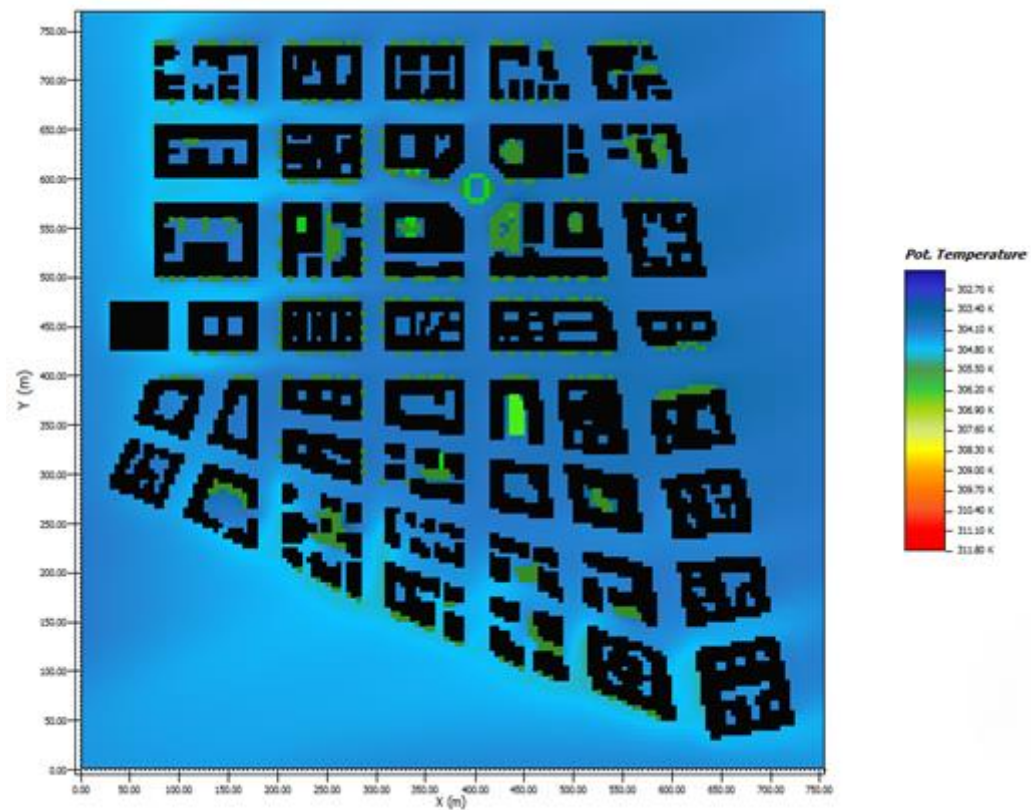


Figure 5.25: Horizontal distribution of potential temperature: Asphalt reflectance 0.65.



## Section 2: Experimental and Numerical Analyses

Through a vertical distribution of temperature, Figure 5.26 allows to observe the phenomenon described previously. The sectioning plane is the y-z plane which passes through the coordinate  $x = 440$  of Figure 5.23, Figure 5.24 and Figure 5.25.

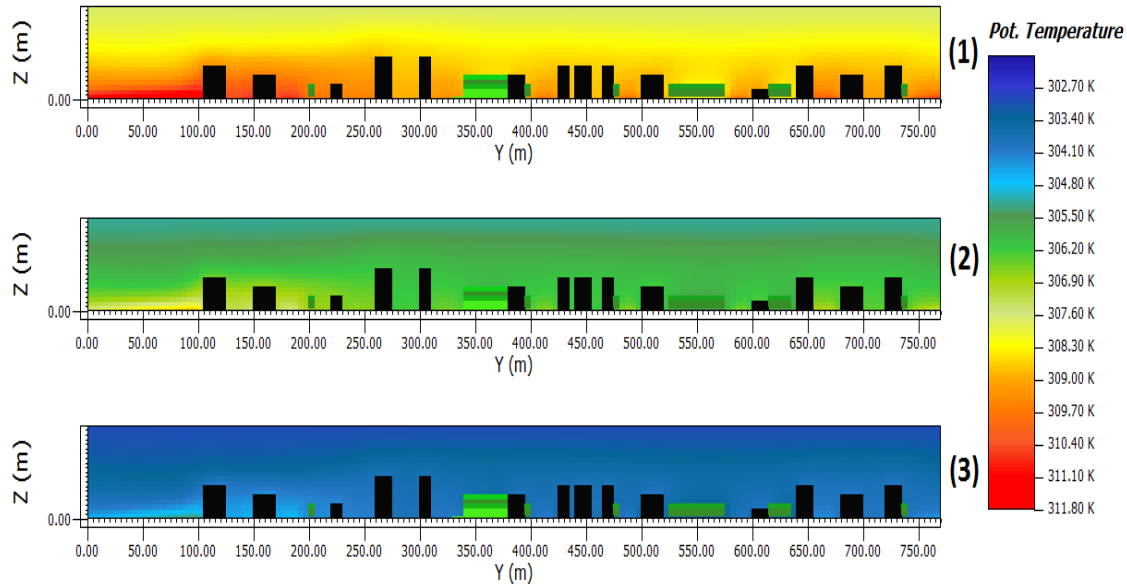


Figure 5.26: Vertical distribution of potential temperature for the three asphalt configuration: 0.1 (1); 0.40 (2); 0.65 (3).

It is possible to note as temperatures tend to decrease with altitude and in proximity to areas with vegetation.

Table 5.10 shows the temperatures detected by receptors at about 4.5 m above the ground. Three hours were chosen: 12:00, 15:00 and 18:00 in order to assess the evolution of temperature in the central part of the day. The selected receptors are: receptor 1, close to the vegetation and receptor 2, near a street intersection. Receptors 3, 4 and 5 show the same temperature values of receptor 2 and were not considered.

Table 5.10: Air temperature recorded by the receptors 1 and 2 to 4.5 meters above the ground for the three levels of solar reflectance of asphalt in July 20. The table shows also the temperature difference between the receptors 1 and 2 and the temperature difference between the configuration characterised by conventional asphalt and cool tints for the receptor 2.

Asphalt solar reflectance [-]		Hours [h]		
		12:00	15:00	18:00
0.1	R1	32.9	35.2	33.9
	R2	33.9	36.2	34.7
	$\Delta T (R2 - R1)$	0.9	1.0	0.7
0.4	R1	30.9	32.5	31.7
	R2	31.7	33.4	32.4
	$\Delta T (R2 - R1)$	0.8	0.8	0.7
0.65	R1	29.2	30.2	29.5
	R2	29.7	30.8	30.1
	$\Delta T (R2 - R1)$	0.6	0.7	0.6
	$\Delta T (0.1 - 0.4) R2$	2.2	2.9	2.3
	$\Delta T (0.1 - 0.65) R2$	4.1	5.4	4.6

As far as receptor 2 is concerned, the differences in air temperature values, as a result of the change in the asphalt reflectance value are evident: 2.9 °C by comparing the conventional asphalt with asphalt stained with cool grey tint and 5.4 °C by comparing conventional asphalt with asphalt

stained with cool off-white tint. The maximum value is reached during the peak temperature at 15:00 as shown in Table 5.10:  $\Delta T$  (0.1- 0.4) R2 and  $\Delta T$  (0.1 - 0.65) R2. Receptor 1, located near the vegetation, shows a temperature lower than the one recorded by receptor 2 with a maximum difference of 1 °C for the configuration with conventional asphalt at the peak temperature. This effect highlights the importance of vegetation as additional technique to mitigate temperatures in densely urbanised areas. However, the influence of vegetation on temperature slightly decreases with the increase of asphalt solar reflectance. This is due to the levelling of the temperature related to the cooling effect operated by these materials. See Table 6:  $\Delta T$  (R2 - R1).

Figure 5.27 shows the vertical profile of the air temperature during the same day, considered previously, at 15:00. The temperature was calculated from a 0 meters to 58.5 meters above the ground; the latter value represents the upper limit in height of the model calculation domain. Temperature trends related to the three configurations are very similar in the shape and the temperature differences stayed almost constant in relation to height. This result is another proof of how cool materials, applied to the asphalts, can influence so clearly and radically the thermal conditions of the affected area, improving comfort even at significant heights, well beyond the average height of the buildings. It should be noted the different behaviour of the two receptors between 0 and 25 m due to the presence of tall plants and trees that change the temperature profile of the receptor 1 (green). The maximum difference is 1 °C at about 4.5 m above the ground, corresponding to the value already discussed in Table 5.10. Beyond the limit of 25 m, the two trends of temperature become overlapped because the receptor 1 is no longer influenced by the effects of the vegetation.

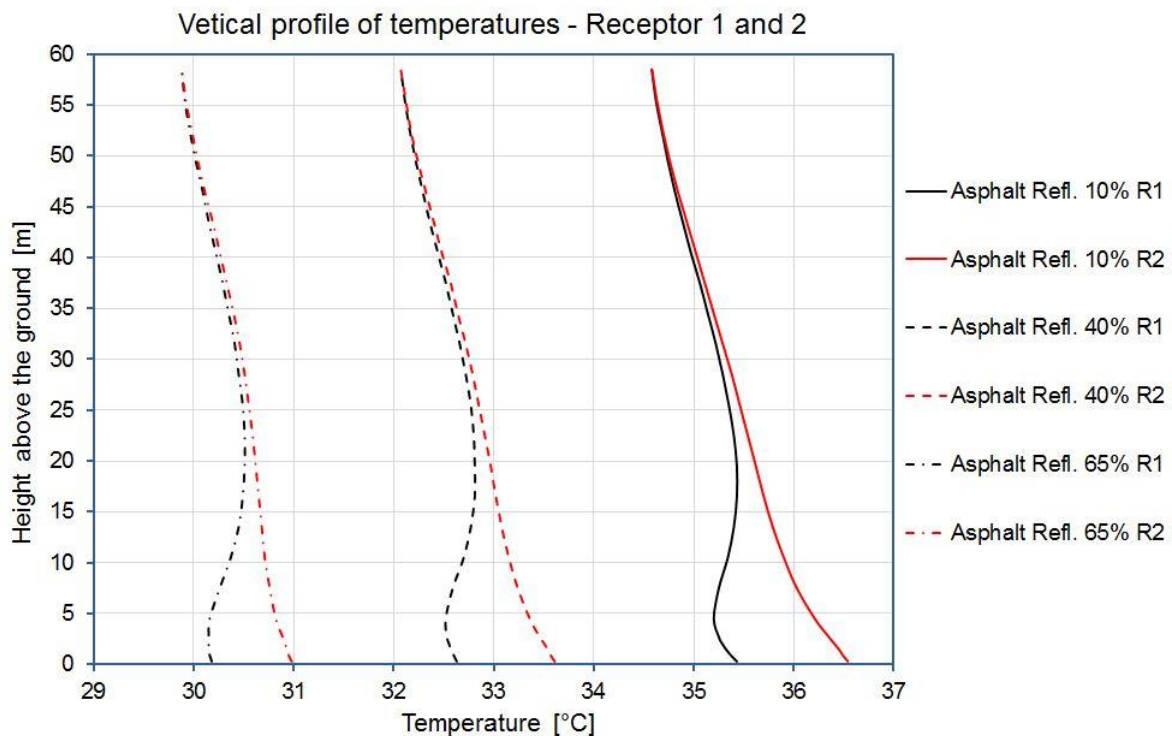


Figure 5.27: Vertical profile of air temperature for receptor 1 and 2 and for the three configurations.

### Cooling Demand Peak Calculation

The air temperature profiles obtained with previous simulations were used to calculate the cooling demand of a typical building within the reference context. The purpose of this study has been the assessment of the influence that an application of asphalts with high solar reflectance can have on cooling demand peaks. The study was conducted with the TRNSYS simulation software [5.47]. As mentioned previously, inputs of external temperature and relative humidity are derived

## Section 2: Experimental and Numerical Analyses

from the previous results obtained with ENVI-met software. These data are representative of one day in July and have been used to modify the default values of the climatic database of Rome (Fiumicino Airport) already existing in TRNSYS.

The structure in question is a residential building spreading over four levels with a flat roof. It represents a typical structure of the buildings assembly of the centre of Rome. Each floor consists of two apartments and it has a total area of 200 m<sup>2</sup>, a net area of 149.2 m<sup>2</sup> and a height of 2.7 m. The plant of the building is shown in Figure 5.28. The longer sides are exposed to North and South, with a windowed area of respectively 3.6 and 7.2 m<sup>2</sup>. The eastern and western sides have a windowed area of 5.4 m<sup>2</sup>. Table 5.11 shows the values of the thicknesses and thermal transmittance of the elements that compose the opaque and transparent envelope. Two levels of insulation were considered in order to quantify the impact of outside temperature on structures with different thermal characteristics to broaden the field of study to new and existing buildings. Ventilation was set to 0.3 volumes / h according to the Italian standard reference for residential use [5.48]. The cooling system was set to turning on when indoor temperature exceeds 26 °C.

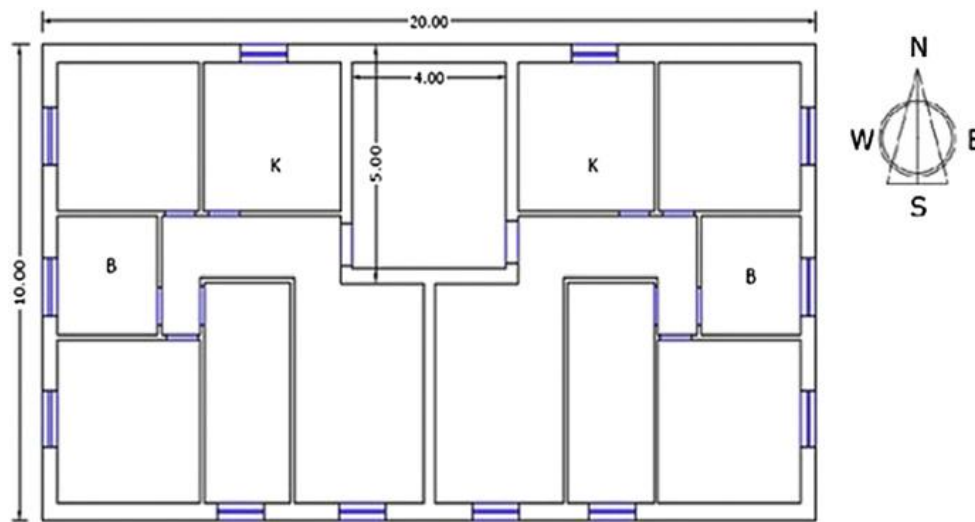


Figure 5.28: Reference building plant.

Table 5.11: Characteristics of opaque and transparent elements of the chosen building envelope.

	NOT INSULATED			INSULATED		
	Thickness [m]	Transmittance [W/m <sup>2</sup> K]		Thickness [m]	Transmittance [W/m <sup>2</sup> K]	
Roof Slab	0.35	1.100		0.35	0.385	
Ground Floor	0.3	1.211		0.3	0.493	
Internal Floor	0.3	1.211		0.3	0.493	
External Wall	0.38	1.128		0.38	0.433	
Internal Wall	0.15	1.726		0.15	2	
Window	Design [mm]	Transmittance [W/m <sup>2</sup> K]	g-value [-]	Design [mm]	Transmittance [W/m <sup>2</sup> K]	g-value [-]
	4	5.68	0.85	4-16-4	2.83	0.76

It has been previously shown that the increase in asphalt reflectance has a significant effect on the reduction of the urban environment temperature. This phenomenon is also reflected with the same intensity on thermal conditions inside the buildings, bringing benefits in terms of energy savings during the summer season. Table 5.12 shows the results obtained with TRNSYS, summarising the values of the cooling load peaks obtained considering the three configuration of road paving: the conventional one and those with cool tints. The table also shows the percentage values of peak reduction with reference to the worst case obtained with the conventional asphalt. For the not insulated building, the maximum cooling load peak was 21.2 kW considering the urban area equipped with a conventional asphalt; it decreases up to 19.0 kW considering the cool grey

## Section 2: Experimental and Numerical Analyses

asphalt tint with a percentage reduction of 10.2%. The use of a cool off-white tint leads to a peak load of 17.2 kW, with a percentage reduction of 18.9%. For the insulated building, the values of the peak cooling loads decreases, but also their percentage of reduction decreases, denoting as the structure suffers less the change in external temperatures due to a lower thermal transmittance. In this configuration, the peak load associated to the conventional asphalt is 16.9 kW while it is 15.6 kW if associated to a cool grey asphalt tint with a percentage reduction of 7.8%. Finally, the cool off-white asphalt tint induces a peak cooling demand of 14.4 kW with a reduction of 14.6%.

Table 5.12: TRNSYS results: peak cooling demands and percentage reductions: two insulation levels, three asphalt solar reflectance values.

asphalt solar reflectance [-]	NOT INSULATED		INSULATED	
	Peak Load [kW]	Peak Reduction [%]	Peak Load [kW]	Peak Reduction [%]
0.10	21.2	-	16.9	-
0.40	19.0	10.2	15.6	7.8
0.65	17.2	18.9	14.4	14.6

### Asphalt Surfaces: Concrete Draining Paving

The third group of simulations is similar to the previous group. In this case, the simulations were conducted both during a spring day and in a summer day, monitoring the middle hours of the day, from 10:00 to 14:00. Reflectance values chosen for road pavements are: 0.10 to simulate a conventional paving, 0.30 to simulate a light grey porous concrete paving (grain size 12 mm) and 0.56 to simulate white porous concrete paving (grain size 12 mm), according to the measurements result previously presented. As in previous cases Figure 5.29, Figure 5.30, Figure 5.31, Figure 5.32, Figure 5.33 and Figure 5.34 show an overview of the ENVI-met results, based on the horizontal distribution of potential temperature at 3 meters above the ground on April 20 and July 20 at 14:00.

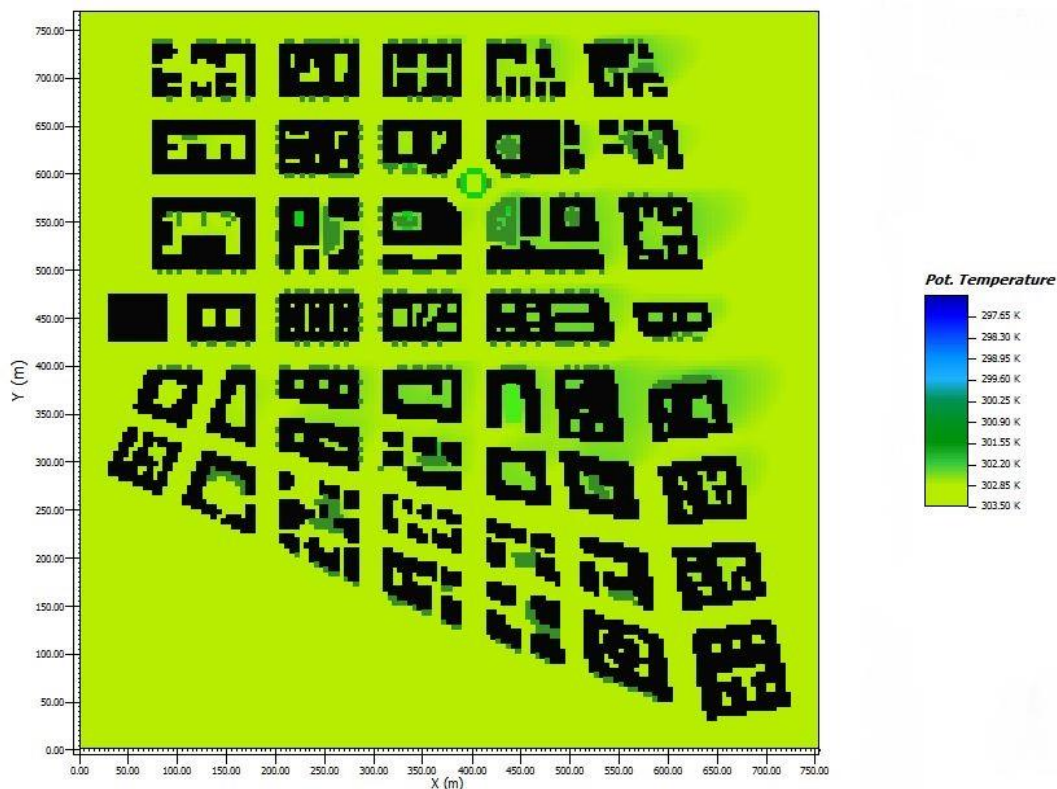


Figure 5.29: Horizontal distribution of potential temperature - Conventional road paving - April 20.



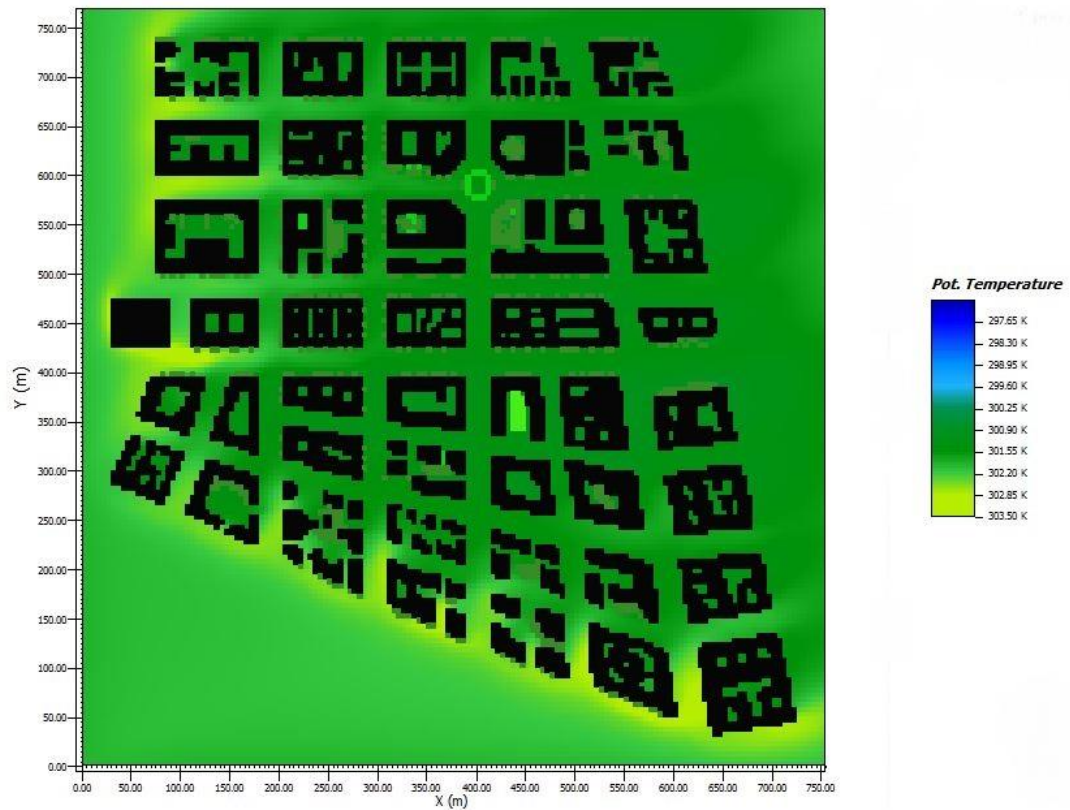


Figure 5.30: Horizontal distribution of potential temperature - Light grey porous concrete - April 20.

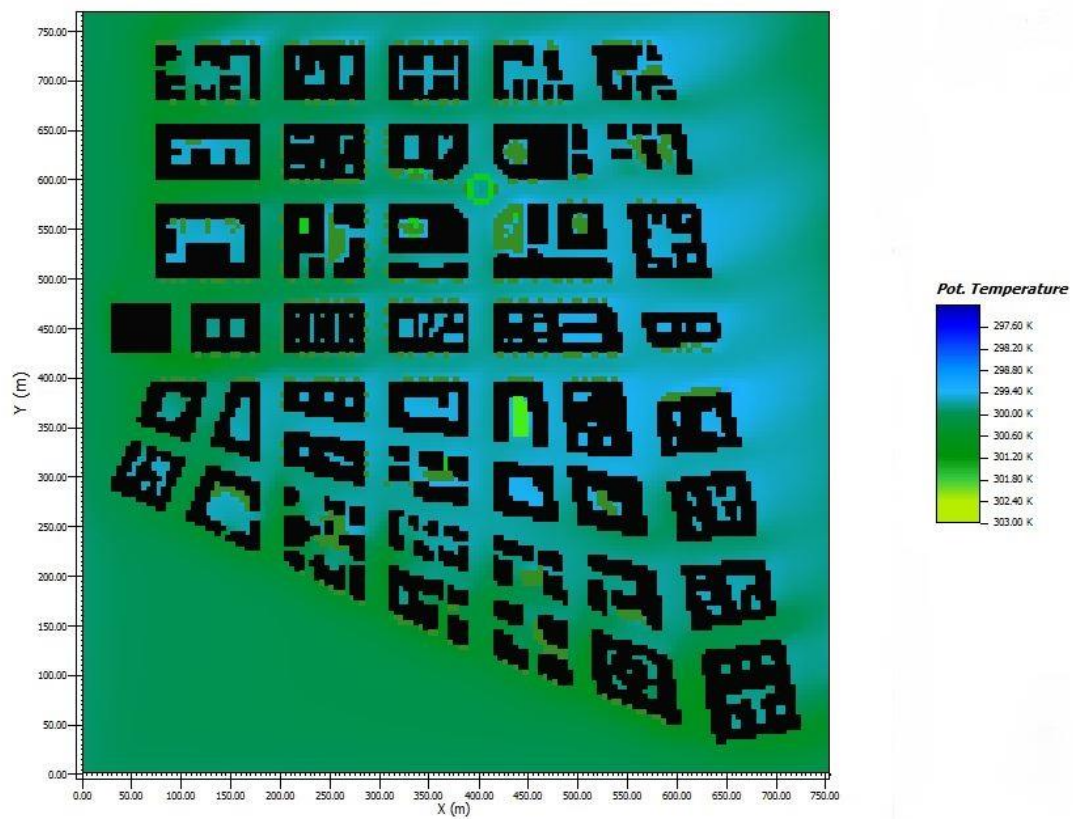


Figure 5.31: Horizontal distribution of potential temperature - White porous concrete - April 20.

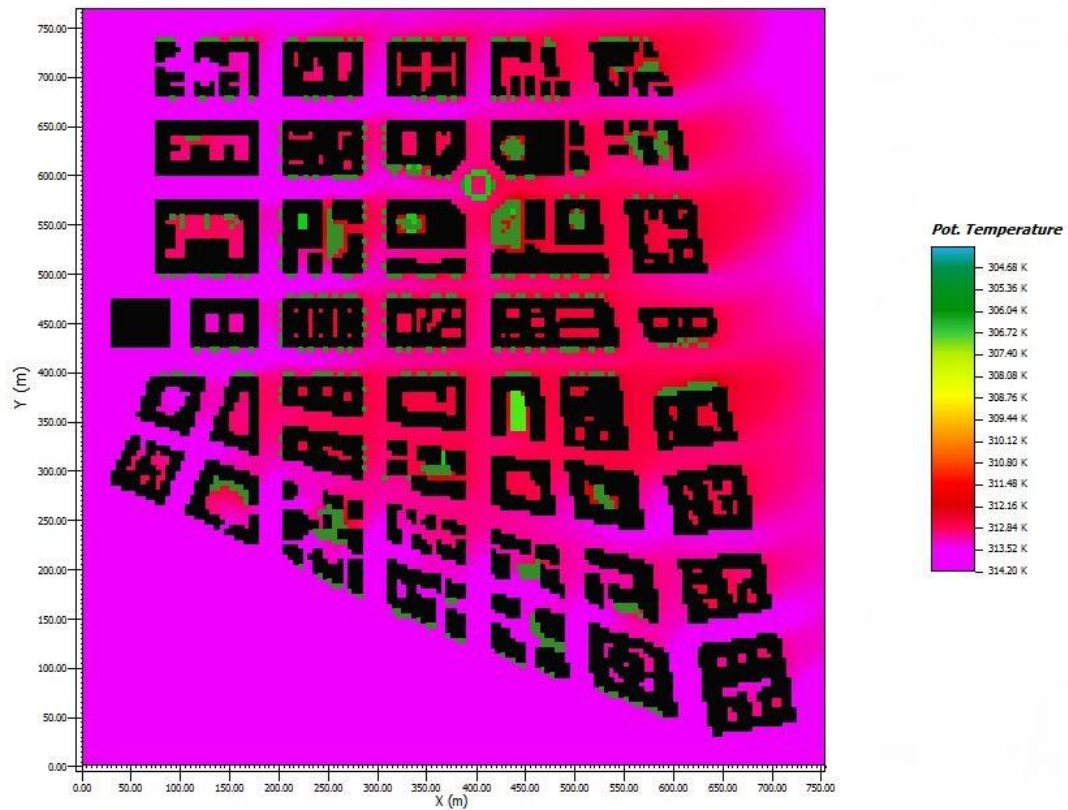


Figure 5.32: Horizontal distribution of potential temperature - Conventional road paving - July 20.

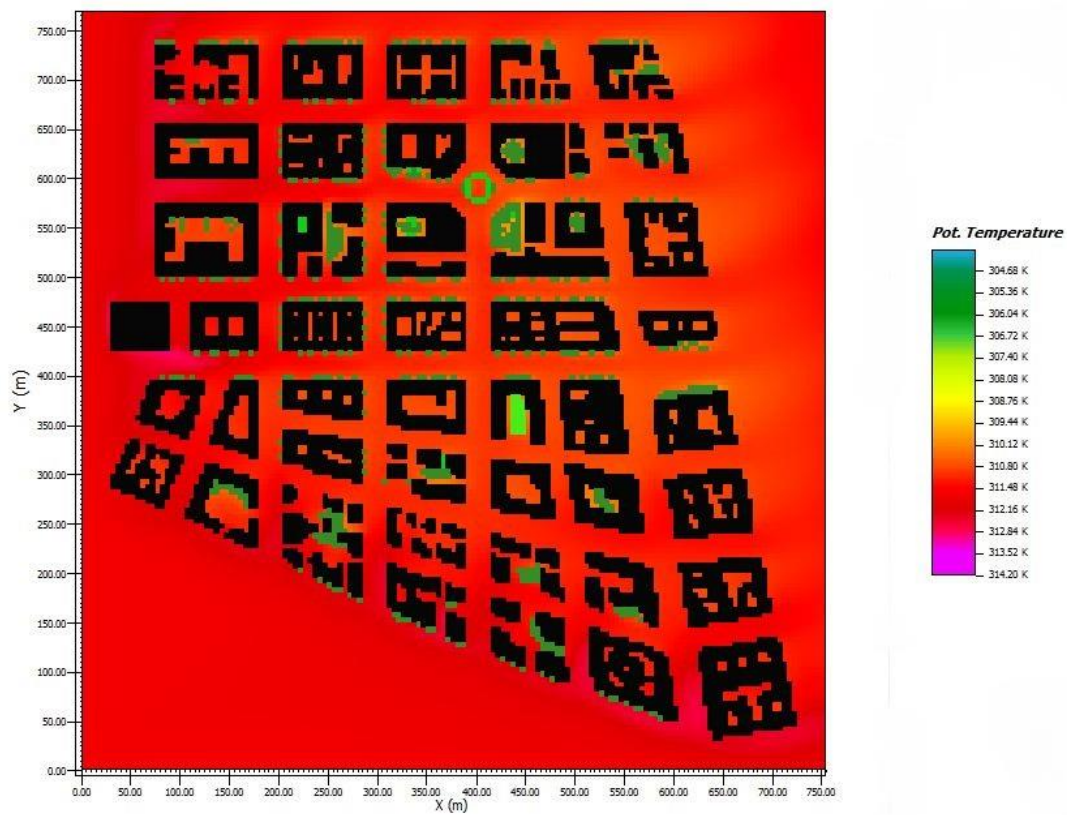


Figure 5.33: Horizontal distribution of potential temperature - Light grey porous concrete - July 20.



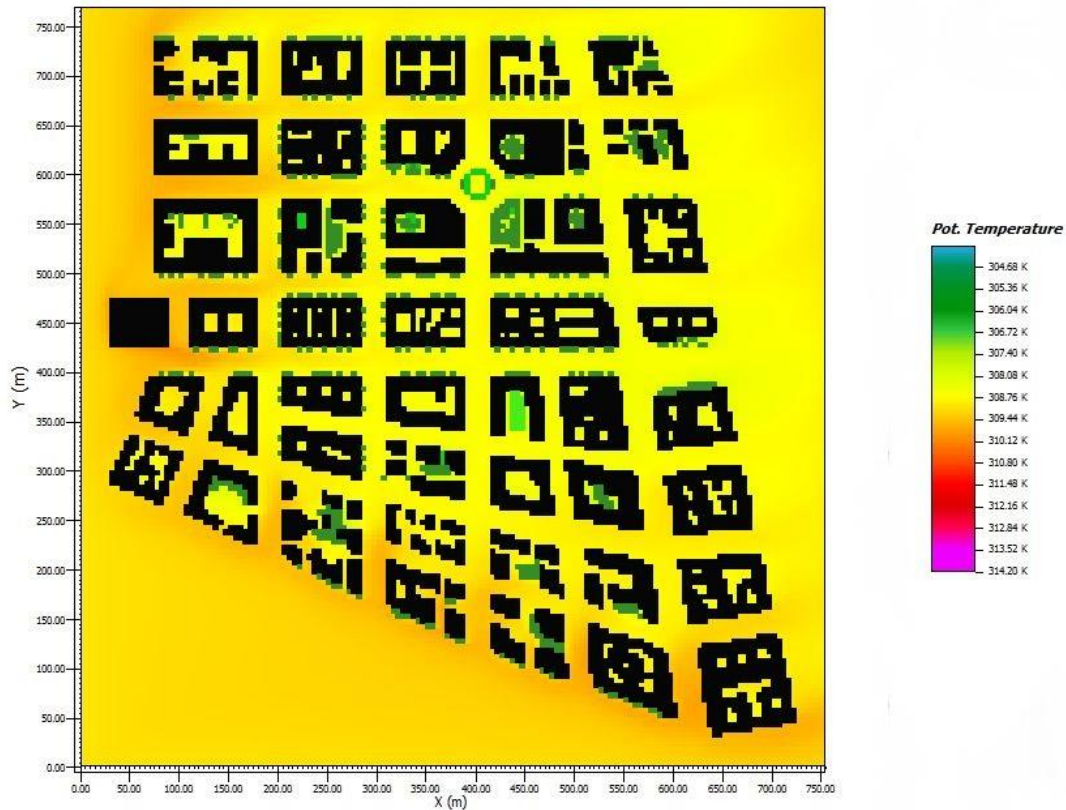


Figure 5.34: Horizontal distribution of potential temperature - White porous concrete - July 20.

According to the chromatic scale, it can be argued that in Spring the temperature decreases by an average of 1.5 °C shifting from an urban area composed of conventional asphalt (Figure 5.29) to an urban area equipped with the porous grey concrete (Figure 5.30). While considering the porous white concrete (Figure 5.31) the temperature decreases further with an average difference of 3.3 °C compared to the conventional material. During summer the temperature decrease reaches even higher values. If compared to the conventional configuration (Figure 5.32), the application of a porous grey concrete reduces the environmental temperature of 2 °C (Figure 5.33). The temperature reduction reaches a value of 4.4 °C for the porous white concrete (Figure 5.34).

The discussion of the results is the same as the results of second group: The grey and white porous concretes remain cooler under the sun than conventional asphalt, because of their high solar reflectance. A lower surface temperature induces a lower convective and radiative heat transfer to the air, decreasing its temperature. The water storing power of these materials was not considered, but it could be a contributory factor to limit the temperature rising by converting the solar irradiation absorbed in evaporation latent heat.

### Comfort Analysis

With the simulation results, the comfort level was calculated using the DI (Discomfort Index), developed by EC Thom [5.49]. It combines, within a single value, the effect of temperature, humidity and air mass movements on the sensation of hot and cold felt by the human body. Air temperature and relative humidity were extrapolated from the data recorded in the more thermally critical receptor: The receptor 2. The index was calculated using the following empirical equation 5.2:

$$DI = 0.4 \cdot (T_a + T_w) + 4.8 \quad (5.2)$$

## Section 2: Experimental and Numerical Analyses

In the equation  $T_a$  and  $T_w$  indicate, respectively, the dry bulb and the wet bulb air temperature. The index was derived both for April 20 and July 20 from 10:00 to 14:00. Figure 5.35 shows how the DI is positively influenced by the progressive increase in reflectance of the surfaces of urban road paving.

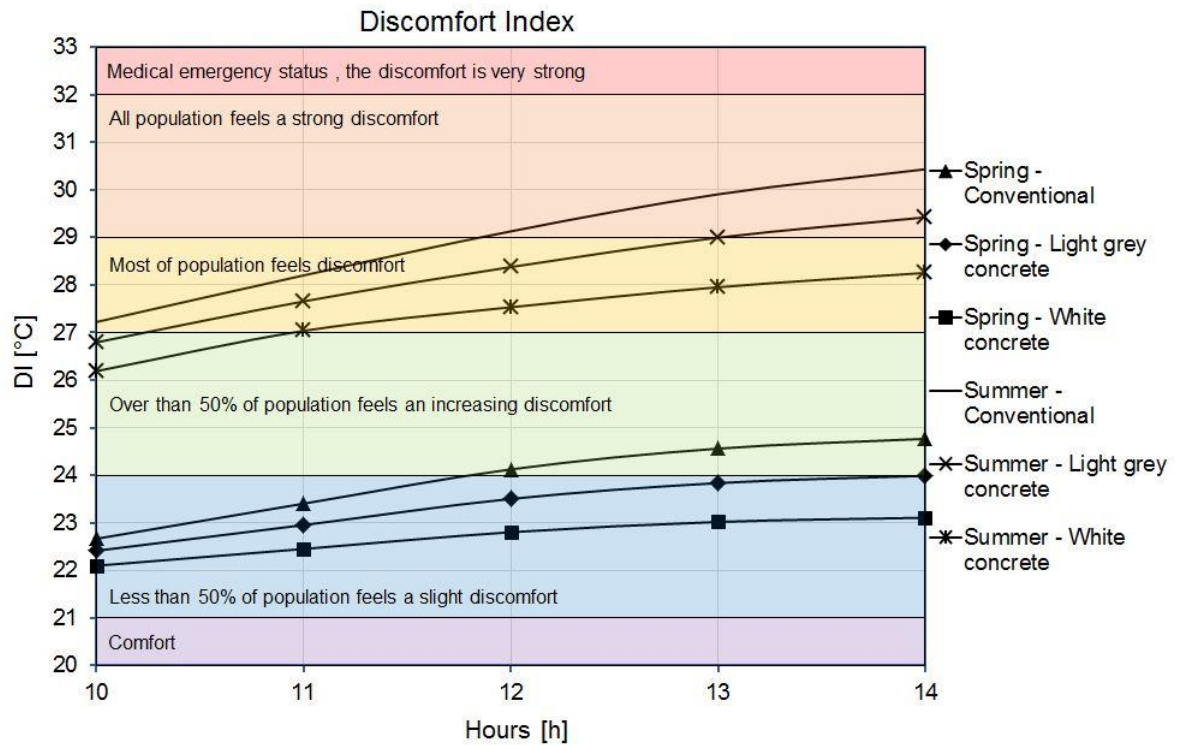


Figure 5.35: Discomfort Index calculated in spring and summer.

## 5.7 Chapter Conclusions

---

The urban heat island effect is a phenomenon that affects cities with a growing intensity. An experimental campaign, detecting the air temperatures, showed the actual presence of the phenomenon in Rome. In fact, from the analysis of data acquired by the thermo-hygrometric sensors, positioned in different points of the city during the summer season, it was obtained a maximum difference in temperature between a densely urbanised area and a rural area that has reached 7 °C. This temperature difference, called UHI (Urban Heat Island Intensity), occurred during night time.

The ability to reflect solar radiation of some materials, used as tints for asphalts and as coatings for road surfaces, was measured by means of optical characterisation in laboratory and outdoor campaigns.

To investigate the potentialities related to the application of materials with high solar reflectance in an urban area, different numerical analysis was conducted through ENVI-met, a software that uses a deterministic method of calculation of the thermo-physical phenomena in an urban environment. The results of this analysis highlight how these tints, used as surface coatings of the built-up environment have a significant impact, thanks to the low surface temperatures, on the decrease in the average air temperature of urban environment, even at considerable heights from the ground. A further numerical analysis conducted with TRNSYS allowed to estimate the effect produced by the decrease in air temperature in urban areas, resulting from the use of cool materials as asphalts coatings, on cooling demands of a typical residential building inserted into a densely populated neighbourhood of Rome. Appreciable reductions were found in the cooling load peak due to the use of these materials applied on road surfaces: 18.9% for non-insulated buildings and 14.6% for the insulated buildings. These results assume a more important connotation if extended to the whole summer season, for the calculation of seasonal energy demand.

In conclusion, the massive use of this innovative technology, combined with an increase in green areas would lead to a significant reduction of the urban heat island and its consequences with improved levels of comfort and a reduction of electric energy uses in buildings due to cooling units.

## 5.8 References

---

- [5.1] Rose LS, Akbari H, Taha H. 'Characterizing the Fabric of the Urban Environment: A Case Study of Greater Houston, Texas'. Lawrence Berkeley National Laboratory Report LBNL- 51448, Berkeley, CA; 2003.
- [5.2] Cambridge Systematics, Inc. Cool pavements draft report, [http://www.epa.gov/hiri/resources/pdf/CoolPavementReport\\_Former%20Guide\\_complete.pdf](http://www.epa.gov/hiri/resources/pdf/CoolPavementReport_Former%20Guide_complete.pdf); available on line at; 2005.
- [5.3] Akbari H, Pomerantz M, Taha H. 'Cool surfaces and shade trees to reduce energy use and improve air quality in urban areas'. Solar Energy; 2001; 70(3): 295 - 310.
- [5.4] Rosenfeld AH, Akbari H, Romm JJ, Pomerantz M. 'Cool communities: strategies for heat island mitigation and smog reduction'. Energy and Buildings 1998; 28: 51 - 62.
- [5.5] Taha H. 'Modelling the impacts of large-scale albedo changes on ozone air quality in the south coast air basin'. Atmospheric Environment 1997; 31(11): 1667 - 1676.
- [5.6] Taha H. 'Meteorological and Air Quality Impacts of Increased Urban Surface Albedo and Vegetative Cover in the Greater Toronto Area, Canada'. Lawrence Berkeley National Laboratory Report No. LBNL - 49210, Berkeley, CA; 2002.
- [5.7] Synnefa A, Karlessi K, Gaitani N, Santamouris M, Assimakopoulos DN, Papakatsikas C. 'Experimental testing of cool colored thin layer asphalt and estimation of its potential to improve the urban microclimate'. Building and Environment 2011; 46: 38 - 44.
- [5.8] Kinouchi T, Yoshinaka T, Fukae N, Kanda M. 'Development of cool pavement with dark colored high albedo coating'. Fifth Conference for the Urban Environment, Vancouver, Canada; 2004.
- [5.9] Carnielo E, Zinzi M. 'Optical and thermal characterisation of cool asphalts to mitigate urban temperatures and building cooling demand'. Building and Environment; 2013; 60: 56 - 65.

## Section 2: *Experimental and Numerical Analyses*

- [5.10] Ferguons B. Porous Pavements; 2005.
- [5.11] Haselbach L. 'Pervious concrete and mitigation of the Urban Heat Island Effect'. Transportation Research Board Annual Meeting; 2009.
- [5.12] Kevern J, Schaefer V R, Wong K. 'Temperature behavior of a pervious concrete system'. Transportation Research Board Annual Meeting; 2009.
- [5.13] World energy outlook 2008 - 2009. Geneva: International Energy Agency; 2008 - 2009.
- [5.14] Howard L. 'The Climate of London deduced from Meteorological Observations made in the metropolis, and at various places around it'; 1833.
- [5.15] Goldreich Y. 'Ground and top of canopy layer urban heat island partitioning on an airborne image'. Remote Sensing of Environment; 2006; 104: 247 - 255.
- [5.16] Hassid S, Santamouris M, Papanikolaou N, Linardi A, Klitsikas N. 'The effect of the heat island on air conditioning load'. Journal of Energy and Buildings; 2000; 32(2): 131 - 141.
- [5.17] Huang L, Li D, Zhao J, Zhu J. 'A fieldwork study on the diurnal changes of urban microclimate in four types of ground cover and urban heat island of Nanjing'. Building and Environment; 2008; 43: 7 - 17.
- [5.18] Kolokotroni M, Zhang Y, Watkins R. 'The London heat island and building cooling design'. Solar Energy; 2007;81(1):102 - 110.
- [5.19] Rosenzweig C, Solecki W, Parshall L, Choppingc M, Pope G, Goldberg R. 'Characterizing the urban heat island in current and future climates in New Jersey'. Environmental Hazards; 2005; 6: 51 - 62.
- [5.20] Santamouris M. 'Heat island research in Europe, the state of the art'. Advances Building Energy Research; 2007;1: 123 - 150.
- [5.21] Taha H, Chang SC, Akbari H. 'Meteorological and air quality impacts of heat island mitigation measures in three U.S. Cities'. Lawrence Berkeley National Laboratory Report, Berkeley, CA; 2000.
- [5.22] RAEE Rapporto Annuale Efficienza Energetica: ENEA; 2014. [www.ENEA.it](http://www.ENEA.it); available online at.
- [5.23] Konopacki S, Akbari H, Pomerantz M, Gabersek S, and Gartland. 'Cooling Energy Savings Potential of Light - Colored Roofs for Residential and Commercial Buildings in 11 U.S. Metropolitan Areas'. LBNL - 39433. Berkeley, CA: Lawrence Berkeley National Laboratory; 1997.
- [5.24] Akbari H. 2005. 'Energy Saving Potentials and Air Quality Benefits of Urban Heat Island Mitigation'. In Proc. of First International Conference on Passive and Low Energy Cooling for the Built Environment, Athens, Greece, May 17 - 24; 2005.
- [5.25] Levinson R., Akbari H, Konopacki S and Bretz S. 'Inclusion of cool roofs in non-residential Title 24 prescriptive requirements'. Energy Policy; 2005; 33: 151 - 170.
- [5.26] Synnefa A, Santamouris M, Apostolakis K. 'On the development, optical properties and thermal performance of cool colored coatings for the urban environment'. Solar Energy; 2007; 81: 488 - 497.
- [5.27] Pomerantz M, Akbari H, Chang SC, Levinson R, and Pon B. 'Examples of cooler reflective streets for urban heat-island mitigation: Portland cement concrete and chip seals'. Lawrence Berkeley National Laboratory: Lawrence Berkeley National Laboratory. LBNL Paper LBNL-49283; 2003. Retrieved from: <http://escholarship.org/uc/item/53w2s92d>; available online at;
- [5.28] Taha H, Chang S, and Akbari. 'Meteorological and Air Quality Impacts of Heat Island Mitigation Measures in Three U.S. Cities'. LBNL - 44222. Berkeley, CA: Lawrence Berkeley National Laboratory; 2000.
- [5.29] Dimoudi A and Nikolopoulou M. 'Vegetation in the urban environment: Microclimatic analysis and benefits'. Energy and Buildings; 2003; 35: 69 - 76.
- [5.30] Takakura T, Kitade S, Goto E. 'Cooling effect of greenery cover over a building'. Energy and Buildings; 2000; 31: 1 - 6.
- [5.31] Santamouris M, Pavlou C, Doukas P, Mihalakakou G, Synnefa A, Hatzibiros A and Patargias P. 'Investigating and analysing the energy and environmental performance of an experimental green roof system installed in a nursery school building in Athens, Greece'. Energy; 2007; 32: 1781 - 1788.
- [5.32] Alexandri E and Jones P. 'Temperature decreases in an urban canyon due to green walls and green roofs in diverse climates'. Building and Environment; 2008; 43: 480 - 493.
- [5.33] Akbari H, Pomerantz M and Taha H. 'Cool surfaces and shade trees to reduce energy use and improve air quality in urban areas'. Solar Energy; 2001; 70: 295 - 310.
- [5.34] Akbari H. 'Shade trees reduce building energy use and CO<sub>2</sub> emissions from power plants. Environmental Pollution; 2002; 116: S119 - S126.
- [5.35] Shashua-Bar L and Hoffman ME. 'Quantitative evaluation of passive cooling of the UCL microclimate in hot regions in summer, case study: Urban streets and courtyards with trees'. Building and Environment; 2004; 39: 1087 - 1099.

## Section 2: *Experimental and Numerical Analyses*

- [5.36] Rosenzweig C, Solecki W, R and Slosberg R. 'Mitigating New York City's Heat Island with Urban Forestry, Living Roofs, and Light Surfaces'. Report 06-06. Albany, NY: New York State Energy Research and Development Authority; 2006.
- [5.37] Stone B and Norman JM. 'Land use planning and surface heat island formation: A parcel based radiation flux approach'. *Atmospheric Environment*; 2006; 40: 3561 - 3573.
- [5.38] Giridharan R, Lau SSY, Ganesan S., Givoni B. 'Urban design factors influencing heat island intensity in high-rise high-density environments of Hong Kong'. *Building and Environment*; 2007; 42: 3669 - 3684.
- [5.39] Emmanuel R, Rosenlund H and Johansson E. 'Urban shading-a design option for the tropics? A study in Colombo, Sri Lanka'. *International Journal of Climatology*; 2007; 27: 1995 - 2004.
- [5.40] Salamanca F, Krpo A, Martilli A and Clappier A. 'A new building energy model coupled with an urban canopy parameterization for urban climate simulations - part I. Formulation, verification and sensitivity analysis of the model'. *Theoretical and Applied Climatology*; 2010; 99: 331 - 344. DOI 10.1007/s00704 - 009 - 0142 - 9.
- [5.41] ISO 9050. Glass in building-Determination of light transmittance, solar direct transmittance, total solar energy transmittance, ultraviolet transmittance and related glazing factors; 2003.
- [5.42] ENVI-met Version 3.1, [www.envi-met.com](http://www.envi-met.com); available online at; 2010.
- [5.43] Huttner S, Bruse M, Dostal P. 'Using ENVI-met to simulate the impact of global warming on the microclimate in central European cities'. 5th Japanese - German Meeting on Urban Climatology (Berichte des Meteorologischen Instituts der Albert-Ludwigs-Universität Freiburg Nr. 18); 307 - 312; 2008.
- [5.44] Bruse M. 'Simulating human thermal comfort and resulting usage patterns of urban open spaces with a Multi-agent System'. *Proceedings of the 24th International Conference on Passive and Low Energy Architecture PLEA*; 699 - 706; 2007.
- [5.45] Lahme E, Bruse M. 'Microclimatic effects of a small urban park in densely built-up areas: Measurements and model simulations'. *ICUC5, Lodz* 1 - 5 September; 2003.
- [5.46] Huttner S, Bruse M. 'Numerical modelling of the urban climate - A preview on ENVI-met 4.0'; *Seventh International Conference on Urban Climate ICUC - 7*, 29 June - 3 July, Yokohama, Japan; 2009.
- [5.47] TRNSYS 16. <http://www.trnsys.com>; Available online at.
- [5.48] UNI 10339. Impianti aeraulici a fini di benessere; 1995.
- [5.49] Thom EC, Bosen JF. 'The discomfort index', *Weatherwise*. 57 - 60; 1959.



## **Section 3: *Development of Numerical Methods***

## 6. Solar reflectance angular dependence of opaque construction materials

---

### 6.1 Introduction

---

Solar gains on opaque surfaces influence energy performances in building energy analysis augmenting the demand for space cooling during summer and decreasing the demand for space heating during winter. They depend on solar irradiation and on solar absorptance that is a property of materials. Absorptance is a coefficient obtained as the ratio between the radiation absorbed by a surface and the incident radiation and, for opaque materials, it is the complement to 1 of reflectance (par. 2.3.2). Reflectance is the ratio between the reflected radiation by a surface and the incident radiation and, being generally easier to measure than absorptance, it is a property well investigated in literature in order to assess the selective capability of materials to reflect radiation at different wavelengths [6.1]. This study is aimed at investigating how reflectance is angular dependent. Solar reflectance is a quantity that varies between a minimum value when a surface is struck perpendicularly by a light beam, to a maximum value corresponding to a light beam parallel to the surface, with a trend depending on the roughness of surface. Typically coloured and painted surfaces of metals or plastic are smooth and glossy presenting a high regular reflectance component strictly dependent on incidence angle. This component follows the Fresnel equation. Instead, a rough surface, due to its irregular features, present many directions of reflection and the reflective coefficient seems to be less sensitive to the incidence angle of the light beam. For this reason a rough surface tends to be similar to a Lambertian surface characterised by a constant distribution of hemispherical radiance.

Solar radiation changes in intensity during the day and can be divided into two components, a diffuse one and a direct one, in percentages that vary with the time of day and with latitude. While the diffuse component always strikes a surface from every direction during daylight, the direct component changes its angle of incidence. Most of thermo-physical models take into account the

aforementioned geometric and energetic distribution of solar radiation, while they may consider constant the solar reflectance of surfaces during the daylight at every incidence angle of direct solar radiation assuming that each surface is Lambertian. This assumption may not be valid for some real materials not perfectly diffusive, which increase their reflection power if struck with a high incidence angle of light beam. This issue induces an overestimation of solar gains.

The cool materials technology is now well-established especially with regard of coatings for roof applications. The latter generally have smooth surfaces with a reflection mode that presents a not negligible regular component. In this perspective the reflectance solar dependence on incidence angle plays an important role on the estimation of solar gains on building components.

The paper introduces a method to compute the reflectance values in order to calculate more accurately the solar gains and therefore the energy fluxes involved in the energy balances of buildings.

## 6.2 Nomenclature

Table 6.1: Chapter 6 nomenclature.

I	Irradiance	[W/m <sup>2</sup> ]
Q	Heat power	[W/m <sup>2</sup> ]
q	Luminance coefficient	[1/sr]
$\alpha$	Absorptance	[-]
$\theta$	Incidence angle	[°]
$\varepsilon$	Angle between the perpendicular to the sample (z-axis) and a reference direction	[°]
$\varphi$	Angle between a reference axis (x-axis) and a reference plane	[°]
$\rho$	Reflectance	[-]
Subscript		
1	Incidence	
2	Reflection	
b	Beam	
b-hem	Incident beam radiation - Hemispherical reflection	
d	Diffuse	
d-d	Incident diffuse radiation - Diffuse reflection	
e	Solar	
g	Global	
SL	Solar load	

## 6.3 Methodology

Solar loads that affected an orientated surface are obtained by multiplying the value of solar irradiance for the absorptance. The latter is determined, for opaque surfaces, by simply subtracting solar reflectance from unity. See equation 6.1.

$$\alpha_e = (1 - \rho_e) \quad (6.1)$$

Typically the physical law which governs solar loads in the most of thermo-physical models is the following equation 6.2:

$$Q_{SL} = I_b \cdot (1 - \rho_e) + I_d \cdot (1 - \rho_e) = (I_b + I_d) \cdot (1 - \rho_e) = I_g \cdot (1 - \rho_e) \quad (6.2)$$

It implicitly considers the surface hit by the solar radiation as Lambertian (perfectly diffusive, with a constant reflectance and therefore absorptance independent from the angle of incidence of direct solar irradiance). This approximation could be considered valid for materials whose surface

is highly rough but it cannot be applied for all materials used as building envelope coatings. As shown in equation 6.2, solar loads change during the day only with global irradiance intensity, having considered the solar reflectance as a constant.

Direct solar irradiance changes its incidence angle on surfaces as a function of time of day, orientation and latitude. A surface increases its reflection power passing from a normal incidence beam to a parallel one. The amount of this increase depends on the intensity of the regular reflectance component that follows the Fresnel equation while the diffuse component remains constant and independent from angle.

The method proposed in this study allows to consider solar gains not only dependent on the change in intensity of global solar irradiance during the daylight but also dependent on the variation of the reflectivity power of the interested surfaces as a function of the incidence angle. Two different reflectance types were considered.

The first one,  $\rho_{e,b-hem}(\theta)$  is the total or hemispherical reflectance including direct component and diffuse component. It is angular dependent and it is obtained from the interpolation of experimental values performed at several incidence angles. This value is correlated to the direct beam of solar irradiance.

The second one,  $\rho_{e,d-d}$ , is a constant value, obtained as an integral average of the previous function from 0 to 90 degrees of incidence, see equation 6.4. It is correlated to the diffuse solar irradiance that strikes a surface in every direction. The solar gains equation turns in the form 6.3:

$$Q_{SL}(\theta) = I_b \cdot [1 - \rho_{e,b-hem}(\theta)] + I_d \cdot (1 - \rho_{e,d-d}) \quad (6.3)$$

with

$$\rho_{e,d-d} = \frac{1}{90} \int_0^{90} \rho_{e,b-hem}(\theta) \cdot d\theta \quad (6.4)$$

Optical measurements were performed on fifteen typical opaque building materials at different incidence angles of a light beam using a gonio-photometer in order to evaluate the spatial distribution of reflections. Further measurements on four selected samples were carried out with a spectrophotometer to obtain the solar reflectance value increasing incidence angles.



The theoretical evolution of regular reflectance with angle, starting from the reflectance value of the samples obtained experimentally for the near normal incidence, was calculated for two materials through Fresnel equation considering a light beam passing from a mean with an unitary refractive index (air) to a mean with a refractive index of 1.5 (specular surface i.e. glass) [6.2]. The experimental and theoretical results were used to find correlations between incidence angles and reflectance in form of equations. The latter were inputted in a building energetic tool, the TRNSYS.

The results allowed to compare several building energetic parameters obtained applying the method exposed in this study, the theoretical regular reflectance and the default calculation preset in the software that consider the solar reflectance of a surface as a constant. Henceforth the first will be called the  $\rho(\theta)$  method, the second  $\rho_{th}(\theta)$  method and the third the  $\rho_{const}$  method.

## 6.4 Description of Selected Materials

The selected samples for the experimental campaign are listed in Table 6.2. They represent typical opaque materials used in building construction.

Table 6.2: Selected materials.

Code	Description	Color	Surface Finishing	Surface Image
8284	Membrane	Grey	Rough	
8285	Textured membrane	Grey	Smooth	
8286	Coating TiO <sub>2</sub>	Grey	Rough	
8287	Bituminous shingle	Dark grey	Rough	
8288	Tile	Light Blue	Smooth	
8289	Tile	Gothic brown	Rough	
8290	Tile	Beige	Smooth	
8291	Tile	Grey	Rough	
8292	Travertine	White	Rough	
8293	Lava stone	Dark grey	Rough	
8294	Porous concrete grain size 6 mm	White	Rough	
8295	Porous concrete grain size 12 mm	White	Rough	
8296	Textured marble tile	Dark grey	Rough	
8297	Marble tile	Light grey	Rough	
8298	Clay brick	Brown	Rough	



## 6.5 Experimental

### 6.5.1 Gonio-Photometric Measurements

In order to know how a surface reflects a light beam and to discover the possible presence of preferential direction of reflection, it was necessary to measure the samples of building materials with a gonio-photometer. This device allows to construct the spatial distribution of the reflection of a surface when struck by an incident light beam.

As reported in Figure 6.1, the geometry of measurement is specified by a polar coordinate system centred on the surface of the sample and with the azimuthal angles referred to an appropriate direction on it. See Table 6.1 for the used symbols.

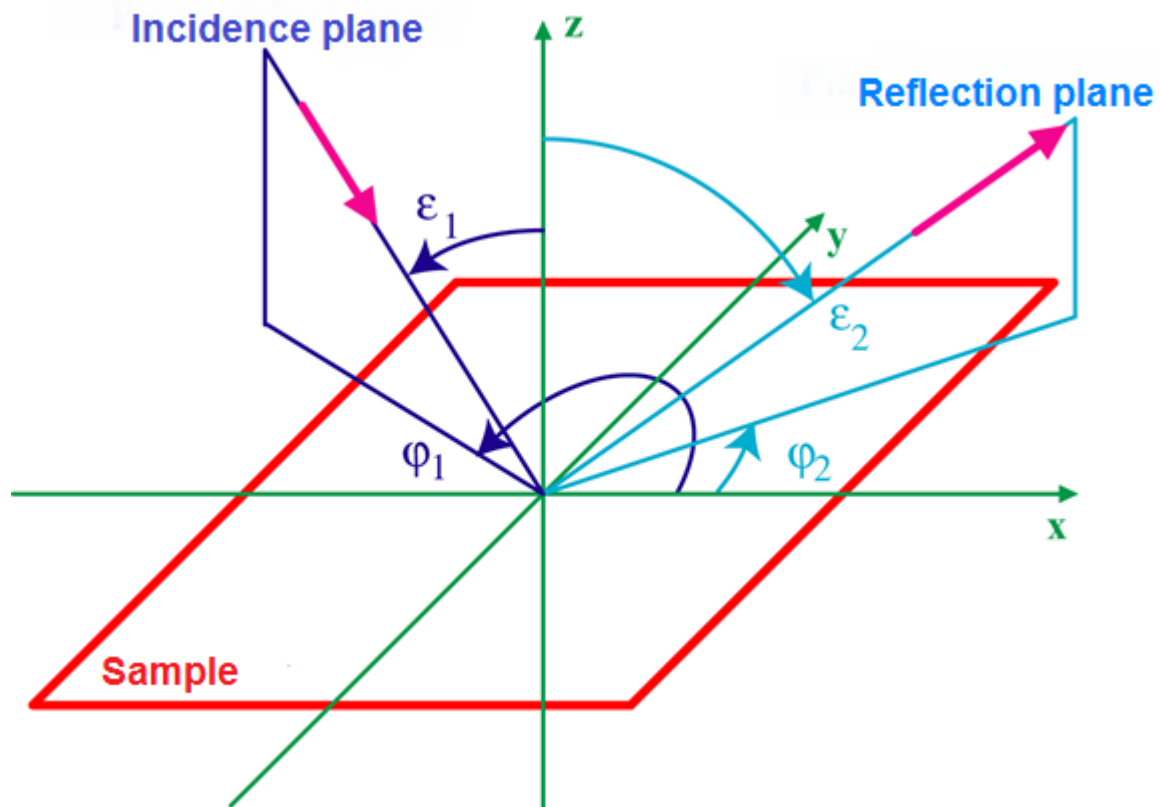


Figure 6.1: Characteristic angles and direction used in gonio-photometric measures.

The gonio-photometer was made available by the optics laboratory of INRIM (Istituto Nazionale di Ricerca Metrologica) of Turin. The characteristics and the method of operation of the instrument were already described (par. 3.4).

The samples were in thermal balance with the laboratory environment temperature ( $25 \pm 2$  °C) and they were measured without any preliminary surface cleaning.

As reported in paragraph 3.4 the output provided by the device is the luminance coefficient “q”. It represents the ratio between the reflected luminance measured in the view direction and the illuminance generated by the light source normally incident on the sample surface.

The size and the weight of some samples made difficult the measurements carried out with the gonio-photometer, not permitting to fully exploit the potentialities of that device. It was possible to measure the luminance coefficient only on a plane normal to the surface and passing through the centre of the sample.

All measurements were performed with an incandescent source (tungsten lamp) at the colour temperature of  $2856 \pm 50$  K being equal to illuminant A and with a photometric detector with a filter to simulate the spectral luminous efficiency function  $V(\lambda)$ .

The measures were carried out at four incidence angles:  $8^\circ$ <sup>1</sup> (near normal to the sample surface),  $30^\circ$ ,  $45^\circ$  and  $60^\circ$ . It was not possible to perform measurements at angles of incidence greater than  $60^\circ$  for problems related to the size of the incident beam that stretched over the sample not allowing a correct measurement.

The incidence angle is typically considered  $0^\circ$  when a light beam hits a surface normally, while is  $90^\circ$  when the light beam is parallel to it.

The Figure 6.2 reports the typical reflection modalities in the measure plane of materials mainly depending on the surface finishing.

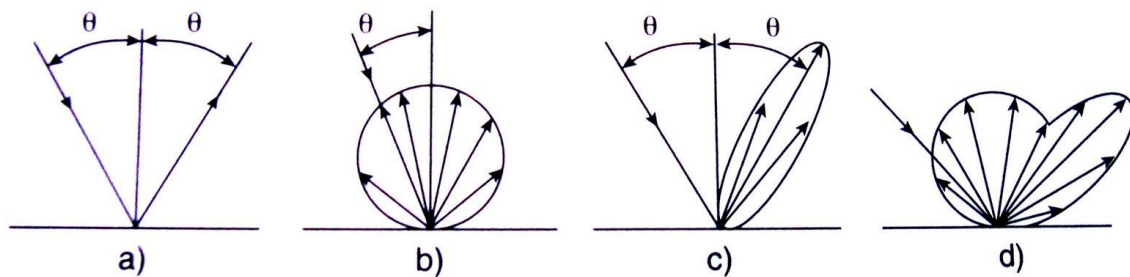


Figure 6.2: Reflection modalities: a) Regular reflection; b) Perfectly diffuse reflection; c) semi-specular reflection; d) semi-diffuse reflection.

Referring to Figure 6.2, the samples can be classified according to their reflection shapes:

- **Samples with a diffuse reflection:** An evident regular component of reflection is not present or a privileged direction of reflection does not exist. This behaviour can be found in samples 8286, 8296, 8297 (see Figure 6.2 b);
- **Samples with a relevant regular reflection:** The regular component of reflection is well detectable and reflection angle is symmetrical to the angle of incidence. This behaviour can be found in samples 8285, 8290, 8291 (see Figure 6.2 c);
- **Samples with reflection mainly contained in the regular reflection half-plane:** A sensible increasing in luminance coefficient is detected in the half-plane opposed to that of incidence, but the interested angles do not concerned exclusively those around the regular reflection. This behaviour can be found in samples 8284, 8288, 8289, 8292 (see Figure 6.2 d);
- **Samples with reflection mainly contained in the incidence half-plane:** A sensible increasing in luminance coefficient is detected in the incidence half-plane. The lack of measurements in the directions next to the retro-reflection make it impossible to assess the numerical importance of this component. This behaviour can be found in samples 8287, 8293, 8294, 8295, 8298.

The following Figure 6.3 and Figure 6.4 report the luminance coefficient distribution in the measure plane for two samples: The first one is a smooth membrane (sample 8285 in Table 6.2), the second one a rough membrane (sample 8286 Table 6.2).

<sup>1</sup> The value of  $8^\circ$  was chosen because it represent the angle of incidence of the light beam on a sample typically used in the spectrophotometric devices equipped with integrating sphere to avoid that the regular component of reflection come out from the opening through which the beam enter in the sphere.

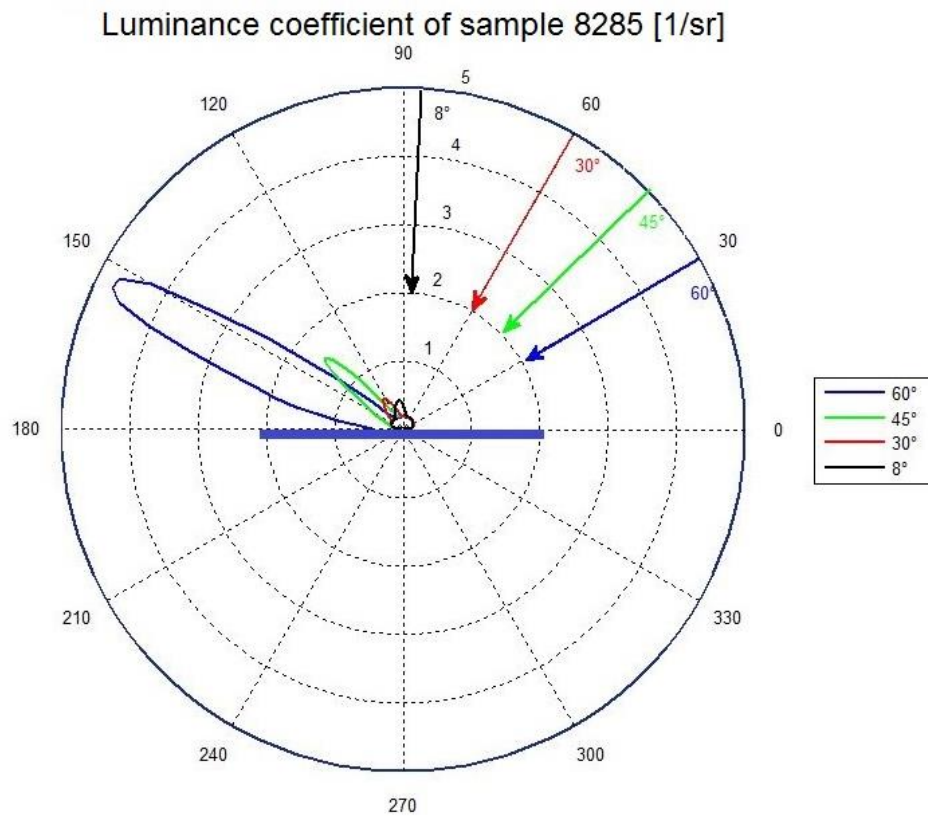


Figure 6.3: Gonio-photometer results: Polar diagram of luminance coefficient of sample 8285 (smooth surface), measured at 8°, 30°, 45°, 60° of incidence of the light beam on the surface sample.

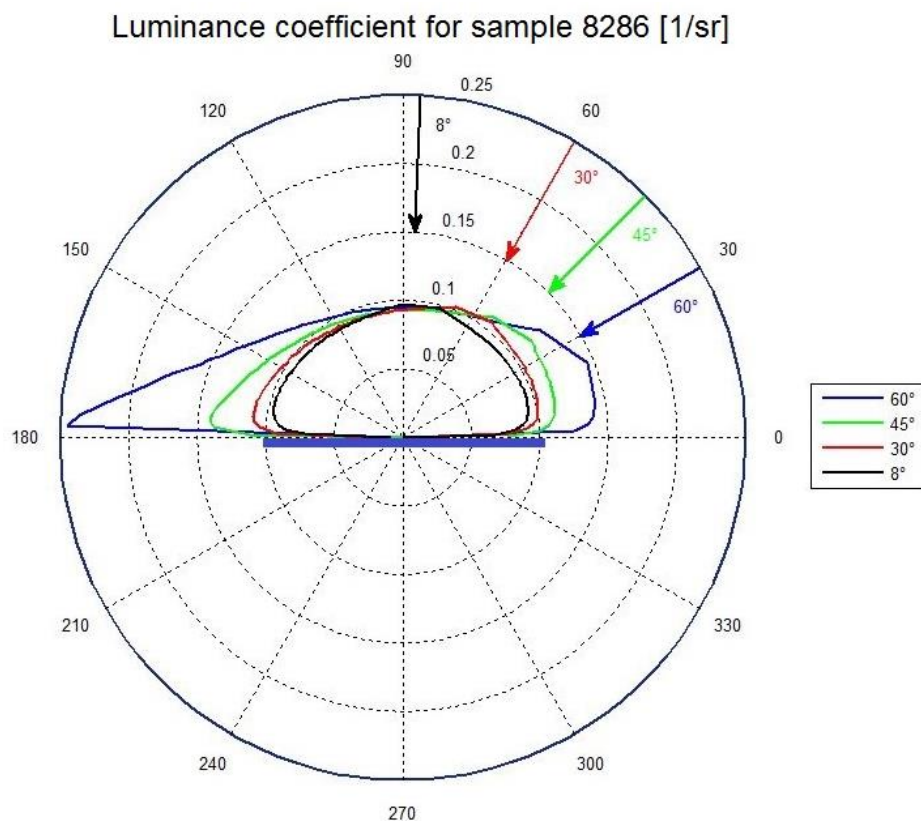


Figure 6.4: Gonio-photometer results: Polar diagram of luminance coefficient of sample 8286 (rough surface), measured at 8°, 30°, 45°, 60° of incidence of the light beam on the surface sample.

More that the intensity of the coefficient of luminance, that takes values significantly different for the two samples, it is important to note the different reflection modalities. The sample 8285 in Figure 6.3 presents a semi-diffuse reflection modality at 8° and a semi-specular modality at 60° with a well-defined regular reflection component. It follows exactly the Fresnel law. With an angle of incidence of 60° the brightness in the direction of view of the regular component increases by about 20 times compared to the measurement made at 8 ° incidence.

Instead, the sample 8286 in Figure 6.4 presents a diffuse reflection with small variations in the intensity of the luminance coefficient in the reflection half-plane.

Once the coefficient of luminance for all directions of observation has been obtained, the directional-hemispherical reflectance factor can be calculated, for an angle of incidence, by the following equation 6.5 (see Table 6.1 for the used symbols).

$$\rho_{\theta,d} = \int_0^{2\pi} \int_0^{\frac{\pi}{2}} q(\theta, \varepsilon_2, \varphi_1, \varphi_2) \cos \varepsilon_2 \sin \varepsilon_2 d\varepsilon_2 d\varphi_2 \quad (6.5)$$

This integral is usually calculated by numerical integration. In this case, since the measurements were conducted not on a three-dimensional hemispherical surface, but on a single plane, the integration cannot be resolved except using approximations. A new procedure developed in a study of the optics laboratory of INRIM was used to calculate directional-hemispherical reflectance and the results were compared to the reflection factor measurement performed with a spectrophotometer in order to verify the results reliability. This procedure calculate the approximate value of the reflectance even if the measurements were performed only in a sample surface normal plane. The procedure is summarised as follow (see Table 6.1 for the used symbols):

- **Samples with a Lambertian reflection:** Values measured in the  $\varphi_2 = 180^\circ$  half-plane are extended to space in which  $90^\circ \leq \varphi_2 < 270^\circ$ . Values measured in  $\varphi_2 = 0^\circ$  half-plane are extended in the space in which  $0^\circ \leq \varphi_2 < 90^\circ$  and  $270^\circ \leq \varphi_2 < 360^\circ$ ;
- **Samples with a relevant regular reflection:** The regular component is readily identifiable and it is integrated considering it symmetric with respect to the plane defined by the regular reflection direction. The remaining component (diffuse component) is integrated as in the previous case of Lambertian samples;
- **Samples with reflection mainly contained in the regular reflection half-plane:** The regular component is clearly identifiable but it is not symmetric. The  $q$  values delimiting the regular component until the peak, in the half-plane  $\varphi_2 = 0^\circ$ , are used as a weighting function applied to the azimuthal angles in order to reproduce a scaled trend of  $q$  maintaining constant its shape. The remaining component (diffuse component) is integrated as in the case of the Lambertian samples;
- **Samples with reflection mainly contained in the incidence half-plane:** As in the previous case but considering the  $\varphi_2 = 180^\circ$  half-plane as reference.

Table 6.3 shows the values of the directional-hemispherical reflectance and its diffuse component obtained with the previously described procedure, for each sample and for each incidence angle. Moreover, to emphasise the importance of regular component as a function of the angle of incidence, the ratio between the diffuse and the total reflectance is also shown.

Table 6.3: Total directional-hemispherical reflectance and diffuse component obtained through the procedure - ratio between diffuse and total reflectance.

Code	Incidence angle											
	8°			30°			45°			60°		
	Total	Diffuse	Ratio	Total	Diffuse	Ratio	Total	Diffuse	Ratio	Total	Diffuse	Ratio
8284	0.278	0.274	0.988	0.284	0.270	0.953	0.292	0.275	0.940	0.312	0.282	0.905
8285	0.505	0.497	0.983	0.515	0.492	0.955	0.529	0.491	0.928	0.566	0.470	0.832
8286	0.242	0.242	1.000	0.260	0.254	0.976	0.278	0.257	0.924	0.305	0.269	0.885
8287	0.321	0.311	0.970	0.330	0.319	0.966	0.337	0.322	0.953	0.349	0.343	0.982
8288	0.346	0.339	0.980	0.350	0.319	0.912	0.362	0.319	0.882	0.362	0.306	0.844
8289	0.275	0.269	0.980	0.277	0.252	0.911	0.297	0.247	0.832	0.350	0.245	0.699
8290	0.482	0.478	0.992	0.490	0.470	0.959	0.504	0.466	0.925	0.524	0.446	0.851
8291	0.145	0.140	0.965	0.146	0.121	0.827	0.162	0.117	0.722	0.205	0.112	0.545
8292	0.621	0.621	1.000	0.623	0.620	0.996	0.634	0.632	0.996	0.646	0.639	0.989
8293	0.171	0.170	0.994	0.183	0.169	0.920	0.198	0.181	0.914	0.221	0.199	0.904
8294	0.548	0.543	0.992	0.576	0.567	0.986	0.617	0.588	0.952	0.700	0.628	0.898
8295	0.559	0.556	0.994	0.604	0.570	0.943	0.654	0.601	0.919	0.696	0.606	0.872
8296	0.309	0.309	0.999	0.322	0.311	0.965	0.341	0.319	0.937	0.365	0.344	0.943
8297	0.416	0.416	0.999	0.426	0.422	0.992	0.441	0.432	0.980	0.470	0.443	0.943
8298	0.313	0.310	0.991	0.329	0.319	0.970	0.351	0.319	0.909	0.382	0.325	0.851

## 6.6 Spectrophotometric Measurements

Spectral measures were performed by means of an experimental facility at the UTEE laboratory (Unità Tecnica Efficienza Energetica) of the ENEA Casaccia Research Centre [6.3]. The coatings samples were tested at five different incidence angles of the light beam: 8° (near normal), 30°, 45°, 60°, and 75°. For issues related to the geometry of the measure instrument it was not possible to perform measures with an incidence angle greater than 75°. An optical characterisation which involves a variation of the angle of incidence of the beam on the sample is typically not feasible with commercial spectrophotometers. Large integrating sphere equipment needed to perform angular measurements on such materials. The experimental facility used for these measurements was described in paragraph 3.3.2.

Measurements were performed between 380 and 1700 nm, covering the 92.7% of the whole solar spectrum energy. The solar and visible reflectance were calculated starting from the spectral measures and operating a weighted average on the solar spectrum as described in the procedure contained in the reference ISO 9050:2003 [6.4]. It was not possible to measure all the fifteen samples due to the weight and size of the most of samples. For this reason, four samples were selected: two membranes (8284, 8285), a shingle (8287) and a tile (8290).

By way of example, Figure 6.5, shows the spectral measured reflectance of the sample 8285 in order to put in evidence the spectral variation at the five incidence angles. The spectral response of reflectance is sensibly affected by the incidence angle. It is important to notice how the trends are parallel translating upward only as a function of the angle. For 8° (near normal) and 30° the trends are very close, almost overlapped. Increasing the angle the reflectance becomes progressively higher. The curve at 75° is much more irregular than the others due to a design limit of the optical bench. At 75° of incidence the spot of the light beam is very elongated going beyond the edges of the sample. To overcome this problem the dimension of the spot was sensibly decreased penalising the amount of incoming energy in the sphere and the accuracy of detectors (par. 3.3.2).

Figure 6.6, Figure 6.7, Figure 6.8 and Figure 6.9 show the evolution of the calculated reflectance broadband values in solar spectrum, increasing incidence angle, for the considered four samples. At a light beam incidence angle of 90° the reflectance was set to 1 as a geometric condition. The increasing of reflectance with angle in the smooth samples (Figure 6.6 and Figure 6.7) seems to be more progressive if compared to the one of rough samples. This factor is due to



### Section 3: Development of Numerical Methods

the higher regular component of reflectance. This component is the main factor that makes the reflectance value dependent on the incidence angle. The rough samples present generally a low regular reflectance and a high diffuse reflectance that is less sensible to an angle variation (Figure 6.8 and Figure 6.9). For these samples, as a matter of fact the trend is almost horizontal even at  $75^\circ$  of incidence.

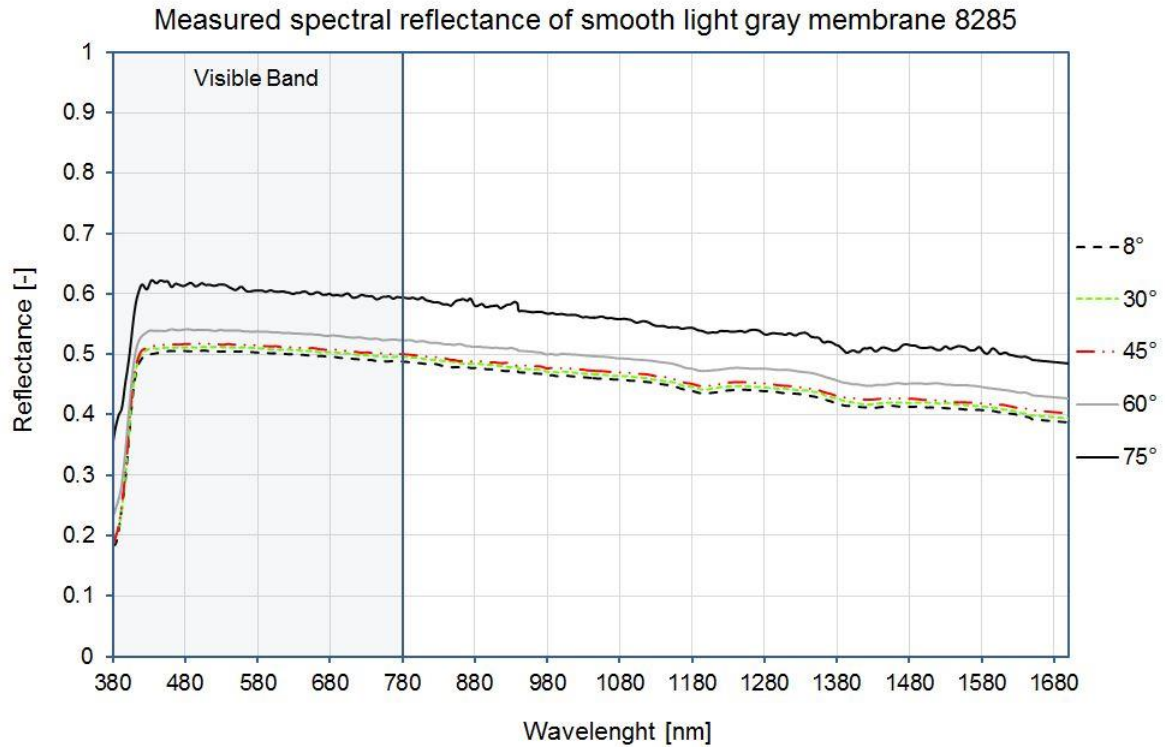


Figure 6.5: Spectral reflectance of sample 8285 at the five considered incidence angles.

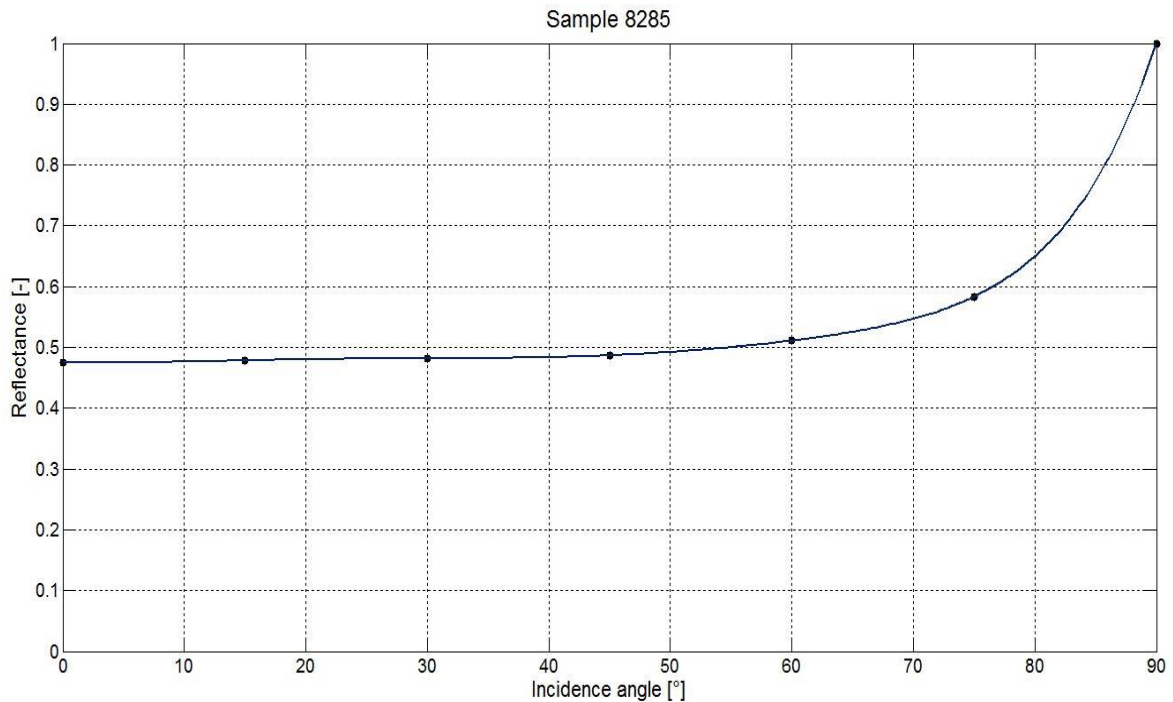


Figure 6.6: Solar reflectance dependence on incidence angle-sample 8285.

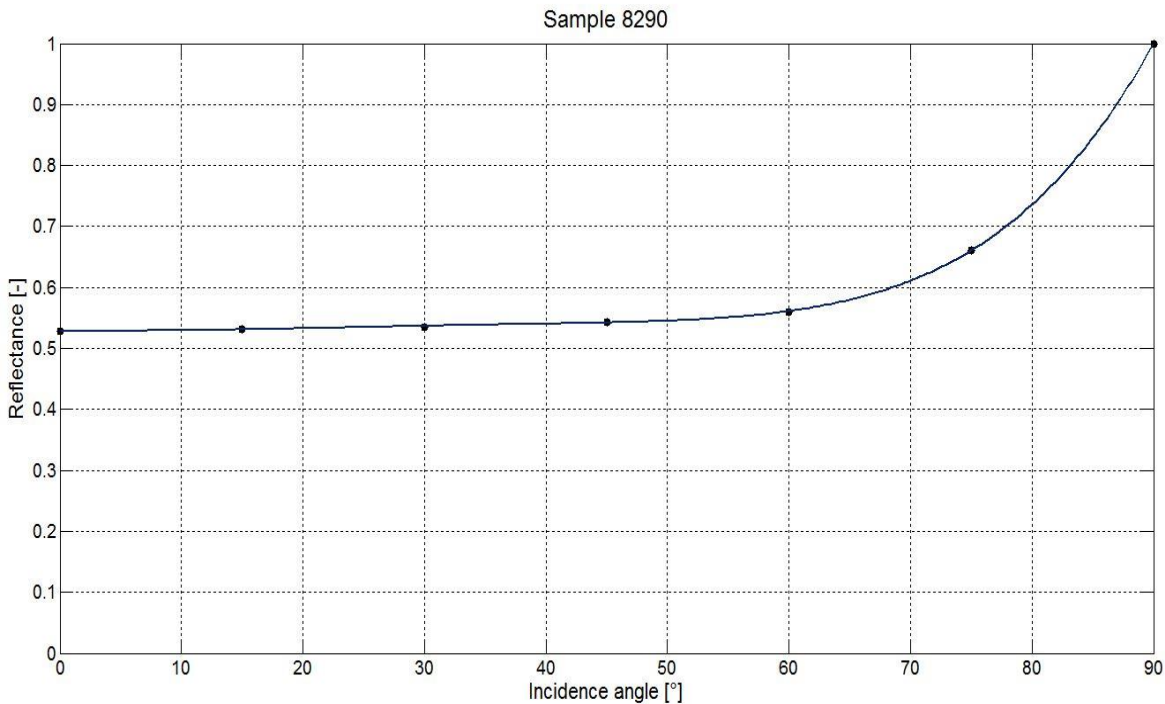


Figure 6.7: Solar reflectance dependence on incidence angle-sample 8290.

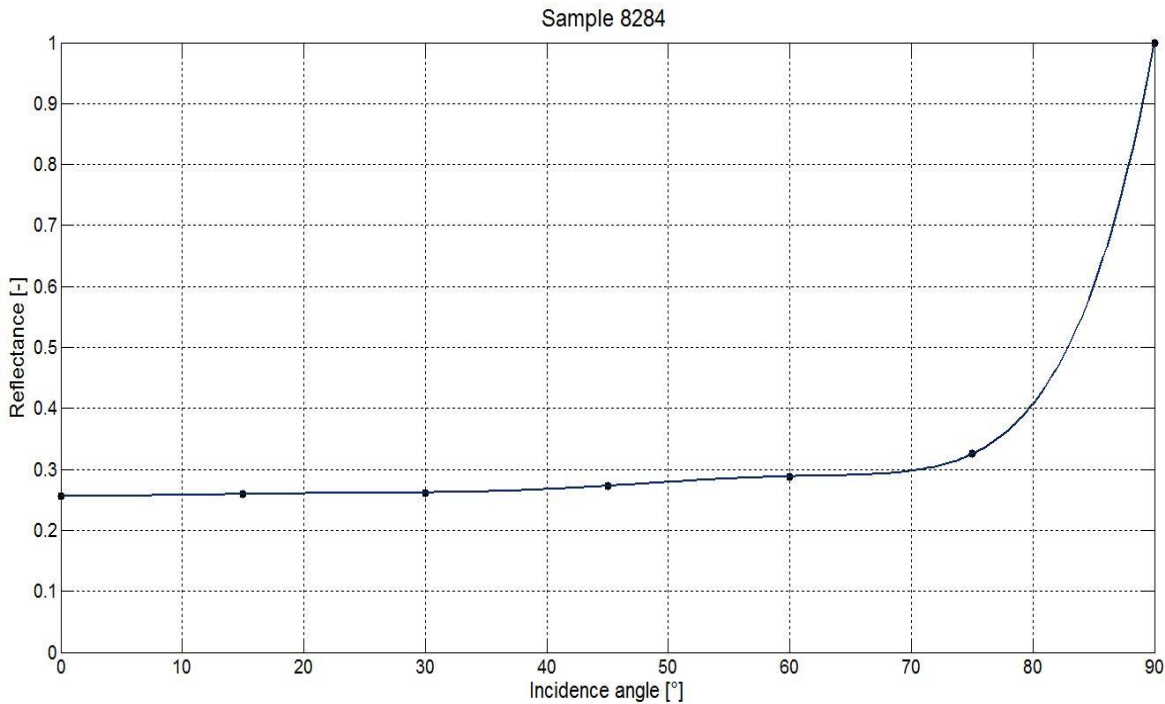


Figure 6.8: Solar reflectance dependence on incidence angle-sample 8284.

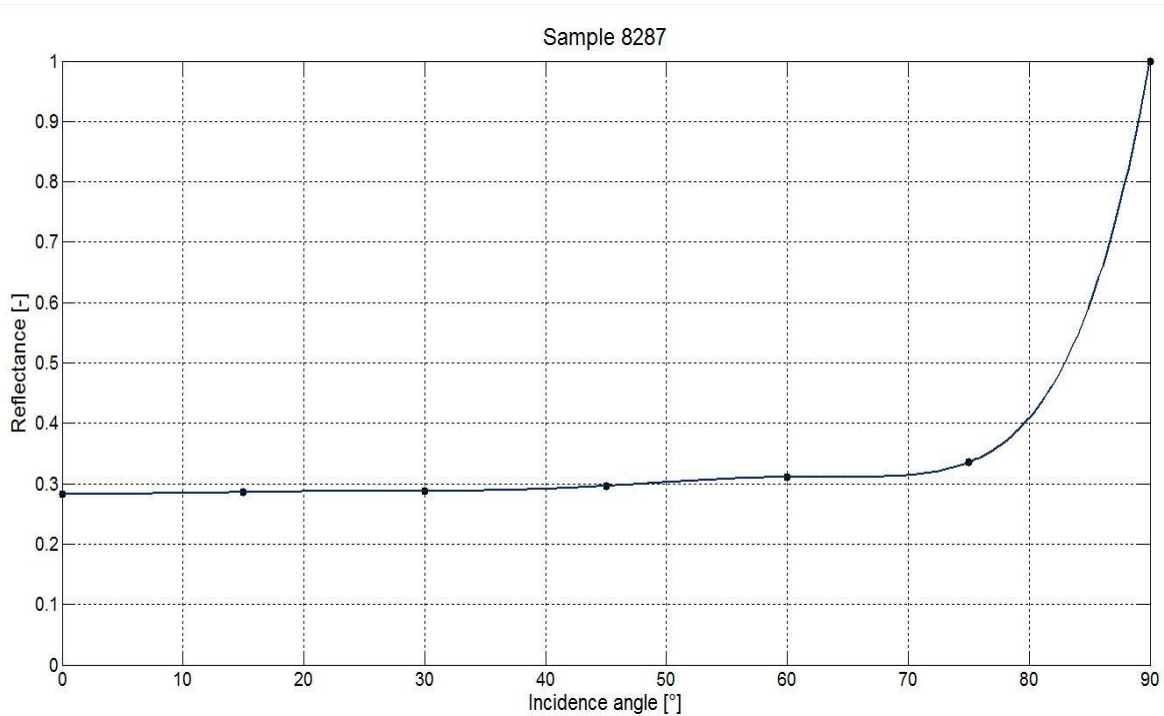


Figure 6.9: Solar reflectance dependence on incidence angle-sample 8287.

## 6.7 Comparison Between the Two Instruments Results

The reflectance broad band values in the visible band for samples 8284, 8285, 8287 and 8290 were calculated starting from the spectral data measured with the spectrophotometer according to the procedure contained in ISO 9050:2003. These values were compared with those obtained by the procedure developed by INRIM processing the coefficients of luminance measured by the gonio-photometer. The measurements with the gonio-photometer were conducted using a photometric detector working in the visible band. For this reason results obtained from this instrument were compared with the broadband values of reflectance in the visible band derived from the spectrophotometer.

The Table 6.4 reports this comparison.

Table 6.4: Comparison between visible reflectance values carried out with spectrophotometer and gonio-photometer.

Sample		Visible Reflectance [-]					Percentage Variation [%]				
		8°	30°	45°	60°	75°	8°	30°	45°	60°	75°
8284	Spectrophotometer	0.279	0.285	0.297	0.314	0.343	0.37	0.51	1.85	0.59	-
	Gonio - photometer	0.278	0.284	0.292	0.312	-					
8285	Spectrophotometer	0.504	0.511	0.515	0.538	0.609	0.25	0.87	2.60	4.89	-
	Gonio - photometer	0.505	0.515	0.529	0.566	-					
8287	Spectrophotometer	0.320	0.324	0.332	0.347	0.369	0.30	1.78	1.43	0.67	-
	Gonio - photometer	0.321	0.330	0.337	0.349	-					
8290	Spectrophotometer	0.456	0.469	0.478	0.496	0.595	5.31	4.33	5.12	5.31	-
	Gonio - photometer	0.482	0.490	0.504	0.524	-					

Although the main function of the gonio-photometer does not apply the calculation of broadband values, but rather the reflection modalities of a materials as a function of its surface characteristics, the results obtained from the comparison are interesting.

The spectrophotometer equipped with an integrating sphere has a measurement error of around  $\pm 0.01$  in reflectance value, then this instrument will be taken as a reference in this comparison.

The gonio-photometer results are obtained through a semi-empirical procedure that allows to obtain the hemispherical reflection factor starting from a measurement made on a single plane normal to the surface sample.

In Table 6.4 the compared results obtained for rough surfaces samples (8284 and 8287) are very close with percentage changes that not exceed 2%. This is due to the reflection shape: Being characterised solely by the diffusing component, it is easier to extend the results obtained for a plan to hemispherical ones, since the shape expected for the luminance coefficient is a semi-sphere.

Regarding samples that have a sensible regular component, to predict the shape of the hemispherical reflection is more complex. The percentage changes are higher and reach values higher than 5%.

## 6.8 Numerical Analysis Calculation

### 6.8.1 Preliminary Comparisons Between Experimental and Theoretical Solar Reflectance

---

The solar reflectance at different incidence angles obtained through the spectrophotometric measurements of two samples, the 8284 and the 8290, was used to find a function  $p(\theta)$  that links reflectance to angle by means of a mathematical fitting using the cubic spline method.

The theoretical evolution of reflectance of these materials was calculated through the Fresnel equation considering a light beam passing from a mean with an unitary refractive index (air) to a mean with a refractive index of 1.5 (specular surface i.e. glass), starting from the reflectance value at the near normal incidence obtained experimentally [6.2]. This equation allows to find the reflectance value for a material with a perfect specular surface. In materials with smooth surfaces but not perfectly specular this equation typically governs the regular component of reflection.

In this manner it was possible to compare the angular evolution of the reflectance, obtained experimentally,  $p(\theta)$ , with the ideal one, obtained theoretically, for a material perfectly specular,  $p_{th}(\theta)$ .

The following Figure 6.10 and Figure 6.11 show the comparison described above. The figures report also a third trend in which the reflectance stays constant regardless of the angle,  $p_{const}$ . The latter trend is typically used in the energy modelling software not considering the change in the reflectivity of a surface by the varying of the incidence angle of direct solar radiation.

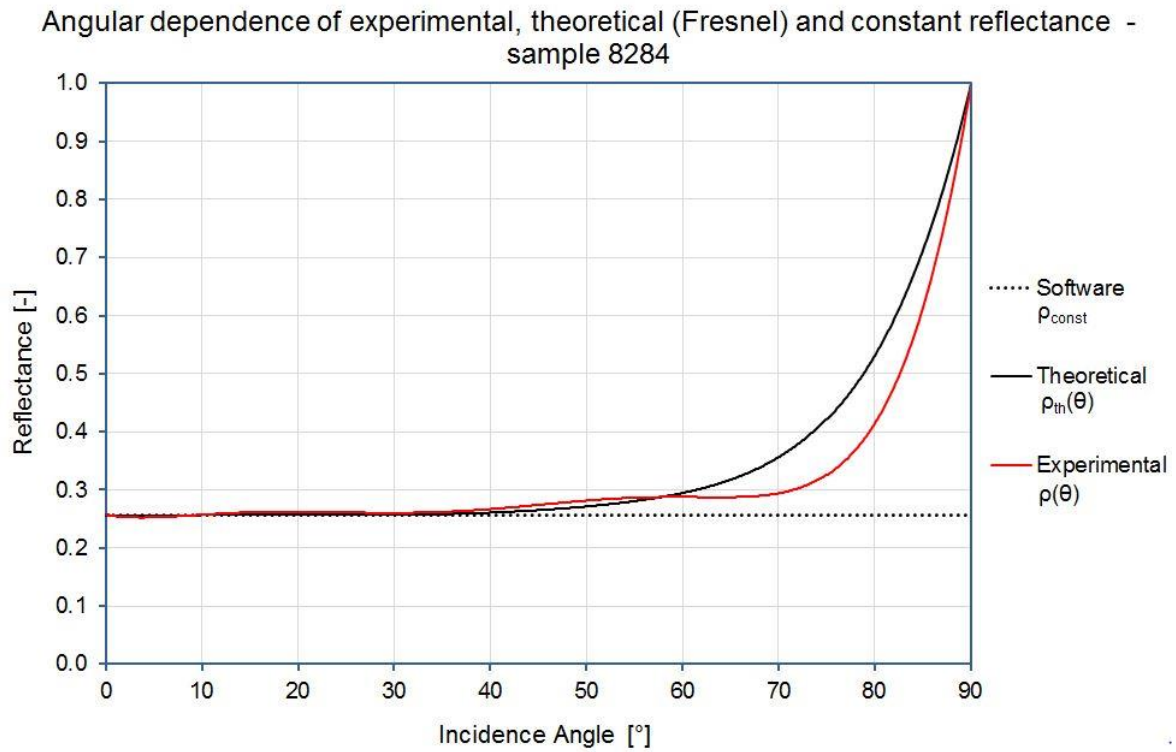


Figure 6.10: Solar reflectance angular dependence, theoretical (Fresnel), experimental and constant (as used in energy modelling software).

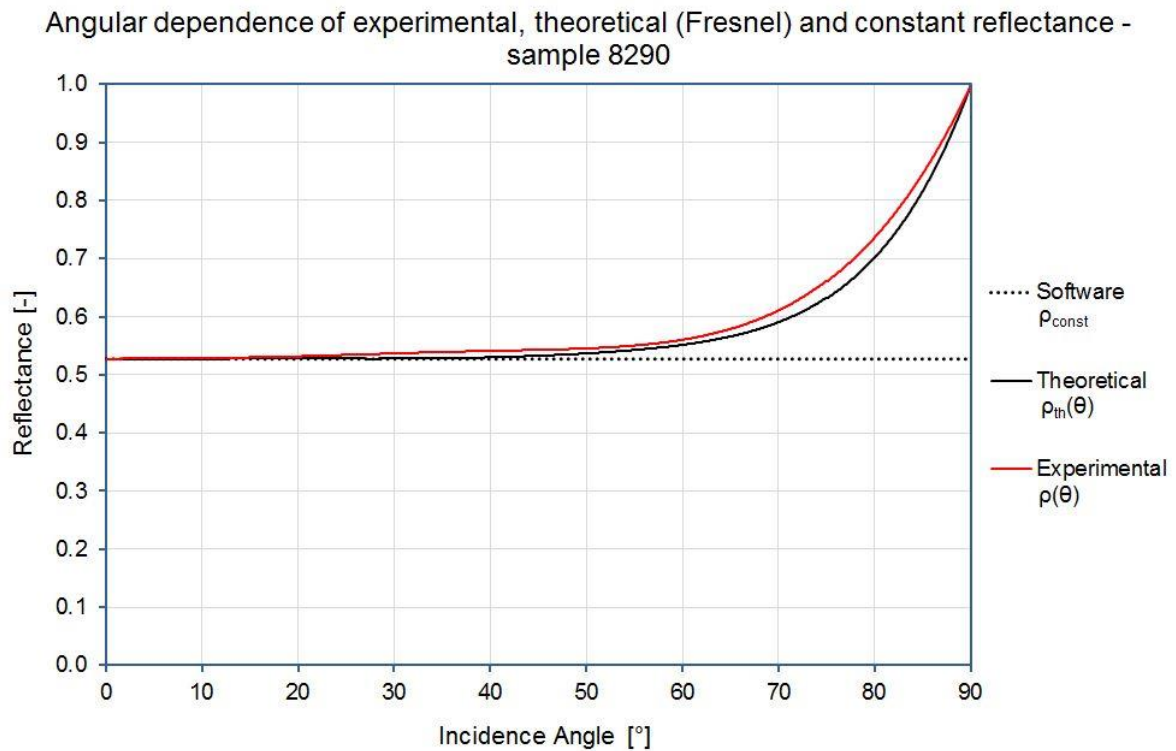


Figure 6.11: Solar reflectance angular dependence, theoretical (Fresnel), experimental and constant (as used in energy modelling software).



### 6.8.2 Model Description

The energy analysis software used in this study is the TRNSYS [6.5].

The examined structure is a simple unique thermal zone box with a plant area of 100 m<sup>2</sup>. The height of the vertical walls is 4 m. In this way all the main expositions were covered (North, South, East, West, and Horizontal). Two insulation levels of the structure were considered: the vertical and horizontal walls thermal transmittance was 1 W / m<sup>2</sup> K in the first case, obtained considering two layers of hollow bricks separated by an air layer and 0.56 W / m<sup>2</sup> K in the second case, replacing the air layer with an insulating material. No windows or other openings were modelled in order to emphasise only the contribution of solar gains on the opaque surfaces in the energetic analysis. The internal temperature was set to 20 °C during winter and 26 °C during summer. The climatic data were extracted from WMO (World Meteorological Organization) database. Three Italian cities were chosen at three different latitudes: Rome, Palermo and Milan.

Simulations were performed for the whole year, but only two seasons were taken into account: winter, from November to the end of February and summer from May 15 to September the 15. The outputs of the simulations are the solar loads and the thermal fluxes through walls.

Using data derived from the analysis of the sample 8284 three simulations were performed for each city and for each insulation level of the structure:

- In the first simulation the solar reflectance of the reference building external surfaces varied with the incidence angle of the direct beam solar radiation following the function  $\rho(\theta)$  described previously;
- Similarly, the second simulation was conducted using the function  $\rho_{th}(\theta)$  derived from the Fresnel equation;
- The third simulation was performed using the default calculation method provided by the software tool which considers the reflectance as constant value regardless of the angle of incidence of direct beam radiation.

The data derived from the sample 8290 were used in a similar manner. In this case the simulation which uses the function  $\rho_{th}(\theta)$  was not performed because of the theoretical curve is essentially overlapped on the experimental one, as can be seen from the previous Figure 6.11.

### 6.8.3 Results

Table 6.5 presents the solar loads on the opaque surfaces in kWh / m<sup>2</sup>, calculated by means of TRNSYS with the  $\rho(\theta)$  method, with the  $\rho_{th}(\theta)$  method and with the  $\rho_{const}$  method, for the three cities, relatively to sample 8284. The values obtained with experimental and theoretical data are very near. The percentage variation between the  $\rho(\theta)$  method and the  $\rho_{th}(\theta)$  method versus the  $\rho_{const}$  were also reported in table. Solar loads obtained with the reflectance angular dependent methods are lower than the ones obtained with constant reflectance method for each orientation and latitude. For  $\rho_{th}(\theta)$  method the maximum percentage variation compared to  $\rho_{const}$  method is 9.6% obtained in Palermo during summer, orientation South, while for  $\rho(\theta)$  method the maximum percentage variation is 8.5% in Palermo orientation North.

Similarly to the previous table, the Table 6.6 presents the solar loads on the opaque surfaces in kWh / m<sup>2</sup>, calculated with the  $\rho(\theta)$  method and with the  $\rho_{const}$  method, for the three cities, relatively to the sample 8290. The optical analyses reported that this sample present a relevant regular component that makes the reflectance more angular dependent. For this reason the percentage variations between the  $\rho(\theta)$  method and the  $\rho_{const}$  method are in average higher than the variations found for sample 8284. The maximum value is 17% obtained for Palermo during summer, orientation South.

Figure 6.12 and Figure 6.13 represent the percentage change in flux respectively for not insulated and insulated configurations for sample 8284. In summer, changes in heat flux are represented with positive values in order to emphasise the decreasing of this value due to the

### Section 3: Development of Numerical Methods

optimisation of the solar loads calculation. Conversely, in winter, the percentage change of thermal flux is represented with negative values indicating the increase of the heat losses towards the outside. It has to be noted that the changes during the summer season are sensibly higher than in winter. The higher variations were registered for South and Horizontal orientations with values higher than 6%.

The variations obtained by comparing the  $\rho(\theta)$  method versus the  $\rho_{const}$  method are higher than the ones obtained by comparing the  $\rho_{th}(\theta)$  versus  $\rho_{const}$ , except for orientation south. As a matter of fact, observing the Figure 6.10, the reflectance values obtained theoretically for an incidence angle that ranges between  $60^\circ$  and  $90^\circ$  are higher than those calculated experimentally. During the summer the sun affects the surface south oriented with incident angles including in that range. The result is a lower solar load (and thus higher variations). Conversely for other orientations the matter is the opposite even if it occurs with less intensity.

Figure 6.14 and Figure 6.15 represent the percentage change in flux respectively for not insulated and insulated configurations for sample 8290. The considerations made for Figure 6.12 and Figure 6.13 concerning the sample 8284 can be replicated for the sample 8290, remembering that no calculations were performed considering the method  $\rho_{th}(\theta)$  because the theoretical and experimental reflectance variations with incidence angle are almost overlapped for this sample. Even in this case the higher variations were registered for South and Horizontal orientations with values higher than 7% (almost 9% for Rome in the insulated configuration, during summer, orientation South).

Table 6.5: Solar loads obtained with sample 8284.

City	Orientation	Solar loads [kWh/m <sup>2</sup> season]						Relative variation [%]			
		Summer			Winter			Summer		Winter	
		$\rho_{const}$	$\rho(\theta)$	$\rho_{th}(\theta)$	$\rho_{const}$	$\rho(\theta)$	$\rho_{th}(\theta)$	$\rho_{const} - \rho(\theta)$	$\rho_{const} - \rho_{th}(\theta)$	$\rho_{const} - \rho(\theta)$	$\rho_{const} - \rho_{th}(\theta)$
Milan	North	162.0	149.1	150.9	41.0	37.9	38.7	7.9	6.8	7.4	5.4
	South	307.2	287.4	284.9	156.2	149.9	151.8	6.4	7.2	4.1	2.8
	East	305.7	288.9	291.8	72.5	68.0	68.4	5.5	4.6	6.3	5.7
	West	308.1	291.6	294.3	71.5	66.9	67.3	5.4	4.5	6.4	5.9
	Hor	533.6	507.5	512.2	110.7	104.0	102.7	4.9	4.0	6.1	7.2
Rome	North	168.5	154.4	155.5	52.7	48.8	49.9	8.3	7.7	7.4	5.4
	South	330.2	309.1	302.7	289.5	279.3	282.7	6.4	8.3	3.5	2.4
	East	353.1	334.1	336.5	119.6	112.2	112.4	5.4	4.7	6.2	6.1
	West	357.2	338.4	341.0	120.9	113.8	113.9	5.3	4.5	5.9	5.8
	Hor	632.8	606.1	610.7	182.1	171.9	168.6	4.2	3.5	5.6	7.4
Palermo	North	172.9	158.1	158.1	60.4	55.9	57.1	8.5	8.6	7.4	5.4
	South	309.4	286.4	279.8	283.9	272.8	276.3	7.4	9.6	3.9	2.7
	East	356.4	337.0	339.3	127.4	119.4	119.9	5.4	4.8	6.3	5.9
	West	365.3	345.9	348.4	128.8	120.9	121.4	5.3	4.6	6.1	5.8
	Hor	658.3	631.8	636.5	204.1	191.9	190.7	4.0	3.3	6.0	6.6

Table 6.6: Solar loads obtained with sample 8290.

City	Orientation	Solar loads [kWh/m <sup>2</sup> season]				Relative variation [%]	
		Summer		Winter		Summer	Winter
		$\rho_{const}$	$\rho(\theta)$	$\rho_{const}$	$\rho(\theta)$	$\rho_{const} - \rho(\theta)$	$\rho_{const} - \rho(\theta)$
Milan	North	103.1	87.4	26.1	22.5	15.2	13.7
	South	195.6	167.7	99.5	91.9	14.2	7.6
	East	194.6	174.2	46.2	40.4	10.5	12.5
	West	196.1	175.5	45.5	39.7	10.5	12.7
	Hor	339.7	307.4	70.4	60.1	9.5	14.8
Rome	North	107.2	90.2	33.6	29.0	15.9	13.7
	South	210.2	177.4	184.3	172.2	15.6	6.6
	East	224.8	201.7	76.2	66.9	10.3	12.1
	West	227.4	204.0	76.9	67.6	10.3	12.1
	Hor	402.8	369.6	115.9	99.9	8.2	13.8
Palermo	North	110.0	92.1	38.4	33.2	16.3	13.7
	South	197.0	163.4	180.7	167.7	17.0	7.2
	East	226.9	203.2	81.1	71.2	10.4	12.2
	West	232.6	208.6	82.0	72.0	10.3	12.2
	Hor	419.1	385.8	130.0	113.6	7.9	12.6

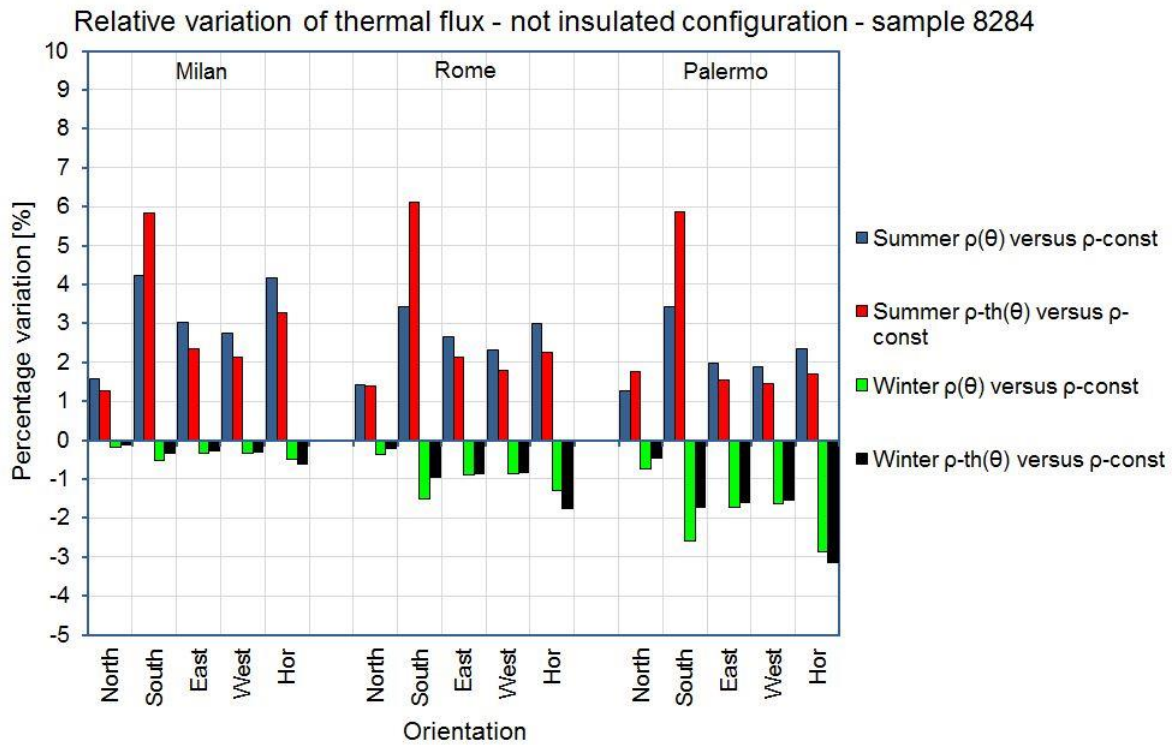


Figure 6.12: Percentage variation of thermal flux for not insulated configuration-sample 8284.

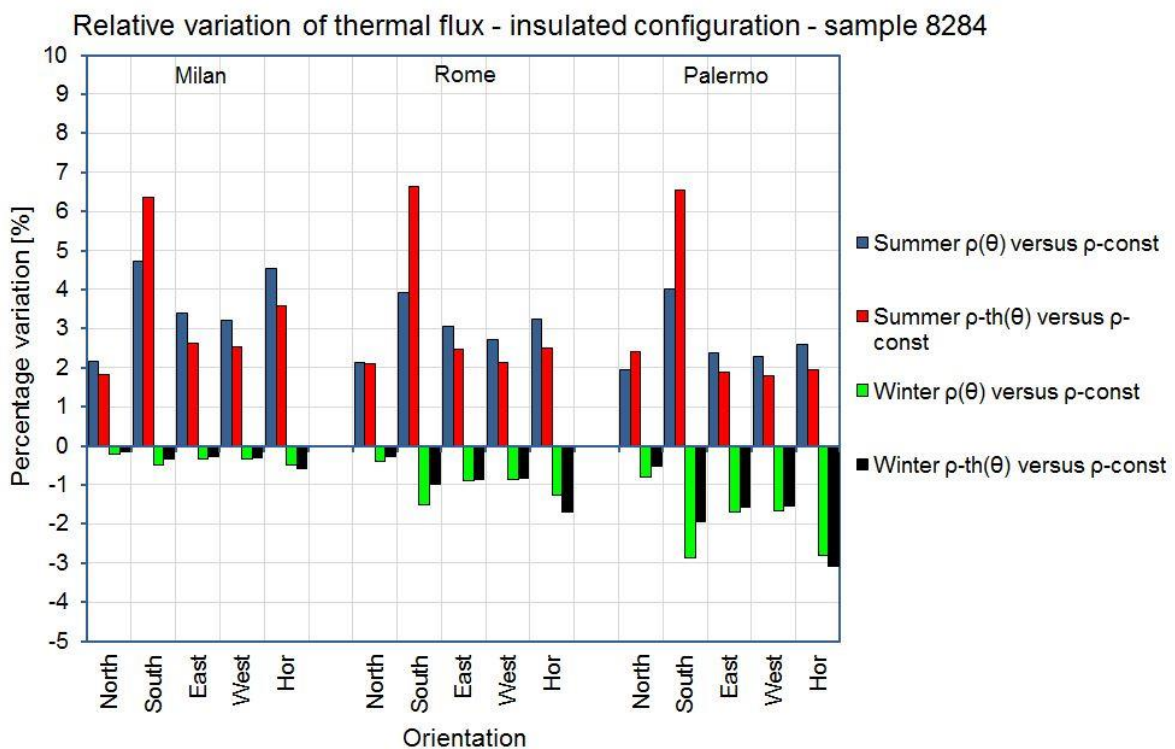


Figure 6.13: Percentage variation of thermal flux for insulated configuration-sample 8284.

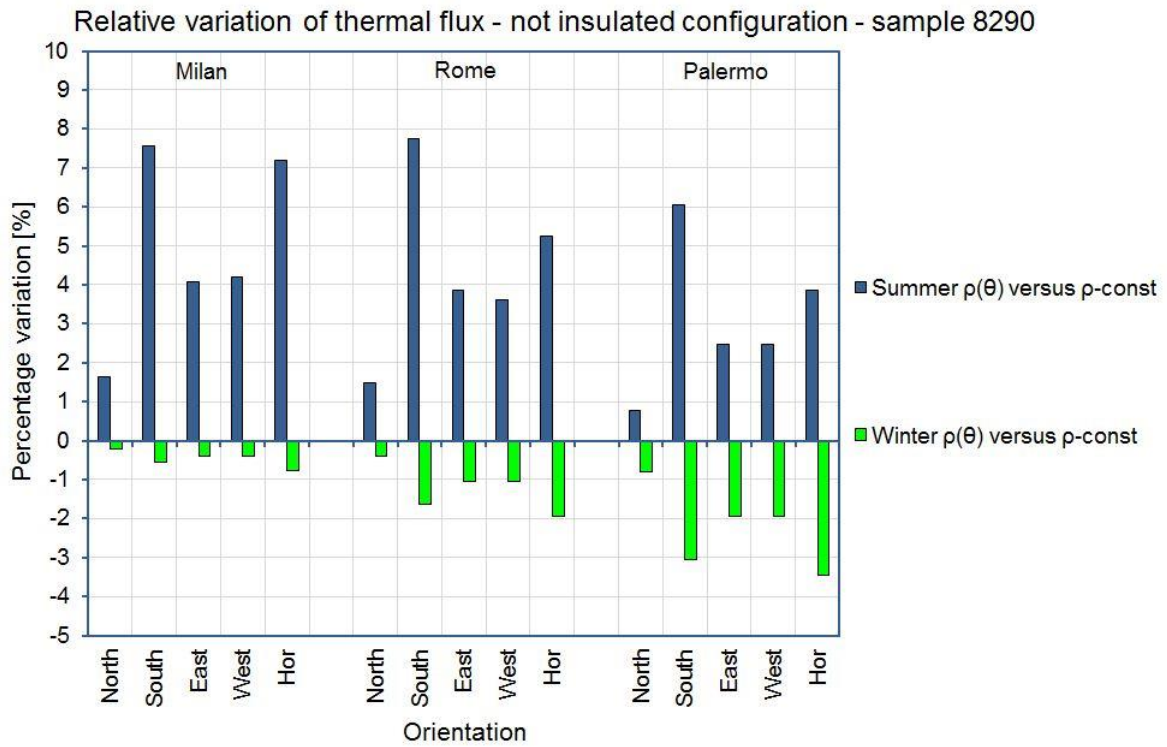


Figure 6.14: Percentage variation of thermal flux for not insulated configuration-sample 8290.

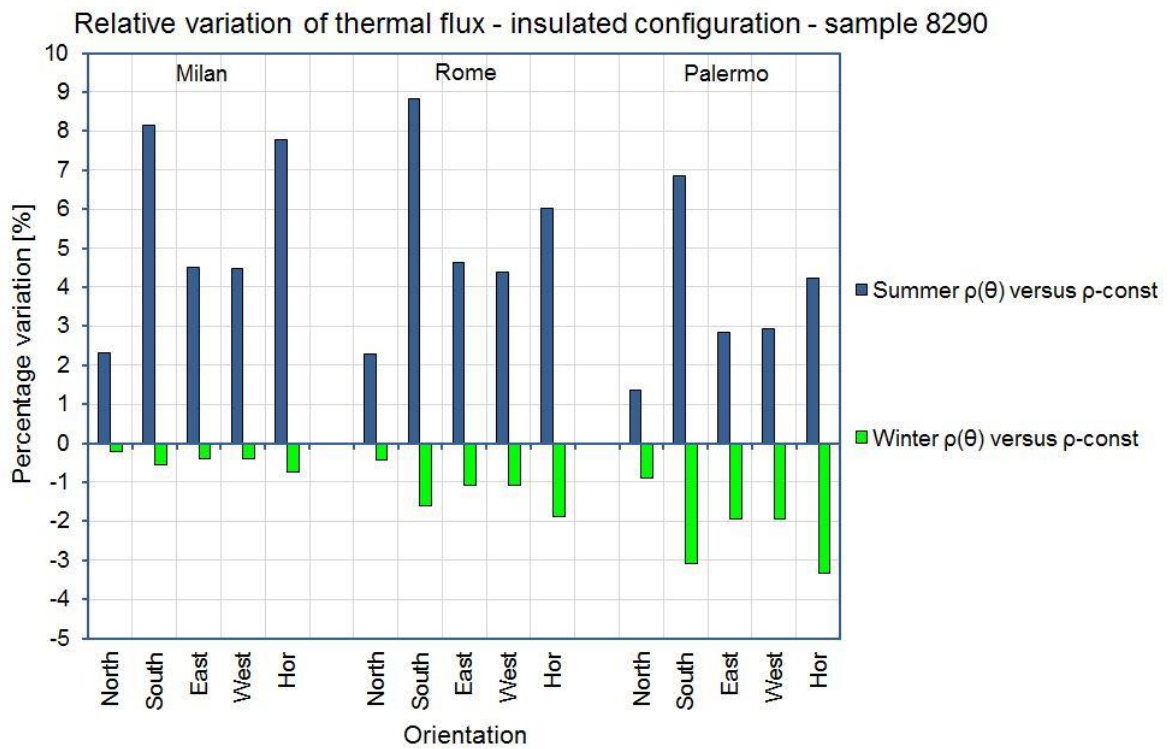


Figure 6.15: Percentage variation of thermal flux for insulated configuration-sample 8290.

## 6.9 Chapter Discussions and Conclusions

---

Solar reflectance is angular dependent. An optical characterisation able to quantify the change in reflectance at different incidence angles demonstrates the extent of this dependence. Several samples of building components used as roof covers were tested with different surface finishing: Smooth and rough. The reflectance of smooth samples showed a high sensibility to an increasing of incidence angle.

The function that links the reflectance to angles was used to find an accurate method of calculation of solar gains. This method was compared to the constant reflectance method typically used in the thermo-physic models. The TRNSYS tool allowed to perform an energetic simulation of a simplified building in order to assess the differences between the two methods by calculating the energy balance of a wall and in particular the thermal flux.

The results showed an underestimation of reflective power of materials in the thermo-physic models leading to an overestimation of solar absorptance and thus of solar gains. Thermal fluxes calculated with the software pre-set method compared with ones obtained with reflectance angular dependent method are higher during summer and lower during winter. The percentage difference between the two calculation method of thermal fluxes reaches not negligible values for South and Horizontal orientations for the three considered cities and for both insulation levels.

The calculation method for reflectance proposed in this paper demonstrated the limits of the thermo-physic models generally used to perform energetic analyses. The concept expressed can also be extended to transparent components for the optimisation of g-value calculation. Further developments will concern a more detailed thermal analysis on building scale in order to assess the importance of this different approach in the evaluation of reflectance on energy demands of buildings.

## 6.10 References

---

- [6.1] Zinzi M. 'Cool materials and cool roofs: Potentialities in Mediterranean buildings'. *Advances in Building Energy Research*; 2010; 4: 201 - 266.
- [6.2] Levinson R, Akbari H, Berdahl P. 'Measuring solar reflectance – Part I: Defining a metric that accurately predicts solar heat gain'. *Solar Energy*; 2010; 84: 1717 - 1744.
- [6.3] Maccari A, Montecchi M, Treppo F, Zinzi M. 'CATRAM: an apparatus for the optical characterization of advanced transparent materials'. *Applied Optics*; 1998; 37: 5156 - 5161 (69 Suppl.) Nos. 1 - 6: 75 - 92.
- [6.4] ISO 9050. Glass in building-Determination of light transmittance, solar direct transmittance, total solar energy transmittance, ultraviolet transmittance and related glazing factors; 2003.
- [6.5] TRNSYS 16. <http://www.trnsys.com>; Available online at.



## 7. Conclusions

---

### 7.1 Achievements

---

The effectiveness of cool materials has been tested through a series of experimental and numerical analysis. The experimental analyses have actually shown as the radiation reflection power in the solar spectrum is higher than that of conventional construction materials. This property, together with the high thermal emissivity, makes the cool material a viable technique for the achievement of goals relative to energy savings and thermo-hygrometric comfort. Being related to solar gains, their effectiveness depends on irradiation and therefore it is a function of latitude. The main results obtained in this research are summarised below:

A reflective membrane was used as roof coating in a reference building. The surface temperatures of the cool roof and the original shingle were constantly monitored during the experimental tests. During summer the reflective membrane subjected to the peak solar radiation showed a temperature of about 25 °C lower than that of the bituminous shingle. Furthermore the variation in temperature between the external and internal surface was halved in the central part of the day limiting the incoming thermal flux in the building. As a matter of fact decreases in mean temperature of the internal environment of about 2.5 °C were detected. A numerical analysis carried out on a calibrated model of the building has shown a decrease in the discomfort number of hours calculated in free-floating conditions as well as a decrease in cooling energy demand of up to 32% (Chapter 4, paragraph 3).

Further numerical analyses have shown that a cool roof, limiting solar gains, leads to a decrease in energy demand during summer and a consequent increase of it during winter. For this reason, the amount of annual energy savings was calculated on several types of residential building obtaining encouraging results with decreases in the annual energy demand up to 50% for not-insulated and insulated buildings (Chapter 4, paragraph 5).

A little investigated aspect of this technology is the durability of its performance over time. Materials, being exposed to the external environment, are subject to phenomena related to climatic agents, ageing and soiling. Tests to detect the reflectance decay in natural exposure imply very long run times. A measurement campaign still in progress has verified the extent of this decay. It has been registered a reduction of about 24% of the reflection power for samples with an initial solar reflectance greater than 0.8. In general, this decay is a function of roughness and reflectance spectrum shape. Nonetheless in many cases spectral data measured after 12 and 18 months demonstrate a convergence trend with broadband values however higher than that of conventional materials (Chapter 4, paragraph 4).

The amply demonstrated effectiveness of cool roofs has still no place in national energy policy (although the cost of this technology is directly comparable to that of conventional materials) providing regulations only to limit the space heating. The data collected during these years of research have produced a proposal for the energy classification of these materials as a function of their solar reflectance and thermal emissivity (Chapter 4, paragraph 5).

This research presents also a detailed study about the potentialities of cool materials used as urban paving coatings to mitigate outdoor temperatures, through experimental and calculation analyses. The optical characterisation highlighted the positive impact of cool materials on the increase of the conventional asphalts solar reflectance. The spectral measurements also evidenced the limits of the tested products; as a matter of facts, excluding samples with light colours, the near infrared reflectance of all the samples resulted to be always lower than 0.46, a value by far poorer than those of cool coloured materials for building roof application. Improving the reflectivity in the near infrared range is a mandatory requirement to exploit the product potentialities, since higher solar reflectance values can be achieved without increasing the visible reflectance and modifying colours, enhancing the architectural and urban integration. The high emissivity values coming from measurements showed that the cool layers do not affect the thermal behaviour of the conventional asphalts. The outdoor monitoring provided useful data about the ability of the coated asphalt to remain cool under the solar radiation. Maximum temperature differences between the green, blue and grey samples respect to the original asphalt range between 8 and 10 °C. Lower values were obtained for the red asphalt, while the difference is close to 20 °C for the off-white samples. The average values during the monitoring period showed that the treated surface temperatures remained several degrees lower than the original asphalts, but increased solar and infrared reflectance values are needed to make these applications competitive. The monitoring also showed significant deviation from the laboratory sample in respect to the road application for the blue sample, being the former more absorptive than the latter. This aspect, which is not relevant for experimental studies, is crucial for the market acceptance of the technology and it needs to be carefully addressed by manufacturers and installers in order to have installations, whose chromatic response is in line with the customer selection, generally occurring through the producers colour palette. Laboratory measurements and monitoring results were conversely in good agreement for the other materials. Numerical analysis was used to investigate the potentialities of cool materials application in an urban texture. The results of this study put in evidence how these colour thin layers, used for roads and paving could have a sensible impact, due to their low surface temperatures, on decreasing the average air temperature of the environment, also at significant heights from the ground. The calculated extent of this decrease, in a summer day, reaches a maximum of 5.5 °C, replacing a conventional asphalt with a cool off-white tint, maintaining this difference almost constant beyond the average height of buildings. A further numerical analysis was aimed at evaluating the effect that the decrease in air temperature in urban areas, resulting from the use of cool materials as asphalt coatings, has on peak cooling loads of a typical dwelling of the densely urbanised building stock of Rome. Sensible reductions of peak cooling demand due to the use of these coatings were registered: 18.9% for the not-insulated configuration, and 14.6% for the insulated building. These results take on a stronger connotation if extended to the whole hot season. The massive use of this innovative technology combined with an increase of green areas leads to a sensible mitigation of urban heat island effect and its

consequences with improvements on comfort levels and a decrease of energy uses in the buildings (Chapter 5).

The use of different energy analysis tools employed for numerical purposes has highlighted a limit concerning the modelling of the building surfaces. These models consider the reflectance as a constant and independent on the incidence angle of radiation that hits the surfaces (Lambertian reflection). Instead, the building materials, especially those used as roof coatings, present mixed reflection modalities with not negligible regular components, which are a function of angle of incidence as demonstrated in the experimental campaign shown in this report. Hence, it was obtained a function that linked the solar reflectance to incidence angle starting from the measured data. It has been used in order to modify the calculation model of a dynamic tool optimising the solar gains calculation. Findings show a percentage changes in solar loads up to 17% for low latitudes and furthermore a percentage change of the heat flux towards the internal environment for the south-facing walls between 7% and 9% for the Italian territory during summer. The results demonstrate the limits of current thermo-physical models generally used to conduct energy analyses (Chapter 6).

## 7.2 Future developments

---

The cool materials technology is in continuous development and research and study activities require continuous updates. The studies highlight the importance of balancing the solar gains during summer with winter losses in order to optimise the performance of the buildings in the whole year. Very promising is the application at urban scale to improve the conditions for summer comfort and mitigate the urban heat island effect.